Building the Biofilm Matrix: Gene Regulation and Cell Organization

by

Janet Elizabeth Price

A dissertation submitted in partial fulfillment
of the requirements for the degree of
Doctor of Philosophy
(Molecular, Cellular, and Developmental Biology)
in The University of Michigan
2020

Doctoral Committee:

Professor Matthew R. Chapman, Chair
Professor Robert A. Bender
Professor Philip C. Hanna
Professor Ursula Jakob
Professor Lyle A. Simmons

Janet E. Price

janetep@umich.edu

ORCID iD: 0000-0002-4385-9283

DEDICATION

For Kyle, Pierce, and Elliot, who always were there to remind me there is life outside of lab.

For my family.

For Mika, my loudest and proudest cheerleader.

ACKNOWLEDGEMENTS

Progress in a PhD would not be possible without a dedicated community of friends and supporters. I have been fortunate to always have an ear to listen to all my ideas and a shoulder to cry on when experiments go awry. Through their actions I am able to complete this dissertation. To all that have been there for me over the years, a heartfelt thank you. To a few individuals instrumental in my success, I wish to acknowledge them individually.

I could not have imagined a better mentor than Sir Dr. Professor Matt Chapman. Matt has an enthusiasm for science that can be felt after spending any amount of time with him. He welcomed me into his lab and pushed me to be a better scientist every day. Knowing that I didn't plan to stay in academia, Matt went above and beyond to encourage me to seek out opportunities to grow in business and communication. While his impressive dance moves never rubbed off on me, I owe him everything for the scientist I am today.

The Chapman Empire has been my home away from home. I want to thank Dave Hufnagel, Maggie Evans, and Neha Jain for showing me the ropes and setting a high bar to aspire to. For a while, Neha and I *were* the Chapman Lab. We spent many long days in lab together and our research bay always echoed with her loving yells. Elizabeth Gichana (eLiz) is one of the most generous people I have ever met. She has looked out for me and helped me get out of my comfort zone by being my wing person at all the intimidating biotech mixers. The whole Chapman Lab has been made full of laughs, inside jokes, poorly drawn turtles, and amazingly supportive friends. For that I thank Sujeet Bhoite, Anthony Balistreri, Kanna Nagamatsu, Hema Swasthi, Nana Britwum, and Mark Gomulinski. I also want to thank the undergraduates I have worked with: Hakam Nouri, Matt Tyl, and Serge Albarian. They were tirelessly dedicated to the lab and their own curated projects.

Our lab is surrounded by brilliant scientists. The Vecchiarelli and Miller Labs have been the ideal neighbors and partners in awesome costumes. Anne Hakim is a tour de force. She was my partner in commiseration and a model of how to have a full family life while taking no quarter in lab. Banter between Joe Basalla, Lisa Tran, and Rees Rillema is sharp and mirthful, but they are always willing to bounce ideas and lend a hand. My favorite time of year is when the Freddolino lab and I travel to Madison, WI for the Phage conference. I cherish times on the patio geeking out over the recent talks with the whole gang. One of the finest minds I met at U of M belongs to Taylor Nye. Her drive and confidence inspired me to always work harder. I will sorely miss our philosophizing over beverages. Shyama Nandakumar was with me through the ups and downs of grad school. I do not know where she finds the energy to do everything she does, but she is kind enough to keep me in the loop. We started together and are now finishing together.

I want to thank the Department of MCDB for all the support. Mary Carr is an invaluable resource and always ready with kind words and advice. She made sure all the i's were dotted

and t's were crossed for everyone in her charge. I also want to thank Gregg Sobocinski for all the help he gave me with imaging. Even without a window, the microscope basement is a cheery place. And Gregg keeps it running like a swiss watch.

I want to thank my committee for always pushing me. Their candid discussions have led to many interesting scientific rabbit holes to explore. A few of which made it into these pages. I am be endlessly grateful for the time and effort they spent shaping me into the scientist I am today.

Finally, I want to thank my family for believing in me.

TABLE OF CONTENTS

LIST OF FIGURES

FIGURE

LIST OF TABLES

TABLE

ABSTRACT

The biofilm lifestyle is the pervasive method for bacteria to resist environmental stress. Biofilm protection results in a decreased ability for human hosts to clear infections and an increased rate of antibiotic resistance among bacteria. In *Escherichia coli,* biofilm formation depends curli and cellulose, which form a protective extracellular matrix around the cells. Cells within a colony biofilm can be divided into at least two physically distinct subpopulations, including a population that produces the extracellular matrix and a population that does not produce matrix. Extracellular matrix production during biofilm formation is under complex regulation that is still poorly understood. My work has identified new pathways and regulators that alter extracellular matrix production and subpopulation development in *E. coli*. We identified over 300 genes including those involved in LPS biosynthesis, gluconeogenesis, purine metabolism, cellular respiration, and other fundamental cellular processes which, when disrupted, result in changed curli production. To better understand subpopulation development, whole transcriptome and proteome data was collected from both the matrix and non-matrix cells. Gene products involved in anaerobic respiration were dramatically increased in the cells comprising the non-matrix subpopulation as compared to the matrix subpopulation. Deletion of *nrfA*, which is a gene involved in anaerobic respiration, resulted in a loss of the non-matrix cells producing subpopulation. Finally, I identified small RNAs and c-di-GMP produced by DgcN that regulate the expression of *csgD*, the master biofilm transcription factor. CsgD levels and matrix production were altered by redox changes sensed by the periplasmic repressor of DgcN, YfiR. Cysteine auxotrophic UPEC isolates were hyper-oxidized and produced more curli under normal and non-permissive biofilm growth temperatures. Deletion of YfiR or supplementation with a reducing agent restored WT curli production in cysteine auxotrophic strains. Taken together this work defines the complex regulatory network controlling biofilm matrix production.

CHAPTER I

Introduction

Life in a Microbial World. Life as we understand it becomes grander and more diverse with each new generation. Existence of living things beyond the limitations of our vision has been discussed for centuries before Antony van Leeuwenhoek set eyes on microbes with his crudely made microscope(1). The five kingdoms of life, which originally had bacteria as a small afterthought at the root, has been redrawn countless times to expand the tree of life with each new bacteria discovery(2, 3). While researchers work through the inability to culture a majority of bacteria in the lab (known as the 'Great Plate Count Anomaly')(4), we are able to sequence the small ribosome subunit of unculturable species and now know bacteria are at least 2/3rds of life on Earth(3). Even by sheer number, humans are outnumbered by prokaryotes (Bacteria and Archea) by about 5×10^{20} to 1(5, 6). While the realization is new to us, fossil records establish the bacterial way of life dating back at least 3,770 million years(7). Bacteria have always found a way to survive.

Bacteria can survive, even thrive, in nearly every environment on Earth. Bacteria are found at the bottom of the oceans, inside volcanoes, and in stable ecosystems in the clouds(8-10). The international space station (ISS) and the Mir space station have both struggled with bacteria contaminating water filtration systems and corroding radiator and navigation components of the station(11, 12). These examples highlight how bacteria can modify their environment to bring it within their tolerable range of many factors (*e.g.* pH, salinity, temperature, oxygen, etc.)(13). But arguably the most important tool for bacterial survival is the ability to form a biofilm.

Biofilms are communities of single-celled organisms, often comprised of many different species, living attached to a surface with the aid of a self-made, extracellular structure(14-16). This secreted structure, called the matrix, provides the underlaying cells protection from stressors such as desiccation, predation, redox changes, and antibiotics(17-21). This resistance is two-fold. First, the matrix forms a physical barrier that is resistant to sheer stress and phagocytosis(18, 22). Second, the bacteria within the biofilm organize into subpopulations with distinct physiological characteristics(14, 19, 23, 24)(Chapter 3). Subpopulation differences in metabolism can attune cells for resistance to unique stresses, such as increased oxygen exposure in outermost biofilm cells, or build resistance, such as persister cells(14, 19, 20, 25). Difference between subpopulation resistance allows for growth in a wider range of environments and a rapid response to changes in environment(14, 26).

The broad resistance of biofilm to antibiotics, environmental stress, and conventional cleaning methods make biofilm a threat to human health and lifestyle. Biofilm formed on medical surfaces serve as major contributors to antibiotic resistance and chronic illnesses(27-32). The CDC estimates 80% of bacterial infections and 65% of hospital acquired infections are caused by biofilm(33). Treatment of the resulting infections costs the US approximately $94 billion annually(34, 35). Biofilm that form on food preparation surfaces or on aquaculture and civil water systems cause equipment breakdown and carry human health risks(36-39). We are unable to control biofilm growth with our current understanding of biofilm formation. Model systems of biofilm formation allow for research into how biofilm is formed and potential biofilm management techniques.

Biofilm Model Systems. Biofilm is the predominant lifestyle in bacteria and, as such, the process of biofilm formation is similar across species(40, 41). First, free-swimming cells will encounter a surface and begin to attach(42, 43). Some attached cells lyse which coats the

surface with extracellular DNA that serves to increase adherence of new cells. Most cells attached to the surface begin secreting extracellular matrix components to build a structure and protect the new community(42, 43). Extracellular matrix can be made up of many substances, such as cellulose, pili, flagella, antigen 43, capsule sugars, and curli among others(42). In *E. coli*, the matrix is primarily composed of curli and cellulose(42). The biofilm continues to grow in size and cell number until dispersal is signaled, breaking open part of the matrix and allowing free-swimming cells back into the environment(42). Biofilm dispersal signals are chemically diverse and not well understood. Dispersal of cells from a mature biofilm has been shown to result from a buildup of toxic waste products or steeply changing oxygen gradients between the cells within the biofilm and the environment(24, 44). Biofilms can also be dispersed through a change in second messenger concentration, such as cyclic-di-guanosine monophosphate (c-di-GMP) or indole(45). Studies have shown that high c-di-GMP and low indole promoted biofilm formation, while low c-di-GMP and high indole can inhibit biofilm formation or facilitate biofilm dispersal(45-48). Biofilm lifestyle as a shared trait among bacteria has allowed researchers to use specific bacteria as systems to model the natural environment and develop strong molecular tools to investigate biofilm.

Escherichia coli is the most well-researched bacteria and will form robust biofilms as part of its lifestyle. *E. coli* was first isolated from a human stool sample in 1886 by microbiologist and pediatrician, Theodor Escherich(49). *E. coli* are commonly found as part of the human microbiome and are among the first to colonize the human GI tract after birth(50). *E. coli* are members of the bacterial family Enterobacteriaceae, gram negative bacteria which colonize the lower intestines mammals, birds, and some reptiles(51). As facultative anaerobes, *E. coli* uses adaptations in respiration and biofilm formation to survive in the oxygen limiting environment of the host(52-54). Since the original isolation of *E. coli*, over 200 different strains have been isolated and studied. Though each individual strain contains roughly 4,800 genes, only slightly over a third of those genes are shared between all strains(55). In this work we used K-12 *E. coli*, a common laboratory strain, and UTI89 *E. coli*, a patient isolate from a bladder infection, to identify genes that play a role in biofilm formation.

K-12 *E. coli* has been serially passaged in the laboratory for over 50 years, causing the strain to lose some characteristics that define other *E. coli* strains(56). K-12 is adapted to grow better in shaking cultures and therefore takes longer to adhere to a substrate and form biofilm(57). Most important for this work, K-12 lacks cellulose due to a mutation in the cellulose synthase(56). While this means K-12 does not model *E. coli* biofilms in nature, lack of cellulose presents the perfect backdrop to ask what genes affect curli production (Chapter 2).

E. coli that exist outside of the intestinal tracts of animals which can cause disease are called extraintestinal pathogenic *E. coli* (ExPEC). ExPEC that infect the urinary tract, such as the UTI89 *E. coli* isolate, are uropathogenic (UPEC) strains. Urinary tract infections (UTIs) are among the most common bacterial infections, representing 25% bacterial infections in women and over 8 million cases in the US per year(58, 59). Many of the UPEC strains originally come from the patient's own GI tract(60). ExPEC strains can also be found on food prep surfaces and lead to infection in consumers(36). ExPEC ability to persist outside of hosts in biofilm contribute to their ability to cause a second infection.

UTI89 *E. coli* forms robust biofilms that contain both curli and cellulose(61) and more closely models *E. coli* biofilm in host environments. UTI89 biofilms form distinct subpopulations of cells, one subpopulation attached to the structure of the matrix and one subpopulation that is unattached(19). The biofilm subpopulations can serve as a reservoir for pathogenic and antibiotic resistant bacteria(25, 62, 63). How these subpopulations develop and the role they play in cell protection remains unclear. UTI89 is the model used to look at biofilm subpopulations (Chapter 3) and regulation of matrix component production (Chapter 3 and 4).

Master Biofilm Regulator, CsgD. CsgD is a FixJ/LuxR/UhpA-type transcription factor that binds DNA using a helix-turn-helix motif(64). Expression of *csgD* is controlled by small RNAs, transcription factors, the sigma factor RpoS, and possibly c-di-GMP. Small RNAs *gcvB, mcaS, omrA, omrB, rprA,* and *rydC* inhibit *csgD* transcription. Low salt and low glucose levels trigger *csgD* expression in the presence of RpoS during stationary phase(65, 66). CsgD level and activity is also dependent on cellular levels of the second messenger c-di-GMP(67-69). Di-guanylate

cyclases (DGCs) contain GGDEF domains that dimerize to produce c-di-GMP, which can be broken down by phosphodiesterases (PDEs) containing EAL domains(70). So far DcgM and DcgN have been shown to affect CsgD activity(68, 71). The mechanism of how the c-di-GMP produced by these DGCs affect CsgD directly is unclear, but transcription factor MlrA which can interact with c-di-GMP is known to bind the *csgD* promoter(72, 73). CsgD promotes curli and cellulose to initiate biofilm formation while inhibiting flagella, causing cells to switch from a motile lifestyle to a sessile lifestyle(74, 75) (Fig. 1.1). While the CsgD regulon is small, CsgD is regulated by over 25 transcription factors in a complex and minimally characterized regulation system.

Components of the Extracellular Matrix. In *E. coli* the extracellular matrix of biofilm is comprised of the polysaccharide component, cellulose, and protein component, curli(61, 76). Cellulose is a linear chain of β-(1,4)-linked glucose monomers(77, 78). Cellulose has long been known to give rigidity to plant cell walls but was not discovered to be part of Enterobacteriaceae biofilm until 2001(77). Cellulose fibers have high tensile strength, surface area, and wettability making cellulose ideal for the flexible structure of biofilm(61, 79-81). In *E. coli* biofilm models specifically, cellulose is required for rugose (agar plate attached) biofilm wrinkling and pellicle (floating) biofilm(61, 78, 82). Cellulose synthesis is under the regulation of the master biofilm regulator, CsgD(61, 77). CsgD binds upstream of *dgcC* to activate transcription. DgcC is a di-guanylate cyclase and possesses the characteristic GGDEF domain required to produce the second messenger, c-di-GMP(83). The cellulose synthase complex BcsAB is activated by c-di-GMP disruption of the salt bridge that tethers a gating loop over the active site, allowing UDP-glucose to be linked together one monomer at a time(84, 85). C-di-GMP is a pooled resource, and some research has shown cellulose production independent of CsgD activation through alternate di-guanylate cyclases(68, 86). Additionally, my research has shown the importance of DgcN (previously YfiN) for cellulose production and CsgD levels under biofilm forming conditions (Chapter 4)(21, 87, 88).

The protein component of the biofilm matrix is curli, polymers of primarily CsgA subunits that have adopted an amyloid fold(66, 76, 89). Amyloids are β-sheet rich protein polymers that are highly resistant to sheer forces and denaturation(66, 76). In *E. coli* biofilms

curli contribute to matrix structure, aid in colony spreading, and contribute to pellicle biofilms(19, 66, 90). Curli production is under control of the master biofilm regulator, CsgD, which binds the intergenic region between diverging curli specific gene (*csg*) operons, *csgDEFG* and *csgBAC*. The *csgDEFG* operon encodes the master biofilm regulator, CsgD, and accessory proteins required for successful curli secretion. CsgG forms a nonameric curli secretion pore on the outer membrane of the cell and is capped on the periplasmic side by a nonameric CsgE(91-93). CsgF is secreted through the CsgG pore before forming a complex with CsgG outside of the cell to act as a binding site for CsgB(76, 94-96). The *csgBAC* operon encodes the major and minor subunits of the curli fibers, CsgA and CsgB respectively, as well as the protein chaperone CsgC(66, 97). Unfolded CsgA and CsgB are secreted into the periplasm, where CsgC prevents CsgA and CsgB from polymerizing within the cell(97). Unfolded CsgA and CsgB are secreted outside the cell through CsgG where CsgB folds and serves as an anchor and template for CsgA folding(98). CsgA subunits outside of the cell are a shared resource, with CsgA monomers contributing to curli on neighboring cells(99).

Identifying Cell Processes Which Effect Biofilm Formation. Biofilm formation is a global shift from free-swimming to sessile life in *E. coli*. The transition in lifestyle requires a minimally understood coordinated change at the transcript and protein level to turn off vegetative growth genes and turn on cell processes required for biofilm formation(42, 100, 101). Because of the interconnected nature of the change in regulation, large-scale screens and analyses are the best way to capture all the relevant changes in the cell.

In my research I utilized genetic screens and whole cell -omics based approaches to understand the global changes required for *E. coli* to transition from vegetative to biofilm growth. The Keio knockout library (102) is a collection of single gene deletions in the BW25113 laboratory *E. coli* strain. The BW25113 strain lacks cellulose, so by screening each knockout for a change in Congo Red binding, indicating a change in curli production, we were able to identify every gene in that strain that effected curli biogenesis (Chapter 2). *E. coli* strains such as UTI89 that produce curli and cellulose have added complexity to biofilm regulation and production. In addition to the regulation for curli and cellulose production, UTI89 biofilms organize cells in to

at least two distinct cell subpopulations: the Matrix and Washout(19). This process of developing subpopulations potentially requires a separate set of cellular processes and transcriptional regulators. To capture the differences between the Matrix and Washout subpopulations, the subpopulations were separated, and the RNA and proteins were isolated. Using RNAseq and Proteomics, the abundance of both transcripts and proteins was quantified relative to the subpopulation. By looking at differential expression comparing the two subpopulations, unique processes required for cell growth in the Matrix or Washout subpopulation can be identified (Chapter 3).

Conclusion. Biofilm protects bacterial communities and is ubiquitous in our environment. Biofilm allows for bacteria growth in harsh and normally unfavorable environments by forming a physical barrier between cells and the environment and creating a space the bacteria can tailor to specific growth requirements, such as oxygen levels. *E. coli* as a model system utilizes many strains and molecular tools to subtly manipulate biofilm to better understand the regulation affecting formation. The process of producing curli and cellulose are well characterized in the *E. coli* system, while the signals that control CsgD, the master biofilm regulator are still unclear. CsgD is an integration point for many signals that describe the conditions in cells, such as growth phase, osmotic or redox stress, and c-di-GMP levels. Through CsgD regulation, the timing of matrix component production can be highly tuned. Studying processes that affect this regulation could lead to potential treatments for biofilm-related infections or anti-biofilm target to be exploited.

Uncontrolled biofilm growth presents an urgent and mounting threat to human health. Cells within biofilms are protected from environmental stress and antibiotics, allowing pathogenic or persister bacteria to evade treatment. Understanding what processes are vital for survival in the non-matrix associated biofilm subpopulation may allow for target treatment of the non-matrix subpopulation.

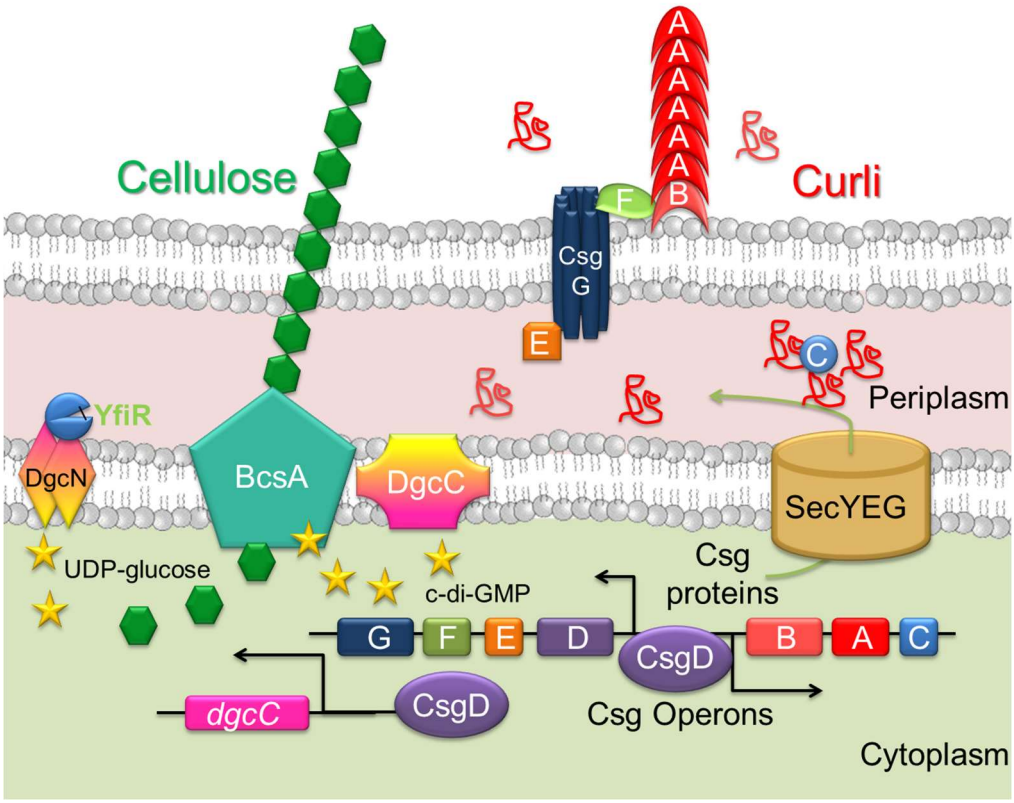

Fig. 1.1. Schematic of matrix component production. Master biofilm regulator, CsgD, promotes production of matrix components curli directly and cellulose indirectly. CsgD binds the intragenic region of the curli (*csg*) operons. Synthesized unfolded proteins pass through the SecY secretion system into the periplasm. CsgGEF form the extracellular curli secretion pore while CsgC chaperones CsgA and CsgB in unfolded form to prevent intracellular amyloid formation before delivery to the curli pore. After secretion, CsgB binds CsgF and adopts an amyloid fold. CsgA uses CsgB as a template and polymerizes into curli fibers. CsgD promotes *dgcC* expression, a diguanylate cyclase (Dgc) that stimulates the cellulose synthase BcsA to link monomers of UDP-glucose into cellulose. DgcN is required for basal expression of *csgD* and is inhibited by YfiR in response to cellular redox.

Chapter II

The Assembly of Curli Amyloids Fibers is Deeply Integrated into the Biology of *Escherichia coli*

Abstract

Curli amyloid fibers are the major protein component of the extracellular matrix produced by Enterobacteriaceae during biofilm formation. Curli are required for proper biofilm development and environmental persistence by *Escherichia coli*. Here, we present a complete and vetted genetic analysis of functional amyloid fiber biogenesis. The Keio collection of single gene deletions was screened on Congo red indicator plates to identify *E. coli* mutants that had defective amyloid production. We discovered that more than three hundred gene products modulated curli production. These genes were involved in fundamental cellular processes such as regulation, environmental sensing, respiration, metabolism, cell envelope biogenesis, transport, and protein turnover. The alternative sigma factors, σS and σE, had opposing roles in curli production. Mutations that induced the σE or Cpx stress response systems had reduced curli production, while mutant strains with increased σS levels had increased curli production. Mutations in metabolic pathways, including gluconeogenesis and the biosynthesis of lipopolysaccharide (LPS), produced less curli. Regulation of the master biofilm regulator, CsgD, was diverse, and the screen revealed several proteins and small RNAs (sRNA) that regulate *csgD* messenger RNA (mRNA) levels. Using previously published studies, we found minimal overlap between the genes affecting curli biogenesis and genes known to impact swimming or swarming motility, underlying the distinction between motile and sessile lifestyles. Collectively, the diversity and number of elements required suggest curli production is part of a highly regulated and complex developmental pathway in *E. coli.*

The contents of this chapter were published in *Biomolecules* by Daniel R. Smith*, Janet E. Price* Peter E. Burby, Luz P. Blanco, Justin Chamberlain, and Matthew R. Chapman. D.R.S. and M.R.C. conceived and designed the experiments; D.R.S performed most of the experiments with J.E.P., P.E.B., L.P.B. and J.C. helping with the RT PCR, CsgD western blots, and the initial screening of the Keio collection on Congo Red plates. The data was analyzed by D.R.S., J.E.P., P.E.B. and M.R.C. D.R.S. wrote the manuscript with help from J.E.P., P.E.B. and M.R.C.

Introduction

Curli are thin aggregative fimbriae produced by many Enterobacteriaceae including *Escherichia coli* and *Salmonella typhimurium*(103, 104). As the major protein component of the extracellular matrix, curli are associated with biofilm development(105). Furthermore, curliated bacteria adhere to and colonize a variety of surfaces(57, 106-109) and are resistant to damage from predation, desiccation, oxidative stress, and other antimicrobial agents(18, 19, 106, 107, 110). Curli fibers have also been implicated in pathogenesis and aid in host cell adhesion, invasion, and immune system activation(111-113).

Curli fibers are the product of a dedicated and highly regulated assembly system encoded by curli specific genes (*csg*), which are arranged on two divergent operons *csgDEFG* and *csgBAC*(66, 114, 115). Found primarily in the genomes of Enterobacteriaceae, *csg* genes are also present in other Gammaproteobacteria including members of the Pseudomonadaceae, Shewanellaceae, and Vibrionaceae families, as well as the more distantly related Bradyrhizobiaceae, Burkholderiaceae, and Flavobacteriaceae families(116). CsgD is the master biofilm regulator, and is required for transcription of the *csgBAC* operon(114, 117). At the cell surface, the major curli fiber subunit CsgA is nucleated into an extracellular amyloid fiber by the minor fiber subunit CsgB(98, 103, 118, 119). Secretion of both curli fiber subunits requires the lipoprotein CsgG, which forms a pore within the outer membrane(91, 92, 103, 120, 121). CsgE acts as the cap for CsgG, blocking the unfolded CsgA from returning into the periplasm(93). CsgF has been shown to interact with CsgG and may aid in its function(92, 121, 122), as well as keeping CsgB associated with the bacterial outer membrane(94, 98). CsgC is dispensable for curli formation; however, it may influence curli fiber morphology, and it potently discourages CsgA amyloid formation within the cell(97, 114, 123, 124). As the first bacterial protein identified as an amyloid(103), curli are part of a growing class of functional amyloid proteins that have evolved to fulfill physiological roles(125).

Regulation of *csgDEFG* operon is complex, and involves several proteins(66). Transcription of the *csgDEFG* operon is under the control of RpoS (σS), Crl, MlrA, H-NS, IHF, and a number of bacterial two component systems(66, 126) (see Table 2.8). The intervening region between the curli operons is the fifth largest divergent operon in *E. coli*, yet previous screens to

find additional accessory factors and regulators have identified only a handful of genes including *nagA*, *ompR*, *dksA*, and *rssB*(114, 127, 128). The current cohort of regulators does not sufficiently account for the diverse conditions that induce *E. coli* expression of curli and other biofilm components(63, 129, 130). Therefore, we performed a comprehensive screen for genes involved in curli production using the Keio collection(102). The Keio collection is a near complete set of single gene knockouts in K-12 *E. coli*. By growing the collection on plates containing the amyloid specific dye Congo red (CR), we identified more than 300 strains that had changes in curli production. These strains lack genes involved in a variety of cellular processes including regulation, environmental sensing, respiration, metabolism, cell envelope biogenesis, transport, and protein turnover. Many of these genes are known to affect RpoS (σS) levels or induce the Cpx or RpoE (σE) stress responses. Induction of either the Cpx or σE stress response system resulted in less curli production, while stimulation of σS levels increased curli expression. Few of the genes identified here are involved in motility, underlying the fact that motility and biofilm formation are distinct microbial behaviors. We propose that curli fiber formation is part of a unique lifestyle in *E. coli* that is tightly linked to key metabolic pathways, including nucleotide synthesis, cell envelope maintenance, and the citric acid cycle.

Results and Discussion

To better understand curli production and regulation, we screened the Keio collection for mutants with altered curli production using Congo red (CR) indicator plates (Figure 2.1A,B). Curliated colonies turn red when grown on CR plates, while strains that do not produce curli remain white(131). The Keio collection consists of 3985 nonessential gene mutants comprising more than 90% of the 4,390 open reading frames of *E. coli* K-12 (named wild type, WT, in the remaining chapter)(102). Following growth in conditions that favor curli production (26 °C for 48 h), strains with changes in CR phenotypes were isolated and scored according to their color, which varied from the white color of *csgA* to the darker red of *cpxR* (Figure 2.1B). Genes known to affect curli production, such as curli specific genes (*csgABEFG*) and previously described transcription factors (*cpxR* and *ompF*) were identified, validating our screening technique.

Strains such as *thyA*, glnA, *ubiE* and *ubiF*, did not grow well under the conditions tested and were not further analyzed (see *ubiF* Figure 2.1A and Table 2.5 strains marked with ‘). Strains with an altered phenotype were regrown on CR indicator plates for verification and scored numerically according to color from lightest to darkest (Figure 2.1B and Table 2.5). We isolated 332 Keio mutants with reproducible CR phenotypes. Of these, 64 strains had two or more phenotypes upon isolation of single colonies. Each genotype from these gene deletion strains was verified by polymerase chain reaction (PCR), revealing that most strains had the correct Kan^r insert for each phenotype (Table 2.6). We excluded the 64 mixed phenotype strains from further study as they likely have second site suppressors. However, we included the strains *cmk*, *fabF*, *mdoG*, *pgm*, *trpD*, *trpE*, *yiaK*, and *ymgE* because both of their CR phenotypes were defective (lighter red than WT cells). The resulting 276 mutants were 14.3% white, 16.5% light pink, 27.2% pink, 18.6% light red, and 23.3% dark red when grown on CR indicator plates (Figure 2.1C). To better quantify curli production in the identified mutants, CsgG and CsgA protein levels were measured in whole cell extracts by Western blotting (sample of color groups Figure 2.1D and Table 2.5). Protein levels were generally consistent with CR phenotypes (Figure 2.1D). In some light pink mutants, the curli secretion protein CsgG(91, 92, 120) was present; however, no CsgA was detectable (Table 2.5).

We divided the gene mutations with altered CR binding into clusters of orthologous groups (COGs)(102, 132-135) and used Echobase(136) to assign a cellular location to each protein product (Table 2.1 and Table 2.7, Figure 2.2). Collectively, the genes identified in the CR screen are predicted to encode proteins that are primarily localized to the cytoplasm. Genes in the transcription COG (K) are likely to have collateral effects as regulators often control multiple gene products, such as the case with cAMP receptor protein (CRP) which has been shown to have 70 unique targets(137). Because of this, of the 43 transcription related genes, only those with previously reported relationships or verified binding sites on the *csg* intragenic region were studied. The CR phenotypes of the Keio collection strains were mostly consistent with the literature: exceptions were found in cyclic-di-guanosine monophosphate (c-di-GMP) and regulatory proteins, some of which are known to have strain-dependent effects on curli

production(89) (Table 2.8). In the following sections, we explore genes from several different functional groups and discuss their likely roles in curli production.

Cell Envelope. Curli assembly occurs at the cell surface, therefore, it is not surprising that genes involved in cell envelope and outer membrane biogenesis have defects in curli assembly (COG family group M)(138). The cell envelope includes the inner membrane, the periplasm, the outer membrane, and extracellular structures including fimbriae and extracellular polysaccharides (EPS)(139). Multiple lipopolysaccharide (LPS) biosynthesis gene mutants, especially those involved in assembling the inner core region of LPS, were defective for curli production (Figure 3A,B). These genes encode hexose and heptose transferases, enzymes that produce the inner core sugar building block adenosine diphosphate (ADP)-l-glycero-d-manno-heptose, the LPS kinase *waaP*, and the transcriptional antiterminator for the *waaQGPSBIJYZK* operon *waaH*(140-143). Western blot analysis showed that many LPS mutants with CR defects had corresponding decreases in CsgA and CsgG levels (Figure 2.3A,C compare WT to *lpcA*, *gmhB*, and *waa* mutants). Mutants in the inner core sugar transferases *waaC*, *waaF*, *waaG*, and the heptose biosynthesis genes *lpcA* and *waaE* were the most defective in CR binding and these strains had lower CsgG levels compared to WT and no CsgA was detected (Figure 2.3C). Previous studies have implicated the LPS biosynthesis genes *waaG*, *ddhC* (*rfbH*), and *lpxM* (*msbB*) as being important for curli production(144, 145). In *Salmonella enterica*, both *waaG* and *ddhC* strains produce less curli than WT(144). Similarly, the *waaG* strain in K-12 *E. coli* has reduced curli production(77, 146). We also looked at other lipid A modifying enzymes to see if they affected curli production. The *lpxL*, *lpxM* (*msbB*), *lpxP*, *pagP*, and *arnT* mutant strains all produced curli at WT levels suggesting the modification state of the lipid A core does not necessarily affect curli production in K-12 strains of *E. coli* (Figure 2.9C, left plate).

Analysis of mutations in other LPS synthesis genes revealed that curli production is likely affected by genes that synthesize or transfer the ADP-l-glycero-d-manno-heptose to Lipid A-KDOII(141) (Figure 2.3A,B). Mutations in *waaD* lead to an accumulation of heptose free LPS(147), and *waaD* mutants had decreased curli production compared to WT (Figure 2.3C

and Figure 2.4A). Mutations in *gmhB* also accumulate heptose-free LPS and, like the *waaD* mutants, the *gmhB* strain had decreased curli production (Figure 2.3A)(148). The composition of the LPS in the *waaD* and *gmhB* strains may explain their intermediate curli phenotype. Unlike the *waaG* mutant strain and other inner core mutants, both *waaD* and *gmhB* strains have a small amount of glucose I and further modified LPS(148, 149) (Figure 2.4A). Accordingly, a mutation in *waaI*, which has fully glucose I modified LPS(141), is unaffected for curli production. Similarly, *waaP*, which lacks phosphorylation of heptose I(141), had less curli production and partially substituted LPS (Figure 2.4A). Thus, it appears that even a small amount of glucose I modified LPS is capable of supporting curli subunit secretion and assembly into an amyloid fiber.

Several LPS mutant strains had a notably dry and crumbly texture when dragged across the plate (Figure 2.8A)(115, 142, 150), including *galU* and *waaG* and to a lesser degree *waaF*. GalU is needed for growth on galactose and trehalose and is required for the production of uridine diphosphate (UDP)-d-glucose, trehalose, the LPS outer core, colonic acid, and periplasmic glucans(151-154). Since WaaG adds UDP-d-glucose to the inner core of LPS, the *galU* and *waaG* mutants should be functionally similar. Both strains displayed a light pink phenotype and had similarly low levels of CsgG by Western blotting. These mutants were also visibly drier than WT, crumbled when scraped from plates(150), autoagglutinated when resuspended in PBS(142), and displayed identical LPS profiles on silver stained polyacrylamide gel electrophoresis (PAGE) gels(154) (Table 2.5, Figure 2.4A, Figure 2.8 compare *galU* and *waaG*). Because of the dry colony phenotype of the *waaG* and *galU* strains (Figure 2.8A), we tested the cell hydrophobicity of the inner core sugar transferase mutants using the bacteria adhesion to hydrocarbons (BATH) method(155). Mutant strains that had less developed LPS cores were more hydrophilic as measured using the BATH method (compare *waaC*,*F*,*G* in Figure 2.8B and Figure 2.4A). As expected, both *galU* and *waaG* had similar cell hydrophobicity profiles. Because of the significant changes made to the membrane in the *galU* and *waaG* mutants, we looked at the integrity of the CsgG protein present within the membrane.

Because CsgG is required for the stability and secretion of CsgA and CsgB(91, 92, 120), and several of the inner core LPS mutants had decreased levels of CsgG protein (Figure 2.4A), we asked if ectopic overexpression of CsgG could rescue the curli assembly defect in the inner core LPS mutants. Expression of *csgG* from plasmid pMC1 increased the amount of CsgG protein in the *waaC*, *waaF* and *waaG* strains, but was unable to restore CsgA protein levels or curli production (Figure 2.4F). Interestingly, the transcript levels of *csgD*, *csgA*, and *rpoS* were near WT levels in the *waaF* strain (Figure 2.10). Taken together, these data suggested that the CsgG present in inner core LPS mutants was not able to properly fold or function in the outer membrane. To test this idea, we supplemented CR indicator plates with divalent cations. Divalent cations interact with LPS molecules in the outer membrane (OM)(141, 156), and their presence can stabilize outer membrane porins(157, 158). When added to CR indicator plates, the divalents Mn^{2+}, Mg^{2+}, and Zn^{2+} all increased CsgG levels and partially complemented CsgA secretion and curli production in inner core LPS mutants (Figure 2.4B–D). Addition of Mn^{2+} near inner core mutants also resulted in increased CR binding (Figure 2.4E). Many LPS mutants displayed an aberrant CR phenotype: a rim of darker stained cells near the edge of the plate (Figure 2.3A and Figure 2.8A) where there is less competition for limiting divalent cations. The mechanism of complementation by addition of divalent cations is unclear. The divalent cations may be interacting with phosporhyl moieties to reshape the OM and decrease the higher phospholipid content of the OM outer leaflet in inner core LPS mutants(156). Alternatively, they may stabilize the interactions between LPS and CsgG or a partner OM protein; however, addition of divalent cations did not alter the heat modified mobility of CsgG from *waaF* relative to WT (Figure 2.4G), suggesting divalent cation rescue of CsgA levels is not due to direct interaction with CsgG.

Other components of the cell envelope, including the enteric common antigen (ECA) and the periplasmic glucans, were found to affect curli production (Figure 2.11). Mutants in ECA biosynthesis with altered curli production include *rffA*, *rffC*, *rffT*, *wzxE*, and *rfe* (Figure 2.114B), which are involved in synthesis or addition of thymidine diphosphate 4N-acetyl-α-d-fucosamine (TDP-Fuc4NAc) to lipid II (Figure 2.11A)(159) and have increased DegP levels via σE and Cpx induction(160). These results suggest ECA was not required for curli production, as only

mutants accumulating lipids II and III were curli deficient. Conversely, the *rfe* strain, which accumulates undecaprenyl-P, produces more curli than WT cells (Figure 2.11B). Mutants in *rfe* suppress the activation of *degP* in the *rffA*, *rffH*, and *rffT* strains suggesting undecaprenyl-P and lipid II accumulation have opposing roles in envelope stress responses and curli production(160). The opposing curli phenotypes within ECA mutants are consistent with previous studies that demonstrated that increased σE activity has a negative effect on curli production(161). ECA mutants that induce the σE or Cpx stress response make less curli than WT, while strains with lower induction produce more curli (Figure 2.11B). Similarly, mutations in *tolA* and pal have higher σE levels(162) and were defective for curli (Table 2.5).

The *rseA* strain, which lacks the anti-sigma factor of σE(163-165), produced less curli and was light pink on CR indicator plates (Figure 2.11C). Furthermore, ectopic expression of the anti-sigma factor *rseA* in WT resulted in increased curli production (Figure 2.11D). The σE stress response may function to limit the production of extracellular fibers during outer membrane stress. However, the *csg* genes lack the σE consensus sequence and overproduction of σE did not significantly affect their transcript levels(166, 167).

Defects in LPS biosynthesis also result in σE induction(168, 169). Inner core LPS mutants such as *waaC*, *waaD*, and *galU* have drastically altered outer membrane protein profiles(142, 150), increased σE-dependent transcription(170-172), and produce little or no curli (Figure 2.3C). The Cpx two-component system, which also negatively regulates curli specific genes(173, 174), is induced in many of these LPS mutants(160, 172). Furthermore, Zn^{2+} rescued curli production in some inner core LPS mutants (Figure 2.4B,C), and has been shown to induce σE and σE-regulated genes(175, 176). The expression of *rseA* or *rseAB* in the *waaC*, *waaF*, or *waaG* mutants(165, 177) could not complement curli production. Thus, while σE and Cpx have a role in modulating curli production, it is more likely that inner core mutants produce less curli due to a secretion defect in CsgG.

Carbohydrate Metabolism, Energy Production, and Gluconeogenesis. Strains with mutations in several genes involved in global carbohydrate flux and sugar import were found to be defective for curli production: *cyaA*, *crp*, *fruR* (*cra*), *ptsH*, *ptsI*, *aceE*, *fbp*, *gnd*, *tktA*, *tpiA* (Table 2.5). The

metabolic flux changes of the Keio *cyaA*, *crp*, and *fruR* strains have been examined under different growth conditions and shown to produce less phosphoenolpyruvate (PEP) from oxaloacetate in glucose limiting conditions(178, 179). PEP is used by the phosphotransferase system (PTS) to transport and phosphorylate many different sugars. FruR increases PEP production from pyruvate through a combination of *pykF* repression and *ppsA* activation(180). The cAMP–CRP complex also activates *ptsHI-crr*(181), and *cyaA* and *crp* mutants, both of which are defective in cAMP–CRP mediated gene activation, and have low levels of glucose uptake due to a PTS defect(182). Combined with the curli phenotype for the PTS genes, *ptsH* (Enzyme I) and *ptsI* (HPr), these results suggest that a defect in the PTS system leads to lower curli production. However, many of these gene products have global effects on gene transcription. The cAMP–CRP complex regulates multiple genes including direct activation of *csgDEFG*(181, 183).

Enzymes for central metabolism, energy production, and their coenzymes also play an important role in curli production. Citric acid cycle (TCA) mutants with reduced curli production include genes encoding enzymes for the complete conversion of α-ketoglutarate to fumarate: *sucA,B,C,D* and *sdhA,B* (Tables 2.5 and 2.9). The restriction of curli defective mutants to the upper TCA cycle and the curli defects in *fruR*, *fbp*, *tpiA*, and *sfcA* (*maeA*) indicate that gluconeogenesis is required for curli production. FruR tightly regulates gluconeogenesis by increasing gluconeogenic enzymes and decreasing glycolytic enzymes to prevent a futile cycle(184). In *S. typhimurium*, a curli producing WT strain had higher levels of gluconeogenic end products including glucose, glycogen, and trehalose as well as lower levels of succinate, fumarate, malate, and polyamines relative to a *csgD* strain (Table 2.9)(185). Gluconeogenic-specific genes including *pckA*, *maeB*, *ppsA*, and *fbp* were also upregulated in the WT strain, and a *ppsA pckA* double mutant in S. typhimurium was defective for curli and glycogen production(185). Thus, gluconeognesis appears to not only be coregulated with but also required for curli production.

Gluconeogenic metabolism is important for pathogenesis in uropathogenic *E. coli* (UPEC)(186). Like urine, the media used to express curli including YESCA and colonization factor antigen (CFA) are mostly composed of amino acids and small peptides. When used as a

carbon source, many amino acids are broken down into pyruvate or compounds of the upper TCA cycle such as α-ketoglutarate, succinate, and formate. Glucose produced by gluconeogenesis is used in LPS, glycogen, trehalose, osmoregulated periplasmic glucans (OPG), or various EPS including cellulose, ECA, and colonic acid. Mutants in most of the pathways utilizing glucose were not defective for curli production. Interestingly, outer core LPS biosynthesis requires UDP-d-glucose which is converted from glucose-6P through the action of Pgm and GalU (Table 2.5) and added to the heptose II of inner LPS core by WaaG(141). The *waaG*, *pgm*, and *galU* strains were all defective for curli production, suggesting gluconeogenic mutants may lack curli due to glucose I defective LPS. Mutants that lack glucose-I LPS modifications can be partially suppressed by the addition of divalent ions (Figure 2.4B). Indeed, the addition of divalent ions to *sdhA* and *sdhB* resulted in increased CR binding, suggesting that the lack of the glucose-I LPS modification is at least partially responsible for the curli defect in gluconeogenesis mutants (Figure 2.11E).

Anaerobic respiration is vital for *E. coli* to persist as a pathogen(52). *oprF* mutants in *Pseudomonas aeruginosa* have impaired anaerobic respiration and as a result, have significantly reduced anaerobic biofilm production(187). Several terminal dehydrogenase components (*sdhA–D*) produced altered CR binding phenotypes (Table 2.5), where loss of the catalytic domains, *sdhAB*, lead to lower CsgA levels and the loss of stabilizing domains, *sdhCD*, lead to higher CsgA levels. Additionally, *narQ*, the primary sensor of the presence of nitrate, has been shown to alter biofilm formation and motility(188, 189), and in our study yielded decreased CsgA and CsgD levels (Table 2.5). Taken together, these respiration mutants point to the involvement of the electron transport chain in curli production.

Previously, our lab investigated the effect of *nagA* mutants on curli production(127). In the Keio collection, we found *nagA*, *nagC*, and *nagK* mutants to be defective for curli production (Table 2.5). For the *nagA* strain, the decrease in curli production was similar to other K-12 strains, and less than seen in the C600 strain(127). Intriguingly, we found *yhbJ* and *pcnB* strains were dark red on CR plates and produced significantly more curli than the WT strain. YhbJ has recently been shown to destabilize the RNA *glmZ*, which increases the *glmS* transcript stability(190, 191). *glmZ* also regulates curli production independent of

CsgD protein levels(192). The *glmS* transcript can be polyadenylated by PcnB and rapidly degraded(193). GlmS transfers ammonia to fructose-6-P to form GlcN-6-P, which is later converted to UDP-GlcNac(152). Fructose-6-P is the product of NagA degradation of GlcNac-6-P(127), suggesting that the curli defect in a *nagA* strain may also be due to lower amounts of fructose-6-P. The resulting lower UDP-GlcNac levels, which are needed for lipid A, ECA, and peptidoglycan biosynthesis, may lead to a compromised cell envelope and subsequently to lower curli expression. The curli defect of the Keio *glmM* mutant would seem to confirm this; however, *glmM* has been reported to be an essential gene(194), and therefore its presence in the Keio collection suggests that the *glmM* strain used in our study has acquired suppressor mutations (Table 2.5). We also found decreased curli in *nanK* and *nanE* (Table 2.5). Both are involved in sialic acid biosynthesis, which ultimately is converted to GlcNAc-6P(152) supporting the role of fructose-6-P in minimal cell envelope development for curli production.

Multiple Regulatory Networks Control Curli Gene Expression. At 754 bases, the non-coding region between *csgD* and *csgB* is the fifth largest region between divergent operons in *E. coli* K-12 and the thirteenth largest intergenic region overall (Table 2.10 and Figure 2.12). The intergenic region has strong inherent curvature and an AT content of 65.5%(195), which aids binding of nucleoid proteins such as IHF and H-NS which can induce sharp bending in DNA(126). At least twelve proteins and five small RNAs have been shown to bind within the intergenic region between *csgD* and *csgB*(75, 126, 152, 196) (Figure 2.12). Previously, most genes found affecting curli production did so through transcriptional changes at one or both curli operons(66) or by modifying cyclic-di-GMP metabolism(197) (Table 2.8). We identified many additional regulatory elements that also affect curli production. In fact, more than a fifth of the genes hit in the CR screen encode either signal transduction proteins or transcription factors (Table 2.1). The high number of regulatory proteins and the large intergenic region between csg operons, are consistent with curli biogenesis being an intricately regulated process. Indeed, 26 of the 32 mapped protein binding sites are within 200 bp of the transcription start of *csgDEFG* operon, the highest such density in *E. coli* (Figure 2.12 and Table 2.10).

Several mutants identified in our screen have been shown to directly or indirectly regulate σS levels or function,

including *crp, clpP, clpX, dksA, dnaK, galU, hns, hfq, nlpD, nuoG, pgm,* and *mdoA* (*mdoGH*)(198-201). Similar to an *rpoS* mutant, an *nlpD* mutant completely lacks curli, probably due to loss of the major *rpoS* promoter within *nlpD*(202). Since DksA affects ppGpp-dependent induction of σS(203), we tested whether altering ppGpp production affected curli production. An MG1655 *relA spoT* double mutant, which is defective in ppGpp synthesis(204), was light pink on CR plates and produced almost no curli proteins (Figure 2.13A). When the same mutants were made in the BW25113 strain, the CR binding phenotype was more severe and no CsgD or curli were detected by western blotting (Figure 2.13B). In addition to *rpoS*, we found that deletion of the sigma factor genes *rpoN* and *rpoZ* decreased curli production (Table 2.5), underscoring the complexity of curli regulation by different sigma factors.

Several genes involved in quorum sensing and virulence were found to affect curli production including *qseB, qseC, aaeR, lsrF, ygiU* (*mqsR*)*, sdiA,* and *flgM*. The qseC strain produced more curli than WT; however, *qseB* had mostly light pink colonies with a few dark red suppressor colonies (Tables 2.5 and 2.8). Previously, QseC but not QseB was found to be important for curli, type I pili, and flagella production in uropathogenic *E. coli* (205). The Keio *flgM* strain overproduced flagella and made less curli consistent with the antagonistic relationship between these two extracellular appendages(75, 206). Similarly, the *hdfR* strain, which lacks a repressor of the *flhCD* operon, was defective for curli. However, *sdiA*, which also overproduces flagella(207), had higher levels of curli production (Table 2.5).

A mutation in the Na^+:H antiporter encoding gene nhaA resulted in cells that stained light pink on CR indicator plates, and had much lower levels of CsgA and CsgG (Figure 2.5A,B,D and Table 2.5). NhaA is one of three sodium ion antiporters which uses the proton electrochemical gradient to expel sodium ions(152), and had been loosely linked to amyloid production in *Shewanella*(208). The *nhaA* mutant was more motile than WT (Figure 2.5C), had more FliC protein when measured by western blot (Figure 2.5B), and more flagella than wild type when examined by transmission electron microscopy (TEM) (Figure 2.5D). When bound to Na^+, NhaR activates *nhaA* and other genes including *pgaABCD* and *osmC*(152). Since high levels

of intracellular Na^+ might result in a constitutively active NhaR, we made a *nhaAR* deletion, which did produce a small amount of curli (Figure 2.5D).

Curli fibers are maximally produced at room temperature in low salt conditions(117). High salt and osmolarity typically repress *csg* transcription through the OmpR/EnvZ and Cpx systems(174), which respond to high osmolarity in the periplasm. However, YESCA is a low salt medium able to support curli production in *E. coli*. High Na^+ also inhibits the proper assembly of FtsZ *in vitro*(209). When we examined *nhaA* and *nhaAR*, we found many filamentous cells (Figure 2.5D). Similary, a *kdpD* mutant displayed cell division defects and had reduced curli production (Figure 2.5B,D). KdpD regulates the influx of potassium, which promotes FtsZ assembly(152). Because high levels of CpxR-P results in aberrant cell division(210), we examined the levels of Cpx and σE regulated genes in *nhaA* and *nhaAR*. Double deletions of *nhaA cpxR* and *nhaAR cpxR* both produced more curli than *nhaA* and *nhaAR* (Figure 2.5F); however, over expression of *rseA* or *rseAB* resulted in lower curli production (Figure 2.5E). Collectively, these results suggest the high intracellular sodium in *nhaA* strains is inhibiting cell division and results in Cpx induction which decreases curli production.

The master biofilm regulator, CsgD, has been shown to affect the transcription of genes outside the curli operon, including those promoting biofilm production, gluconeogenic metabolism, and peptide import (see Table 2.9). CsgD also plays an important role in decreasing flagella rotation and production, promoting the switch from single planktonic growth to community behavior, through the activity of AdrA, ci-di-GMP, and σS as well as direct repression of the *fliE* and *fliFGHIJK* operons(75, 206). Here, *flgM, flhC, fliI, fliG,* and *fliT* had altered curli production (Tables 2.5 and 2.8). To further explore the intersection of flagella and curli we compared the results from our screen on CR indicator plates with other screens involving the Keio collection. Inoue *et al*.(211) screened the Keio collection for defects in swarming motility using Eiken Agar and subsequently checked the swarming mutants for reduced swimming motility(211, 212). Using GeneVenn(213), motility genes identified by Inoue *et al*. were compared to the genes identified in our screen (see Figure 2.6). Very few genes were found to overlap, especially between swimming motility and curli production. Half the genes that affect both swimming motility and curli encode for either adenosine triphosphate

(ATP) synthase or LPS biosynthesis genes (Figure 2.9). A second study looked for biofilm defective mutants in the Keio collection using crystal violet and 96-well plates(214). The biofilm mutants were subsequently tested for flagella, type I pili, and curli production(215). For curli production, growth was for three days on CFA amended with CR but not Coomassie brilliant blue. Comparison of flagella, curli, and type I pili genes also identified little overlap between flagella and curli associated genes (Figure 2.6). However, fewer curli genes were identified, perhaps due to the use of LB (Luria-Bertani) media in the initial biofilm screen(215). LB media has relatively high salt concentration, which inhibits curli production(117). Additionally, the CR phenotypes presented here are different for several strains listed in the LB screen; for example, several inner core LPS mutants are listed as WT for CR binding in their study(215). Consequently, we tested our strains using similar conditions and found that several of the phenotypic differences were due to media, growth, or staining differences (Compare CR plates in Figure 2.9, Table 2.11).

CsgD Transcript and Protein Levels Are Altered in Several Strains with CR Phenotypes

CsgD is considered the "master" biofilm transcription factor(117, 216). We selected a total of 38 mutant strains, sampling each CR phenotype and representing each COG, to further investigate the regulation of *csgD* at both transcript and protein level. *csgD* transcript levels were measured in all 38 strains using quantitative real time polymerase chain reaction (RT-qPCR) (Table 2.2 and Table 2.12) and CsgD protein levels were measured by Western blot analysis (Table 2.12 and representative blot Figure 2.7). Twenty-one of the 38 strains had *csgD* transcript levels that were significantly different from WT (Table 2.3). There was a correlation of CR phenotypes with *csgD* transcript and CsgD protein levels. For example, of twelve mutants tested that had increased CR binding, eight had increased levels of *csgD* transcripts and ten had increased levels of CspD protein (Table 2.2 and Table 2.12). Mutants *mdoC*, *perR*, and *cusB*, which presented increased *csgD* transcripts, did not have a detectable change in CsgD protein levels while *truB* and *qseC* exhibited no change in *csgD* transcripts to account for the increase of CsgD levels (Table 2.2 and Table 2.12). Of 19 mutants that were white, light pink, or pink on CR plates, 57% of them also had significantly decreased *csgD* transcript levels (Table 2.2) and all but *nagA, dksA, aaeR, glvG, cmr,*

and *php* had decreased CgsD levels consistent with their CR coloring and qPCR data (Table 2.12). There were also notable cases where the *csgD* transcript or protein levels did not predictably correlate with CR binding.

Two mutants that were pink on CR plates, *nagA* and *dksA*, had significantly increased *csgD* transcript levels (Table 2.2). However, it appears that the 16s ribosomal RNA (rRNA) levels were changed in these mutants and when we normalized by total RNA, the *csgD* transcript levels were similar to WT (Table 2.4). It is also worth noting that a threefold increase in *csgD* transcripts was observed in *cysB*, but CsgD protein levels were half of WT, whereas *fes* was observed to have *csgD* transcript levels nearly identical to wild-type with approximately half the levels of CsgD protein (Table 2.12).

The *csgD* transcript data presented here agree with some previously published findings. For instance, mutants in pyrimidine synthesis, *pyrC*, were shown to have decreased *csgD* transcripts(217) and we observed similar decreases in *csgD* expression in a *purD* mutant (Table 2.2). It is interesting to speculate that these two mutants act through the same mechanism, but more work is needed to elucidate how *pyrC* and *purD* contribute to curli biogenesis. *Hfq*, a chaperone protein responsible for RNA stability, is required for *csgD* expression in *S. enterica*(218), and we confirmed that this is true in *E. coli* (Table 2.2). Additionally, RcsB represses the *flhDC* operon(219), induces expression of the small RNA (sRNA) *rprA*(220). In turn, the sRNA *rprA* can reduce *csgD* transcription and CsgD protein levels(220). We observed that an *rcsB* mutant strain had increased *csgD* transcripts and CsgD protein levels (2.12). Taken together, these data suggest that the increased CR binding observed in *rcsB* mutants is likely the result of lower RprA levels. Two other sRNAs, McaS and GcvB, have also been shown to target *csgD* transcripts(221). McaS has been found to interact with Hfq implicating additional levels of sRNA control on *csgD*(222).

The CR screen also revealed possible post-translational control of CsgD (Table 2.12). For example, *hdfR, mltA*, and *fabH* mutant strains had normal *csgD* transcripts, but decreased CsgD protein levels, suggesting that these genes are required for the proper translation of *csgD* or CsgD protein stability (Figure 2.10 and 2.5). Consistent with this, *hdfR* and *mltA* have been shown to interact with the *csgD* messenger RNA (mRNA)(223). The FabH protein is an initiator

of fatty acid synthesis capable of conjugating acetyl-CoA to acyl-carrier protein (ACP), and lack of *fabH* or overexpression leads to decreased fatty acid chain length and abundance(224-226). The mechanism behind how FabH changes CsgD protein levels warrants further investigation. An intriguing result from the screen was that there were multiple mutants, *ddpD*, *glvG*, and *php*, which had altered CR binding phenotypes, yet normal *csgD* transcript and CsgD protein levels (2.12). For example, the *php* mutant was white on CR plates, had undetectable levels of CsgA and CsgG, but had WT levels of CsgD protein (Tables 2.5 and 2.12). Taken together, we suggest that CsgD is inactive in these mutant strains, or that CsgBA cannot be produced or appropriately secreted because CsgG is not present. In any case, it is clear that *php* is essential for curli biogenesis and it acts downstream of CsgD transcription and translation.

Materials and Methods

Bacterial Strains and Growth Conditions. The Keio collection(102) was made by the Datsenko and Wanner method in *E. coli* strain BW25113(227). The collection was shipped to us after being grown on LB. Freezer stocks made with LB broth (10 g tryptone, 5 g yeast extract, 10 g NaCl) with 20% glycerol were maintained in 96-well microplates at −80 °C. Additional strains and plasmids used are listed in Table 2.13. A complete curli deletion strain was made in BW25113 so that both the *csgDEFG* and *csgBAC* operons were deleted using *csgG* and *csgC* terminal primers(102) the method of Datsenko and Wanner, 2000(227). Typically, bacteria were grown for 48 h at 26 °C on YESCA plates (1 g yeast extract, 10 g casamino acids, and 20 g agar per liter). Congo red indicator plates are YESCA media amended with 50 μg/mL CR and 10 μg/mL Coomassie Brilliant Blue (CBB). CFA agar (1.5 g yeast extract, 10 g Casamino Acids, and 20 g agar per liter containing 0.4 mM $MgSO_4$ and 0.04 mM $MnCl_2$ buffered to pH 7.4) with 100 μg/mL CR or 50 μg/mL CR and 10 μg/mL CBB were sometimes used. For the experiments looking at the effect of divalent cations, salts were added to CR indicator media prior to autoclaving. To remove residual salts in these experiments, strains were grown to saturation in LB overnight, washed and diluted five-fold in YESCA, and spotted onto the appropriate plates. LPS mutants were always surrounded by other strains due

to differences in CR binding near the colony edge. Antibiotics were added when appropriate in the following final concentrations: 25 μg/mL kanamycin; 25 μg/mL chloramphenicol; or 100 μg/mL ampicillin.

To screen the Keio collection, we used sterile toothpicks and plate bolt replicators to copy the collection onto CR indicator plates amended with 25 μg/mL kanamycin. Following growth for 48 h at 26 °C, the strains were scored for color as indicated. If a colony was pink or darker red than the surrounding strains it was restreaked for single colonies. The CR phenotype of each strain was verified by comparison to BW25113. To emphasize CR phenotypes in the pictures captured, the levels were uniformly adjusted by setting the gray point to a clear spot on the red agar in Adobe Photoshop.

Western Blotting and LPS Silver Staining. Bacteria were scraped off YESCA plates and resuspended in phosphate buffered saline (PBS) (pH 7.4) before normalization of optical density at 600 nm (OD_{600}). To solubilize CsgA, samples were briefly treated with formic acid as described(104) or with hexafluoroisopronol (HFIP)(228). Whole cell samples were electrophoresed on 13% sodium dodecyl sulfate (SDS)-polyacrylamide and blotted onto polyvinylidene difluoride using standard techniques. CsgA and CsgG polyclonal antibodies were raised in rabbits with the purified proteins (Proteintech, Chicago, IL, USA) and were used at 1:10,000 and 1:100,000 dilutions, respectively. The CsgD antibodies were kindly provided by Ute Romling and were used at a 1:5000 dilution. Goat anti-rabbit IgG-HRP (immunoglobulin G-horseradish peroxidase) (Sigma, St. Louis, MO, USA) was used at a 1:10,000 dilution for CsgA and CsgG blots and a 1:5,000 dilution for the CsgD blots. CsgD blots were transferred onto nitrocellulose membranes using pH 11.2 buffer containing 25 mM N-cyclohexyl-3-aminopropanesulfonic acid (CAPS) and 10% Methanol. Western blots were developed using the chemiluminiscent Pierce super signal detection system (Thermofisher Scientific, Waltham, MA, USA). LPS was extracted as described(229) from OD_{600} of 10 cells grown on YESCA plates for 48 h at 26 °C. Samples were normalized to 10 ng of keto-deoxy-d-manno-8-octanoic acid (KDO) per lane using the Thiobarbituric Acid Assay and were separated and silver stained in a 14% Tricine SDS-PAGE gel(229).

RNA Extraction. RNA extraction was performed as described(230) with modifications. Briefly, overnight cultures grown in LB media were normalized to an OD_{600} of 1 and 4 µL were plated on YESCA agar. Plates were incubated at 26 °C for 24 h. Colonies were harvested for RNA extraction by resuspension in a 2:1 solution of RNA protect (Qiagen, Hilden, Germany):YESCA. Cells were pelleted via centrifugation: 7000× g for 5 min at room temperature. Cell pellets were immediately frozen and stored at −80 °C. Pellets were thawed at room temperature and resuspended in RNA extraction solution (18 mM ethylenediaminetetraacetic acid (EDTA), 0.025% SDS, 1% β-mercaptoethanol, 95% formamide). Cells were lysed by incubation at 100 °C for 7 min. After centrifugation: 16,000× g for 5 min at room temperature, the supernatant was transferred to a new microcentrifuge tube. The solution was diluted with 4 volumes RNase-free H2O, and then 0.1 volume 3 M sodium acetate pH 5.2 and 2 volumes ethanol. The solution was placed at −80 °C for at least 1 h or overnight. Precipitated nucleic acids were pelleted via centrifugation: 16,000× g for 20 min at 4 °C and washed with ice-cold 75% ethanol. The pellets were resuspended in 1× DNase I buffer (New England Biolabs, Ipswich, Massachusetts, USA) and incubated at 55 °C for 10 min. The solutions were clarified via centrifugation: 16,000× g for 5 min at room temperature and the supernatant was transferred to a new microcentrifuge tube and digested with DNase I (NEB) for 45 min at 37 °C. RNA was precipitated by adding 0.1 volume 8 M LiCl and 3 volumes ethanol and placing at −80 °C overnight. RNA was pelleted via centrifugation: 16,000× g for 15 min at 4 °C and washed with ice-cold 75% ethanol. The RNA pellet was dried and resuspended in RNase free H2O.

R**everse Transcriptase Complementary DNA Synthesis and Real-Time Quantitative PCR.** Reverse transcriptase complementary DNA (cDNA) synthesis was performed using Promega Go-Script (A5003) (Promega, Madison, WI, USA) according to the manufacturer's instructions with random primers (Invitrogen, Carlsbad, CA, USA). Real-time quantitative PCR was performed using Invitrogen Power Sybr green master mix (Invitrogen, Carlsbad, CA, USA) according to the manufacturer's instructions. Briefly, reverse transcriptase reactions were diluted 1000-fold for reactions using *csgD* primers and 10,000-fold for reactions using 16s primers. The data were

analyzed using the Pfaffl method(231). The amplification efficiencies of each primer pair were calculated via a standard dilution and relative RNA levels were calculated for each primer for each sample. Transcript levels of *csgD* were normalized to 16s levels.

Quantitative Real Time-PCR Analysis. The mRNA extraction was based on protocols for the RNeasy Mini Kit (Qiagen) with minor changes. Briefly, bacteria were normalized to an OD_{600} of 1 and 30 uL were spread onto YESCA plates and allowed to grow at 26 °C. After 24 h, bacteria were resuspended in 1.5 mL of RNAprotect (Qiagen) vortexed and incubated for 5 min. Cells were pelleted at 5000× g for 10 min and treated with lysozyme (Thermo Fisher Scientific, Waltham, MA, USA) (200 µL of freshly prepared 1mg/mL stock in 30 mM Tris-HCl 10 mM EDTA pH 8.0) for 5 min at room temperature. RNA was purified using the RNeasy Mini kit (Qiagen, Venlo, The Netherlands) and included an in column treatment with RNase free DNase (Qiagen, Venlo, The Netherlands). The RNA yield and purity were quantified in an Infinite 200 Pro NanoQuant Tecan reader (Tecan, Männedorf, Switzerland) and only samples with a 260/280 nm ratio equals or over 2 were further used. Aliquots of 2 ug/mL of mRNA were used to synthesize the cDNA using the Promega ImProm II reverse transcription kit and adding betaine 5 mM solution to the pre-annealing step with the random primers. Three serial dilutions (10−1, 10−2 and 10−3) by duplicate of each sample were analyzed using the ABsolute Blue QPCR SYBR Green Low ROX supermix from Thermo Scientific (Waltham, MA, USA) (3:5), the absolute quantification plate type and a standard 7500 run mode in an Applied Biosystems 7500 Fast Real-Time PCR System (Applied Biosystems, Foster City, CA, USA). The primers were designed using Primer 3 software, sequences are indicated in the Table 2.12, and were commercially acquired from Integrated DNA Technologies. Primers were used at 1.225 pM final concentrations each in 20 µL total reaction volume. As internal controls 16s and *rpoA* gene expression were measured, both worked similarly but 16s was more consistent and abundant, so 16s was used in the experiments described in this work. After confirming that the 16s primers and the target gene primers had similar efficiencies using the cycle threshold values generated from the ABI 7500 Fast System software analysis (Applied Biosystems, Foster City,

CA, USA), all the calculations for the fold gene expression data were done applying the ΔΔCt standard calculation.

Motility Assay. Cells were grown overnight in YESCA with appropriate antibiotics. Saturated cultures were diluted 1/100 in fresh YESCA and grown to mid log phase (OD_{600} of 0.3–0.6). Strains were normalized to 0.2 OD600 in YESCA and 2 uL were inoculated into 0.2% Agar YESCA motility plates. Plates were grown for 8 h at 26 °C. The strains tested for motility were also tested for growth rates in YESCA at 26 °C using a Klett meter (Kats Enterprises, Denton, TX, USA). No appreciable growth rate differences were measured.

Electron Microscopy. Bacteria were grown on YESCA plates for 48 h at 26 °C. Samples were resuspended in PBS and stained with 2% uranyl acetate as previously described(103). Grids were viewed using a Phillips CM10 microscope (Philips Electron Optics, Eindhoven, The Netherlands).

PCR verification of strains with multiple CR phenotypes. Strains with multiple phenotypes were chosen for PCR verification. Primers were designed 2-300 bp upstream of each gene and are listed in Table 2.8. Each strain with an altered CR phenotype was struck from the Keio collection to make a clean freezer stock. At least two independent colonies for each phenotype were resuspended in sterile water and subjected to colony PCR. The individual colony mixtures were added to master mixes of GoTaq Flexi (Promega). Mixture A contained the appropriate upstream primer and primer K1(102) and was used to verify the location of the kanamycin insert in the genome. Mixture B contained the primers KT and K2(102) and was used to verify the presence of the insert. If each phenotype gave a positive PCR product for both mixtures then it was added to Table 2.6. Mutations in energy production, coenzyme metabolism, cell envelope biogenesis, and DNA repair genes were more likely to have more than one CR phenotype (Table 2.6).

Cell hydrophobicity. Cell hydrophobicity was measured as described(155) using Xylene (X5-1; Fisher Scientific Co., Pittsburgh, PA), which gave more consistent results than a mixture of linear hexanes(232). The assay was performed with 2 mL of cells resuspended to 1 OD_{600} in PBS pH 7.4 amended with 2 M ammonium sulfate(155, 233), which helps distinguish between the relatively hydrophilic K-12 strains. Cells were tested in 16x125 mm glass culture tubes overlaid with increasing amounts of Xylene. Following incubation for 10 minutes at room temperature, the mixtures were vortexed for 1 minute using a Barnstead Thermolyne 16700. Following phase separation for 15 minutes at room temperature, a sample from the lower aqueous layer was removed and measured at OD_{600}. Each strain was independently tested at least twice.

Conclusions

More than 300 gene deletions that altered curli amyloid levels were identified in our CR screen. Several of the mutants focused on in this study are part of regulatory cascades, including stress response systems, which affect *csg* transcription. General themes arose for two major stress response systems, σS and Cpx. Mutations that that result in elevated σS levels produced more curli, while, those that induced σE or the Cpx system, produced less curli. An intact cell envelope was required to support curli biogenesis, as mutations in LPS and OPG resulted in less extracellular amyloid. Curli amyloid production was tied to key metabolic pathways such as the TCA cycle, the nucleotide synthesis pathways, and the catabolite utilization pathways. Collectively, the number and diversity of mutations that result in altered CR binding demonstrate that amyloid biogenesis is a complex and highly regulated developmental pathway in *E. coli*.

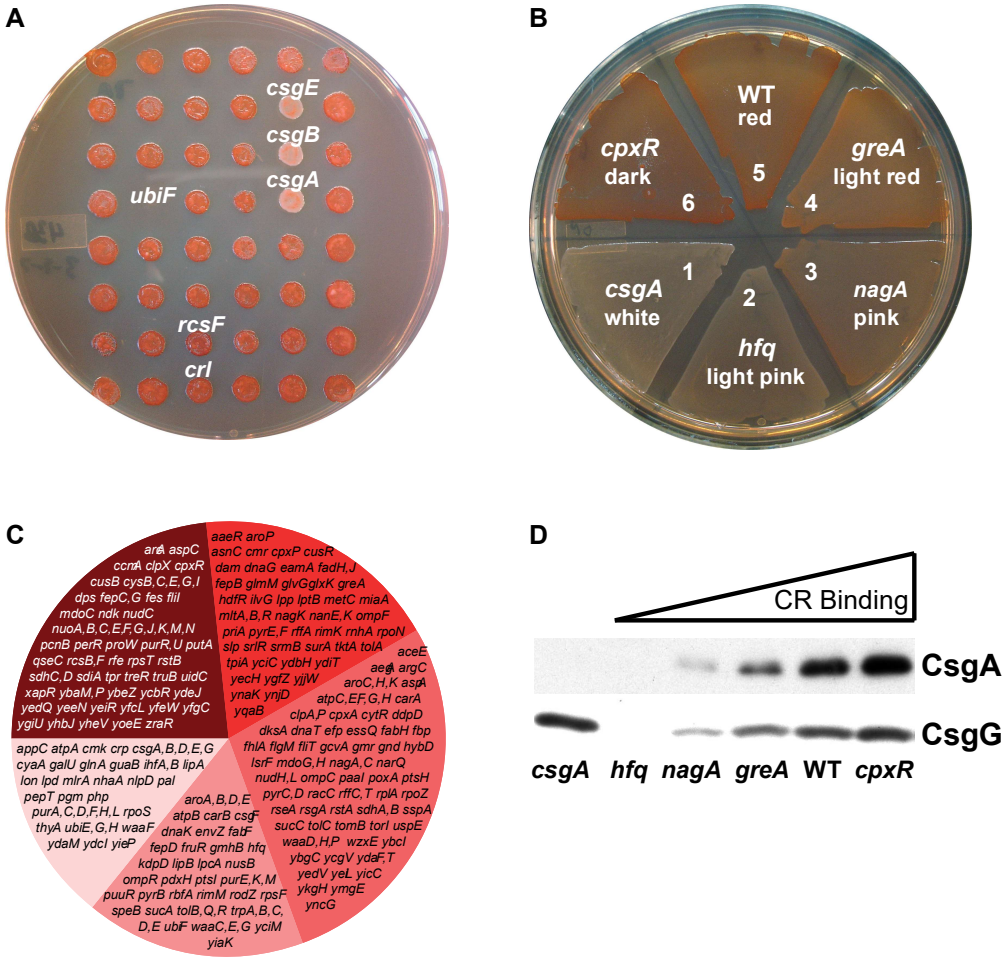

Figure 2.1. Overview of screen for mutants affecting curli production. A) The Keio collection was screened on CR indicator plates after inoculation with a bolt replicator and incubation for two days at 26 °C. The collection was screened three times. B) Associated phenotype scoring: 1 or white = *csgA*; 2 or light pink = *hfq*; 3 or pink = *nagA*; 4 or light red = *greA*; 5 or wild type (WT) = BW25113; and 6 or dark red = *cpxR*. C) Distribution of Congo red (CR) phenotypes based on scoring from white to dark red. D) Whole cell Western blots of strains probed with anti-CsgG and anti-CsgA antibodies.

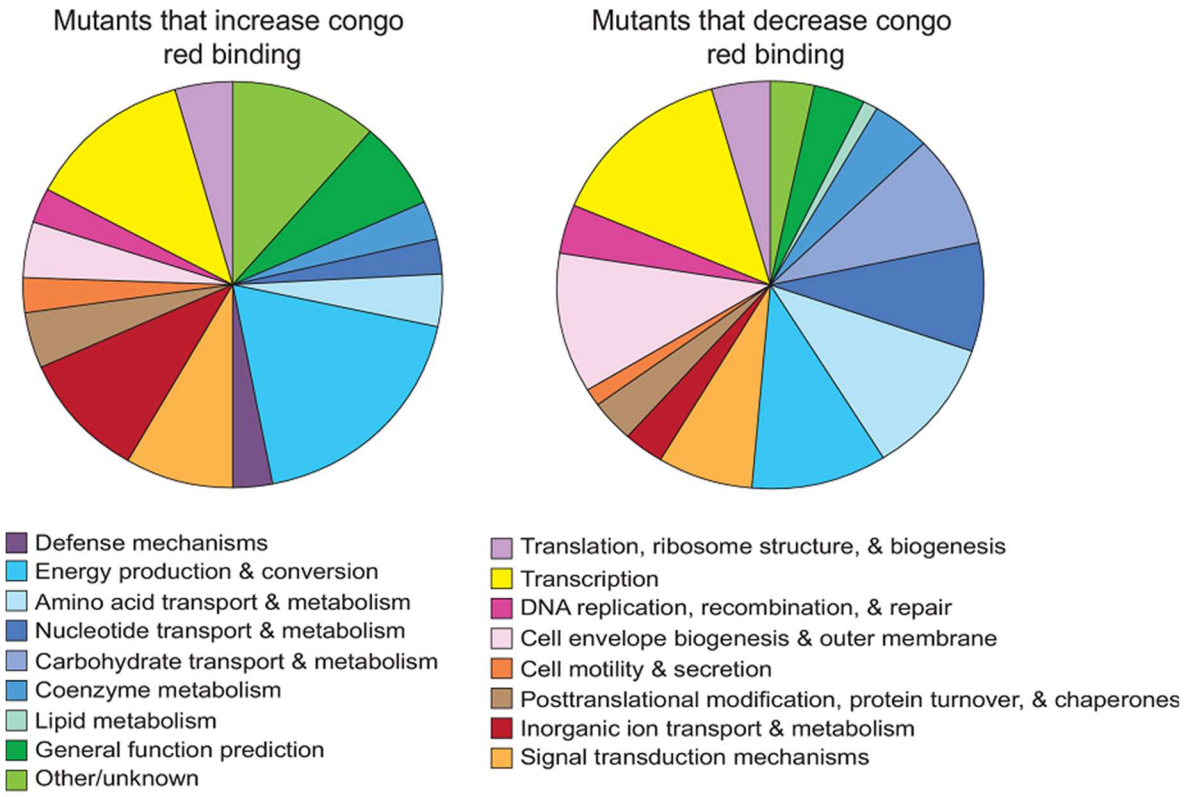

Figure 2.2. Genes affecting curli production perform diverse roles. Genes identified for altered curli production sorted by clusters of orthologous groups (COGs) showed involvement of regulation, environmental sensing, metabolism, cell envelope biogenesis, transport, and protein turnover in curli production.

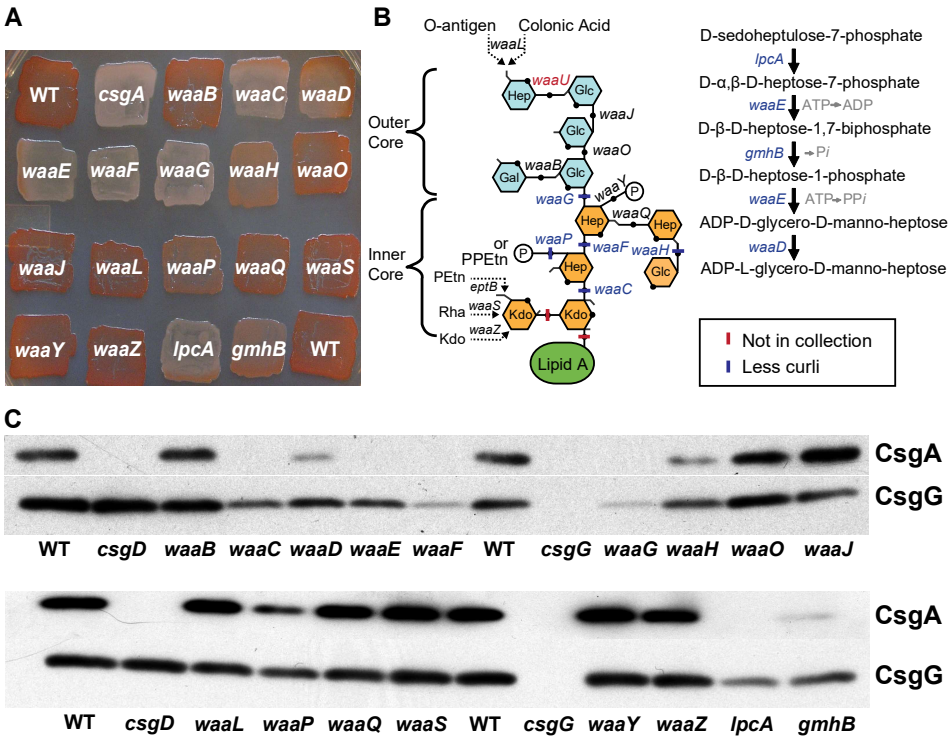

Fig. 2.3. Lipopolysaccharide (LPS) mutants are defective for curli production. A) LPS mutant strains and BW25113 (WT) grown on CR indicator plates at 26°C for two days. B) A schematic of LPS structure. Blue lines represent curli defective LPS mutants. Red lines represent LPS genes not in the Keio collection. C) Whole cell Western blots of LPS mutants probed with anti-CsgG and anti-CsgA antibodies. All samples were grown on YESCA plates at 26°C for two days and treated with formic acid.

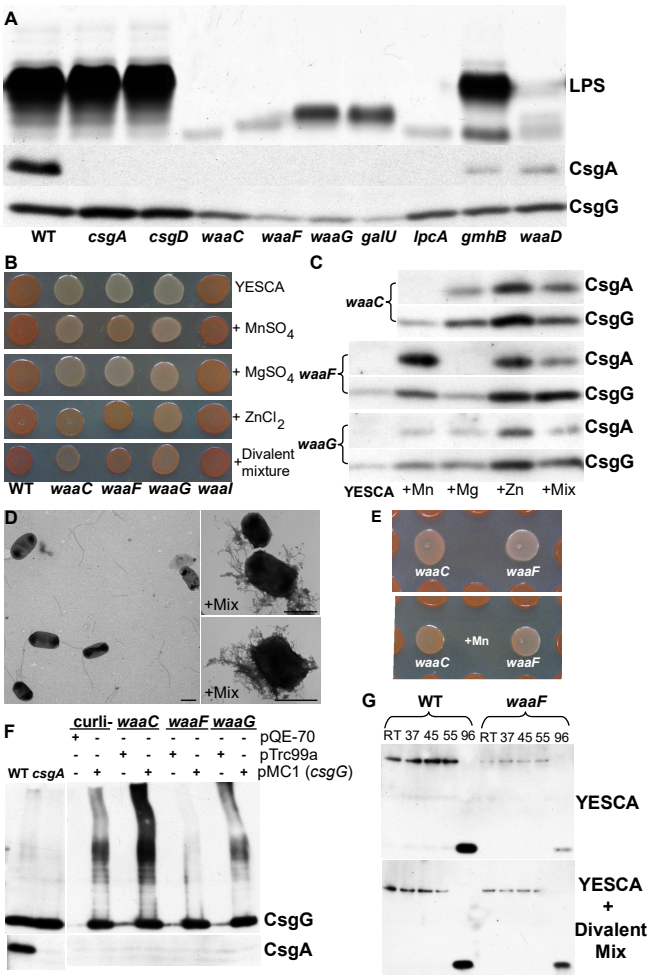

Fig. 2.4. Effects of inner core LPS mutants on curli production. A) Silver stain of LPS from LPS mutants and BW25113 (WT) resolved on a 14% polyacrylamide gel electrophoresis (PAGE) Tricine gel (top panel), and the respective whole cell Western blots probed with antibodies to CsgA and CsgG are shown in the bottom part of panel A. B) Addition of divalent salts $MnSO_4$ (0.5 mM), $MgSO_4$ (0.5 mM), $ZnCl_2$ (0.1 mM), or a mixture of all three divalent and $CaCl_2$ (0.5 mM) to CR indicator plates had varying abilities to suppress the CR phenotype of the indicated LPS mutants. C) Whole cell Western blots of LPS mutants probed with anti-CsgG and anti-CsgA antibodies. All samples were grown on YESCA plates supplemented with the indicated salts at 26 °C for two days and treated with hexafluoroisopropanol (HFIP). D) Transmission electron microscopy (TEM) images of *waaF* grown on YESCA and YESCA amended with a mixture of divalent cations. Scale bar equals 1 µM. E) The addition of 2 µL of 0.1 M $MnSO_4$ to LPS mutants *waaC* and *waaF* resulted in their ability to bind CR only when they were grown on plates surrounded by BW25113. F) Overexpression of *csgG* from pMC1 did not rescue CsgA secretion in inner core LPS mutants. G) The CsgG of WT (BW25113) and *waaC* had similar mobility in a 13% sodium dodecyl sulfate (SDS)-PAGE gel after a 10 min treatment at the indicated temperatures as in previous studies(121) except samples were 10 µL of 0.5 OD_{600} resuspended cells grown on YESCA for 2 days at 26 °C. The Divalent mix was $MnSO_4$ (0.5 mM), $MgSO_4$ (0.5 mM), $ZnCl_2$ (0.1 mM), and $CaCl_2$ (0.5 mM).

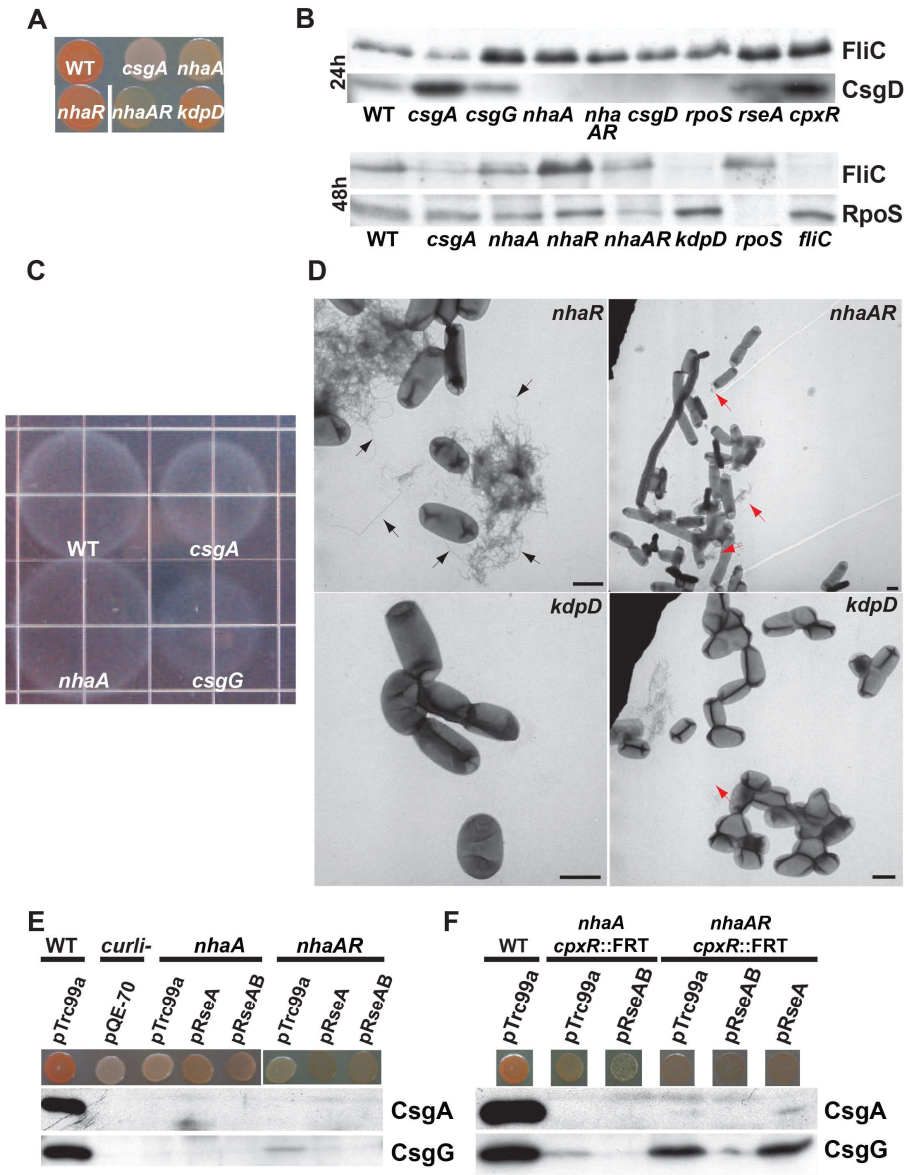

Fig. 2.5. Sodium antiporter gene *nhaA* is required for curli production. A) Strains were grown on CR indicator plates at 26 °C for two days. B) Whole cell Western blots probed with antibodies to CsgA, CsgG, and FliC at 24 and 48 h. All samples were treated with HFIP; C) Motility of WT, *csgA*, *csgG*, and *nhaA* strains in 0.2% YESCA motility plates at 26 °C. D) TEM images from cells grown for 26 °C for two days on YESCA plates. Black arrows indicate flagella. Red arrows indicate curli. Green arrows indicate filamentous cells. Scale bar equals 1 µm. E) Expression of *rseA* in trans using pRseA or pRseAB does not rescue curli expression in *nhaA* or *nhaAR* strains as detected by CR binding or Western blot probed with antibodies to CsgA or CsgG. F) Expression of *rseA* in trans from pRseA or pRseAB does not rescue curli production in *nhaA cpxR* or *nhaAR cpxR* double deletions as detected by CR binding or Western blot probed with antibodies to CsgA or CsgG.

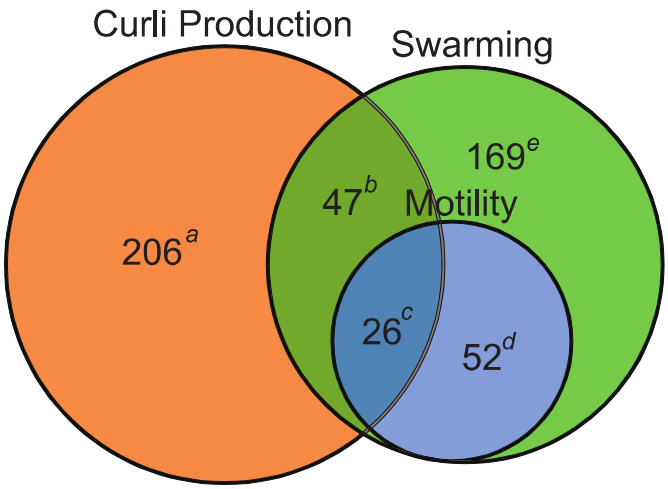

Fig. 2.6. Venn diagrams demonstrating few genes associated with curli affect swarming or swimming. Comparison of genes found to affect curli with swimming and swarming associated genes. Sections of Venn diagrams: [a] (orange), curli associated genes that do not affect swarming or swimming motility; [b] (dark green), curli associated genes that affect swarming motility; [c] (dark blue), curli associated genes that affect swimming motility; [d] (light blue), swimming defective genes that do not affect curli; and [e] (light green), swarming defective genes that do not affect curli.

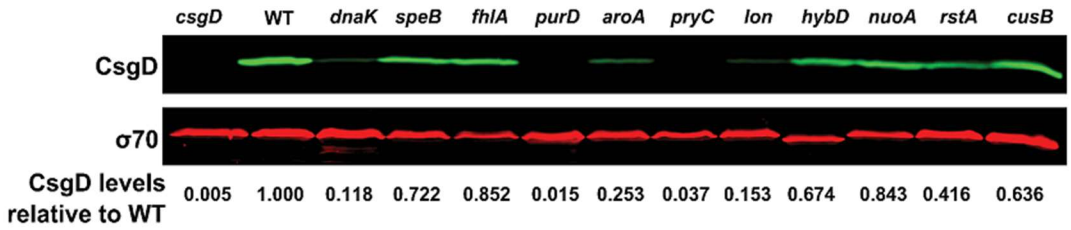

Fig. 2.7. CsgD protein levels are changed in several mutants. A representative western blot is shown for the data presented in Table 2.12. CsgD protein levels are shown in green and σ70 levels are shown in red as a loading control. CsgD levels were normalized to σ70, and then each mutant was normalized to WT to yield the relative CsgD protein levels for each mutant list of genes. σ70 migrates father in the *hybD* line consistently over multiple trials on different days.

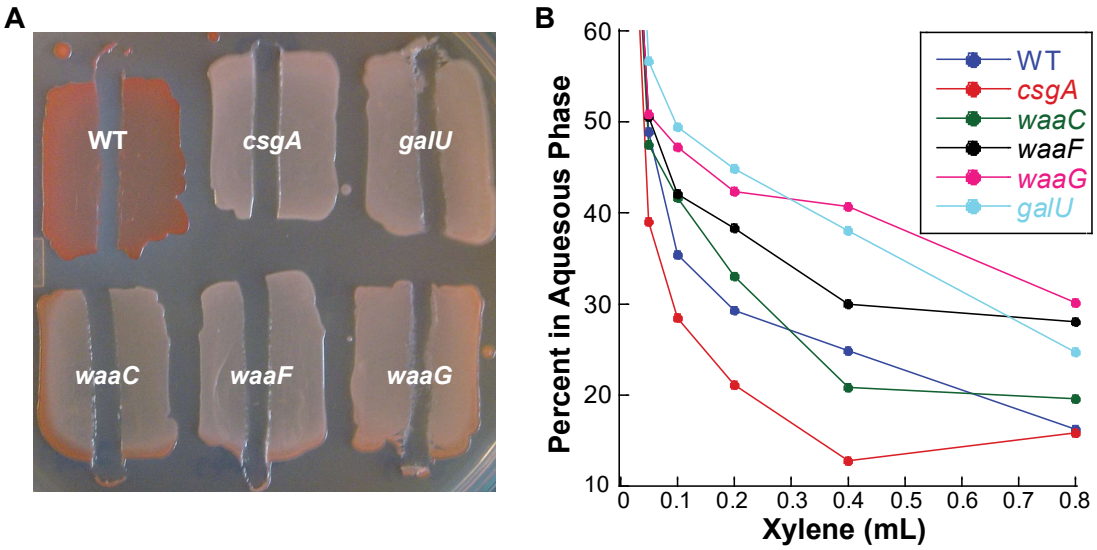

Fig. 2.8. Congo Red and hydrophobicity of different LPS mutant *E. coli* strains. A) Congo Red indicator plates of WT (BW25113), *csgA*, *galU*, *waaC*, *waaF*, and *waaG* grown for 2 days at 26°C. A sterile loop was scraped through each strain to show the dry, friable phenotypes. B) Cell hydrophobicity of LPS mutant strains in phosphate buffered saline (PBS) amended with 2 M ammonium sulfate. Similar results were obtained in independent replicates (data not shown).

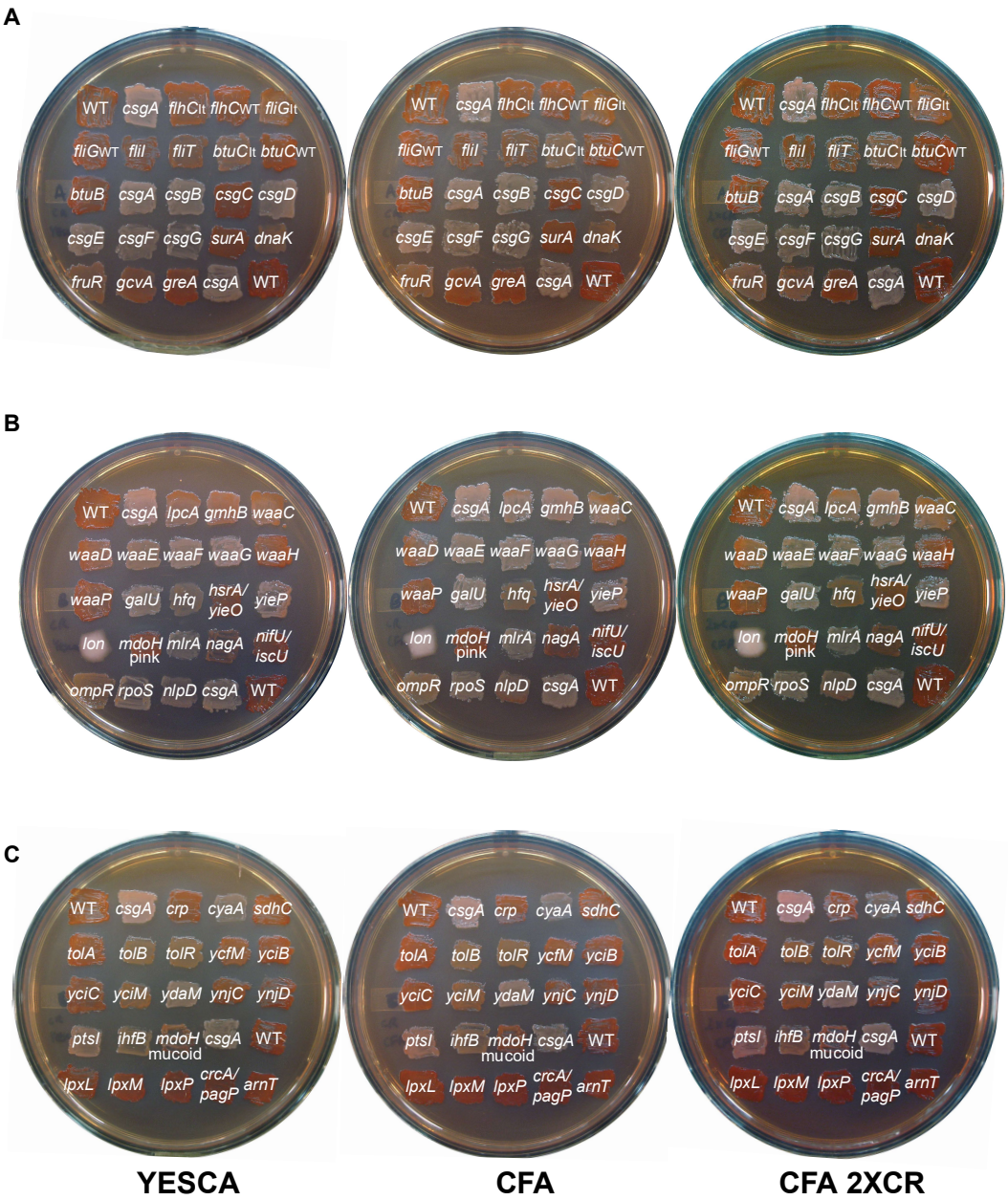

Fig. 2.9. Differences in Congo Red phenotypes of Keio collection strains on YESCA and CFA plates and CFA plates without Coommassie Brilliant Blue counterstain. Niba et al 2007 (215) performed a screen of the Keio collection for biofilm defective mutants. The biofilm mutants were subsequently tested for their motility, Type I pili formation, and curli production. For curli production they grew strains on CFA agar with twice the usual amount of Congo Red and no Coommassie Brilliant Blue (CBB) counterstain. Some of their CR phenotypes which were scored as +, -, or ± were different than ours. We tested these strains on YESCA and CFA plates with CR and CBB and on CFA plates without CBB and twice the CR as in Niba et al 2007 (215). Sets (A) (B) and (C) were scored based on their CR phenotypes from 1-6 at 24, 48, and 72 hours at 26^{o}C (See Table 2.11). Shown here is 48 hours growth. Some of the phenotypic differences are due to plating differences. CBB aids in detecting subtle differences between strains. The *crp* shown in (C) was found to have a suppressor; a new mutant had a white CR phenotype like *cyaA.*

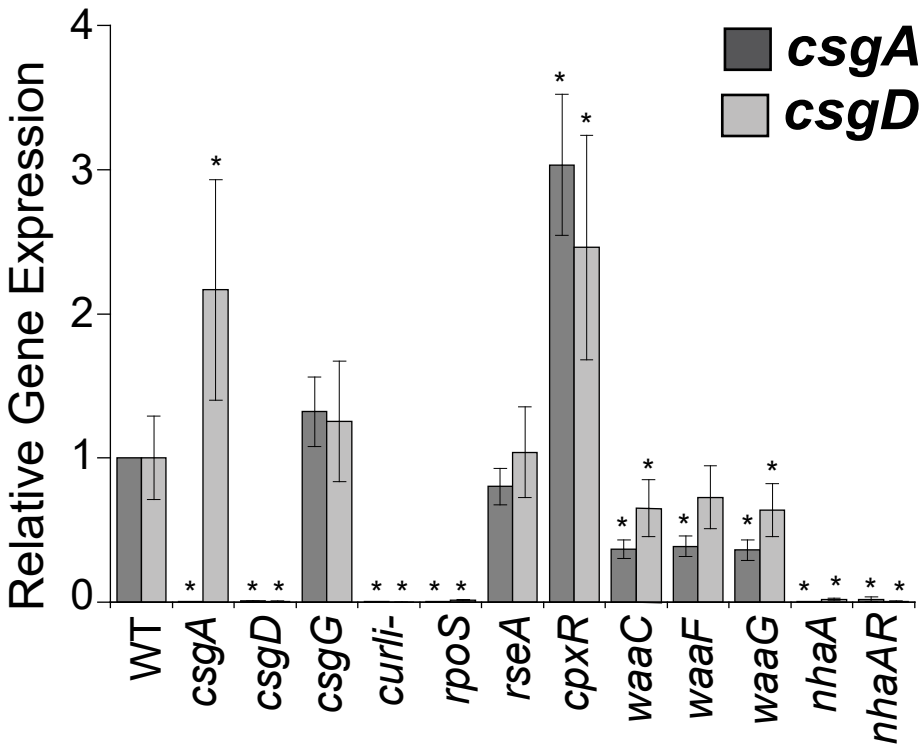

Fig. 2.10. qRT-PCR of inner core LPS and nhaA mutants. Relative levels of the indicated transcripts to BW25113 (WT) following 24 hours growth at 26°C as measured by RT-PCR. *csgA* and *csgD* transcript levels were graphed. Error bars are standard error of the mean of at least five measurements. * indicates $p < 0.05$ from student t-test.

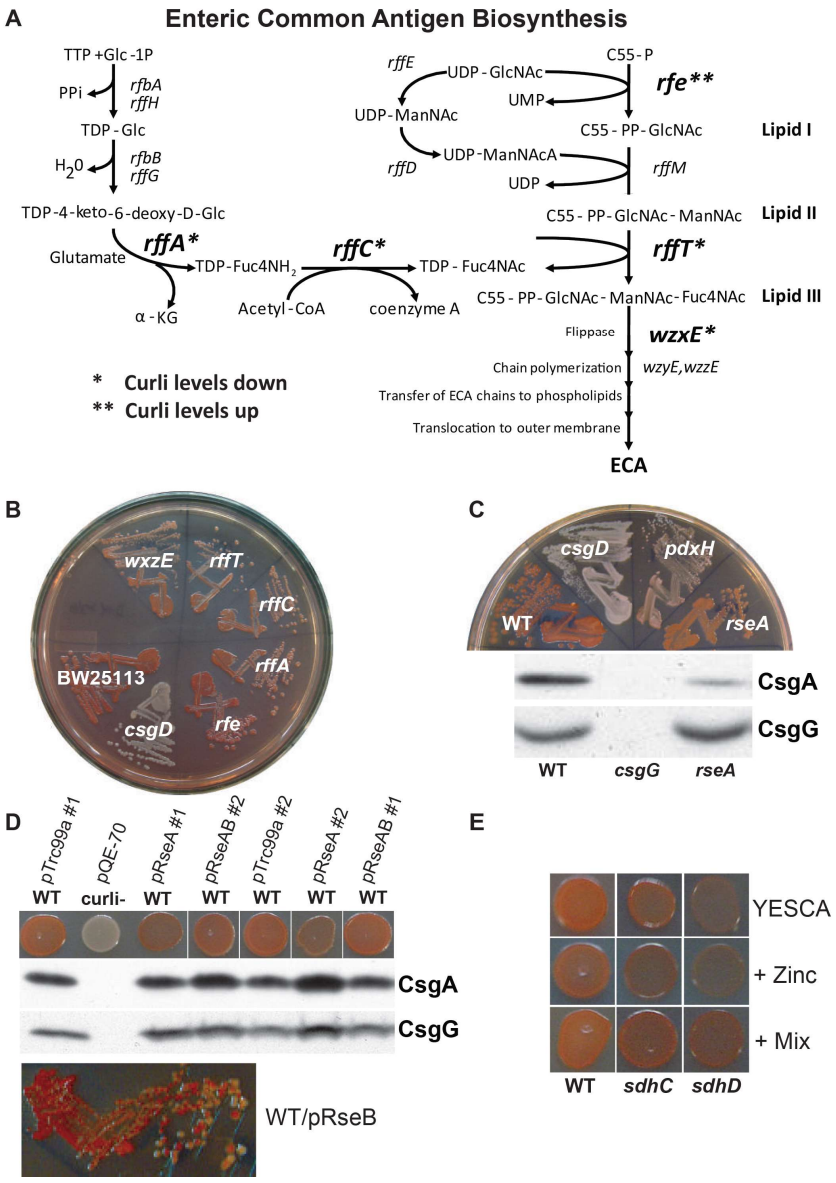

Fig. 2.11. Effects of σ^E induction on curli production. A) Diagram of Enteric Common Antigen biosynthetic pathway. B) Curli deficient strains: *rffA, rffC, rffT, wxzE*. Strains with increased curli production: *rfe.* C) Congo Red binding and whole cell Western blots of BW25113, *csgG*, and *rseA* mutants probed with antibodies to CsgA and CsgG. The *rseA* strain has a mucoid phenotype. D) Expression of *rseA in trans* using pRseA or pRseAB initially increased curli production in BW25113; however, these strains often reverted to normal curli production or variable CR phenotypes and colony morphologies (data not shown). When WT was transformed with pRseB, both pink and white colonies appeared in a near equal ratio of pink to red. When either colony phenotype was streaked again, both phenotypes appeared with a slight bias towards the original color. The streak shown was originally a red colony that arose from streaking a pink colony. Retransformation of pRseB plasmids obtained from different colony phenotypes displayed similar mixed phenotypes. E) Addition of ZnCl2 (0.25mM) or divalent mix to CR indicator plates partially rescues the curli defect in *sdhA* and *sdhB.*

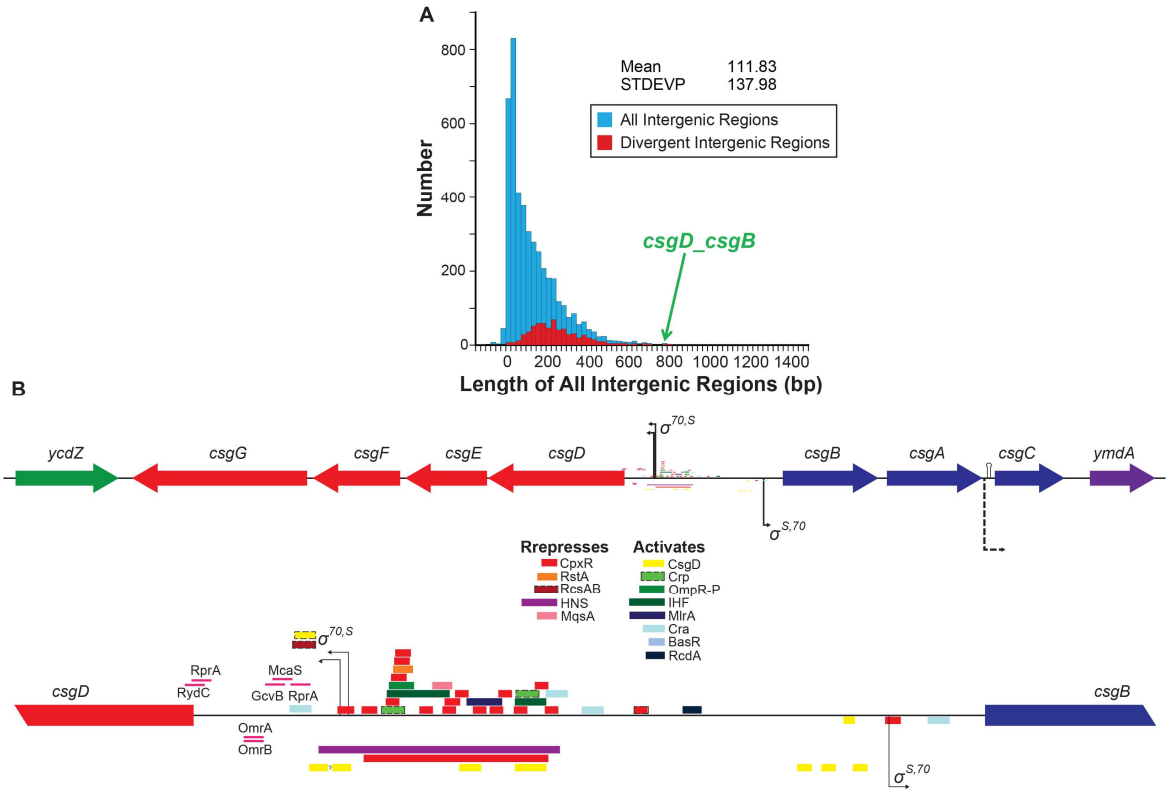

Fig. 2.12. The intergenic region between *csgD* and *csgB* has many transcriptional binding sites. A) Histogram of the length of all intergenic regions (blue) with an overlay of histogram of divergent intergenic regions (red). Divergent intergenic regions are shifted to larger sizes. B) Genomic context of *csg* genes (top) and the mapped transcriptional binding sites for the intergenic region between *csgD* and *csgB* (bottom) to scale. The scale of the intergenic region is one base pair per 0.25mm. Binding sites with number designations are from Ecocyc; the labeled CsgD and RcsAB binding sites near the transcription start of the *csgDEFG* operon have not been mapped(126). CpxR sites are depicted as separate binding sites at Ecocyc; however, they were originally a single large CpxR binding region. This large CpxR binding site and large HNS binding site are not currently annotated in Ecocyc(75, 126). Dan is also proposed to bind in the intergenic region and in the *csgB* ORF; however, the exact site or sites have not been mapped(196). The HNS and IHF binding sites may be multiple individual sites; their large size is much greater than their consensus sequences of 10 and 13bp, respectively(152).

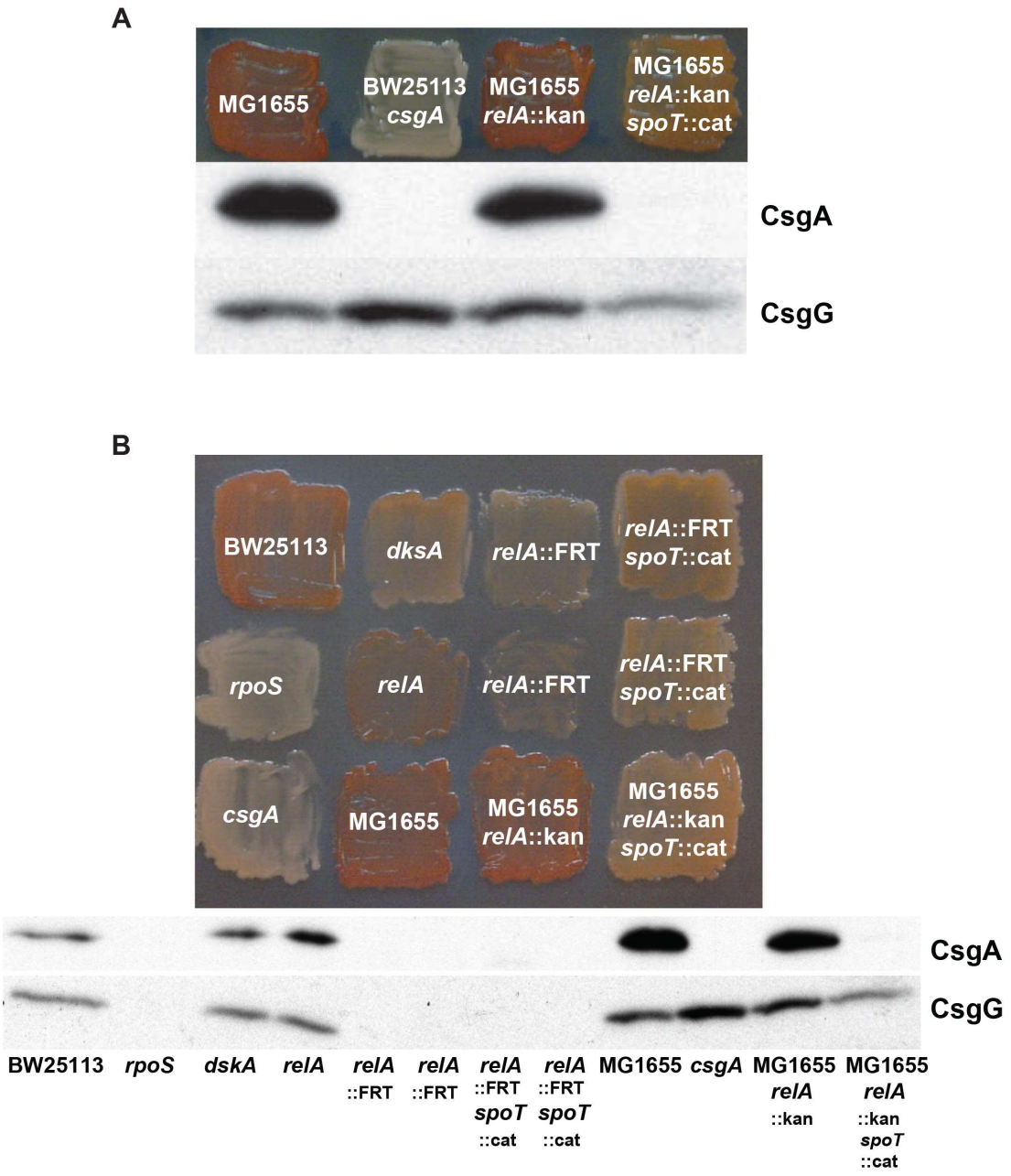

Fig. 2.13. Low ppGpp strains and *dksA* mutants produce less curli. Congo Red binding and Western blots of strains deficient for producing ppGpp. A) Background is *E. coli* strain BW25113(102) unless noted as MG1655. Strain *relA*::FRT has had the kanamycin cassette of the *relA* Keio strain (*relA*::FRT-*kan*-FRT) excised using pCP20 which encodes Flp recombinase(227). B) The FRT clean deletions were compared to keio collection strains. The *spoT*::cat (*ΔspoT207*::cat) was moved into the *relA*::FRT strain by P1 transduction; however, the *relA*::FRT strain is more defective than the *relA* Keio strain. The duplicate strains of *relA*::FRT and *relA::FRT spot*::cat shown were independent isolates. MG1655 *relA*::kan denotes MG1655 *relA*251::kan. Strains were grown on YESCA plates for two days at 26°C.

Table 2.1. Primary cellular role of genes that affect curli production.

Function	COG Group	Number (% total)	Genes (dark mutants are bold)
Information storage			
Translation, ribosome structure, & biogenesis	J	13 (4.2)	*efp, miaA,* ***pcnB****, poxA, rbfA, rimK, rimM, rplA, rpsF,* ***rpsT****, rsgA, srmB,* ***truB***
Transcription	K	43 (13.8)	*aaeR,* ***arcA****, asnC,* ***cpxR****, crp, cra, csgD, cusR,* ***cysB****, cytR, dksA, fliT, fhlA, flgM, gcvA, greA, hdfR, hfq, ihfA, ihfB, mlrA, mtlR, nagK, nanK, nusB, ompR,* ***perR, purR****, puuR,* ***rcsB****, rfaH, rffC, rpoN, rpoS, rpoZ, rstA,* ***sdiA****, srlR,* ***treR, xapR,*** *ydcI, yieP, ynaK*
DNA replication, recombination, and repair	L	11 (3.5)	***atl****, dam, dnaG, dnaT, ihfA, ihfB,* ***nudC****, nudL, priA, rnhA, rppH*
Cellular processes			
Cell envelope biogenesis, outer membrane	M	29 (9.3)	*csgA, csgB, csgE, csgF, csgG,* ***cusB****, galU, lpp, mdoH, mltA, mltB , nlpD, ompC, ompF,* ***rcsF****, pal, rfaC, rfaD, rfaE, rfaF, rfaG, rfaP,* ***rfe****, rffA, rffT, slp, tolc, wzxE, ycgV*
Cell motility & secretion	N	5 (1.6)	*cpxP, flgM,* ***fliI****, tolA,* ***ycbR***
Posttranslational modification, protein turnover, chaperones	O	11 (3.5)	***ccmA****, clpA, clpP,* ***clpX****, dnaK, lon, sspA, surA,* ***yfgC****, yjjW, yncG*
Inorganic ion transport & metabolism	P	14 (4.5)	*cpxP,* ***cysC, cysI****, ddpD,* ***dps****, fepB,* ***fepC****, fepD,* ***fepG****,* ***fes****, mdfA, mdoG, nhaA,* ***yoeE***
Signal transduction mechanisms	T	23 (7.4)	***arcA****,* ***clpX****, cpxA, cpxP,* ***cpxR****, crp, cusR, dksA, envZ, fhlA, gmr, kdpD, narQ, ompR,* ***qseC****, rseA, rstA,* ***rstB****, uspE, ydaM, yedV, yeiL,* ***zraR***
Defense Mechanism	V	2 (0.6)	***cusB****,* ***yfeW***
Metabolism			
Energy production & conversion	C	37 (11.9)	*aceE, aegA, appC, aspA, atpA, atpB, atpC, atpE, atpF, atpG, atpH, dlgD, fadH, hybD, lpd,* ***nuoA, nuoB, nuoC, nuoE, nuoF, nuoG, nuoJ, nuoK, nuoM, nuoN, putA,*** *racC, sdhA, sdhB,* ***sdhC, sdhD****, sucA, sucC, ubiF, ubiH, ydiT, yjjW*
Amino acid transport & metabolism	E	28 (9.0)	*argC, aroA, aroB, aroC, aroD, aroE, aroH, aroK, aroP, aspA,* ***aspC****, carA, carB,* ***cysE****, ddpD, eamA, glnA, gmhB, mdfA, metC, pepT,* ***proW****, speB, trpA, trpB, trpC, trpD, trpE*
Nucleotide transport & metabolism	F	22 (7.1)	*carA, carB, cmk, cyaA, guaB,* ***ndk,*** *purA, purC, purD, purE, purF, purH, purK, purL, purM,* ***purU****, pyrB, pyrC, pyrD, pyrE, pyrF, thyA*
Carbohydrate transport & metabolism	G	21 (6.7)	*eamA, fbp, glmM, glvG, glxK, gmhA, gnd, lapB, lsrF, mdfA, nagA, nagC, nagK, nanE, nanK, pgm, ptsH, ptsI, rafD, tktA, tpiA*
Coenzyme metabolism	H	8 (3.8)	***cysG****,* ***fepC****, lipA, lipB, pdxH, rimK, trpA, trpB, ubiE, ubiF, ubiG, ubiH*
Lipid metabolism	I	3 (1.0)	*fabF, fabH, fadJ*
Secondary metabolites	Q	2 (0.6)	*fabF, paaI*
Poorly characterized			
General function prediction	R	14 (4.5)	*essQ, ilvG, iptB, nudL, php,* ***rapZ****, rppH,* ***uidC****, ybcI, ybgC,* ***ydeJ****,* ***yeiR****, ygfZ,* ***yheV****, ynjD, yqaB*
Unknown/Other	S,U	22 (7.1)	***mdoC****, rodZ, tolB, tolQ, tolR, tomb, torI,* ***tpr****,* ***ybaM****,* ***ybaP****, yciC, ydaF, ydaT, ydbH, yecH,* ***yedQ****,* ***yeeN****,* ***yfcL****,* ***ygiU****, yicC, ykgH, ymgE*

Table 2.2. Selected mutant *csgD* levels as compared to Wild Type.

CR Phenotype	Strain	Average relative to BW25113	Standard Deviation	Outcome of T-test
Red	BW25113	1	N/A	N/A
White	*csgD*	N.D.	N/A	N/A
White	*nhaA*	0.018	+/-0.0068	P-value<0.001
White	*php*	0.841	+/-0.130	Not significant
White	*purD*	0.036	+/-0.053	P-value<0.001
White	*lon*	0.392	+/-0.187	P-value<0.05
Light Pink	*rfaC*	1.118	+/-0.363	Not significant
Light Pink	*dnaK*	0.221	+/-0.034	P-value<0.001
Light Pink	*speB*	0.578	+/-0.114	P-value<0.05
Light Pink	*hfq*	0.06	+/-0.080	P-value<0.001
Light Pink	*aroA*	0.223	+/-0.057	P-value<0.05
Pink	*fabH*	1.171	+/-0.315	Not significant
Pink	*flgM*	0.86	+/-0.254	Not significant
Pink	*ddpD*	0.766	+/-0.337	Not significant
Pink	*pyrC*	0.045	+/-0.020	P-value<0.001
Pink	*nagA*	3.38	+/-1.946	P-value<0.05
Pink	*fhlA*	0.695	+/-0.132	P-value<0.05
Pink	*dksA*	5.115	+/-1.076	P-value<0.001
Pink	*hybD*	0.278	+/-0.043	P-value<0.05
Pink	*gmr*	0.54	+/-0.142	Not significant
Pink	*rstA*	0.492	+/-0.187	P-value<0.05
Light Red	*priA*	0.023	+/-0.004	P-value<0.001
Light Red	*aaeR*	2.324	+/-0.755	P-value<0.05
Light Red	*glvG*	1.316	+/-0.175	Not significant
Light Red	*cmr*	1.586	+/-0.561	Not significant
Light Red	*dam*	0.967	+/-0.268	Not significant
Light Red	*hdfR*	0.752	+/-0.254	Not significant
Light Red	*mltA*	0.874	+/-0.170	Not significant
Dark Red	*cysB*	3.06	+/-0.982	P-value<0.001
Dark Red	*pcnB*	1.602	+/-0.354	P-value<0.05
Dark Red	*truB*	1.371	+/-0.240	Not significant
Dark Red	*rcsB*	3.723	+/-0.970	P-value<0.05
Dark Red	*sdiA*	2.952	+/-0.684	P-value<0.05
Dark Red	*fes*	0.999	+/-0.217	Not significant
Dark Red	*nuoA*	2.302	+/-0.678	Not significant
Dark Red	*qseC*	2.861	+/-2.190	Not significant
Dark Red	*arcA*	1.603	+/-0.219	P-value<0.05
Dark Red	*mdoC*	1.581	+/-0.309	P-value<0.05
Dark Red	*perR*	1.923	+/-0.537	P-value<0.05
Dark Red	*cusB*	2.224	+/-0.998	P-value<0.05

Table 2.3. *csgD* qPCR significance for selected mutants.

Outcome of T-test	Number of strains
Not significant	15
P-value<0.05	14
P-value<0.001	7
Uncertain	2
Total	38

Table 2.4. *csgD* levels altered by decreased ribosome levels.

Strain	Aveage *csgD* levels	Std Dev	p-value	Average *16s* levels	Std Dev	p-value
BW25113	3.141E-02	1.652E-02	N/A	1.38E-02	7.56E-03	N/A
dam	4.605E-02	1.173E-02	0.107	2.05E-02	4.31E-03	8.93E-02
hfq	1.742E-04	3.279E-05	9.36E-04	6.46E-03	6.48E-03	1.02E-01
nagA	2.407E-02	2.143E-03	0.306	4.79E-03	4.23E-03	2.94E-02
dksA	3.777E-02	9.779E-03	0.436	3.14E-03	8.50E-04	6.51E-03

Table 2.5. Congo Red Phenotypes and Western blot data from Keio strains with Altered Curli Production (Inset removed genes)

Name	JW Strain	Keio Location	Primary COG Class	Original Color	Color For chart	Checked Color(s) at 26C (5 is WT)	Checked Color(s) at 37C (4 is WT)	CsgG Levels	CsgA Levels
aaeR	JW3212	53-10C	K	light red	4	4	3	+++	++++
aceE	JW0110	5-9F	C	light red	3	3	3	++	+++
aegA	JW2452	53-9D	C	pink to orange	3	3	3	+	++
appC	JW0960	3-1F	C	white to lt pink	1	1	4	+/-	+/-
arcA	JW4364	5-3F	T	dark red	6	5-6	ND	++++	+++
argC	JW3930	9-4G	E	pink to light red	3	3	4	+	+/-
aroA	JW0891	41-4D	E	white to lt pink	2	2-3,2	2,3	++,++	+/-,+/-
aroB	JW3352	51-10D	E	white to lt pink	2	2-3,4	3,2	+/-,+	-,+/-
aroC	JW2326	41-8E	E	pink to orange	3	4,3	2,3	+,++	+/-,++
aroD	JW1683	41-6E	E	white to lt pink	2	1,2	2-3,3	+,+/-	+/-,-
aroE	JW3242	41-10E	E	white to lt pink	2	2-3,2	2,3	++,++	+/-,+
aroH	JW1694	41-6F	E	light red	3	3-4	4	+++	++
aroK	JW5947	89-1H	E	pink to orange	3	4,3	4,4	+++,+++	++++,++
aroP	JW0108	39-11C	E	light red	4	4	4	+	+++
asnC	JW3721	1-1G	K	dark red	4	4,4	4,4	+++++,++	++++,+++
aspA	JW4099	63-11A	E	pink to orange	3	3(SG)	4(SG)	++	+
aspC	JW0911	41-4E	E	red	6	6	2-3	+++	++++(+)
atpA	JW3712	93-1H	C	slow growth/other	1	1,1(SG)	2,1(SG)	+/-,-	-,-
atpB	JW3716	93-2D	C	slow growth/other	2	2,3(SG)	1,1(SG)	++,+	-,+++
atpC	JW3709	93-1E	C	slow growth/other	3	3,2-3(SG),3(SG)	2,1(SG),2(SG)	++++,+/-	++++,-
atpE	JW3715	93-2C	C	slow growth/other	3	3,3(SG)	2,2(SG)	++,+++	++,+++
atpF	JW3714	93-2B	C	slow growth/other	3	3,3(SG)	2,2(SG)	++,+++	+,++
atpG	JW3711	93-3D	C	slow growth/other	3	3,3(SG)	2,2(SG)	+++,+++	++++,++++
atpH	JW3713	93-2A	C	slow growth/other	3	3,3(SG)	1,1(SG)	+,+	+/-,+++
carA	JW0030	85-4C	E	pink to orange	3	3	4	+++	+
carB	JW0031	49-4D	E	white to lt pink	2	2	5(SG)	+	+/-
ccmA	JW5366	69-2G	O	dark red	6	5-6	4	+++	+++++
clpA	JW0866	7-11F	O	pink to light red	3	3	4	+++	+++
clpP	JW0427	7-10F	O	light red	3	3	4	+++	+++
clpX	JW0428	7-10G	O	dark red	6	6	4	+++++	+++++

cmk	JW0893	49-7C	F	pink to orange	1	1 dry, 1 dry	4,5	-,-	-,-
cmk	'	49-7C	'	'	'	2,2 dry	4,4	+/-,+/-	+/-,-
cmr	JW0826	55-2B	P	light red	4	3-4	4	++	++
cpxA	JW3882	5-2D	T	pink	3	3	4	+++	+++
cpxP	JW5558	73-7H	T	light red	4	4	4	+++	+++
cpxR	JW3883	5-2E	T	dark red	6	6	4	+++++	++++
crp	JW5072	1-2F	T	see notes	1	1	ND	ND	-
csgA	JW1025	43-11D	M	white to lt pink	1	1	4-5	+++++	-
csgB	JW1024	43-11C	M	white to lt pink	1	1	4	+++++	-
csgD	JW1023	1-2G	K	white to lt pink	1	1	4	++++	-
csgE	JW1022	43-11B	M	white to lt pink	1	1	4	+	-
csgF	JW1021	29-9E	M	white to lt pink	2	2-3	4	++	+
csgG	JW1020	29-9D	M	white to lt pink	1	1	4	-	-
cusB	JW0563	3-5G	M	dark red	6	5-6	4	+++++	++++
cusR	JW0560	5-10A	T	light red	4	4	4	++++	+++
cyaA	JW3778	53-10F	F	white to lt pink	1	1	3	+/-	-
cysB	JW1267	95-7A	K	dark red	6	6	3-4	+++++	++++
cysC	JW2720	47-7D	P	dark red	6	6,5	4,4	++++	+++++
cysE	JW3582	41-10H	E	dark red	6	5-6	3	++++	+++++
cysG	JW3331	31-1F	H	dark red	6	6	4	+++++	+++++
cysI	JW2733	47-7H	P	dark red	6	6,5	4,3	++++	+++++
cytR	JW3095	1-3A	K	white to lt pink	3	3, 3	4, 4	+++, +	+/-, ++
dam	JW3350	81-1E	L	pink to orange	4	4,4	4,4	+++,+++	++++,+++
ddpD	JW1479	55-6C	P	pink to orange	3	3	4	++	++
dksA	JW0141	29-11E	T	light red	3	3	3	++++	++
dnaG	JW3038	81-1C	L	pink to orange	4	3-4	4	++++	+++
dnaK	JW0013	95-2C	O	white to lt pink	2	2	6	+/-	-
dnaT	JW4326	93-1B	L	pink to orange	3	2-3	5	+/-	+/-
dps	JW0797	3-9F	P	dark red	6	6	4	++++	+++++
eamA	JW5250	77-2C	E*	pink to orange	4	4	4	+++	+++
efp	JW4107	61-7A	J	pink to orange	3	3	4	++	+
envZ	JW3367	5-10B	T	white to lt pink	2	2	4-5	+/-	+/-
essQ	JW5255	77-2F	R*	pink to orange	3	3	4	+++	+
fabF	JW1081	49-2E	I	pink to orange	2	2	4	+/-	-
fabF	'	49-2E	'	'	'	3	4	++	+

fabH	JW1077	95-2F	I	pink to orange	3	3	4	++	+++
fadH	JW3052	51-9E	I*	light red	4	4,4	4,4	++++,+++	+++
fadJ	JW2338	85-1C	I	pink to orange	4	3-4	3	+++	+++
fbp	JW4191	5-9H	G	pink to orange	3	3,2	4,4	++,++	+,++
fepB	JW0584	53-11F	P	light red	4	3-4	3	++	+++++
fepC	JW0580	41-2B	P	dark red (slow growth)	6	5-6	2	++++	+++++
fepD	JW0582	53-11E	P	white to lt pink	2	2-3	3	++	++++
fepG	JW0581	85-6A	P	dark red	6	6	3	+++++	++++
fes	JW0576	41-1H	P	dark red	6	5-6	2	++++	+++++
fhlA	JW2071	85-2A	K	light red	3	3	4	+	+
flgM	JW1058	89-12H	K*	light red	3	3-4	4	+++	++
fliI	JW1925	45-3B	N	dark red	6	6,6,5-6	4,4,4	+++++,+++++,+++	++++,+ (NA?),+++++
fliT	JW1911	45-2G	O*	pink to orange	3	3,3	4,4	+++	+++
fruR	JW0078	1-10C	K	white to lt pink	2	2	4	++	+/-
galU	JW1224	49-12C	M	white to lt pink	1	1	4	+/-	-
gcvA	JW2799	83-3E	K	white to lt pink	3	2-3	4	++	+++
glmM	JW3143	95-2E	G	light red	4	3-4,3-4	4,4	++,+++	++++,+++
glnA	JW3841	41-11H	E	slow growth/other	1	1(VSG),1(VSG),1(VSG)	1(VSG),1(VSG),1(VSG)	NA,NA,-	NA,NA,-
glvG	JW3658	55-10F	G	red	4	4,4	4,4	+++,+++	++++,++++
glxK	JW0502	89-10D	G	light red	4	4	4	+++	+++
gmhB	JW0196	81-5D	M*	white to lt pink	2	1,2-3,2-3	4,ND,ND	++,+,+	+,-,+
gmr	JW1278	23-8B	T	red	3	3-4	4	++++	+++(+)
gnd	JW2011	3-3E	G	pink to orange	3	3	4	+	++
greA	JW3148	61-3D	K*	pink to orange	4	3-4	4	+++	+++
guaB	JW5401	95-7D	F	slow growth/other	1	1(SG),1	5(SG),6	-	-
hdfR	JW5067	87-6G	K	light red	4	3-4	4	+++	++
hfq	JW4130	31-2B	R	white to lt pink	2	2,1-2	5-6,5	+/-	-,-
hybD	JW2961	9-3H	C	light red	3	3	4	+	+
ihfA	JW1702	1-10D	L	white to lt pink	1	1	4	-	-
ihfB	JW0895	1-4F	L	white to lt pink	1	1	4	-	-
ilvG	JW3740	65-10D	R*	light red, slight muccoid?	4	4	4	+++	+++++
kdpD	JW0683	3-9E	T	pink to orange	2	2	4-5	++	++

lipA	JW0623	43-2E	H	slow growth/other	1	1,2,2(VSG)	1,2,1(VSG)	+/-,++,+/-	NA,+/-,+/-
lipB	JW5089	89-6E	H	slow growth/other	2	2(SG),2(VSG)	1(SG),1(VSG)	ND,+/-	ND,+++
lon	JW0429	7-10H	O	slow growth/other	1	1(mucoid)	4	-	-
lpcA	JW0212	49-9A	M*	white to lt pink	2	2,1,2,2	5,5,ND,ND	++,++,+,+/-	-,-,-,-
lpd	JW0112	5-9G	C	slow growth/other	1	1(SG), 1(SG)	2, 1	+/-, -	-, -
lpp	JW1667	31-2C	M	light red	4	4, 4	5, 4	++++, ++	++, +++
lptB	JW3168	59-1D	M*	light red	4	3,4,4	3,4,4	NA,++++,+++	++++,++++,+++
lsrF	JW1510	21-3E	G	light red	3	3	4-5	++	++++
mdoC	JW1034	13-4H	M*	red	6	6,6	4,4	+++++, +++++	+++++,++++
mdoG	JW1035	65-4H	M*	light red	3	3	4	++	+++
mdoG	'	65-4H	'	'	'	1 mucoid	4	-	-
mdoH	JW1037	65-3C	M	light red	3	3	4	++	+++
metC	JW2975	41-10C	E	pink to orange	4	3-4	4	+++	++
miaA	JW4129	61-7B	J	light red	4	3-4	4	++++	++
mlrA	JW2115	53-9B	K	white to lt pink	1	1	3	-	-
mltA	JW2784	7-2C	M	red	4	4	4	+++	+++++
mltB	JW2671	7-2D	M	red	4	4	4	+++	+++
mtlR	JW3575	85-3E	K	light red	4	3-4	4	+++	++
nagA	JW0663	47-3D	G	pink to orange	3	3	4	++	++
nagC	JW0662	1-7A	G	pink	3	3	4	+++	++
nagK	JW1105	21-1H	G	light red	4	4-5	3	+++	+++(+)
nanE	JW3192	47-9H	G	red	4	3-4	ND	++++	++
nanK	JW5538	69-10D	G	light red	4	4,3-4	4,ND	++,+++	++++,++
narQ	JW2453	3-12E	T	light red	3	3	4	++	+
ndk	JW2502	85-5F	F	dark red	6	6,6	4,4	++++,+++++	++,+++++
nhaA	JW0018	39-10E	P	white to lt pink	1	1,1	5,5	-,-	-,-
nlpD	JW2712	9-3A	M	white to lt pink	1	1	4	+/-	-
nudC	JW5548	37-6H	F*	red	6	5-6,5-6	4,4	++++,++++	+++++,+++++
nudH	JW2798	23-2H	R	pink to orange	3	3	3	+	+
nudL	JW1802	23-12G	R*	light red	3	3-4	4	++	++++
nuoA	JW2283	3-5B	C*	dark red	6	6	3	+++++	++++
nuoB	JW5875	3-5A	C	red	6	6	3	+++++	++++
nuoC	JW5375	87-5H	C	dark red	6	6	3	++++	+++++
nuoE	JW2280	3-4H	C	dark red	6	6	3	+++++	++++
nuoF	JW2279	3-4G	C	dark red	6	6	2	++++	+++++

nuoG	JW2278	3-4F	C*	dark red	6	6	3	+++++	+++++
nuoJ	JW2275	3-4C	C	dark red	6	6	3	++++	+++++
nuoK	JW2274	3-4B	C	dark red	6	6	3	++++	+++++
nuoM	JW2272	3-3H	C	dark red	6	6	3	+++++	++(NA)
nuoN	JW2271	3-3G	C	dark red	6	6	3	++++	+++++
nusB	JW0406	95-4D	K	white to lt pink	2	2, 3	5-6, 6	+/-, -	-, -
ompC	JW2203	7-4F	M	light red	3	3,3	3,3	+++,++	++,+++
ompF	JW0912	7-4G	M	light red	4	4	3	++++	+++
ompR	JW3368	5-1F	T	white to lt pink	2	2	5	-	-
paaI	JW1391	41-6A	Q	pink to orange	3	3-4	4	++++	++++
pal	JW0731	7-2F	M	white to lt pink	1	1	5	+	-
pcnB	JW5808	87-7B	J	dark red	6	6	ND	+++	+++++
pdxH	JW1630	43-6H	H	pink to orange	2	2	3	+	+
pepT	JW1113	7-12A	E	white to lt pink	1	1	4	+/-	+/-
perR	JW0244	1-7E	K	dark red	6	5-6	4	+++++	++++
pgm	JW0675	5-5E	G	white to lt pink	1	1 mucoid	5	-	-
pgm	'	5-5E	'	'	'	2 mucoid	5	+/-	+/-
php	JW3342	51-10C	R	white to lt pink	1	1,2	4,4	-	-
poxA	JW4116	85-10G	J	pink to orange	3	3	4	+	++
priA	JW3096	93-1A	L	pink to orange	4	4	3	+	+++
proW	JW2653	57-10D	E	dark red	6	6,6	4,4	+++++,+++++	++++,+++++
ptsH	JW2408	57-8F	G	light red	3	3,3-4,2-3	3,3,4	++,++,++	++,++,+++
ptsI	JW2409	57-8G	G	white to lt pink	2	2,3,2	2,3,1	+,+/-,+/-	+,+/-,+
purA	JW4135	53-6D	F	pink to orange	1	1(SG),3,2	4(SG),3,4-5	+/-,-,+/-	-,ND
purC	JW2461	85-4F	F	pink to orange	1	1(SG),1	5,4-5	+/-,-	-
purD	JW3969	53-6C	F	white to lt pink	1	1(SG),2,2	5-6,6,4-5	-,-,-	-,ND
purE	JW0512	49-6D	F	white to lt pink	2	2(SG),2	2(SG),4-5	-,-	-
purF	JW2309	53-4B	F	white to lt pink	1	1,3,1	5(SG),3,4	-,-,-	-,ND
purH	JW3970	85-5C	F	pink to orange	1	1(SG),1	5,5	+/-,-	-
purK	JW0511	49-6C	F	white to lt pink	2	2,2	4,4	+/-,-	-
purL	JW2451	53-4H	F	white to lt pink	1	1(SG),2,1	4(SG),1,4	-,-,-	-,ND
purM	JW2484	53-4E	F	white to lt pink	2	2,3,2	5-6,3,5	-.-,-	-,ND
purR	JW1650	1-7H	K	dark red	6	5, 6,6	5, 4,4	++++, +++++,+++++	+++++, ++++,+++++
purU	JW1220	49-7F	F	red	6	6	4	+++	++++

putA	JW0999	47-4B	C	dark red	6	6	4	+++	+++++
puuR	JW1292	23-8D	K	pink to light red	2	2	4	+	+
pyrB	JW4204	53-7A	F	white to lt pink	2	2	4	+/-	-
pyrC	JW1049	49-7E	F	light red	3	3(SG)	4(SG)	+++	++
pyrD	JW0928	49-7D	F	light red	3	3-4	2	+++	++
pyrE	JW3617	53-6A	F	light red/slow growth	4	4(SG),2-3(SG)	3,3(SG)	+++,+	+,+
pyrF	JW1273	53-2C	F	light red	4	4(SG)	3	+++	+
qseC	JW2994	5-1C	T	dark red	6	6	3-4	+++++	++
racC	JW1345	63-2A	C	pink to orange	3	3	4	-(NA)	++
rbfA	JW3136	95-6B	J	pink to orange	2	2	4	+	+/-
rcsB	JW2205	3-11H	K	dark red	6	ND	ND	ND	ND
rcsF	JW0192	48-9G	T*	dark red	6	6,6	4	+++++,+++++	+++++,+++++
waaC	JW3596	95-5H	M	white to lt pink	2	2,2,2,2	5,5,ND,ND	++,++,+,+	-,-,-
waaD	JW3594	45-5C	M	white to lt pink	3	2-3,2-3,2-3,2-3	4-5,4,ND,ND	++,++,++	-,+/-,+/-
waaE	JW3024	95-4E	M	white to lt pink	2	2,2,2-3,2	5,5,ND,ND	++,+,+,+	-,-,-
waaF	JW3595	45-5D	M	white to lt pink	1	1,1,1-2,2	4-5,4,ND,ND	+/-,+/-,+/-,+/-	-,-,-,-
waaG	JW3606	45-6C	M	white to lt pink	2	1,2,2	4-5,ND,ND	+/-,+/-,+/-	-.-,-
waaH	JW3818	45-7E	K	light red	3	3,3,3-4	4,ND,ND	++,++,++	+.+,++
waaP	JW3605	45-6B	M	pink to orange	3	4,3-4,3,3	4,4,ND,ND	+++,+++,+++,+++	+,++,+/-,++
rfe	JW3758	45-6G	M	dark red	6	6	ND	+++	+++++
rffA	JW3765	49-3F	M	light red	4	3-4	ND	+++	+++
rffC	JW5597	37-3D	M	light red	3	3,3,4,3,3	4,4,4,ND,4	++,++++,+++,+++,+++	+++++,++,+++,++,++
rffT	JW5596	73-8G	M	light red	3	3	ND	+++	+++++
rimK	JW0836	57-4E	J*	dark red	4	4,4	4,4	++,+	++++,++
rimM	JW5143	95-5C	J*	white to lt pink	2	2	5	+/-	-
rnhA	JW0204	49-5C	L	pink to light red	4	4	4	+++	+++
rodZ	JW2500	21-11H	M*	white to lt pink	2	2-3,2, 2	4,4-5, 4	++,++,+/-	+++,-
rplA	JW3947	95-6E	J	pink to orange	3	3	4	++	+++
rpoN	JW3169	5-1D	K	light red	4	3-4	3	++	++
rpoS	JW5437	79-1H	K	white to lt pink	1	1	3	-	-
rpoZ	JW3624	5-1G	K	pink to orange	3	3	4	++++	+++
rpsF	JW4158	95-3G	J	white to lt pink	2	2	4	-	-

rpsT	JW0022	89-5G	J	dark red	6	6	4	++++	+++++
rseA	JW2556	91-1B	T	light red	3	3,3	5,6	++++,+++++	++,+++++
rsgA	JW4122	95-4G	J*	pink to orange	3	3	4	++	+
rstA	JW1600	3-10F	K	light red	3	3	4	++	+
rstB	JW1601	3-10G	T	dark red	6	5-6	4	+++	+++
sdhA	JW0713	1-12C	C	pink to orange	3	3	3	++	++
sdhB	JW0714	1-12D	C	white to lt pink	3	3	3	++	++
sdhC	JW0711	1-12A	C	dark red	6	6,5	4,3	++++,+++++	+++++,+++++
sdhD	JW0712	1-12B	C	dark red	6	6,6	4,3	+++,++++	+++,+++
sdiA	JW1901	1-10F	K	dark red	6	6	4	+++++	+++++
slp	JW3474	7-3E	M*	light red	4	3-4	4	++++	+++
speB	JW2904	89-5F	E	pink to orange	2	2-3	4	+++	++
srlR	JW2676	1-10G	K*	pink to orange	4	3-4	4	++	++
srmB	JW2560	7-9G	J	light red	4	3-4	4	++++	+++
sspA	JW3198	43-8A	O	pink to orange	3	3	5	++	++
sucA	JW0715	1-12E	C	pink (slow growth)	2	2(SG)	3(SG)	+/-	++
sucC	JW0717	1-12G	C	pink to orange	3	3	3	+	+
surA	JW0052	95-4C	O	light red	4	3-4	5	+++	++++
thyA	JW2795	93-3E	F	slow growth/other	1	1(VVSG)	1(VVSG)	slow growth	slow growth
tktA	JW5478	5-6A	G*	red	4	4	4	+++	+++
tolA	JW0729	61-12C	N*	light red	4	4,4	ND,4	++++,+++++	++,++++
tolB	JW5100	95-5A	N	white to lt pink	2	2,2	5,2	+,+/-	-
tolC	JW5503	79-4B	N	light red	3	3,3	4,4	+++,++	++++,++
tolQ	JW0727	95-7F	N	white to lt pink	2	2,2	5,5-6	+,+/-	-,-
tolR	JW0728	61-12b	N	white to lt pink	2	2-3	5	+	-
tomB	JW0450	81-9H	T*	pink to light red	3	3	3	+	++
torI	JW5387	69-3C	K*	pink to orange	3	3	4	++	+/-
tpiA	JW3890	3-6G	G	red	4	4	3	+++++	+++
tpr	JW1219	67-2B	J*	dark red	6	6	4	++++	++++(+)
treR	JW4200	1-8G	K	dark red	6	6	4	+++++	+++++
trpA	JW1252	41-4H	E	white to lt pink	2	2,1	3,3	+,+/-	+/-.+/-
trpB	JW1253	41-5A	E	white to lt pink	2	2	3	+	+/-
trpC	JW1254	59-8F	E	white to lt pink	2	2,3,2	3,3,4	NA,+/-,+/-	++++,-,-
trpD	JW1255	41-5B	E	white to lt pink	2	2,2	3,4	+,+	++,+/-
trpD	'	41-5B	'	'	'	3,2-3	4,3	+,+	++,+

trpE	JW1256	41-5C	E	white to lt pink	2	2,2	4	++,+/-	++,+/-
trpE	'	41-5C	'	'	'	3,3	4	+++,++	++++,++
truB	JW3135	61-5B	J	dark red	6	5-6	4	+++++	++++
ubiE	JW5581	43-8D	H	slow growth/other	1	1,2,1(SG)	2,1,2(SG)	-,+,-	-,-,-
ubiF	JW0659	25-8G	H	slow growth/other	2	2,2(SG)	2,2(SG)	+,+/-	+/-,-
ubiG	JW2226	95-7B	H	slow growth/other	1	1(SG),1(SG)	1(SG),1(SG)	ND,-	ND,-
ubiH	JW2875	79-10B	H	slow growth/other	1	1,1(SG)	1,1(SG)	-	-
uidC	JW1607	67-2E	G*	dark red	6	6	4	++++(+)	++++
uspE	JW1327	19-11H	T	light red/other	3	3-4	4	+++	+
wzxE	JW3766	49-3G	M*	pink to orange	3	3,3	4,ND	+++,++	++,++
xapR	JW2396	1-9D	K	pink to light red	6	6,5	4, 4	++,+++	+++, +++
ybaM	JW0455	15-5E	S*	light red	6	6	4	+++++	+++++
ybaP	JW0471	15-5G	S	dark red	6	5-6	4	+++++	+++++
ybcI	JW0516	15-6E	R	pink to orange	3	2-3	3-4	++	++
ybeZ	JW0657	65-4E	T	dark red	6	6	4	+++++	+++++
ybgC	JW0726	21-3D	R	light red	3	3	4-5	+++	+++
ycbR	JW0922	43-11A	U	red	6	5-6	4	+++	+++
ycgV	JW1193	23-7D	M	light red	3	3	4	++++	++++
yciC	JW1247	13-7G	S*	light red	4	3, 4	4, 4	+++, +++	++, ++
yciM	JW1272	95-1C	G	pink to orange	2	2,3,2	5,4,ND	+, ++,++	+++, ++,+/-
ydaF	JW1349	13-9G	S*	light red	3	2-3,2-3	4,4	++,++	+++
ydaM	JW5206	75-10G	T	white to lt pink	1	1	4	+	-
ydaT	JW1353	13-9H	S*	pink to orange	3	3,2-3	4-5,4-5	++++, ++	++,+++
ydbH	JW1376	13-10G	S*	pink to light red	4	4	4	+++++	++++
ydcI	JW5226	75-12C	K	white to lt pink	1	1	4	+	-
ydeJ	JW1530	19-9G	R	dark red	6	6	4	+++++	+++++
ydiT	JW1690	29-6D	C	light red	4	3-4	3	+++	++
yecH	JW1894	11-12A	R*	light red	4	4	4	+++++	+++++
yedQ	JW5832	87-9H	T	red	6	6	4	+++++	+++++
yedV	JW1951	3-11D	T	light red	3	3	4	++	+
yeeN	JW1964	19-8G	S	dark red	6	5-6	4-5	+++++	++
yeiL	JW2150	9-7G	T*	pink to orange	3	3	4	+	+/-
yeiR	JW2161	21-8E	R	dark red	6	6	ND	+++++	++++
yfcL	JW2322	9-10E	S*	dark red	6	5-6	4	+++++	++++(+)
yfeW	JW5495	77-11E	M	dark red	6	6,5-6	3,4	++++,++++	+++++,+++++

yfgC	JW2479	29-10D	R	dark red	6	6	4	+++++	+++++
ygfZ	JW2866	33-3E	R	slow growth/other	4	3-4	3	+++	+++
ygiU	JW2990	33-6G	T*	dark red	6	6	4	+++++	+++++
yhbJ	JW3172	35-2B	R	dark red	6	6,6	4	+++	+++++
yheV	JW3312	61-4C	S*	dark red	6	6	4	+++++	+++
yiaK	JW3457	29-12G	C	light red	2	2,2	4,4	+/-	-
yiaK	'	29-12G	'	light red	'	3-4,3-4	4,4	++++	+++
yicC	JW3619	35-12G	S	light red	3	2,3	4,4	++,++	++++,++
yieP	JW5068	87-1G	K*	white to lt pink	1	1	4	+/-	-
yjjW	JW4342	39-5F	O	light red	4	4-5	4	+++	+++
ykgH	JW0302	31-5F	S	light red	3	3-4	4	+++	++
ymgE	JW1184	49-11H	S	pink to orange	3	3	4	++	++
ymgE	'	49-11H	'	pink to orange	'	3-4	4	+	+
ynaK	JW1359	13-10C	K	light red	4	4	4	+++(+)	+++++
yncG	JW1449	81-6A	O	pink to orange	3	3	4	+++	+(+)
ynjD	JW5286	67-11H	R	light red	4	4	4	+++	+++++
yoeE	JW1980	25-2D	P	dark red	6	5-6,5-6	4,3	++++,+++++	+++++,+++++
yqaB	JW2665	23-1G	R	light red	4	4	3	++	+++
zraR	JW3968	5-2G	T	dark red	6	5-6	4	+++++	++++
			* Best pick / change		Commas delimit separate experiments in respective order. NA = not available				

Strains removed after second check.

Name	JW Strain	Keio Location	Primary COG Class	Original Color	Color For chart	Checked Color(s) at 26C (5 is WT)	Checked Color(s) at 37C (4 is WT)	CsgG Levels	CsgA Levels
alaS	JW2667	95-4B	J	light red	N/A	5	4	++++	++++
appB	JW0961	3-1G	C	red	N/A	5-6,5	3-4,4	++++,++++	+++++,++++
arnT	JW2251	21-9E	M	red	N/A	5	ND	++++	++++
aroF	JW2582	41-9F	E	red	N/A	5	4	++++	++++
atpD	JW3710	93-1F	C	red	N/A	4-5	5	++++	++++
bioH	JW3375	89-5D	R	red	N/A	4-5	4	++++	++++
btuD	JW1699	55-7D	H	dark red	N/A	5,5-6	4,4	++++,++++	++++,++++

cbpA	JW0985	45-9D	O	red	N/A	5,4,4	4,4,4	++++,++++,++++	++++,++++,++++
csgC	JW1026	91-3B	M*	red	N/A	5, 5	4, 3	++++	++++
cspC	JW1812	63-3F	K	light red	N/A	5	4	++++	+++(+)
cusS	JW5082	75-3A	T	red	N/A	5, 5	4, 4	++++	++++
emtA	JW5821	87-8F	M	red	N/A	4-5	4	++++	+++(+)
fecC	JW4249	57-3B	H	dark red	N/A	4-5	4	++++	++++
guaA	JW2491	95-6C	F	red	N/A	4-5,4-5,5-6,5	4,4,4,4	++++,++++,++++,++++	++++,++++,++++
ilvB	JW3646	41-11B	E	red	N/A	5	4	++++	++++
lpxL	JW1041	93-3C	M	red	N/A	5	ND	++++	NA
lpxM	JW1844	45-1G	M	red	N/A	5	ND	++++	++++
paaF	JW1388	43-4F	I	dark red	N/A	5	5	++++	++++
pagP	JW0617	81-4A	M*	red	N/A	5	ND	NA	++++
phoP	JW1116	3-10A	K	red	N/A	5	4	++++	++++
phoQ	JW1115	3-10B	T	red	N/A	5	4	++++	+++(+)
purT	JW1838	53-3B	F	dark red	N/A	5,5,5	4,4,4	++++,++++,++++	++++,++++,++++
pyrI	JW4203	53-6H	F	red	N/A	5	4	++++	NA
pyrL	JW4205	39-2G	K*	dark red	N/A	4-5	5	++++	NA
waaB	JW3603	83-10D	M	red	N/A	5,5,5	4,ND,ND	++++,++++,++++	++++,++++,++++
waaI	JW3602	45-5H	M	red	N/A	5,4-5,4-5,4-5	4,4,ND,ND	++++,++++,++++,++++	+++,++++,+++++,++++
waaL	JW3597	45-5E	M	red	N/A	4-5,4-5,5,5	4,4,ND,ND	++++,++++,++++,++++	++++,++++,ND,++++
waaQ	JW3607	45-6D	M	red	N/A	4-5,5,5	4,ND,ND	++++,++++,+++++	++++,++++,+++++
waaY	JW3600	45-5F	M*	red	N/A	5,5,5,5	4,4,ND,ND	++++,++++,++++,++++	++++,+++++,++++,++++
waaZ	JW3599	83-10C	M*	red	N/A	5,5,5	4,ND,ND	++++,++++,++++	++++,++++,++++
rph	JW3618	65-9H	J	red	N/A	5	4	++++	++++
tktB	JW2449	3-5F	G	red	N/A	5	4	++++	++++
ubiC	JW5713	71-10F	H*	light red	N/A	4	4	++++	++++
yceP	JW5152	75-7E	T*	light red	N/A	5	4	++++	++++
ycjU	JW1310	47-4F	R	dark red	N/A	5,5,5	4,4,4	++++,ND,++++	++,ND,++++
ygiH	JW3031	33-8H	S,I*	dark red	N/A	5	4	++++	++++
yhaK	JW3077	5-4E	R	red	N/A	4-5	4	++++	++++
yjiK	JW5869	89-2C	S	red	N/A	4-5	4	++++	++++
yniD	JW5911	67-11F	S*	light red	N/A	4-5	4	++++	++++
yoaE	JW1805	23-12H	N	light red	N/A	5	4	++++	++++
ypfG	JW2450	11-1C	S*	light red	N/A	4-5,5	4,4	++++	++++
yqeC	JW5464	69-5H	S*	dark red	N/A	5-6	4	++++	++++

yqiK	JW3023	33-8E	S	dark red	N/A	5	4	++++	++++
yecH	JW1894	11-12A	S*	pink to light red	N/A	4-5	4	++++	++++
argF	JW0266	41-3E	E	light red	N/A	5,4-5(dry),5	4,4,ND,ND	++++,+++++,+++++	++++,+++++,+++
argI	JW4211	65-12G	E	red	N/A	5	ND	++++	+++
aroG	JW0737	65-2F	E	red	N/A	5	4	+++++	+++++
aroL	JW0379	41-3G	E	red	N/A	5	4	+++++	+++++
crl	JW0230	43-9H	K*	red	N/A	5	4	+++	++++
fre	JW3820	43-8E	C	red	N/A	4-5	2	+++	+++(+)
fucO	JW2770	85-2B	C	light red	N/A	5	4	+++	+++
galM	JW0739	1-12H	G	red	N/A	5,5	4,4	++++,++++	+++++,+++++
gltA	JW0710	5-5F	C	dark red	N/A	5-6	4	+++(+)	+++
hisG	JW2001	41-7D	E	light red	N/A	5	4-5	+++++	++++
hns	JW1225	95-1A	K*	red	N/A	5, 5	4, 3	+++++,+++	++,+++++
lpxP	JW2375	59-12C	M*	red	N/A	5	ND	+++, -	+++
nanA	JW3194	41-10D	M	red	N/A	5	ND	++++	+++
pdxJ	JW2548	43-6H	H	light red	N/A	4-5	3-4	+++	+++
waaJ	JW3601	45-5G	M	red	N/A	4-5,5,5,5	4,4,ND,ND	++++,++++,++++,++++	++++,++++,+++++,+++++
waaS	JW3604	45-6A	M*	red	N/A	5,5,5,5	4,4,ND,ND	++++,++++,++++,++++	++++,+++++,+++++,++++
rpmE	JW3907	95-3H	J	red	N/A	5	4	++++	+++
rumA	JW2756	85-8B	J	dark red	N/A	5	4	+++++	+++
sbmC	JW1991	39-8F	L	dark red	N/A	5	4	+++	+++++
skp	JW0173	29-8D	M	dark red	N/A	5	4	++++	+++
sucD	JW0718	83-2D	C	dark red	N/A	5	1-2	++	+++
treC	JW4198	47-12E	G	red	N/A	4-5	4	+++	++++
ycfM	JW5157	75-7H	R	light red	N/A	5	4	++++	+++++
ydiZ	JW1713	31-11G	S*	dark red	N/A	5	4	+++++	++++
ygiF	JW3026	33-8F	S	dark red	N/A	6,5,5	4,4,4	+++++,+++++,+++++	+++++,+++,+++++
yiiS	JW3893	37-6B	S	red	N/A	5	3	++++	+++
yiiU	JW3899	37-6C	D*	red	N/A	5	4	+++++	+++++
yjbB	JW3980	83-7D	P	light red	N/A	5	4	++++	+++
ylcG	JW5076	79-11F	S*	red	N/A	4-5	4	+++++	+++++
ymjB	JW5203	67-9D	S*	dark red	N/A	5	4	++++	+++

Table 2.6 Phenotypes of Suppressor Strains with More Than One CR Phenotype and the Primers Used.

Gene	Strain	Location	Phenotypes	Predominate Phenotype (>4:1)	PCR Gel	PCR Results	Upstream Primer	COG Family
bhsA	JW1098	13-5H	1,5	white	8	both correct	GAG AAG TCG CTT CAT AAC CG	M*
btuC	JW1701	55-7F	3,5	-	13	both correct	CGC TTA CAA AAG CTG AAA TGT C	H
cysH	JW2732	47-7G	3.6	dark red	10	both correct	CGA AAC ATG GTG TCA GCG	H
dcuC	JW0616	89-4A	3,5	pink	9	both correct	CGA GAT ACA ACA ATC ATC TTA ACG	C
dnaQ	JW0205	53-11C	1,2,3,4	white	13	all correct	GCA TCA AGA CGT TGC CAG	L
fepE	JW0579	41-2A	2,6	light pink	J3,16	both correct	CTG TTT GTT GCT GAA CGC	P,M
flhC	JW1880	45-2B	3,5	pink	13	both correct	GTG AAA CCG CAT AAA AAT AAA GTT GG	K*
fliG	JW1923	45-3A	2,5	-	3	both correct	GCT CAA TGT CGT TAA CTC G	N
glcD	JW2946	47-9B	3,4	pink	13	both correct	GCG TAC TGA ACA GAT GGA TC	C
gshB	JW2914	43-7H	4,5	lt red	6	both correct	GCG TTA AAC TGG ATA GTG AAC G	H
gsiA	JW5897	75-5A	2,5	light pink	10	both correct	GCG GAA TGA CCA ATA AAT TAC C	H*
hepA	JW0058	7-9C	3,4	pink	7	both correct	CGA TGA AGA AAA CCA AAA GCG	K
hycI	JW2687	9-2H	3,5	pink	4	both correct	GAA AAG GTG GTG TTC AGT CAA C	C
hypE	JW2700	85-1H	3,5	pink	8	both correct	CGA TTG CCG ATG TGT TCT G	O
kbl	JW3592	47-10F	3,5	pink	1	both correct	CTA TCT GGG GAG AGG AAA ATG G	H
manY	JW1807	85-6E	3,5	-	4	both correct	CAC ACG TAG TTG ATG TTG C	G
mfd	JW1100	39-7C	3,5	pink	15	both correct	GCT GAA TGT GAT TGG CTC C	L*
mppA	JW1322	59-9B	2,5	light pink	1	both correct	CGG CAT TCT CAT TAT TTA TAG ATA GG	E
mutL	JW4128	39-9E	2,3,5	-	J1	all correct	GTC TGA CCC CTA TTT AAG CC	L
nuoH	JW2277	3-4E	5,6,1	-	6	all correct	CAA ATT CCA GGA CGA AGT GG	C
nuoI	JW2276	3-4D	2,5,6	dark red	12	all correct	CCG CAA TTC TTT GGT TTT ATT ACC	C
nuoL	JW2273	3-4A	2,5,6	-	10	all correct	GCC AAT CAG TGC TAA AGC	C
pdxB	JW2317	43-6F	*1 mucoid,5*	wild type	*5,17*	both correct	*CGC CAG ATT ATG CTC AGC*	H*
purN	JW2485	53-4F	2,5	light pink	8	both correct	GGT AAG CCA TTA GCC GAT C	F
qseB	JW2993	5-1B	2,6	light pink	J1	both correct	GCA TCT TTG AAC ACG TAG AGA TC	K
rbsK	JW3731	53-1E	2,4	-	2	both correct	GCG CAG AAT GAT GAA ATG G	G
rbsR	JW3732	1-10E	2,5	wild type	10	both correct	CCA TCA AAA TAA GAC TAT CGT TGC	K
rdgC	JW0384	19-5F	3,5	pink	4	both correct	GTC TTT ATC GAA TGG CTG ACC	L
rlmF	JW5107	75-4F	3,6	pink	3	both correct	CAG GTT ACT CAT CGG TTG C	J*

rnk	JW0602	49-6E	2,5	light pink	3	both correct	GCA GTT AAG CTA ACG TGC	K
rssB	JW1223	3-10E	*3,5*	pink	*12,16,17*	*NONE*	*GAA TGG TGA TTC TCT GCC G*	T
rsxC	JW1621	81-6D	2,5	light pink	J1	both correct	GAA GCC ATC AGC TGT AAC G	C
sbcD	JW0388	49-5F	3,5	pink	9	both correct	GGT GTT TGA TGA ACT GGA TAC C	L
sfcA	JW5238	77-1B	2,5	light pink	15	both correct	CGG CAA CCT AAT TTA GGG G	C
ssnA	JW2847	61-1F	*2,5*	light pink	J2,16	both correct	*GTA ACT ACG TTT GCA GCA AG*	R*
sucB	JW0716	1-12F	2,6	dark red (SG)	15	both correct	GTA GTG ATG TGT TCT GGT AAG G	C
tonB	JW5195	67-9A	2,5	light pink	7	both correct	CCC TGG ATC GTT ACT GTC	M
uup	JW0932	55-3C	3,4-5	pink	7	both correct	GCA ACC TGC GTC TGA ATG	R
wcaD	JW2041	43-5F	3,5	pink	9	both correct	GGC GAC AAA ATT GAA CTG C	M*
ybaB	JW0460	25-7F	2,5	lt pink	14	both correct	GCT ACC AAA ACT GGT CGA AC	S
ybjN	JW0837	15-10H	3,5	pink	11	both correct	GAT TTT CGT TCC AAT TTG CAT CG	R*
ycbL	JW0910	23-3C	3,5	pink	14	both correct	GGC TAT ATT CAG GAA GAA TTG GC	R
ycbQ	JW5122	67-7H	3,5	pink	11	both correct	GAG AAG GAA AGC GAG GAC	U
yciU	JW1240	17-1F	2,5	light pink	5	both correct	CGA TGA TTT ACT TCA TGC GAT TTG	S*
ydeP	JW1495	81-6B	3,5	pink	5	both correct	CAG GAA ACA AGG TTT CAG C	C
ydfD	JW1567	11-6D	3,5	pink	11	both correct	CGG TAT CAG TTT TAC TCC GTG	S*
ydiY	JW1711	11-8F	3,5	-	J3,16	both correct	GGA TAA ATT TGC GGG GTA ATT G	M
ydjI	JW1762	19-9H	1 mucoid,5	wild type	14	both correct	CTA TTG CAC GCT GTC AGC	G
yebY	JW1828	11-10F	3,5	pink	12	both correct	CGA TTC ACC TGA TTT GTG C	S*
yehE	JW2099	13-2A	3,6	pink	1	both correct	GGT GGT GCA GAG AAA CTG	S*
yfjW	JW2623	11-3G	3,5	pink	8	both correct	CAT CCA CGG AGA TCA TAA CG	R*
yjbI	JW3998	37-8B	3,5	pink	4	both correct	CTA AGA ATA TCC ATT ATC TCA ATG CC	S
ynfH	JW5261	67-11B	5,6	-	15	both correct	GCA ATG CAT AAG CGT GAA G	C*
cmk	JW0893	49-7C	1,2	white	J1	both correct	GCG CTA TCA ATG CTA AAT ACT CC	F
fabF	JW1081	49-2E	2,3	light pink	3	both correct	CGA AAA CCA TCG CGA AAG C	Q
mdoG	JW1035	65-4H	3,1 mucoid	pink	5	both correct	GGT TCA TAT ATG GTT AAC TAA TCT CGG	M*
pgm	JW0675	5-5E	1 mucoid,2 mucoid	lt pink mucoid	12	both correct	GCC GGT CAA AAC GAT TAA AGA C	G
trpD	JW1255	41-5B	2,3	light pink	9	both correct	CCA AAG TTG ACC GTT ATT CC	E
trpE	JW1256	41-5C	2,3	light pink	11	both correct	CGT GAA ATT TCC TCT CTT GC	E
yiaK	JW3547	29-12G	2,3	light pink	14	both correct	GCA ATA AGC GAT GGA CGG	C

ymgE	JW1184	49-11H	3,3-4	pink	7	both correct	CGA TGT TGT CTT CGG CTT G	S
fhlA	JW2701	85-2A	3,5	pink	6	only 3's	GGT TGT GGT ATT GAA CTT TCA G	K
sdhC	JW0711	1-12A	2,6	dark red	J2	only 6	GCA TTA TAT GCT TTT CCT GGT AAT G	C
sdhD	JW0712	1-12B	3,6(SG)	-	6	only 6(SG)	CAT GTG GGC GTT ATT CAT GAT AAG	C
								* Best guess or changed

Table 2.7 Cellular localization of identified gene products.

	Number	
Location	**(% tot.)**	**Gene(s)**
Cytoplasmic	211 (75.6)	*aaeR, aceE, aegA, arcA, argC, aroA, aroB, aroC, aroD, aroE, aroH, aroK, asnC, aspA, aspC, atpA, atpC, atpG, atpH, carA, carB, ccmA, clpA, clpP, clpX, cmk, cpxR, crp, csgD, cusR, cyaA, cysB, cysC, cysE, cysG, cysI, cytR, dam, ddpD, dksA, dnaG, dnaK, dnaT, dps, efp, fabF, fabH, fadH, fadJ, fbp, fepC, fes, fhlA, flgM, fliI, fliT, fruR, galU, gcvA, glmM, glnA, glxK, gmhB, gmr, gnd, greA, guaB, hdfR, hfq, hybD, ihfA, ihfB, ilvG, lipA, lipB, lon, lpcA, lpd, lptB, lsrF, metC, miaA, mlrA, mtlR, nagA, nagC, nagK, nanE, nanK, ndk, nudC, nudH, nudL, nuoB, nuoC, nuoE, nuoF, nuoG, nusB, ompR, paaI, pcnB, pdxH, pepT, perR, pgm, php, poxA, priA, ptsH, ptsI, purA, purC, purD, purE, purF, purH, purK, purL, purM, purR, purU, putA, puuR, pyrB, pyrC, pyrD, pyrE, pyrF, racC, rbfA, rcsB, rffA, rffC, rffT, rimK, rimM, rnhA, rplA, rpoN, rpoS, rpoZ, rpsF, rpsT, rsgA, rstA, sdhA, sdhB, sdiA, speB, srlR, srmB, sspA, sucA, sucC, thyA, tktA, tomB, torI, tpiA, tpr, treR, trpA, trpB, trpC, trpD, trpE, truB, ubiE, ubiF, ubiG, ubiH, uspE, waaC, waaD, waaE, waaF, waaG, waaH, waaP, xapR, ybaM, ybaP, ybeZ, ybgC, ycgV, ydaF, ydaM, ydaT, ydcI, ydeJ, ydiT, yecH, yeeN, yeiL, yeiR, yfcL, ygfZ, ygiU, yhbJ, yheV, yiaK, yicC, yieP, yjjW, ynaK, yncG, ynjD, yoeE, yqaB, zraR*
Periplasmic	11 (3.9)	*cpxP, csgE, csgF, fepB, mdoG, surA, tolB, ycbR, yciM, yfeW, yfgC*
Integral Membrane Proteins	35 (12.5)	*appC, aroP, atpB, atpE, cmr, cpxA, eamA, envZ, essQ, fepD, fepG, kdpD, mdoC, mdoH, narQ, nhaA, nuoA, nuoJ, nuoK, nuoM, nuoN, proW, qseC, rfe, rseA, sdhC, sdhD, tolQ, wzxE, ybcI, yciC, yedQ, ykgH, ymgE, rstB*
Membrane Anchored	8 (2.9)	*atpF, cusB, glvG, rodZ, tolA, tolR, yedV, ydbH*
Outer membrane Lipoproteins	8 (2.9)	*csgG, lpp, mltA, nlpD, pal, rcsF, slp, mltB*
Outer Membrane ß-barrel proteins	4 (1.4)	*ompC, ompF, tolC, uidC*
Extracellular	2 (0.7)	*csgA, csgB*

Table 2.8 Genes required for or known to affect curli production.

Gene	Effect on Curli production	Source	Color in screen
cpxA,R	-	(126, 173, 174)	WT, dark red
crl	+	(234-236)	WT
csgA,B	Fiber subunits	(76, 114)	white
csgC	Fiber morphology [b]	(123)	WT
csgD	*csgBAC* transcription	(114)	white
csgE,F[a],G	Secretion, chaperone	(76)	white
ddhC (rfbH)	+ [d]	(144)	N/A [e]
dksA	+ [o]	(128)	pink
envZ	+	(174, 237)	white
hns	variable [j]	(65, 126, 237, 238)	WT
ihfA,B	+	(126, 237)	light pink
fis	- [f]	(239)	WT
flhC,D	-	(206)	WT[l]
fliZ	-	(206)	WT
lon	+	(240)	mucoid white
lpp	+ [f]	(241)	light red
lpxM (msbB)	+ [f]	(145)	WT
mlrA	+	(72)	white
nagA [o],C	+	(127, 128)	pink
ompR	+ [o]	(115, 126, 128, 174, 237, 240)	white
pal	+ [c]	(240)(68)	light pink
rcsA,B,C	-	(174, 240, 242)	WT[m]
waaG	+ [d]	(144)	light pink
rpoS	+	(65, 115, 235, 238)	white
rssB	+ [o]	(128)	pink & WT [n]
rstA,B	-	(126, 243)	pink, dark red
qseB,C	none, +	(205)	variable, dark red
sdiA	-	(244)	dark red
tolA,B,Q,R	+	(240)	light pink
ycfR	+	(232)	white & WT [g]
ymgA (ariR)	- (via Rcs)	(245)	WT
ymgB [p]	- (via Rcs)	(245)	WT
Cyclic-di-GMP (GGDEF or EAL)			
***adrA* (*yaiC*)**	+ [i]	(246)	WT [i]
ycgF	- (via Rcs)	(71, 245)	WT
***yciR* (*gmr*,STM1703)**	-	(71, 247, 248)	pink to light red[h]

ydaM	+	(71, 248)	white
yeaP	+	(71)	WT
yedQ	Cellulose only[k]	(71, 86, 248)	dark red
***yegE* (STM2123)**	+	(71, 206, 246)	WT
yhdA	+	(71)	WT
***yhjH* (STM3611)**	-	(71, 206, 246, 247)	WT
***yjcC* (STM4264)**	-	(247)	WT
STM3388	+	(246)	N/A[e]
STM1827	-	(247)	N/A[e]
STM4551	+	(249)	N/A[e]

Notes: Genes in bold had different CR phenotypes compared to results found in the literature.
Bas(R) and Zur were also listed as primary transcription factors, those that directly regulating curli specific genes (250); however, we were unable to find supporting data in the indicated article (126). a Some curli production occurs but is not cell associated (94). b Larger, more stable fibers (123). c Inferred from (240). d In *Salmonella enterica serovar Typhimurium* (DT104 Rv or LT2)(144). Abequose is not used for *E. coli* O-antigens (251). e No homolog in BW25113 (102, 152). f In *Eschrelichia coli* O157:H57 EHEC strain 4304. g Mostly white colonies with few red suppressors. h Pink to light red on CR plates but WT levels of CsgG and CsgA. i AdrA is also regulated by CsgD (77); positive feedback on CsgD was seen in *S. Typhimurium* MAE52 but not UMR1 (246). j (-) in *E. coli* K-12 (+) in *S. typhimurium*. k No effect when tested in *E. coli* W3110, a BW25113 relative (71, 102, 252). l *flhC* had mostly pinkish/light red colonies with a few WT colonies. m *rcsF* is dark red. n Mostly pink colonies with few red suppressors. o Found in screens for additional genes affecting curli production (128). p *ycgZ*, the mutant of which was WT for curli here, antagonizes the repression of curli through *ymgB*; however, *ycgZ* itself does not influence *csgB* transcription or curli production. Table 2.5 excludes the RNAs *omrA* and *omrB* which postranscriptionally inhibit *csgD* translation (253).

Table 2.9 CsgD regulon excluding *csgBAC* and *csgDEFG*.

Activates/Increases/Required	Represses/ Decreases	Evidence	Strain	Ref
adrA(*yaiC*), *yhiE, yjbR, chbG*(*ydjC*), *recT*	*yagS, pepD, glnS, thyA*	Microarray, Lux fusions, Primer extension	*E. coli* MG1655/ ompR234 strain*	(254)
adrA(*yaiC*), *gsk, iraP*(*yaiB*), *yjgW, ymdA, yoaD, ytfI, glyA*	*cspA, cspB, cspG, fecR, fhuE, gatA, gatC, gatZ,* (*gatY, gatB, gatD*)†, *infA, metA,* <u>*ompF*</u>*, ompT,* <u>*pyrB*</u>*, pyrI, pepD,* <u>*dps,*</u> <u>Dps</u>	Microarray, RT-PCR, Mass Spec of PAGE gel band	*E. coli* MG1655/ pT7-CsgD*	(255)
glyA, GlyA		Increased SHMT activity, β-Galactosidase	*E. coli* MG1655/ CsgD expression plasmids	(256)
hmp, glyA		β-Galactosidase	*E. coli* K-12	(257)
yiHU-O-yshA‡	*yihVW*‡	Activity *csgD* strain Luciferase	*S. enterica* serovar Enteritidis	(258)
PflB, GadA, WrbA, <u>Dps</u>, OmpW, <u>*dps*</u>*, pflB, osmB,* <u>RpoS</u>, *iraP*(*yaiB*)	TnaA, GatZ, GatY	SDS-PAGE, MALDI-TOF, RT-PCR, Western Blots	*E. coli* MG1655/ pT7-CsgD*	(259)
adrA		Very Low activity in a *csgD* strain, β-Galactosidase	*S. typhimurium* ATCC14028	(216)
bapA		Low levels in a *csgD* strain RT-PCR	*S. enterica* serovar Enteritidis	(260)

adrA, rpoS, rpoD, pckA, fbaA, sdhCDAB, mdh, maeB, ppsA, fbaB, *fumAC, fbp, pgmI, gapA, gpmA,* ***yehZYWX, osmY, osmE, kdpFABC,*** *otsBA, proP,* ***wrbA, STM4267,*** *yghA, sodA, STM0402, cadBA,* ***entCEBA, fhuA,*** *fhuF****,yrbFEDCB, oppABCDF, lsrACDBFGE, gltIJKL,*** *argT****, gcvTHP, fadBA, glnA, csrA,*** *yncE, yqhE, adk,* **GlpX, YrbC, OppA, GltI, MglB, UgpB, DppA, RbsB, GcvT, WrbA, SodA, STM0402**		Relative to a *csgD* strain Luciferase, MALDI-TOF proteome analysis	*S. typhimurium* ATCC14028	(232) **
csgBA, yccT, adrA, wrbA(data not shown)	*fliE, fliFGHIJK, yhbT*	β-Galactosidase	*E. coli* BW25113 or *csgD*/pBADcsgD	(75) ***
csgA, csgB, csgD, adrA, flgB, fliC, SMT3670	*fimC*	Microarray, RT-PCR	*S. typhimurium* UMR1 & MAE50,2	(261) ****

Underlined had altered curli production (Table 2.5 or 2.6) and include *sdhCDAB, fbp, glnA, dps, ompF, pyrB, rpoS, lsrF, fliG, and fliI.*

† Not listed in main table, levels down 2.7 to 3.3 fold (255).

‡ *yihVW* and *yihU-PyshA* are divergent operons.

* Higher levels of CsgD (262).

** Only listed genes with P values >0.05. Bold genes are <2.0 fold change. Genes with P >0.05 include *mlrA, aceBA, sucAB, glpFKX, proP, proVWX, soxS, gshA, speA, spec, speB, mglBAC, ugpBAECO, fliY, dppABCDE, rbsDACBKR, ppa* Metabolites higher in WT: Glucose, Trehalose1, Glutathione, Betaine, Acetamide, Glutamate, NAD+, Octanoic acid, Carnitine, Imidazole, Glycogen, Methionine, Glycerol-3-osphate, Galactose, Mannose, Pyroglutamate, and Galactinol. Metabolites higher in *csgD*: Succinate, Fumarate, AMP, Malate, Cadaverine, Putrescine, Proline, and Adenine.

**** In contrast to *S. enterica serovar Enteritidis*, the *bapA* and capsule operons (258, 260) were not regulated in *S. typhimurium*.

*** The use of ChIP on chip, generating a consensus sequence, and DNase protection assays revealed several new CsgD binding sites, most within intergenic regions. Not all of the possible twenty regulons are listed here as only a few were assayed for transcription activity

Table 2.10 40 Largest Intergenic Regions in *E. coli* and the Number of Transcriptional Binding sites in Divergent Intergenic Regions

Name	Length	Orientation	L_END	R_END	Cs
nanC_fimB	1455	Divergent	4537525	4538979	97.8
ygcE_ygcF	1372	Convergent	2901397	2902768	62.53
iap_ygbF	950	Convergent	2875641	2876590	61.98
lrhA_yfbQ	919	Divergent	2404664	2405582	51.83
dppA_proK	910	Codirectional-	3705729	3706638	79.87
betT_yahA	874	Codirectional+	330721	331594	7.13
yiiD_yiiE	858	Codirectional+	4076462	4077319	87.86
mngB_cydA	846	Codirectional+	769835	770680	16.59
hdeD_gadE	798	Codirectional+	3655591	3656388	78.79
araF_ftnB	796	Divergent	1984153	1984948	42.76
matA_ykgL	775	Divergent	310561	311335	6.69
ycgV_ychF	768	Codirectional-	1255176	1255943	27.05
csgD_csgB	**754**	**Divergent**	**1102420**	**1103173**	**23.76**
essQ_cspB	753	Codirectional-	1638610	1639362	35.32
ydfJ'_ydfK	753	Divergent	1630310	1631062	35.14
ypjC'_ileY	750	Codirectional-	2783034	2783783	59.98
yncH_rhsE'	749	Codirectional+	1525177	1525925	32.87
ychE_oppA	737	Codirectional+	1298469	1299205	27.99
ycdU_serX	735	Convergent	1096053	1096787	23.62
eco_mqo	714	Convergent	2302416	2303129	49.62
gltA_sdhC	708	Divergent	753692	754399	16.24
ynaE_ttcC'	700	Codirectional-	1432282	1432981	30.87
iraM_ycgX	699	Codirectional-	1211227	1211925	26.11
dinQ_arsR	694	Divergent	3645857	3646550	78.58
yfcV_sixA	680	Codirectional-	2453669	2454348	52.88
yjiC_iraD	672	Divergent	4554344	4555015	98.16
yobF_yebO	669	Codirectional-	1905616	1906284	41.07
stpA_ygaW	668	Divergent	2796518	2797185	60.27
leuL_leuO	659	Divergent	83709	84367	1.8
wza_yegH	658	Divergent	2135268	2135925	46.02
yjdN_yjdM	657	Codirectional-	4323765	4324421	93.19
gltP_yjcO	641	Convergent	4293818	4294458	92.55
nuoA_lrhA	630	Codirectional-	2403095	2403724	51.79
arsC_yhiS'	628	Codirectional+	3648686	3649313	78.64
yjjP_yjjQ	618	Divergent	4600882	4601499	99.16
atpI_rsmG	616	Codirectional-	3920464	3921079	84.5
yaiS_tauA	615	Divergent	383841	384455	8.27
purH_rrsE	614	Divergent	4205556	4206169	90.64

Table 2.11 Congo Red phenotypes of Keio strains on YESCA and CFA plates or CFA plates without Coommassie Brilliant Blue.

Set A	Niba Results	24H			48H			72H			Different
Name		YESCA CR	CFA CR	CFA 2XCR	YESCA CR	CFA CR	CFA 2XCR	YESCA CR	CFA CR	CFA 2XCR	
flhC lt	+	3	3	3	3	3	3	3	3	3	Yes
flhC WT	+	4-5	5	5	4	5	5	4-5	4-5	5	no
fliG lt	+	2	2	2	3	2	2	3	3	2-3	Yes
fliG WT	+	4-5	4-5	4-5	4-5	5	5	5	5	5	no
fliI	+	6	6	6	6	6	6	6	6	6	Yes***
fliT	+	3	3-4	3	3	3-4	3	2-3	3	3	Yes
btuC lt	Not Tested	2	2	2	2	2	2	2	2	2	
btuC WT	Not Tested	4-5	4-5	4-5	4	4-5	5	4-5	4	4	
btuB	variable	4-5	4-5	4-5	6	5	6	4-5	5	5	unclear
csgA	-	1	1	1	1	1	1	1	1	1	no
csgB	-	1	1	1	1	1	1	1	1	1	no
csgC	Not Tested	4-5	4-5	4-5	5	5	5	6	6	6	
csgD	-	1	1	1	1	1	1	1	1	1	no
csgE	-	1	1	1	1	1	1	1	1	1	no
csgF *	+	1	1	1	1	1	1	1	1	1	Yes*
csgG	-	1	1	1	1	1	1	1	1	1	no
surA	+	2-3	3	3	3-4	3-4	4-5	4	4	4	Yes****
dnaK	+	1	1-2	2	2	2	2	2-3	2	3	Yes
fruR	+	2	1-2	2	2	2	2	3	2	2	Yes
gcvA	+/-	2	2	2	2-3	2-3	2	3	3	2	no
greA	+	2-3	2-3	2-3	3	3	3	4	4	3	Yes
Set B	**Niba Results**	**24H**			**48H**			**72H**			**Different**
Name		YESCA CR	CFA CR	CFA 2XCR	YESCA CR	CFA CR	CFA 2XCR	YESCA CR	CFA CR	CFA 2XCR	
lpcA	+	1-2	1	1	1-2	1	1-2	2	1	1-2	Yes
gmhB	+	2	2	1	2	1	1	2	1	1	Yes

waaC	Not Tested	2	2	1	2	1	2	2	1	2	
waaD	+	2	2	2	2-3	2	3	2-3	1-2	2	Yes
waaE	+	1-2	1	1	2	1	1-2	2	1	1-2	Yes
waaF	+	1	1	1	1	1	1	1	1	1	Yes
waaG	+/-	1	1	1	1	1	1	1	1	1	no
waaH	+	2-3	3	3	3	3	3	3	3-4	4-5	Yes****
waaP	+	2-3	3	3	3	4	3	3	4	3	Yes
galU	+	1	1	1	1	1	1	1	1	1	Yes
hfq	+/-	1	1	1	1-2	2	2	2-3	3	3	no
hsrA/yieO	-	3-4	4-5	4	5	5	3-4	4	4	4	Yes****
yieP	Not Tested	1	1	1	1**	1**	1**	1**	1**	1**	
lon	-	1 mucoid	1 mucoid	1 mucoid	1 mucoid	1 mucoid	1 mucoid	1 mucoid	1 mucoid	1 mucoid	no
mdoH pink	+	3	4-5	4	3-4	4	3-4	3	5	4	Yes****
mlrA	-	1	1	1	1	1	1	1	1	1	no
nagA	+	2	3	3	2-3	2-3	2	2	3	3	Yes
nifU/iscU	+/-	3	3	3	3-4	4	3	3-4	4	4	no
ompR	-	1	1	1	2	2	2	2	2	2	no
rpoS	-	1	1	1	1	1	1	1-2	1-2	1-2	no
nlpD	-	1	1	1	1	2	1-2	1	2	2	no
Set C	**Niba Results**	**24H**			**48H**			**72H**			**Different**
Name		**YESCA CR**	**CFA CR**	**CFA 2XCR**	**YESCA CR**	**CFA CR**	**CFA 2XCR**	**YESCA CR**	**CFA CR**	**CFA 2XCR**	
crp †	+/-	6	6	6	6	5-6	5	4-5	4-5	4-5	Yes*****
cyaA	-	1-2 slow	1 slow	1 slow	1 slow	1 slow	1 slow	1 slow	1 slow	1 slow	no
sdhC	+	6	5	6	5-6	5	5	5-6	5	5	Yes***
tolA	+	3-4	4	4	4	4	4-5	4	5	5	Yes****
tolB	+/-	2	2	2	2	2	2	2	2	3	no
tolR	+/-	2	2	2	2	2	2	2	2	3	no

ycfM	+	2-3	3	3	3	3	3	3	3	3	Yes
yciB	+	3	4	4	5	5	5	4	4	4-5	no
yciC	Not Tested	3	3-4	3-4	4	5	4	4	4	4	
yciM	+/-	2	2	2	2-3	2	2-3	2-3	2-3	3	no
ydaM	+/-	1	1	1	1	1	1	1	1	1	no
ynjC	+	3	3-4	3	3	4	3-4	3	4	4-5	Yes****
ynjD	Not Tested	6	6	6	6	6	6	6	6	6	
ptsI	+	1-2	2	2	1	1-2	1-2	1	1	1	Yes
ihfB	-	1	1	1	1-2	1-2	2	2	2	2	no
mdoH mucoid	+	2**	2-3**	2-3**	2**	2-3**	2-3**	2-3	3	3	Yes
lpxL	Not Tested	3-4	3-4	4	5	5	5	4-5	5	5	
lpxM	Not Tested	3-4	3-4	4	5	5	5	5	5	5	
lpxP	Not Tested	4-5	3-4	5	5	5	5	5	5	5	
crcA/pagP	Not Tested	4-5	3-4	5	5	5-6	5	5	5	5	
arnT	Not Tested	3-4	3-4	4	4-5	4-5	5	5	5	4-5	

**csgF* has red fibers underneath the colonies in the agar and can appear pinkish
All strains in Table 2.6 were tested for this phenotype and only *csgF* displayed it.
**Somewhat mucoid
*** Niba et al did not test for higher curli expression
**** May be due to plate differences(Yesca vs CFA) or dye differences (CR w CBB vs 2XCR) or time (48 vs 72 hours)
†*crp* was found to have suppressor mutation. A fresh strain looked like *cyaA.*

Table 2.12 CsgD protein and Transcript levels Relative to WT.

Strain	CR phenotype	WB 1	WB 2	WB 3	*csgD* transcripts relative to WT	CsgD protein levels relative to WT
BW25113	red	1.0000	1.0000	1.0000		
csgD	white	0.0126	0.0055	0.0135		
nhaA	white	0.0142	0.0082		Decreased	Decreased
php	white	0.9445	0.9423		Unchanged	Unchanged
purD	white	-0.0439	0.0155		Decreased	Decreased
lon	white	0.1457	0.1527		Decreased	Decreased
waaC	light pink	0.6878	0.5203	1.0482	Unchanged	Decreased
dnaK	light pink	0.0816	0.1182		Decreased	Decreased
speB	light pink	0.5322	0.7222		Decreased	Decreased
hfq	light pink	-0.0398			Decreased	Decreased
aroA	light pink	0.1219	0.2532		Decreased	Decreased
fabH	pink	0.4979	0.8522		Unchanged	Decreased
flgM	pink	0.6672	1.0713	0.4800	Unchanged	Decreased
ddpD	pink	1.0434	0.6480		Unchanged	Unchanged
pyrC	pink	-0.0468	0.0369		Decreased	Decreased
nagA	pink	0.6095	0.5059		Unchanged	Decreased
fhlA	pink	0.9006	0.8524		Decreased	Decreased
dksA	pink	0.8364	0.7521	0.6623	Unchanged	Decreased
hybD	pink	0.6723	0.6738		Decreased	Decreased
gmr	pink	0.4931	0.4825		Unchanged	Decreased
rstA	pink	0.6088	0.4164		Decreased	Decreased
priA	light red	0.0413			Decreased	Decreased
aaeR	light red	0.9616	1.2935	0.8055	Increased	Unchanged
glvG	light red	0.7299	1.1921		Unchanged	Unchanged
cmr	light red	1.2507	0.8003		Unchanged	Unchanged
dam	light red	0.6988			Unchanged	Decreased
hdfR	light red	0.4839	0.8262		Unchanged	Decreased
mltA	light red	0.6086	0.6473		Unchanged	Decreased
cysB	dark red	0.6711	0.4694	0.5832	Increased	Decreased
pcnB	dark red	1.9168	0.8719		Increased	Increased
truB	dark red	1.1641	1.7952	0.7562	Unchanged	Increased
rcsB	dark red	1.5940	1.1027	0.7657	Increased	Increased
sdiA	dark red	1.7794	0.8559		Increased	Increased
fes	dark red	0.4200	0.4536	0.3477	Unchanged	Decreased
nuoA	dark red	1.2107	0.8432		Unchanged	Unchanged
qseC	dark red	0.9838	1.7053		Unchanged	Increased
arcA	dark red	2.1738			Increased	Increased
mdoC	dark red	0.9017	0.6071		Increased	Unchanged
perR	dark red	0.7418	0.9590		Increased	Unchanged
cusB	dark red	1.1105	0.6361		Increased	Unchanged

Table 2.13 Strains, plasmids, and primers used.

Strains			
Strains	**Genotype or Description**	**Ref, Source†**	**CR Phenotype**
			Notes
BW25113	*rrnB3 ΔlacZ4787 hsdR514 Δ(araBAD)567 Δ(rhaBAD)568 rph-1*	(102), JM	WT
MG1655	$F^- \lambda^-$ *ilvG- rfb-50 rph-1*	(263), SH	Like BW25113
UTI89	MedImmune UPEC isolate.	(264), SH	Makes celluose
NU14	Cystitis isolate.	(265), SH	
C600	F- *thr leu thi lac tonA*	(266), SH	Like BW25113
MC4100	F^- *[araD139]$_{B/r}$ Δ(argF-lac)169* &lambda$^-$ e14-flhD5301 Δ(fruK-yeiR)725 (fruA25)‡ relA1 rpsL150(strR) rbsR22 Δ(fimB-fimE)632(::IS1) deoC1*	(267, 268), SH	Like BW25113, nonmotile
Keio library	3985 single-gene deletions of *E. coli* K-12 strain BW25113. Each is *gene::*FRT-kan-FRT	(102)	variable
curli-	BW25113 *csgGFED_BAC*::FRT-*kan*-FRT	this study	No curli
cpxR::FRT	BW25113 *cpxR::FRT*	this study	Like *cpxR*
cpxR::FRT waaG	BW25113 cpxR::FRT waaG::FRT-kan-FRT	this study	Like waaG
nhaA::FRT	BW25113 nhaA::FRT	this study	Like nhaA
nhaAR	BW25113 nhaAR::FRT-kan-FRT	this study	More curli than nhaA
nhaAR::FRT	BW25113 nhaAR::FRT	this study	Like nhaAR
nhaA::FRT cpxR	BW25113 nhaA::FRT cpxR::FRT-kan-FRT	this study	More curli than nhaA’
nhaAR::FRT cpxR	BW25113 nhaAR::FRT cpxR::FRT-kan-FRT	this study	More curli than nhaAR’
nhaA::FRT osmC	BW25113 nhaA::FRT osmC::FRT-kan-FRT	this study	Like nhaA
nhaA::FRT pgaA	BW25113 nhaA::FRT pgaA::FRT-kan-FRT	this study	Like nhaA
nhaA::FRT pgaC	BW25113 nhaA::FRT pgaC::FRT-kan-FRT	this study	Like nhaA
nhaA::FRT flhC	BW25113 nhaA::FRT flhC::FRT-kan-FRT	this study	Like nhaA
nhaA::FRT flhD	BW25113 nhaA::FRT flhD::FRT-kan-FRT	this study	Like nhaA
nhaA::FRT fliZ	BW25113 nhaA::FRT fliZ::FRT-kan-FRT	this study	Like nhaA
nhaA::FRT yhjH	BW25113 nhaA::FRT yhjH::FRT-kan-FRT	this study	Like nhaA
JM4962	BW25113 *relA*::FRT	(204), JM	
JM4977	BW25113 *relA*::FRT *ΔspoT207::cat*	(204), JM	Like *relA*::FRT
ΔrelA251::kan	MG1655 *ΔrelA251::kan*	(204, 269), JM	

CF1693	MG1655 *ΔrelA251::kan ΔspoT207::cat*	(204, 269), JM	
Plasmids			
pTrc99a	Expression vector.	(270), SH	
pQE-70	Expression vector.	Qiagen	
pMC1	*csgG* in pTrc99a	(76)	
pRseA	pLC252: *rseA* in pTrc99a	(177, 271), CG	
pRseB	pRseB–ATS: *rseB* in pFLAG-ATS	(164), CG	
pRseAB	pLC253: *rseAB* in pTRC99a	(177, 271), CG	
† SH – Scott Hultgren, JM – Janine Maddock, CG – Carol Gross			
Genetic Primers			
Curli deletion Kan 5'	CCGGATGATAATTCCGGCTTTTTTATCTGTCAGGATTCCGGTGGAACCGAGTGTAGGCTGGAGCTGCTTC		
Curli deletion Kan 3'	ATTCATCTTATGCTCGATATTTCAACAAATTAAGACTTTTCTGAAGAGGGCATATGAATATCCTCCTTAG		
Curli deletion check 5’	GTGACTGGAAACTGGTGTTACC		
Curli deletion check 3’	GGCTACTGTCGAATATTAATACCGG		
qRT-PCR Primers			
16s-RT-F	GGTGCAAGCGTTAATCGGAA		
16s-RT-R	CTTCCGTGGATGTCAAGACC		
cpxP L1	TCAACGCTGGCAGTCAGTTC		
cpxPR1	TCACCCGGATGCCAGTTATC		
csgA-RT-F	CGGTAATGGTGCAGATGTTGG		
csgA-RT-R	TGCCGTTCCACTGATCAAGAG		
csgBP2L	TAGCAACCGGGCAAAGATTG		
csgBP2R	CGTTGTGTCACGCGAATAGC		
csgDP2L	GCGGCGAATGCTACTTTACG		
csgDP2R	CGCTGATGAACAACGAACGA		
csgGP1L	ACCGGCGAGATCCTTTCTTC		
csgGP1R	CCCTGTTTCGATAGCCGACA		
rpoAP1L	GTTCGACGCACGCCAAGGTGA		
rpoAP1R	ACGTGCGGCTTGACGAT		
rpoHL1	TGCATTACCATGGCGATCTG		

CHAPTER III

Establishment of Biofilm Subpopulation and Structure Requires Anaerobic Respiration

Abstract

Bacteria biofilms allow for cell growth in diverse and harsh environments due largely to the protection conveyed by the extracellular matrix in which the cells are encased. Cells within a biofilm stratify into matrix associated and non-matrix associated subpopulations. In this work, we compared the transcript and protein profiles of the two biofilm subpopulations and what is required for subpopulation structure development. We identified 54 transcripts and related proteins that were differentially expressed between the subpopulations. Differences in motility, some amino acid breakdown, and anaerobic respiration were represented. Additionally, 29 transcriptional regulators were differentially expressed at either the transcript or protein level, indicating additional regulation on the levels of these transcription factors between the different subpopulations. The non-matrix associated subpopulation was functionally anaerobic, allowing for Fnr activation and promotion of the Fnr regulon, including the anaerobic respiration complexes. Of the anaerobic respiration complexes upregulated, NrfA showed the greatest fold change increase relative to matrix associated cells and was investigated further. Mutant variants that lacked *nrfA* were unable to form distinct matrix and washout subpopulations, although they made curli and cellulose in approximately the same amounts as wild-type cells. Anaerobic respiration is required for development of subpopulations and protective benefits of biofilm in UTI89 *E. coli*.

The contents of this chapter are an unpublished manuscript by Janet E. Price, Catherine Barnier, and Matthew R. Chapman. J.E.P. and M.R.C. conceived and designed the experiments; J.E.P. performed most of the experiments with help from the U of M RNAseq and Proteomics Cores. The data was analyzed by J.E.P., C.B. and M.R.C. J.E.P. wrote the manuscript with help from C.B. and M.R.C.

Introduction

Biofilms are communities of single or multiple bacteria species growing on a surface with the aid of a self-produced, extracellular structure(14). Bacteria within a biofilm can be protected from stressors, including desiccation, antibiotics, redox changes, and predation(18-20). While matrix production can be energetically exhaustive(272), biofilms are formed regularly in conditions of low nutrients, low salt, or low temperature and are the prevailing lifestyle for bacteria(5, 40). The extracellular structure or matrix, can be comprised of polysaccharides, protein, and extracellular DNA(14, 273). In *Escherichia coli*, cellulose serves as the polysaccharide component and curli fibers (CsgA) serve as the main protein component(61, 76). A strict balance between curli and cellulose is required for protection of the biofilm(80, 273, 274).

Because biofilm cells can be resistant to antibiotics and conventional cleaning methods, biofilm has broad health and economic impacts on humans. Biofilms outside our intestinal tract are major contributors to antibiotic resistance and chronic illnesses(27-32). The CDC estimates 80% of bacterial infections and 65% of hospital acquired infections are caused by biofilm(33). Treatment of these infections costs the US approximately $94 billion annually(34, 35). Biofilm that form on food preparation surfaces or on aquaculture and civil water systems cause equipment breakdown and carry human health risks(36-39). Difficulty in removing hazardous and unwanted biofilm stems from minimal knowledge of initiation and dispersal factors that dictate biofilm development.

Initiation and dispersal signals that regulate biofilm formation are extremely diverse and include mechanical changes, stress-induced cell responses, or changes in signaling molecule concentrations(45). Cells can initiate biofilm formation through direct contact by compression of pili that signals the presence of a surface(275, 276). Dispersal of cells from a mature biofilm has been shown to result from a buildup of toxic waste products or steeply changing oxygen gradients between the cells within the biofilm and the environment(24, 44). Biofilms can also be formed or dispersed through a change in second messenger concentration, such as c-di-GMP or indole(45). Studies have shown that high c-di-GMP and low indole promoted biofilm formation, while low c-di-GMP and high indole can inhibit or disperse

biofilms(45-48). New specialized enzymes and small molecules are constantly being added to lists of compounds that can modulate biofilm formation without clear insight to what the integration point or master regulation pathway controls these transitions in the biofilm lifestyle. This gap in knowledge on biofilm modulation limits our ability to target areas for biofilm removal or prevention.

Recent studies have shown that protection for cells within a biofilm is not uniform but is instead based on structure. Biofilm communities are organized into at least two subpopulations based on structure, cells that are directly interacting with the matrix components organized into a approximately 30μm thick, wrinkled layer(Matrix) and an underlying, non-matrix associated subpopulation (Washout)(19). Oxygen, useful substrates, and nutrient availability exists on a gradient that create unique environments at varying depths within a biofilm(14, 19, 23, 277). Any disruption of the matrix structure leaves Washout cells susceptible to antibiotics and phage infection until matrix structure encases the exposed cells again(26, 278-280). Subpopulations are minimally characterized hallmarks of biofilms and understanding minimal requirements for biofilm organization into subpopulations will advance our ability to exploit weaknesses in protection for removal of biofilms.

We asked what cellular processes are characteristic of Matrix and Washout subpopulations in UTI89 *E. coli*. We found that Matrix and Washout subpopulations were transcriptionally and translationally distinct. Differences between subpopulations included genes involved in motility, chemotaxis, amino acid metabolism, and anaerobic respiration. Washout cells were functionally anaerobic, though some oxygen remained available(19). This is supported by other studies that have shown microenvironments within biofilm that were able support obligate anaerobe growth(281). Creation of regular, wrinkled matrix structure depended on set gradient of anaerobic respiration in the Washout cells. Increased respiration through nitrate supplementation caused temporary smoothing of biofilms while matrix components were unchanged. Similarly, a knockout of *nrfA*, an anaerobic nitrite respiration complex, produces smooth colonies that lack the regular, wrinkled biofilm structure even though the overall amount of curli and cellulose produced was comparable to WT biofilms. In summary, anaerobic respiration is a key driver of subpopulation development of UTI89 biofilms.

Methods

Strains and Growth Conditions. All experiments were carried out in the UTI89 *E. coli* background. Starting cultures were grown at 37°C with 220 rpm agitation in Luria Broth (LB) media. Mutant lines were constructed using the lambda red recombinase technique (227). Primer sets and strain list can be found Table 3.2.

Rugose colony biofilms were grown from 4µL drops of suspended cells at an optical density at 600nm (OD_{600}) of 1.0. Starting cultures were diluted to the correct concentration. Cell suspensions were pelleted at 12,000 xg for 1 minute. The liquid was aspirated off, resuspended in sterile YESCA media (10g Bacto Casamino Acids, 1g Fisher yeast extract/liter), and pelleted again to wash cells 3 times. Prepared cells were plated on either aerobic YESCA or YESCA + Congo Red (CR) media plates (50µg CR/mL and 20g agar/liter) or anaerobic YESCA or YESCA + Congo Red (CR) media plates (50µg CR/mL and 20g BD noble agar/liter). Pellicle biofilms were grown in sterile 48-well falcon tissue-treated polystyrene plates using a 1:1000 dilution of starting cultures in YESCA media. Pellicles were mixed on an orbital shaker on low for 10 minutes. Bacteria in both pellicles and rugose biofilms were then incubated for 48 hours (unless stated otherwise) at 26°C before imaging with a digital camera. Where indicated, 20mM $NaNO_3$ or 20mM NaCl was added prior to autoclaving as addition to media before or after autoclaving showed no difference in situations tested.

Subpopulation Separation. The Matrix and Washout subpopulations in rugose biofilms were separated as described (19). Briefly, the rugose biofilms were excised with the agar beneath them using a sterile metal spatula and moved to a 24-well falcon tissue-treated polystyrene plate containing 750µL of 1:2 YESCA media:Qiagen RNA protect for RNA isolation or 50mM potassium phosphate buffer (KPi) (ph 7.2) for western blot analysis. The plate containing biofilms was gently shaken on an orbital shaker until the matrix fraction fully dissociates from the agar (between 5-10 minutes). The cells released into the media were deemed the Washout cells and transferred to an Eppendorf tube. An additional 750µL of buffer was added to the wells to wash any remaining unattached cells into the media through an additional 5 minutes of

gentle shaking. The media was again transferred to combine with the initial Washout cells to make the Washout cell portion for testing. The Matrix fraction was transferred to an Eppendorf tube containing 500µL of buffer using a sterile inoculating loop. To separate cells from the matrix structure, a Fisher Scientific Tissuemiser Homogenizer was inserted into the Eppendorf tube, set to medium speed, and run for 20 seconds. Large aggregates were allowed to settle and suspended cells at the top of the tube were used in assays as the Matrix cell portion.

RNA Isolation. Rugose biofilms were grown at 26°C for 30 hours. Biofilm subpopulations were separated as described and 3 collected biofilm colonies were pooled in 15mL falcon tubes for each of the 3 replicates. Suspended matrix cells were moved to a fresh falcon after homogenization to limit matrix structure in the RNA preparation. Both subpopulations were pelleted at 5000 xg for 10 minutes before flash freezing in liquid nitrogen to limit transcription or mRNA turnover. Samples were then thawed, and the supernatant aspirated off before resuspending the cell pellets in 50uL of methanol and pelleting again at 5000 xg for 20 minutes. Remaining methanol was removed, and the pellets were dried in a laminar flow hood before storing at -20°C overnight.

Isolating RNA from the prepared cells required a hybrid of the Invitrogen PureLink RNA kit and a phenol-chloroform extraction. Freshly prepared Lysozyme solution (10mM Tris-HCl (pH 8.0), 0.1mM EDTA with 1mg lysozyme and 0.5µL of 10% SDS per 100µL) was used to resuspend the cell pellets and then incubated at room temperature for 5 minutes. 350µL of lysis buffer from the PureLink was prepared with 1% β-mercaptoethanol and added to each sample. Cells were pipetted up and down to mix thoroughly. An equal volume of phenol-chloroform (25 phenol: 24 chloroform: 1 isoamyl alcohol, pH=6.8) was added, samples vortexed, then centrifuged at 4600 xg for 10 minutes. The aqueous phase was collected, and equal parts phenol-chloroform was added, mixed, and centrifuged for an additional 3 times. Samples were washed twice with equal parts chloroform and centrifuged at 4600 xg for 10 min. Twice the volume of 100% ethanol was added to the final aqueous collection and mixed by inversion. RNA was precipitated on ice for 30 minutes before being pelleted at 7700 xg for 15 min. The supernatant was removed, and the pellet gently washed using 500µL of 70% ethanol.

RNA was pelleted again at 7700 xg for 10 minutes before being treated with Promega DNase I following the published protocol. The RNA was then purified using the Invitrogen PureLink RNA kit following the published protocol. RNA quality and quantity were measured using a DeNovix DS-11 and an agarose gel. Purified RNA was flash frozen and stored at -80°C.

RNAsequencing. RNAsequencing was performed by the University of Michigan Advanced Genomics Core facility. RNA quality was measured by bioanalyzer to establish that samples had RIN scores above 8 before proceeding. Purified RNA was ribo-depleted using the ribo-depleted Stranded TruSeq kit from Illumina before being library prepped for sequencing on an Illumina HiSeq 4000 using a stranded mRNA single-ended, 51 cycle protocol. Reads were aligned to the published UTI89 genome(264) and differential expression assessed using the program Rockhopper(282, 283). Results were trimmed using the expression value to account for genes that were differentially expressed between Matrix and Washout populations at a level of log_2fold change of greater than one with significance of less than 0.05 using q-value calculations.

Proteomics. Rugose subpopulations were separated as described, samples standardized to $4x10^9$ cells as measured by OD_{600}, flash frozen, and turned over to the University of Michigan Proteomics & Peptide Synthesis Core for analysis. The samples were prepped for unlabeled protein expression profiling using urea extraction, in-solution digestion with trypsin and 3hr LC-MS/MS. Samples were lysed in urea buffer (8M urea, 150mM NaCl. 50mM Tris pH8, 1X Roche complete protease inhibitor) and sonicated using a Q Sonica probe. Extracts were further incubated for 1 hour at 37°C in a ThermoMixer. The extracts were then quantified by Qubit fluorometry to quantify yields. Protein samples were reduced using 15mM dithiothreitol at 60°C followed by alkylation with 15mM iodoacetamide at room temperature before an overnight digestion with Promega Trypsin at 37°C. The reaction was quenched with formic acid and desalted using an Empore SD solid phase extraction plate. Samples were lyophilized and reconstituted in 0.1% trifluoroacetic acid. Mass spectrometry was completed using a nano LC-MS/MS with a Waters M-Class HPLC system interfaced to a ThermoFisher Fusion Lumos.

Peptides were loaded on a trapping column and eluted over a 75µm analytical column at 350nL/minute; both columns were packed with Luna C18 resin. The 3-hour gradient-generated data was collected with the Orbitrap operating at 60,000 FWHM and 15,000 FWHM for MS and MS/MS respectively. The data was processed using Matrix Science Mascot and validated through Proteome Software Scaffold. Data were filtered using at 1% protein and peptide FDR and requiring at least five unique peptides per protein. Proteins detected in only one or two replicates of a subpopulation were excluded. Results were trimmed to account for proteins that were differentially expressed between Matrix and Washout populations at a level of log_2fold change of greater than one with significance of less than 0.05 using p-value calculations.

iPAGE Analysis. We performed gene ontology (GO) term enrichment analysis using iPAGE(284) on the RNA-seq log2FC values. IPAGE identifies significantly over- or under-represented GO terms based on whether significant mutual information is found between the membership of each gene within a given bin and within a given GO term. All settings used were default except for exptype, which was set to continuous to reflect the nature of log2FC values, and only 7 bins were used here. The database used was a UTI89 index file based on annotations obtained from Uniprot(285).

Permutation Test. We performed a permutation test to assess whether the average log_2fold-change value observed across the Fnr regulon was significant. In order to preserve more of the regulatory effects present in the RNA-seq data, the data were shuffled at the level of transcriptional units (i.e. genes within the same operon were kept together). The data was shuffled 100,000 times and the average log 2 fold-change value was calculated after each permutation to generate a distribution of the average expected value for average log_2fold-change across the Fnr regulon by chance. All analysis was performed using Python (v2.7.17) base packages and the Pandas (v0.24.2) and numPy (v1.16.6) packages. The figure was generated using the Python Matplotlib (v2.2.5) package. The log_2fold-change value of Fnr was added using Photoshop.

Western Blot. CsgA Western blots were performed as previously described (68). Rugose biofilms were separated and collected in 0.5mL of 50mM potassium phosphate buffer (KPi) (pH 7.2) and homogenized with a Fisher Tissuemiser for 20 seconds on medium. Cells were spun down and resuspended in KPi to achieve an OD_{600} of 1.0, then 150µL of cells were pelleted and resuspended in hexafluoroisopropanol (HFIP). The HFIP-treated samples were vortexed briefly before drying in a Savant SPD140 SpeedVac at 45°C for 45 minutes. The dried samples were resuspended in 2x SDS-running buffer and heated at 95°C for 10 minutes. After cooling, 10µL of sample was loaded into a 15% SDS-PAGE gel along with 2µL of Fisher BioReagents EZ-Run Prestained Rec Protein Ladder and run at 25mA for 50 minutes. Gels were transferred to polyvinylidene difluoride (PVDF) membranes using transfer buffer in a semidry transfer apparatus at 25V for 10minutes at room temperature. CsgD blots were performed in the same manner with slight alterations: HFIP was excluded and gels were semi-dry transferred using cold CAPS buffer (10mM CAPS, 10% Methanol, pH 11.0). All membranes were blocked in Tris-buffered saline-Tween 20 (TBS-T) + 5% skim milk for 1 hour at room temperature. The membranes were incubated with primary antibody overnight at 4°C on a tilt table (1:15,000 α-CsgA, 1:4,000 CsgD) followed by three 5-minute washes in TBS-T. The membranes were incubated with secondary antibodies for 1h at room temperature (1:15,000 LiCor infrared dye anti-rabbit antibodies) followed by three 5-minute washes in TBS-T. Membranes were dried at room temperature before visualizing on a LiCor Odyssey CLX imager. Bands were quantified using the LiCor Odyssey program.

S4B Staining. Rugose biofilms were collected from plates using blue inoculating loops and transferred to Eppendorf tubes containing 500µL of KPi and disrupted using a Fisher Tissuemiser for 20 seconds on medium. The cells were stained by incubation with 0.05 mg/mL S4B dye (68, 286) at 37°C, 200 RPM shaking for 10 minutes. Cells were pelleted, the excess dye gently removed using a pipette, and the cell pellet resuspended in 100µL of KPi. Shaking was repeated for 5 minutes to remove any excess dye. Cells were then pelleted and resuspended in 100µL of KPi. Stained and unstained cells were diluted 1:10 into 98-well black with flat clear bottom polystyrene plates and measured on a Tecan M200 Infinite Plate Reader using

parameters for 535 nm excitation and 595 nm emission. Unstained cells were used to measure OD_{600} to normalize dye reading by cell number. Error bars represent the standard deviation of biological triplicate reactions.

NAD/ NADH Measurement. Rugose biofilms were separated and collected in KPi buffer. Samples were prepared using NAD/NADH-Glo™ Assay from Promega according to their protocol for measuring both NAH and NADH. Cells were incubated for 1 hour before being measured in a GloMax Microplate Reader using a 1 second exposure. Each sample was normalized by cell number and measured in 5 technical replicates.

ATP Measurement. Rugose biofilms were separated and collected in KPi buffer. Samples were prepared using CellTiter-Glo™ Assay from Promega according to their protocol. A 1µM ATP stock was diluted 1:10 four times to generate a standard curve. Cells were incubated for 1 hour before being measured in a GloMax Microplate Reader using a 1 second exposure. Each sample was normalized by cell number and measured in 5 technical replicates.

Confocal Microscopy. Whole biofilm confocal images were taken using biofilms grown from UTI89 strains expressing GFP from the curli promoter and constitutively expressing mCherry on filters as previously reported (19). Nitrocellulose 0.45µm membranes were added on top of the YESCA and YESCA + 20mM $NaNO_3$ plates for easy biofilm removal. After 48 hours of growth, the filters beneath the biofilm were trimmed and the entire biofilm moved to a glass slide. 4 spacers ~0.3mm deep were added outside of the filter on the slide to ensure the coverslip did not put pressure on the biofilm structure. Invitrogen ProLong Diamond Antifade Mounting media was added slowly before adding a Fisherbrand No. 1.5 glass coverslip and sealing with clear nail polish. Confocal images were collected using a Leica SP8 laser scanning confocal microscope at equal depths within the biofilms using a 40x objective. A double-dichroic 488/561 beam splitter and a 488-nm argon laser and a 561-nm diode-pumped solid-state laser were used for image capture. Images were analyzed with LAS AF v2.6.3 build 8173 software.

Growth Curves. Starting cultures of WT and *nrfA*- were pelleted and washed twice in filter sterilized YESCA media. For aerobic growth curves, cells were back diluted to obtain OD_{600} 0.1 of cells in 3mL of YESCA or YESCA + 20mM $NaNO_3$ in Fisherbrand snap cap glass culture tubes. Culture tubes were incubated at 37°C with 220 rpm agitation for 24 hours. OD_{600} was measured every hour using a spectrophotometer with a YESCA only as the blank. For anaerobic growth curves, YESCA and YESCA + 20mM $NaNO_3$ medias were equilibrated in an anaerobic chamber for 72 hours before use. Sterilized Pyrex™ Vista™ Reusable Glass Tubes with Phenolic Screw Caps 13mm and washed cells were brought into the anaerobic chamber. Cells were diluted into the anaerobic media to OD_{600} of 0.01 in 10mL. Caps were securely fastened before removing the chamber and incubating stationary at 37°C for 48 hours. Cultures were vortexed briefly before OD_{600} was measured every hour using a spectrophotometer with a YESCA only as the blank. Graphs were generated using the Python package brokenaxes. Error bars represent standard deviations of 3 biological replicates.

Results

Biofilms stratify into two transcriptionally and translationally distinct subpopulations. UTI89 forms rugose colony biofilms on agar plates or pellicle biofilms at the liquid-air interface(82). Rugose biofilms can be separated into matrix component-associated (Matrix) and non-matrix associated (Washout) cell subpopulations(19). To identify pathways that were unique to biofilm subpopulations, Matrix and Washout cells were separated and characterized using RNA sequencing (RNAseq) and liquid chromatography– tandem mass spectrometry (LC-MS/MS).

WT cells were grown under biofilm forming conditions for 30h and then the Matrix and Washout subpopulations were separated as described for RNAseq analysis. Approximately 10 million reads per replicate were collected for the RNAseq analysis. Comparing differential transcript expression levels, distinct profiles arose for each subpopulation (Table 3.1 Left). The *csg* genes (*csgACDF*) and amino acid metabolism (*astABCD, trpABCDE*) were upregulated in the Matrix subpopulation compared to the Washout Subpopulation (Table 3.1 Left). Flagella genes (*fliACDS, flgDEGKLMN*), anaerobic respiration (*napABFGH, narGHJ, nirB, nrfABC*), and many

poorly characterized y-genes (*ygeWXY, yqeAB, yccT*) were upregulated in the Washout cells compared to the Matrix subpopulation (Table 3.1 Left).

To visualize patterns in transcripts that were differentially expressed between the Matrix and Washout subpopulations, an iPAGE analysis was completed to identify overrepresented gene ontology terms (GO terms). Established subpopulation characteristics served as internal controls to confirm subpopulations were efficiently separated. For example, washout cells are known to be flagellated (280, 287) and flagella-related genes were overrepresented in the Washout cell subpopulation compared to the matrix subpopulation(Fig. 3.1). iPAGE revealed that Washout cells have increased expression of genes that are associated with anaerobic respiration (Fig. 3.1). Nitrate reductase is the active component in nitrate respiration, which requires genes under the nickel cation binding and cytochrome assembly GO term for proper production and insertion of heme groups into the reductases. Matrix cells had increased representation of arginine, thiamine, and histidine amino acid breakdown pathways (Fig. 3.1). The amino acid pathways highlighted by iPAGE all pool into inosine monophosphate (IMP), the precursor of c-di-GMP and c-di-AMP(288, 289). Our results support that the Washout and Matrix subpopulations were successfully separated and have unique transcriptional profiles.

Between 20 thousand and 52 thousand protein spectra per replicate were collected and analyzed from the LC-MS/MS. Comparing the normalized spectral abundance factor (NSAF) of the Washout subpopulation relative to the Matrix subpopulation, protein profiles for both subpopulations arose. Proteins involved in amino acid metabolism (IlvBCN, LeuCD, ThiCEG.), free radical stress response (SodAC, KatE) and protein chaperones (CsgC, Spy) were increased in the Matrix subpopulation. Chemotaxis proteins (CheABWYZ, Tar, Tsr), anaerobic respiration (NapBFGH, NarGHP, NirB, NrfABC), and 65 y-proteins were increased in the Washout subpopulation (Table 3.1).

We next looked to identify transcript/protein pairs present in the RNAseq and proteome data that were differentially expressed in the biofilm subpopulations. The 1,699 transcript/protein pairs that were present in both data sets were further analyzed. RNAseq

reads and protein spectra that met a 2-fold change difference in expression ($p<0.05$) between Matrix and Washout subpopulations were considered significant. 127 transcripts met the 2-fold threshold between the Matrix and Washout subpopulations but were not significantly different in the proteomics. 323 proteins met the 2-fold threshold between the Matrix and Washout subpopulations but were not significantly different in the RNAseq data. 54 transcript/protein pairs were significantly differentially expressed at both the RNA and protein level (Fig 3.2A and Table 3.1). The 54 transcript/protein pairs that were differentially expressed are primarily enriched in the same population at the RNA and protein levels (Fig. 3.2BC). A subset of the 54 with the $\log_2$FC values and p-values are presented in Fig. 3.2D. Flagella-related genes (*fliC*, *flgE*) were increased in the Washout subpopulation as compared to the Matrix cells, while curli-related genes (*csgC*) were increased in the Matrix subpopulation as compared to the Washout cells. All nitrate and nitrite respiration complexes were represented in the significant hits for both data sets (*nrfABC, napB, narG, nirB*) indicating an important role for anaerobic respiration in Washout cells. The presence of *ccmH* in the differentially expressed hits highlights the importance of respiration that requires heme C groups for activity, such as *nrfABC* and *nirB*. The Washout subpopulation appears to be anaerobic based on nitrate respiration complexes and heme processing. Collectively, the protein and RNA profiles both show 54 significant transcript/protein pairs involved in motility, chemotaxis, anaerobic respiration, and amino acid catabolism that are different between the two subpopulations.

Washout subpopulation is respiring anaerobically. Transcripts and proteins important for anaerobic respiration were overrepresented in the Washout subpopulation. Fnr is known to regulate nearly 300 genes in response to low oxygen availability(290) and many of the anaerobic pathways found in the iPAGE analysis are regulated by Fnr (Fig. 3.1). A permutation test on the $\log_2$FC values from the RNAseq data yielded a distribution of log2FC values for the Fnr regulon expected by chance (Fig. 3.3). The experimental $\log_2$FC observed for the Fnr regulon in the RNAseq data was 0.533, representing 6.4 standard deviations from the randomly generated distribution (Fig. 3.3). The Fnr regulon is significantly activated in the Washout

subpopulation versus Matrix subpopulation, suggesting that the Washout cells are functionally anaerobic.

Biofilms were grown in an anaerobic chamber to test whether aerobic respiration was necessary for matrix production. Biofilms grown under anaerobic conditions did not adopt the wrinkled morphology that biofilms grown under aerobic conditions display (Fig. 3.4A). Anaerobic biofilms did not produce matrix as shown by lack of Congo red binding (Fig. 3.4A) and by Western blot for CsgA and CsgD (Fig. 3.4B). Cells grown anaerobically on YESCA lack a terminal electron acceptor and may be starved for energy. We supplemented agar plates with $NaNO_3$ to act as an electron acceptor during anaerobic growth, which resulted in colonies that appeared thicker, more opaque, and had faint Congo red binding (Fig. 3.4A). Western blot analysis revealed that when nitrate was supplemented to anaerobically grown cells, biofilms had increased CsgD and CsgA levels compared to biofilms without nitrate supplementation (Fig. 3.4B). Similarly, cellulose levels increased with nitrate supplementation as compared to anaerobic growth without supplementation (Fig. 3.4C). Anaerobic biofilms did not form biofilm subpopulations, with or without $NaNO_3$ supplementation. Together these data demonstrate that a functioning electron transport chain is required for matrix component production, though other apparent factors are at work given that the matrix component levels were still far below that of aerobically grown biofilms. To test whether the lack of matrix in anaerobically grown biofilms was due to decreased energy, we turned to aerobically grown biofilms and used the functionally anaerobic Washout subpopulation as a proxy for anaerobic biofilm growth. Biofilm subpopulations were separated, and cellular ATP levels were measured. The Washout subpopulations had 4-5 times more ATP than the Matrix subpopulations (Fig. 3.4E). Congo red binding in anaerobically grown biofilms appeared to be localized to the agar surface where respiration was occurring. We followed up this observation by asking whether the oxygen-exposed Matrix cells have more reducing power than the Washout cells. The NAD to NADH ratio was 6.8 in the Matrix subpopulation compared to 9.93 in the Washout subpopulation, demonstrating that the anaerobic Washout population has a greater redox potential than Matrix cells (Fig. 3.4D). While respiration is required for matrix component production, the

wrinkled biofilm morphology and establishment of subpopulations are not caused by insufficient reducing power or insufficient energy in non-matrix producing cells.

Limited anaerobic respiration through NrfA complex is required for biofilm structure. Anaerobic respiration was overrepresented in the Washout subpopulation. To test whether nitrate respiration rates effected matrix component production, aerobically grown biofilms were supplemented with $NaNO_3$. Nitrate in the agar plates was available to the underlying Washout cells, thus increasing anaerobic respiration in Washout cells. We found that the regular, wrinkled rugose morphology was lost in WT biofilms that were supplemented with $NaNO_3$ (Fig. 3.5A). This change in structure was due to nitrate addition and not the buffering capacity of the added sodium (Fig. 3.7). Using WT cells expressing eGFP from a curli promoter on the chromosome and mCherry constitutively expressed from a plasmid, the wrinkled matrix structure of biofilms was visualized with confocal microscopy. In WT biofilms without nitrate, GFP was localized to the Matrix producing cells forming the outside of the wrinkles while mCherry was expressed by all cells, including the Washout cells within the wrinkles (Fig. 3.5B Left). In WT biofilms supplemented with $NaNO_3$, the wrinkle structures are lost, and all cells are expressing both GFP and mCherry, indicating a loss of the non-matrix associated Washout subpopulation (Fig. 3.5B). Western blot analysis of WT biofilms with and without nitrate supplementation showed approximately equal levels of CsgA and CsgD proteins (Fig. 3.5C). $NaNO_3$ supplemented biofilms did not yield significant cell number differences by OD_{600} (data not shown). Increased anaerobic respiration through $NaNO_3$ supplementation was sufficient to block biofilm subpopulation development but did not inhibit matrix component production.

To determine if NrfA was required for subpopulation development during biofilm formation a *nrfA*$^{-}$ deletion strain was constructed. NrfA is part of the NrfABC complex, a nitrite cytochrome c-type respiration complex. Overrepresentation of *cmmH* in our data sets indicated the importance of heme C groups, and *nrfABC* presented the greatest fold changes among type c respiration complexes. A knockout strain of UTI89 was generated replacing *nrfA* with a kanamycin cassette (*nrfA*-). The *nrfA*- cells exhibited a slow growth defect in both YESCA (Fig.

3.8) and LB (data not shown). Biofilms grown from *nrfA*- cells exhibit a smooth rugose morphology while retaining Congo red staining, indicating the continued production of matrix components (Fig. 3.6A). Western blot analysis confirms that *nrfA*- biofilms produce CsgA at comparable levels to WT cells, while CsgD production is reduced to approximately half that of WT levels (Fig. 3.6B). There was no significant difference in cellulose production (Fig. 3.6C). While all matrix components were present, organization into the biofilm structure was lost. This held true for pellicle biofilms as well, with cultures unable to form a floating biofilm with or without nitrate supplementation (Fig. 3.9). NrfA is required for organization of matrix components into the regular, wrinkled biofilm structure and establishment of cell subpopulations.

Discussion

The difference in availability of compounds such as oxygen, nutrients, and substrates within biofilm subpopulations allow for heterogeneity of cells within the biofilm community(14, 291). The subpopulations have differences in movement, biofilm components, and respiration among others (Fig. 3.1) that hold true at both the transcript and protein level (Fig. 3.2). The only exception was YidB, a currently undescribed gene, which was the only transcript/protein pair that switched subpopulations between analyses. The Matrix subpopulation is defined by cells that are producing CsgA and CsgB, but CsgA and CsgB were not found in the significant proteomic data, possibly because amyloids would not be solubilized in the proteomics preparation. Based on our proteomics results, we failed to capture many membrane proteins, such as curli pore CsgG and biofilm related DgcC and DgcN, which were expected in the Matrix subpopulation as seen previous biofilm studies(61, 68, 274). Transcriptional regulators *bolA*, *chaB*, and *osmE* were increased at the transcript level of Washout cells with no differential expression found at the protein level (Table 3.1), indicating a possible difference in transcript stability, targeted degradation, or functions at the transcript level. BolA has been previously connected to biofilm formation through direct regulation of c-di-GMP levels, matrix component production, and flagella production(100, 292). Similarly, transcriptional regulators CysB, Fis,

ModE, NarP, and RseB among 16 others were differentially expressed at the protein level without significant differences in subpopulations at the transcript level (Table 1), indicating a possible difference in protein stability or targeted degradation. Over 100 Y-genes were identified as differentially expressed between the subpopulations at the transcript, protein level, or both. Of these identified Y-genes, YdcI was recently shown as a transcription factor able to bind the *csgD* promoter region(293). The identified Y-genes are fertile ground for new research.

The production of extracellular matrix components is dependent on aerobic respiration(291, 294, 295). Our work demonstrated that changing availability of terminal electron acceptors oxygen and nitrate dramatically altered matrix component production and overall biofilm structure (Fig. 3.4-3.6). Biofilm grown anaerobically do not produce curli and cellulose compared to biofilm grown aerobically (Fig. 3.4ABC). Curli and cellulose production can be partially rescued in anaerobically grown biofilm with nitrate supplementation (Fig. 3.4ABC). Because cells grown anaerobically do not form distinct Matrix and Washout subpopulations, we turned to the anaerobic Washout cells to understand the role of anaerobic respiration. In the functionally anaerobic Washout cells, lack of curli and cellulose was not due to loss of reducing power (Fig. 3.4D) or lack of ATP (Fig. 3.4E), excluding these as limiting factors for matrix production. Instead, we looked at respiration as a way of driving a chemical gradient within a biofilm.

Regulators of nitrate respiration are likely responsible for the lack of subpopulations observed in nitrate supplementation and *NrfA*- knockouts (Fig. 3.5A and 3.6A). The tandem NarQ/NarP and Narx/NarL two-component systems are known sense nitrate and nitrite in cells. NarL responds to nitrate while NarP, which was found to be increased in the Washout subpopulation (Table 3.1), responds to nitrite(296). NarL and NarP compete for many of the same DNA recognition sites and act as on/off switches dependent on nitrate and nitrite levels(296, 297). Together, NarPL regulate genes in anaerobic respiration, ammonia breakdown, and cysteine/glutathione import directly(296, 298) and modulate biofilm production indirectly(54, 299). Additionally, NarPL binding to promoter sites, including sites upstream of the *nrf* operon, modulate the binding of other transcription factors, such as IHF and Fnr(300-

302). In our study we changed the ratio of nitrate to nitrite in cells through supplementing biofilms with nitrate or knocking out *nfrA*- which reduces nitrite to ammonium. Knocking out the primary nitrite respiration complex *nrfA*- and supplementing with nitrate, thereby causing nitrite to build up in the cells, produced biofilms that retained matrix component production but were unable to form biofilm subpopulations (Fig. 3.6) or the floating pellicle biofilms (Fig. 3.9). These results indicate a breakdown in organization of matrix components. Previous work has showed that increasing nitrate in biofilms by knocking out nitrate respiration complexes and supplementing nitrate in the media led to increased CsgA and CsgD levels and smooth colony morphologies in *E. coli*(54). The increases of CsgA and CsgD were blocked in the nitrate respiration knockout strain by also knocking out *narL*(54). Taken together with our study, increased levels of nitrate in biofilm cells, as sensed by NarL, cause increased production of curli, while increased levels of nitrite in biofilm cells, as sensed by NarP, cause biofilms to lose subpopulation structure. The ratio of nitrate to nitrite in biofilms can be re-established in WT biofilms. WT biofilms supplemented with nitrate are smooth for 7-9 days, when biofilms begin to wrinkle (data not shown). We hypothesize that a ratio of higher nitrate to lower nitrite may be required to switch cells further down in the biofilm from actively producing matrix components to remaining motile, thereby generating the biofilm subpopulations. Washout cells would be required to respire anaerobically to maintain the ratio of nitrate to nitrite, but Washout cells can remain primed for biofilm dispersal. If the matrix becomes compromised, letting in more oxygen, Fnr is rapidly inactivated and motility is restored through decreased c-di-GMP production.

This work describes expression profiles unique to the subpopulations UTI89 of *E. coli* biofilms, and how organization of these subpopulations is dependent on anaerobic respiration. WT biofilm subpopulations experience unique microenvironments(14, 19, 23, 277) that drive changes in biofilm cell motility, chemotaxis, anaerobic respiration, and amino acid catabolism (Fig. 3.1 and 3.2). By establishing a densely packed outer layer of matrix encased cells, exposure to oxygen can be limited in the Washout subpopulation past the threshold of Fnr inactivation (Fig. 3.3). Supplementing aerobically growing cells with nitrate resulted in defective subpopulation development (Fig. 3.5AB). Curli production in nitrate supplemented biofilms

remained at levels equal to WT aerobically grown biofilms (Fig. 3.5C). Blocking respiration through a *nrfA*- knockout mutant resulted in a similar lack of shell structure with matrix component production intact (Fig. 3.6). We hypothesize that cells building a biofilm use a fixed ratio of higher nitrate to lower nitrite in establishing which cells produce and become encased in curli and cellulose. A required nitrate to nitrite ratio is supported by our findings that WT cells exposed to high nitrate levels having all cells producing matrix components (Fig. 3.5) while lacking organization until presumably nitrate is reduced to normal levels and subpopulations return at 7-9 days of growth (data not shown). Intriguingly, NarL has already been identified to promote biofilm in response to nitrate(54, 296). We postulate that the tandem NarQ/NarP and Narx/NarL two-component systems act to modulate downstream expression of biofilm lifestyle-related genes to establish biofilm subpopulations based on nitrate and nitrite(296, 297, 299).

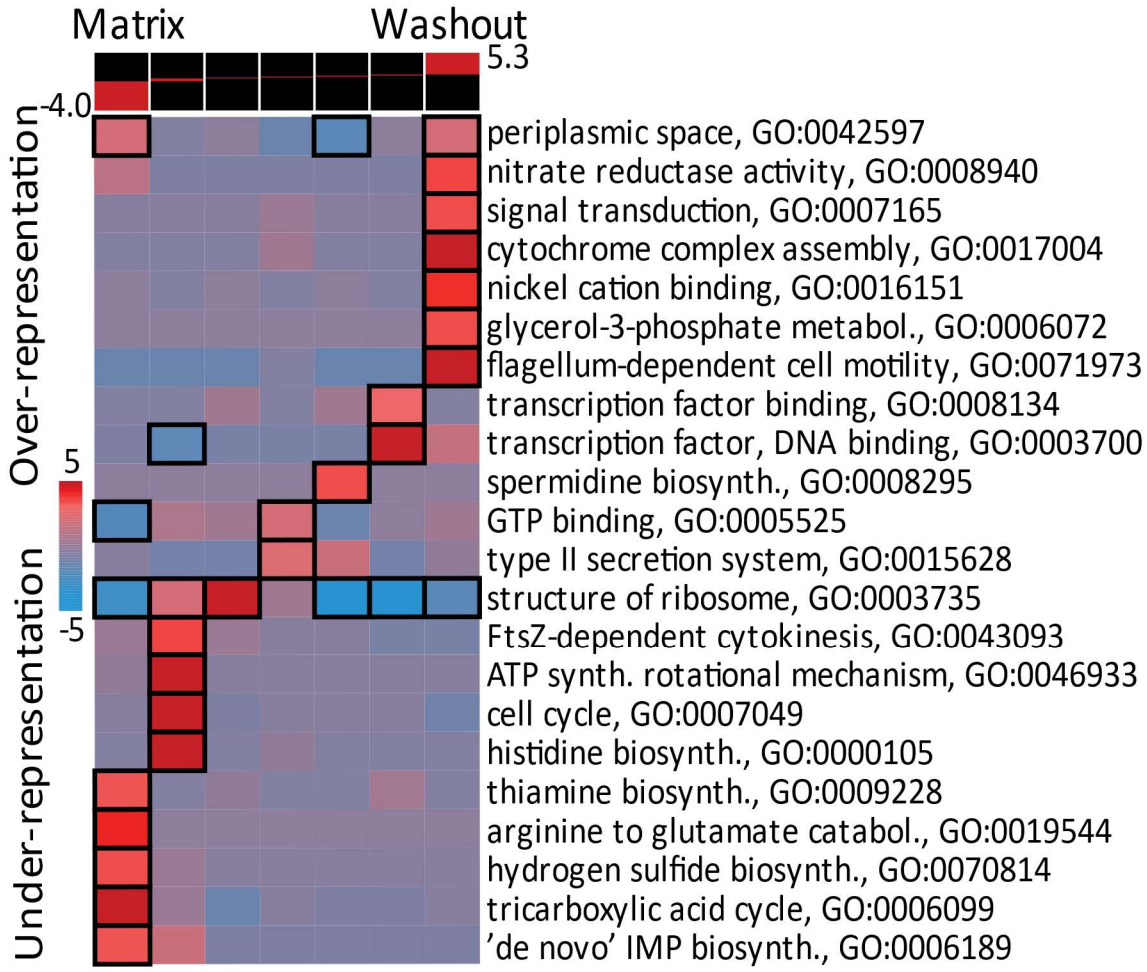

Figure 3.1. Pathways identified by iPAGE analysis of over-representation in the Washout subpopulation relative to the Matrix subpopulations. Red and blue bins, respectively, indicate the over- and under-representation of a pathway based on separately calculated log transformed p-values, from a hypergeometric distribution. Genes are binned based on the order of $\log_2$fold change (l2fc) with a positive l2fc (on the right) indicating genes that were more prevalent in the Washout subpopulation and a negative l2fc (on the left) indicating genes that were more prevalent in the Matrix subpopulation. Thus, a red bin on the right-hand side indicates a pathway that was found to be significantly over-represented in the Washout subpopulation.

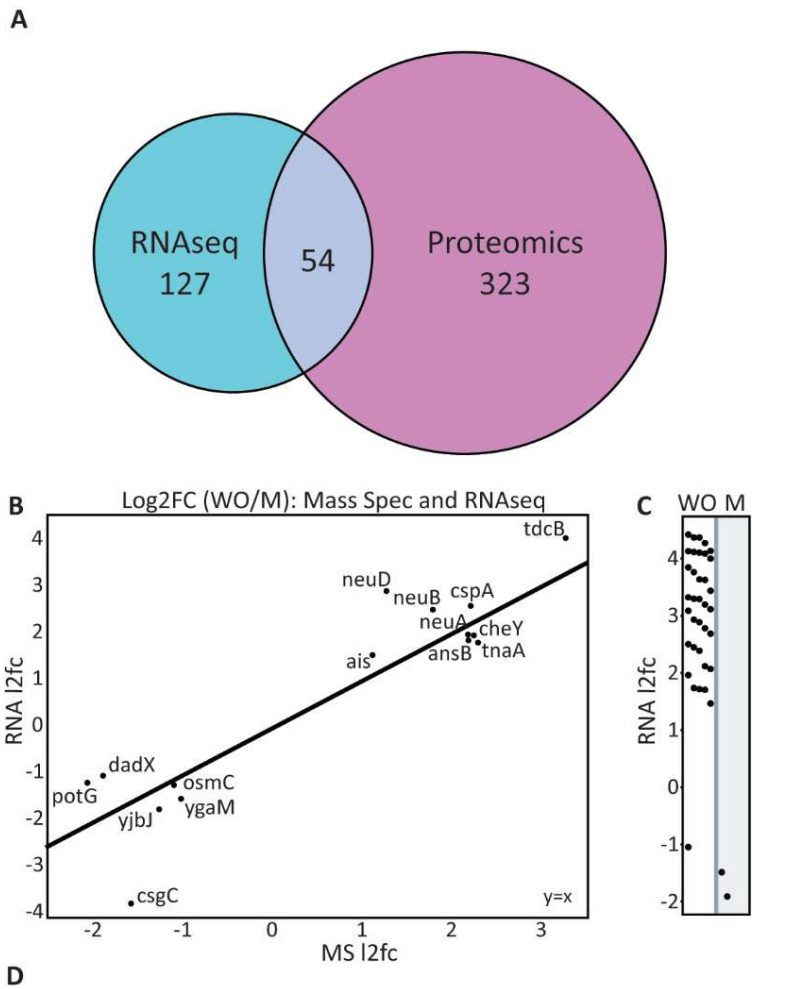

D

Gene Name	RNA Log_2FC	p-value*	Protein Log_2FC	p-value
fliC	4.71	0	2.41	0.00281
flgE	4.10	0	N/A	0.00203
csgC	-3.70	0	-1.57	0.00679
nrfA	4.27	0	N/A	0.00288
nrfB	4.14	0	N/A	0.000249
nrfC	4.42	0	N/A	0.000134
napB	3.63	0	N/A	0.000249
narG	1.72	0.0126	N/A	0.00513
nirB	3.09	4.25 E-107	N/A	0.0315
ccmH	1.96	8.33 E-12	N/A	0.00999

Figure 3.2. Highlights of significant differentially expressed transcript/protein pairs between the Matrix and Washout cell populations. A) 1,699 genes were represented in both data sets. 128 genes were identified as only significantly changed in the RNAseq data, while 323 proteins were identified as only significantly changed in the proteomics. 54 transcript/protein pairs were significantly differentially expressed between the subpopulations in both analyses. B) Log_2Fold changes (l2fc) from both RNAseq and proteomics data sets were plotted against each other to highlight near-linear relationship between RNA and protein expression. Negative l2fc values

denote hits differentially expressed in Matrix cells while positive l2fc value denote hits differentially expressed in Washout cells. Gene names were added using Photoshop. C) Proteins measured in only one biofilm subpopulation are represented as dots with the population represented by the column and the l2fc values for RNA expression along the y-axis. The transcript/protein pair that was up in the Matrix subpopulation at the RNA level but up in the Washout subpopulation at the protein level is YidB. D) A subset of hits to be discussed have been presented with their log2foldchange values, adjusted p-values*, and p-values. Negative log_2FC values indicate that the transcript/protein pair up in the Matrix subpopulation. Positive log_2FC values indicate that the transcript/protein pair was up in the Washout subpopulation. N/A denotes that the proteins were only detected in the Washout subpopulation.

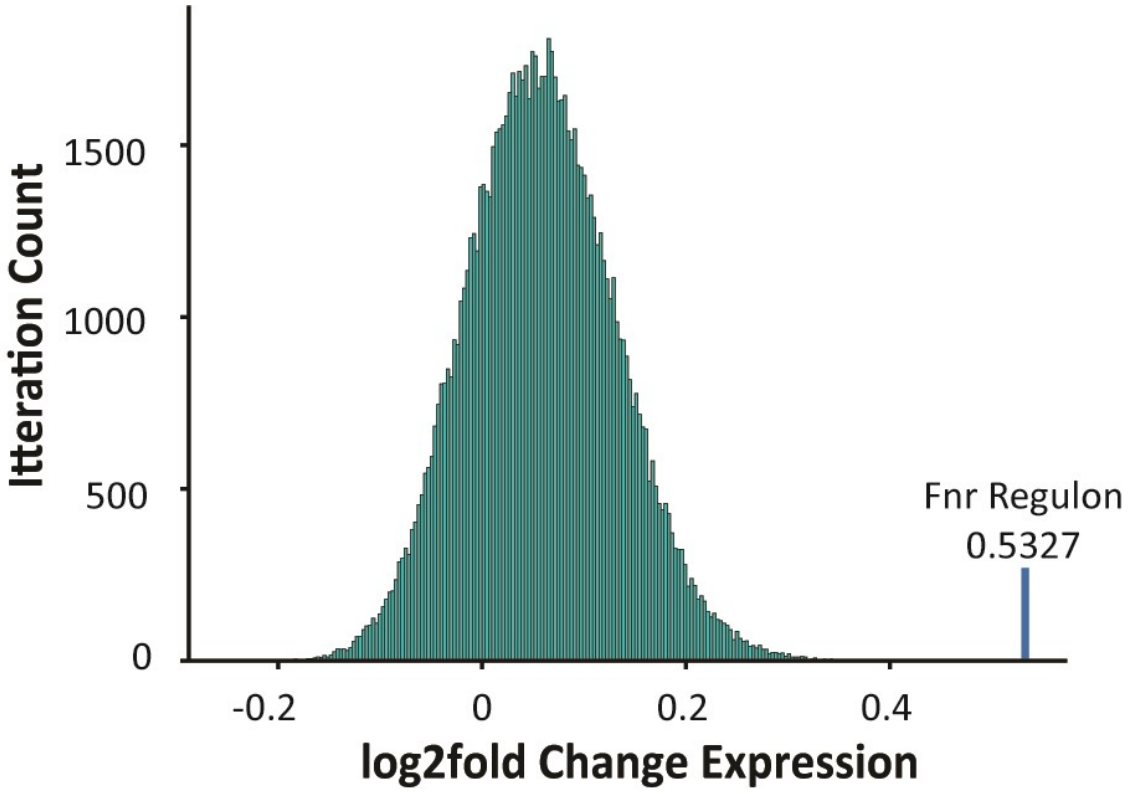

Figure 3.3. The Fnr regulon is significantly upregulated in Washout cells indicating Washout cells are functionally anaerobic. Randomized iterations of the RNAseq data was broken down by transcriptional operons. 100,000 iterations of the RNA log2fold values established a normal curve of background noise for the data. The average log2fold change across the Fnr regulon is 6.4 standard deviations above the curve.

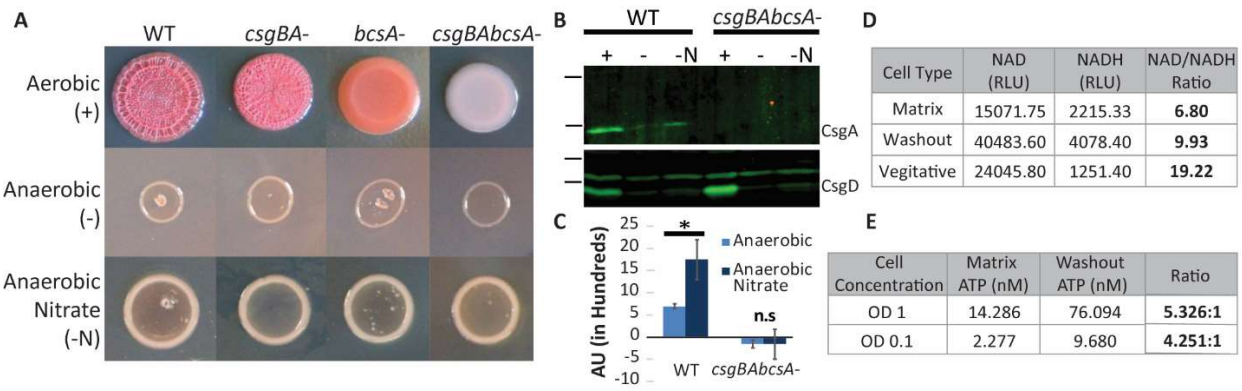

Cell Type	NAD (RLU)	NADH (RLU)	NAD/NADH Ratio
Matrix	15071.75	2215.33	**6.80**
Washout	40483.60	4078.40	**9.93**
Vegitative	24045.80	1251.40	**19.22**

Cell Concentration	Matrix ATP (nM)	Washout ATP (nM)	Ratio
OD 1	14.286	76.094	**5.326:1**
OD 0.1	2.277	9.680	**4.251:1**

Figure 3.4. Inhibition of respiration is sufficient to block rugose biofilm formation. A) Rugose biofilms of matrix component mutants grown under aerobic and anaerobic conditions. Congo red staining indicates matrix component production. B) Western blot of WT and mutant lacking both matrix component indicates decrease of both curli (CsgA) and CsgD under anaerobic conditions. Header +, -, and -N represent biofilms grown aerobically, anaerobically, and anaerobically supplemented with nitrate, respectively. Ladder markers represent, from top to bottom, 26, 17, 34, and 26kDa. C) Cellulose stain of anaerobic biofilms indicate increase of cellulose production after nitrate is supplemented. D) Separated aerobic biofilm cell populations and vegetative control were normalized by OD for measurement of NAD and NADH using NAD-NADH Glo assay, measured in Relative Light Units (RLU). Washout cells have a higher NAD/NADH ration than Matrix cells, indicating increased metabolism, oxidation state, and energy production. E) Separated aerobic biofilm cell populations were normalized by OD for measurement of ATP using NAD-NADH Glo assay. A standard curve of ATP was generated to quantify the light unit signal from Matrix and Washout cells. Ratio denotes the number of Washout cell ATP to Matrix cell ATP. Consistently Washout cells have higher ATP levels than Matrix cells.

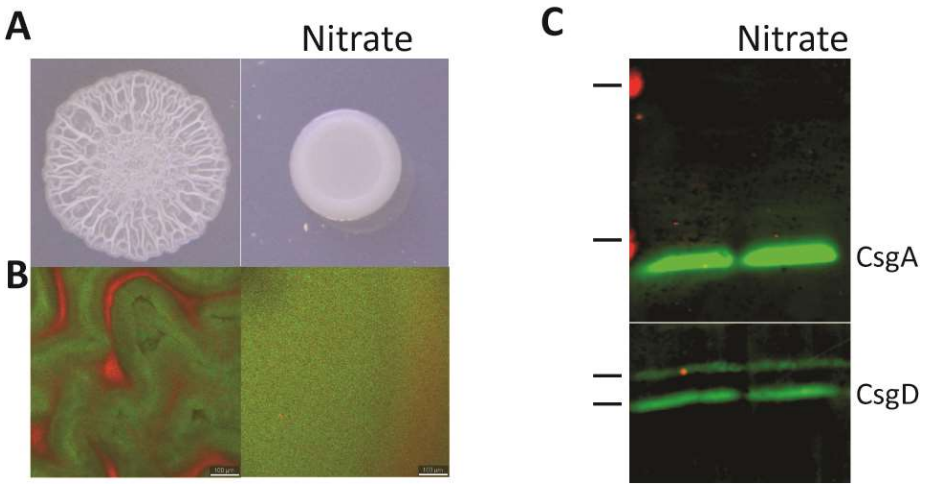

Figure 3.5. Nitrate supplementation causes biofilms to lose regular wrinkled structure without blocking matrix component production. A) Rugose biofilms wild type cells grown with and without nitrate supplementation. B) Confocal image optical slice at same depth within a biofilm. Wild type cells are expressing GFP from a curli specific promoter on the chromosome while expressing mCherry in all cells from a constitutive promoter. C) Western blot to measure CsgA and CsgD levels in wild type biofilms with and without nitrate. Samples are normalized by cell number. Ladder markers represent, from top to bottom, 26, 17, 34, and 26kDa respectively.

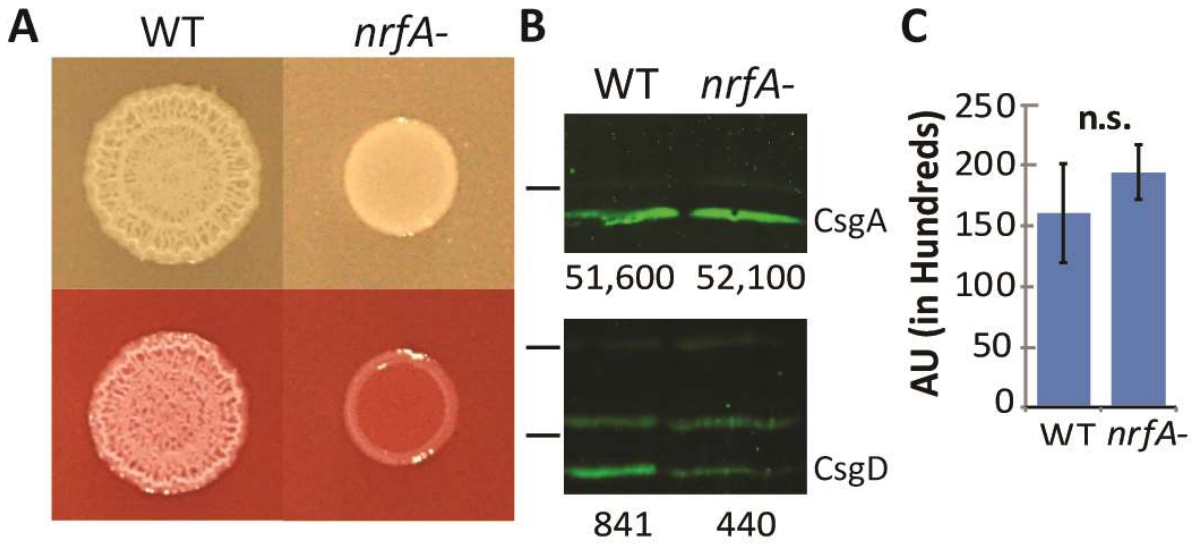

Figure 3.6. Anaerobic respiration is required for wrinkled structure of rugose biofilms. A) Rugose biofilms of wild type and *nrfA*- mutant on YESCA and YESCA congo red (bottom). *nfrA*- mutant cells form smooth, non-wrinkled colonies, but still stain red with Congo red. B) Quantitative western blot of CsgA and CsgD in wild type as compared to *nrfA*- biofilms. Ladder markers represent, from top to bottom, 17, 34, and 26kDa respectively. C) SB4 cellulose stain of wild type and *nrfA*- biofilms.

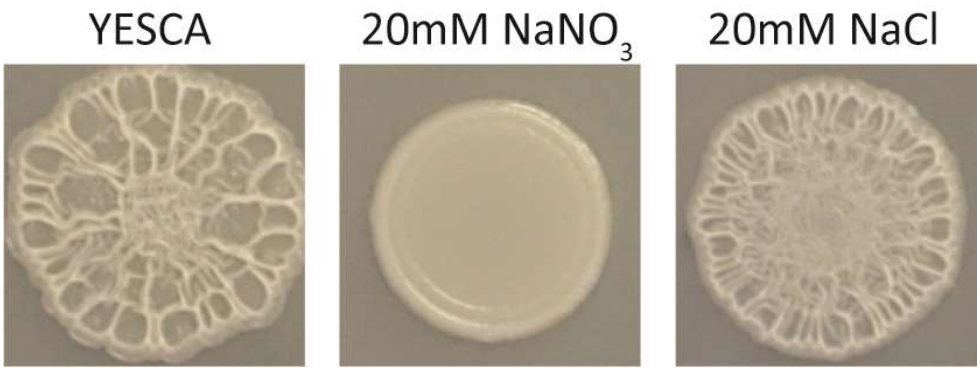

Figure 3.7. Loss of wild type rugose biofilm wrinkling is due to NO_3 addition, not buffering caused by additional sodium ions.

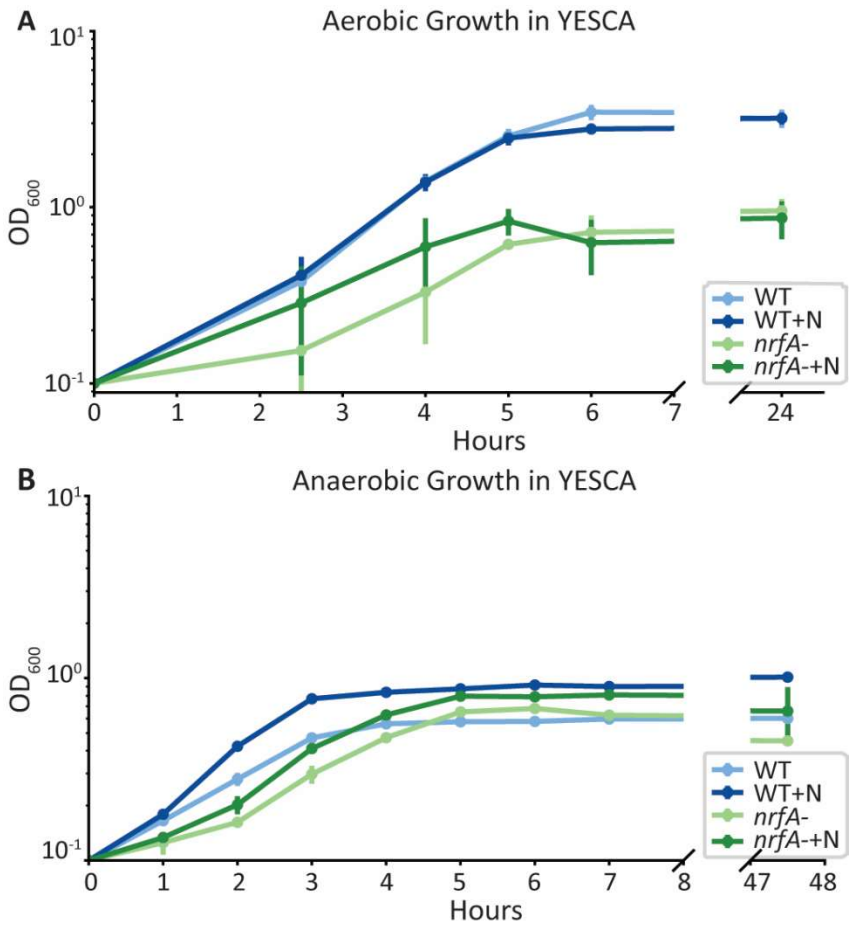

Figure 3.8. Characterizing growth defect of *nrfA*- mutant. A) 24-hour aerobic growth curves of WT and *nrfA*- mutants in shaking, baffled cultures with and without sodium nitrate supplementation with OD_{600} measurements taken regularly. Error bars represent standard deviation of 3 biological replicates. B) 48-hour anaerobic growth curves of WT and *nrfA*- mutants in static, enclosed test-tube cultures with and without sodium nitrate supplementation with OD_{600} measurements taken regularly. Error bars represent standard deviation of 3 biological replicates.

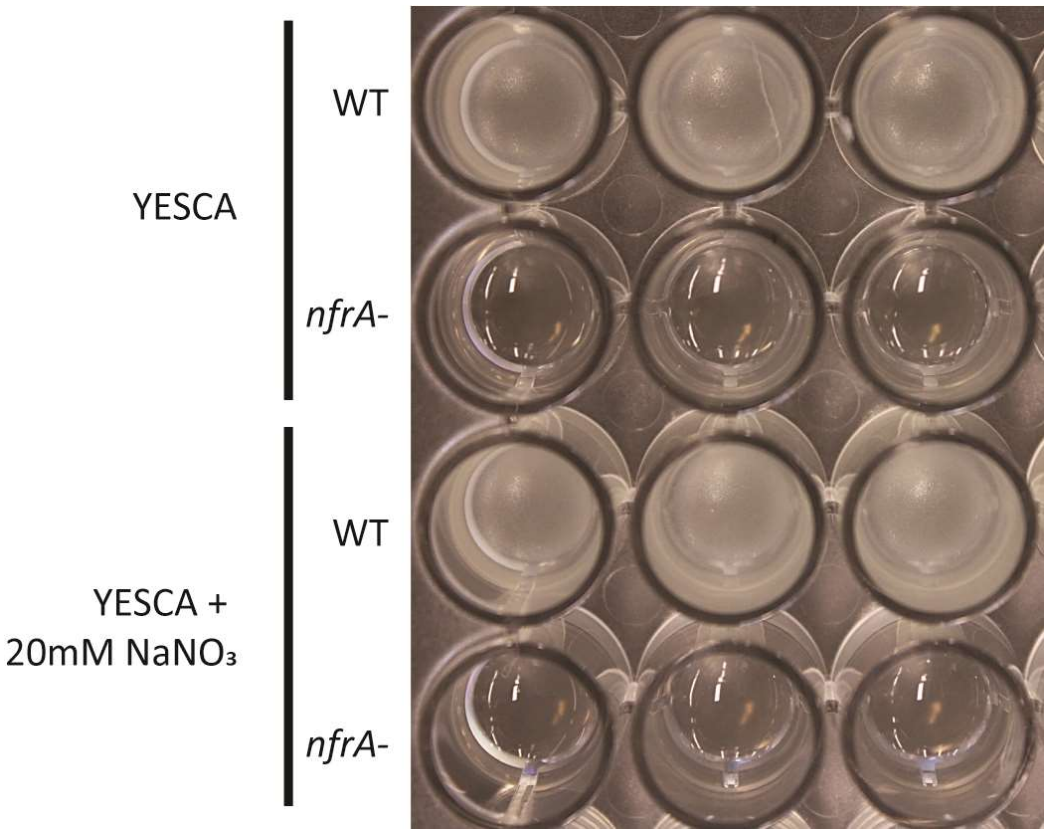

Figure 3.9. *nrfA*- mutants are unable to form pellicles though they possess both curli and cellulose levels comparable to wild type cells. $NaNO_3$ addition does not block pellicle formation of WT cells.

Table 3.1. Average expression, differential expression, and significance for transcript/protein pairs represented in Fig. 2A Venn diagram.

	RNAseq				Proteomics				
Name	Average Expression Matrix	Average Expression Washout	q-Value	(wash/matrix) log2fold change	Average NSAF Matrix	Average NSAF Washout	p-value	Fold Change NSAF Matrix / NSAF Washout	Excluded
aceA	532	243	6.34E-40	-1.130469932	0.001097149	0.000550942	0.0122	1.991405321	
acpP	6011	4609	1.05E-07	-0.383151252	0.00113839	0.002560794	0.00296	0.444545702	
acs	532	258	7.98E-36	-1.04405518	0.001182	0.000861038	0.072391	1.372761058	
add	23	35	0.231419	0.605721061	0	0.00028454	0.001965	0	
aer	17	42	0.184527	1.304854582	0	0.000107271	0.011162	0	
agaV	5	7	1	0.485426827	0	7.65903E-05	0.018841	0	
ais	24	70	0.000188	1.544320516	0.000182818	0.000394395	0.00439	0.463541595	
alsA	10	22	1	1.137503524	0	2.0754E-05	0.000249	0	
amiC	58	53	1.27E-13	-0.130060541	0	4.83451E-05	0.020936	0	
ansB	248	897	0.000246	1.854767865	0.000882122	0.003978212	0.000269	0.221738336	
argF	1	29	1	4.857980995	0	9.35485E-05	0.035658	0	
aroL	94	107	1.47E-06	0.186878135	0.000514896	0.000217761	0.004304	2.364494936	
asnC	360	303	2.25E-09	-0.248679113	5.44111E-05	0.000138559	0.28113	0.392693088	
astA	537	231	1.05E-67	-1.217029237	0.000703326	0.000424274	0.011218	1.657717186	
astB	495	224	5.66E-43	-1.143929793	0.000500793	0.000299839	0.085728	1.670207005	
astC	808	335	6.59E-47	-1.270194197	0.001632794	0.001146656	0.008606	1.423962034	
astD	494	204	5.28E-53	-1.27594189	0.000566039	0.000449395	0.014317	1.25955974	
baeR	52	49	8.13E-09	-0.085729874	0.000302132	0.000126374	0.045389	2.390771252	
barA	30	36	1.7E-06	0.263034406	0	2.32246E-05	0.020936	0	
basR	65	90	0.001722	0.469485283	0	0.00020511	0.002023	0	
birA	44	49	3.61E-06	0.155278225	0	6.75987E-05	0.000249	0	
bisC	27	20	1	-0.432959407	0	2.27867E-05	0.03394	0	
blc	240	258	1.07E-07	0.10433666	0.000639927	0.000217553	0.011746	2.941469526	
bolA	7693	2789	7.05E-65	-1.463798374	0.001171321	0.000802098	0.133595	1.460321076	
btuB	55	73	0.000189	0.408464845	6.40616E-05	0.000138626	0.021854	0.462120009	
btuD	115	81	4.81E-23	-0.505640048	0	4.3814E-05	0.000249	0	

caiD	3	3	1	0	0	5.51253E-05	0.030558	0	
ccmF	9	51	5.16E-31	2.502500341	0	2.49509E-05	0.032966	0	
ccmH	19	74	8.33E-12	1.961525852	0	0.000115854	0.00999	0	
celA	76	61	4.09E-13	-0.317190176	0.000554109	0.000551969	0.988879	1.003876476	
chaB	346	119	6.6E-114	-1.539810464	0.000936112	0.000612065	0.024942	1.529431359	
cheA	2	34	0	4.087462841	0	0.000146701	0.005449	0	
cheB	1	15	1	3.906890596	0	6.39447E-05	0.000249	0	
cheW	6	60	1.6E-167	3.321928095	0	0.000186205	0.041467	0	
cheY	9	35	1.56E-12	1.959358016	0.000191524	0.000900997	0.00051	0.212568981	
cheZ	10	42	3.4E-22	2.070389328	0	0.000402449	0.005246	0	
chuA	108	80	1.35E-18	-0.432959407	0.000213866	0.000103789	0.007911	2.060593159	
coaD	134	103	7.55E-17	-0.379588663	0.00071103	0.000339562	0.002905	2.093959381	
cpxP	370	1145	0.00482	1.629750422	0.00011158	0.000197083	0.277398	0.566154987	Y
crr	3766	2398	5.62E-09	-0.651201341	0.004296836	0.001489262	0.008945	2.885210407	
csgA	74527	4812	0	-3.953054639	0.001953221	0.000321548	0.019469	6.074433789	Y
csgC	845	65	0	-3.700439718	0.000637139	0.000214338	0.006793	2.972585576	
csgD	1274	180	0	-2.823296466	0.000594176	1.56518E-05	0.025951	37.96209647	Y
csgF	812	119	0	-2.770518154	0.000477722	5.13846E-05	0.044994	9.296988759	Y
cspA	378	2264	2.83E-21	2.582415819	0.001080596	0.00496002	0.002859	0.217861273	
cspG	106	263	0.055363	1.310998535	0	0.000860902	0.004131	0	
csrA	17602	8832	8.05E-10	-0.994927285	0	0.000960646	0.019609	0	
cstA	534	360	9.11E-17	-0.568842835	0.00026425	7.07998E-05	0.004084	3.732350425	
cutA	44	45	6.59E-06	0.032421478	0	0.000131568	0.016332	0	
cydB	773	815	1.39E-05	0.076331645	0	6.55784E-05	0.003307	0	
cysB	366	875	1	1.257439368	0.000123269	0.000262966	0.043709	0.468763997	
cysG	56	52	3.93E-12	-0.106915204	0.000212877	9.40699E-05	0.009928	2.262965902	
dadX	673	336	8.57E-31	-1.002145272	0.000718163	0.000194831	0.036337	3.686076522	
dbpA	71	48	1.75E-26	-0.564784619	0	3.20677E-05	0.012367	0	
dcd	229	166	1.91E-23	-0.464164357	0	0.000319144	0.000868	0	
deaD	127	365	0.077304	1.523067967	9.02352E-05	0.000585861	0.002469	0.15402164	
deoA	144	118	9.35E-15	-0.287281952	0.000134067	0.000347245	0.00233	0.386087397	
deoR	55	60	2.18E-06	0.125530882	0	8.44984E-05	0.000249	0	
dinD	18	27	1	0.584962501	0	9.88608E-05	0.017767	0	

dmsB	32	70	0.309452	1.129283017	0	0.000231581	0.00474	0	
dnaB	78	76	1.04E-10	-0.037474705	6.71048E-05	0.000156917	0.02117	0.427644681	
dnaE	117	80	2.86E-18	-0.548436625	0	1.06048E-05	0.018841	0	
dnaT	78	155	0.848307	0.990722186	0	0.000279473	0.009707	0	
dnaX	92	92	3.46E-08	0	0	3.88345E-05	0.018841	0	
dxr	91	90	3.11E-10	-0.015941544	0	0.000110219	0.007099	0	
elaB	3318	1803	2.68E-28	-0.87991449	0.001018652	0.000341367	0.006998	2.984038939	
erfK	135	193	0.005112	0.51564144	0.000494722	0.000115976	0.013394	4.265727171	
exbB	459	735	0.078706	0.679250096	0	0.000144424	0.013139	0	
exoX	83	78	2.83E-10	-0.089637212	0	6.32709E-05	0.017767	0	
fadB	82	50	3.95E-33	-0.713695815	0.000365411	0.000167514	0.01195	2.18138059	
fadD	86	75	2.98E-13	-0.197446064	0	5.14736E-05	0.002006	0	
fadJ	118	49	4.22E-81	-1.267933205	0	1.03583E-05	0.183648	0	Y
fdnG	21	58	0.189514	1.465663572	5.50753E-05	0.000275443	0.010317	0.19995161	
fdnH	26	56	0.524206	1.106915204	0	0.000159354	0.02291	0	
feoA	103	478	8.85E-20	2.214366281	0.000510769	0.000197722	0.076886	2.583274427	
feoB	53	230	2.65E-09	2.117569596	0	3.48282E-05	0.01383	0	
fepC	24	24	1	0	0	5.90503E-05	0.032966	0	
fis	372	493	0.000265	0.406285025	0	0.000447009	0.004375	0	
flgD	3	64	0	4.415037499	0	2.40865E-05	0.42265	0	Y
flgE	5	86	0	4.10433666	0	0.00024393	0.002039	0	
flgG	5	49	2.5E-156	3.292781749	0	7.02556E-05	0.007704	0	
flgK	7	52	9.87E-82	2.893084796	3.65519E-05	1.67643E-05	0.244777	2.180347207	Y
flgL	13	78	2.93E-42	2.584962501	2.82254E-05	0.000115541	0.1822	0.244288526	Y
flgM	16	103	4.14E-60	2.686500527	0	0.000690517	0.001688	0	
flgN	18	116	5.95E-62	2.688055994	0	7.47743E-05	0.183648	0	Y
fliA	6	65	1.4E-227	3.437405312	0	0.000161741	0.00086	0	
fliC	25	655	0	4.711494907	0.001561902	0.008283704	0.002815	0.188551134	
fliD	3	55	0	4.196397213	2.43883E-05	5.59967E-05	0.22459	0.435530227	Y
fliF	1	22	1	4.459431619	0	1.93931E-05	0.000249	0	
fliG	3	23	1	2.938599455	0	0.000174877	0.027835	0	
fliH	4	23	1	2.523561956	0	0.000136384	0.008331	0	
fliM	1	23	1	4.523561956	0	9.84318E-05	0.001288	0	

fliS	4	47	5.7E-202	3.554588852	0	6.48219E-05	0.2005	0	Y
fliY	163	211	0.00049	0.372371034	0.000825279	0.000120793	0.015711	6.832182653	
fliZ	17	43	0.03116	1.338801913	0	3.44209E-05	0.183788	0	Y
folC	66	56	7.63E-16	-0.237039197	0	0.000131109	0.011162	0	
frdA	221	544	0.981563	1.299560282	0.000614011	0.001243473	0.000215	0.493787267	
frdB	239	503	1	1.073547782	0.000471002	0.001452552	0.005753	0.324258199	
fruK	71	73	1.25E-09	0.040077439	0	0.000156176	0.009707	0	
fucO	109	99	2.79E-12	-0.138827705	0.000203923	0.000422704	0.004739	0.482425921	
fumB	6	55	8.5E-138	3.196397213	0	0.00052233	0.001354	0	
gabD	573	286	1.57E-30	-1.002519992	0.001881174	0.001323788	0.024134	1.421053859	
gabT	1032	441	2.11E-49	-1.22659241	0.002421801	0.001491807	0.008365	1.623400449	
galK	57	49	1.94E-13	-0.21818017	6.53984E-05	0.000182845	0.000903	0.357670653	
galR	63	108	0.104761	0.777607579	0	6.38648E-05	0.018751	0	
gldA	221	284	0.004855	0.36184456	0.000423721	0.000745224	0.011501	0.568582507	
glmU	177	179	1.56E-08	0.016210227	0.000173602	0.000354178	0.000538	0.490154566	
glnA	203	766	2.22E-05	1.915864665	0.000815057	0.001324273	0.026825	0.615474728	
glnH	992	933	8.62E-08	-0.08846304	0.005586877	0.002277544	0.010183	2.453027511	
glpA	8	75	6.2E-147	3.22881869	0	3.00988E-05	0.282286	0	Y
glpB	2	29	1	3.857980995	0	2.62884E-05	0.000249	0	
glpE	63	50	5.07E-13	-0.333423734	0	0.000303671	0.003796	0	
glpK	92	157	0.231965	0.771058793	0.000376713	0.0010772	0.00619	0.349715398	
glpQ	62	100	0.021756	0.689659879	0.000128809	0.000663145	0.002444	0.194240075	
gltL	242	146	5.11E-34	-0.729038678	0.000441495	0.000116503	0.011621	3.789548238	
glyQ	227	217	8.47E-10	-0.064997255	0.000252591	0.000506523	0.002152	0.498676856	
gmk	222	417	1	0.909487707	0	0.000131379	0.003603	0	
gnsB	13	15	1	0.206450877	0	0.000337993	0.000249	0	
hemK	33	35	3.32E-06	0.084888898	0	7.01052E-05	0.010188	0	
hisI	77	58	2.07E-16	-0.408805546	0	9.48158E-05	0.037285	0	
hisJ	337	359	4.59E-06	0.091235253	0.001077872	0.000487635	0.002679	2.210405106	
hmpA	57	186	0.004152	1.706268797	0	0.000107239	0.012524	0	
hsdS	16	25	1	0.64385619	0	0.000106109	0.009481	0	
hybA	58	175	0.023301	1.593230117	0.000172875	0.000301097	0.011426	0.574151302	
hybC	83	162	1	0.964810572	0.000226178	0.000578217	0.013744	0.391164504	

hybD	106	171	0.020528	0.68993206	0	0.00018546	0.020601	0	
hypB	30	72	0.251097	1.263034406	0	0.00022783	0.000351	0	
hypD	24	43	0.880548	0.841302254	0	3.35529E-05	0.016648	0	
ihfA	5750	3366	3.59E-17	-0.772526779	0.003214048	0.001504657	0.021005	2.136067141	
ilvB	73	71	2.9E-10	-0.040077439	8.66615E-05	0.000193853	0.046607	0.447047841	
ilvC	29	23	7.13E-14	-0.334419039	8.03491E-05	0.000226068	0.005464	0.355420694	
ilvN	102	89	5.34E-11	-0.196691911	0	0.00026954	0.016006	0	
intB	123	91	3.57E-20	-0.434719865	0	4.48406E-05	0.048541	0	
ispB	221	251	2.88E-06	0.183640995	0	0.000196953	0.027471	0	
katE	211	119	2.29E-30	-0.826281425	0.000403544	0.000166224	0.020142	2.427714714	
kefA	30	34	4.15E-07	0.180572246	0	9.31478E-06	0.000249	0	
kpsF	84	119	0.001193	0.502500341	0.000153501	0.000393556	0.013927	0.390035096	
kpsT	5	33	7.14E-55	2.722466024	0	5.56268E-05	0.194871	0	Y
lamB	146	440	0.01576	1.591535155	1.59337E-05	0.000200451	0.010361	0.079488877	Y
lasT	43	84	1	0.966052668	0	0.00011415	0.016702	0	
leuC	17	11	1	-0.628031223	0	5.91489E-05	0.000249	0	
leuD	23	15	1	-0.61667136	0	9.43612E-05	0.009053	0	
lpp	74321	25676	6.55E-16	-1.533349447	0.001948855	0.001332895	0.044181	1.462121665	
lpxD	826	650	9.26E-12	-0.345702064	0	0.000290019	0.000787	0	
luxS	1211	493	1.29E-71	-1.296539313	0.002174332	0.001702062	0.179839	1.277469309	
lysC	14	24	1	0.777607579	0	4.41389E-05	0.005948	0	
maa	151	790	2.69E-14	2.387304104	0	9.88807E-05	0.013282	0	
malE	148	407	0.038131	1.459431619	0.000983281	0.000948192	0.784075	1.03700637	
malK	41	142	0.000318	1.792195115	8.55486E-05	0.000177891	0.187882	0.480906115	Y
malQ	71	85	3.79E-05	0.259643817	0	7.69515E-05	0.02388	0	
mdaB	36	35	1E-07	-0.040641984	0	0.000241425	0.025919	0	
mglA	51	51	1.09E-10	0	6.47082E-05	0.000215247	0.005836	0.300623141	
mnmA	113	126	6.33E-07	0.157100961	0	0.000187506	0.013288	0	
mntR	74	64	1.77E-11	-0.209453366	0	0.000196329	0.032449	0	
moaC	70	85	0.000333	0.280107919	0.000157726	0.0003366	0.001537	0.468585168	
moaD	61	85	0.03351	0.478653599	0	0.000473941	0.007099	0	
modA	1161	638	2.15E-26	-0.863739643	0.004010155	0.000284404	0.014199	14.10023031	
modE	37	44	0.000402	0.249978253	0	0.000218607	0.005714	0	

moeA	34	43	0.000124	0.338801913	0	0.000222859	0.02425	0	
mqo	14	26	1	0.893084796	0	5.93231E-05	0.012248	0	
mraZ	317	218	1.22E-24	-0.540154705	0.000257904	0.000114227	0.011537	2.257826713	
mrp	132	183	0.002916	0.471305719	0	6.24781E-05	0.005459	0	
mrr	19	36	1	0.921997488	0	0.000121556	0.005332	0	
mscL	1812	734	3.2E-55	-1.303730987	0.00013278	0.000118298	0.92387	1.122426491	Y
mtlD	88	68	3.7E-20	-0.371968777	0.00013456	0.000324309	0.044893	0.414911528	
murD	140	94	2.57E-25	-0.574694165	0.000263834	0.000105001	0.006631	2.512675362	
mviM	79	82	2.18E-09	0.053771256	0	8.70705E-05	0.01383	0	
napA	22	354	0	4.008173931	5.25036E-05	0.00082008	0.000328	0.064022543	
napB	14	173	0	3.627273306	0	0.000382728	0.000249	0	
napF	23	286	2.7E-275	3.636309381	0	9.85814E-05	0.000249	0	
napG	16	230	0	3.845490051	0	0.000102464	0.005459	0	
napH	10	160	0	4	0	4.93381E-05	0.016332	0	
narG	21	69	0.012596	1.716207034	0	0.000200977	0.005129	0	
narH	21	58	0.033784	1.465663572	0	0.000197188	0.00238	0	
narJ	20	52	0.00757	1.378511623	0	4.49221E-05	0.226982	0	Y
narP	97	94	1.45E-10	-0.045323991	0	0.000205528	0.008563	0	
ndh	32	63	0.634057	0.977279923	0	0.000147654	0.001099	0	
nemA	39	38	1.42E-08	-0.037474705	0.000111253	0.000353307	0.002593	0.314889468	
neuA	16	63	1.59E-12	1.977279923	8.20817E-05	0.000369022	0.017656	0.222430282	
neuB	12	68	1.84E-37	2.502500341	0.000196043	0.000672716	0.004867	0.291419657	
neuC	15	54	5.11E-10	1.847996907	4.81821E-05	0.000340246	0.009817	0.141609662	Y
neuD	9	67	1.21E-93	2.896164189	0.000171327	0.000411144	0.009415	0.416706851	
neuS	2	16	1	3	0	6.95475E-05	0.020601	0	
nfo	55	47	4.49E-12	-0.226770862	0	0.000140115	0.003746	0	
nikR	47	40	3.29E-10	-0.232660757	0	0.000223052	0.002006	0	
nirB	4	34	4.3E-107	3.087462841	0	3.40973E-05	0.031474	0	
nmpC	207	279	0.012732	0.430634354	0	0.000121911	0.000591	0	
nrdD	62	181	0.011515	1.545649577	6.02336E-05	0.000118204	0.024496	0.509573202	
nrfA	25	483	0	4.272023189	0	0.000525987	0.002883	0	
nrfB	21	369	0	4.135159583	0	0.000140831	0.000249	0	
nrfC	12	257	0	4.420662048	0	0.000504558	0.000134	0	

nth	25	31	1	0.310340121	0	6.57841E-05	0.016332	0	
nuoH	296	214	1.2E-19	-0.467986379	0	3.82951E-05	0.018841	0	
nuoK	193	146	1.32E-16	-0.402632478	0	0.000179101	0.009247	0	
nuoL	232	180	1.12E-11	-0.366127899	0	3.5803E-05	0.018751	0	
ompF	684	1764	0.149008	1.366782331	0.000149363	0.000354036	0.007977	0.42188753	
oppF	162	130	4.88E-16	-0.31748219	0.000557748	0.000255939	0.013483	2.179223988	
osmC	1090	474	6.56E-66	-1.201369171	0.003007406	0.001407136	0.012926	2.137254071	
osmE	3217	1550	7.34E-37	-1.05344772	0.000768474	0.001231018	0.027939	0.624259296	
osmY	2994	1488	6.48E-24	-1.008699695	0.004693908	0.008072647	8.29E-05	0.581458308	
pabC	61	46	5.14E-16	-0.407175382	0	5.91489E-05	0.000249	0	
pcm	118	91	8.76E-18	-0.374848409	0	8.52025E-05	0.03394	0	
pdxA	148	134	6.71E-12	-0.143364175	4.55247E-05	0.000129692	0.250603	0.351022237	Y
pepE	63	77	6.01E-05	0.289506617	0.000207988	0.000543451	0.012108	0.382716137	
phnB	244	126	2.66E-46	-0.953457414	0.000548534	0.000184371	0.0462	2.975155198	
potD	260	193	2.52E-18	-0.429910776	0.000940247	0.000232629	0.045545	4.041834173	
potF	287	150	1.1E-41	-0.936088236	0.000683969	0	0.006721	#DIV/0!	
potG	160	72	5.59E-72	-1.152003093	0.000199311	4.78957E-05	0.020925	4.161356749	
proX	6	6	1	0	0	0.00013338	0.003107	0	
psiF	562	265	2.77E-66	-1.084577771	0.000434752	0.00016393	0.056153	2.652062984	
pspE	298	281	1.29E-12	-0.0847422	0	0.000213221	0.004278	0	
pspF	26	41	0.209874	0.657112286	0	5.18451E-05	0.009247	0	
pstS	91	107	1.19E-06	0.233672346	0.000648527	5.83743E-05	0.041951	11.10979043	
ptsN	266	268	4.17E-09	0.010806755	0.000760845	0.000248809	0.045906	3.057953328	
putP	394	232	2.83E-21	-0.764070824	0.000335998	0.000142728	0.013011	2.354112281	
pyrB	98	84	9.26E-16	-0.222392421	0.000268829	0.000631375	0.019378	0.4257844	
pyrH	176	180	6.74E-09	0.032421478	0.000202455	0.000453951	0.014816	0.445985281	
rbn	174	160	2.72E-11	-0.121015401	0	9.56378E-05	0.026224	0	
rbsR	82	41	3.17E-46	-1	0	1.04158E-05	0.42265	0	Y
rfaF	96	120	2.72E-05	0.321928095	0	6.56063E-05	0.004278	0	
rfaJ	57	58	9.64E-09	0.025090981	0	5.17673E-05	0.007704	0	
rffG	79	60	5.66E-20	-0.396890153	0	0.000137715	0.003307	0	
ribA	99	157	0.015837	0.665264129	0	0.000188386	0.010731	0	
ribD	53	71	0.000113	0.421826665	0	0.000152985	0.036601	0	

rimI	51	54	2.59E-06	0.08246216	0	9.30455E-05	0.017767	0	
rimJ	97	96	2.07E-09	-0.014950341	0	9.39065E-05	0.027504	0	
rmf	34274	14805	1.24E-11	-1.211030083	0.000113812	0	0.42265	#DIV/0!	Y
rnd	57	67	1.57E-06	0.233199176	0	6.42965E-05	0.006764	0	
rnt	39	49	0.000981	0.329307625	0	0.000237989	0.000414	0	
rph	103	92	2.19E-13	-0.162938571	0	0.000387486	0.01622	0	
rpoN	285	227	4.26E-11	-0.328269622	0	7.99103E-05	0.021988	0	
rpoS	3358	1704	4.97E-09	-0.978676895	0.000250847	0.000106165	0.000242	2.362807129	
rseB	340	418	0.001579	0.297968196	0.000446408	0.000159032	0.003546	2.807031193	
rsmC	72	72	1.88E-10	0	0.000147773	0.000409732	0.038559	0.360657582	
rspA	12	9	1	-0.415037499	0	2.93324E-05	0.018841	0	
rstA	41	145	5.85E-08	1.822357085	0	8.14279E-05	0.055498	0	
secB	479	445	8.03E-11	-0.10622032	0.000445971	0.001620708	0.007273	0.275170651	
selD	221	210	2.72E-10	-0.073657042	0.000227703	0.000489878	0.001803	0.464815307	
sgbH	8	8	1	0	0	7.36235E-05	0.032449	0	
slyA	671	605	3.72E-10	-0.149377624	0.001327307	0.000661517	0.008125	2.006459865	
smpB	146	202	0.000308	0.468386924	0	6.5721E-05	0.000249	0	
sodA	1370	907	4.73E-18	-0.595001437	0.00078142	9.39065E-05	0.018642	8.321253731	
sodC	271	174	1.7E-30	-0.639205546	0.001001426	0.000325171	0.003458	3.079691205	
sohB	107	85	4.31E-19	-0.33207605	0	7.03548E-05	0.029616	0	
speC	29	24	1.02E-13	-0.273018494	0	5.4792E-05	0.012576	0	
speD	44	58	0.004717	0.398549376	0	0.000216728	0.007636	0	
speF	15	26	1	0.793549123	0	6.17801E-05	0.002023	0	
spoT	178	184	1.14E-05	0.047828525	0	4.49232E-05	0.000249	0	
spy	303	152	2.4E-55	-0.99524647	0.002197314	0.000886147	0.025476	2.479626864	
srlR	39	37	3.24E-08	-0.075948853	0	9.13802E-05	0.004278	0	
sucA	614	517	0.000239	-0.248074375	0.001238678	0.001146789	0.036388	1.080127832	
sufB	129	149	3.64E-06	0.207941265	0	7.71091E-05	0.022786	0	
sufC	126	121	5.96E-12	-0.058416686	0.000468407	0.000183028	0.033702	2.55920315	
sufD	136	129	6.01E-10	-0.076235586	0	4.19173E-05	0.009247	0	
sufS	110	96	2.36E-13	-0.196397213	0	6.25976E-05	0.003307	0	
tar	3	52	0	4.115477217	0	0.000196598	0.010753	0	
tdcA	9	69	2.34E-82	2.938599455	0	6.69168E-05	0.113945	0	

tdcB	20	323	0	4.01346226	0.000143671	0.001369517	0.002277	0.104906283	
tdcC	22	337	0	3.937173163	0	6.43163E-05	0.100855	0	
tdcD	12	210	0	4.129283017	0	0.000497151	1.31E-05	0	
tdcE	10	212	0	4.40599236	3.76449E-05	0.000788405	0.000372	0.047748127	Y
tdcG	17	135	3.43E-88	2.989352756	1.62588E-05	0.000494065	0.000369	0.032908263	Y
thiC	123	87	1.01E-20	-0.499571009	0.000537639	0.0002604	0.002472	2.064669508	
thiE	117	78	2.22E-23	-0.584962501	0.001145293	0.000514466	0.042568	2.22617696	
thiG	108	78	1.16E-21	-0.469485283	0.000742519	0.000345249	0.036263	2.15067776	
thiH	130	87	2.33E-27	-0.579424317	0	3.2061E-05	0.018841	0	
thrC	84	61	5.54E-23	-0.461580085	0.000110632	0.000255734	0.031755	0.432604108	
tnaA	12	42	9.35E-08	1.807354922	8.49403E-05	0.000412587	0.00267	0.205872314	
treB	15	111	2.28E-68	2.887525271	0	0.000135133	0.002145	0	
treC	6	59	1.6E-142	3.297680549	0	0.00025567	0.009511	0	
treF	51	99	0.403917	0.956931278	0	4.0025E-05	0.005459	0	
trpA	585	276	7.3E-55	-1.083768358	0.001991159	0.001215683	0.027142	1.637893982	
trpB	459	223	5.27E-44	-1.041450443	0.000807652	0.0006933	0.041265	1.164939107	
trpC	333	156	7.42E-56	-1.093976148	0.000653327	0.000366068	0.0033	1.784713989	
trpD	345	135	7.1E-85	-1.353636955	0.000246322	0.000262674	0.575882	0.9377502	
trpE	186	93	7.66E-50	-1	0.000776231	0.000469214	0.001825	1.654322574	
truA	40	32	1.9E-14	-0.321928095	0	4.58557E-05	0.016648	0	
trxA	1262	1146	1.77E-08	-0.139104866	0.002098803	0.000910851	0.019354	2.304222561	
trxB	231	234	3.63E-08	0.018615678	0.000427873	0.00086372	0.026314	0.495383718	
tsr	8	55	4.22E-64	2.781359714	0	0.000256677	0.019883	0	
tyrS	228	199	1.13E-11	-0.196265394	0.000313476	0.000632002	0.001183	0.496004808	
ubiG	85	62	3.1E-18	-0.455194626	0	0.000321746	0.003746	0	
ugpB	183	100	2.65E-41	-0.871843649	0.001435901	0.000562895	0.016261	2.550920642	
usg	81	77	2.86E-12	-0.073063462	0.000155501	0.000537136	0.029014	0.289500069	
uvrB	67	53	5.36E-18	-0.338168736	0	3.89526E-05	0.01383	0	
uxaA	19	20	1	0.074000581	0	4.3814E-05	0.000249	0	
waaW	63	61	1.4E-10	-0.046542586	0	4.02902E-05	0.012367	0	
xdhD	12	61	1.01E-23	2.345774837	0	4.26999E-05	0.342303	0	Y
xseA	74	97	0.000165	0.390459477	0	2.27496E-05	0.000249	0	
xylA	35	27	3.8E-16	-0.374395515	0	6.26436E-05	0.042754	0	

xylB	29	22	4.19E-16	-0.398549376	0	3.36778E-05	0.04042	0	
yaiI	33	64	1	0.955605881	0	6.25304E-05	0.016648	0	
yajO	216	148	8.97E-24	-0.545434137	0.000217617	0.000476395	0.020935	0.456799538	
ybaA	970	264	1.1E-246	-1.877446818	0.001024081	0.000242091	0.050771	4.230151455	
ybaY	1622	607	1.14E-61	-1.418005398	0.001110276	0.000757836	0.098994	1.46506184	
ybdK	102	80	3.97E-19	-0.350497247	0	8.44984E-05	0.000249	0	
ybeJ	1059	737	1.6E-15	-0.522966065	0.007904565	0.002620871	0.016462	3.016007541	
ybfE	22	37	1	0.750021747	0	0.000154697	0.030243	0	
ybgA	56	72	0.002836	0.362570079	0.0002011	0	0.003062	#DIV/0!	
ybgF	416	331	3.53E-14	-0.329752311	0.000143643	0.000387173	0.019715	0.371004271	
ybhA	21	23	1	0.131244533	0	0.000164055	0.009504	0	
ybhB	361	166	1.26E-68	-1.120815596	0.000672973	0.000405919	0.085408	1.657897904	
ybiC	67	53	5.13E-17	-0.338168736	0	0.00017698	0.001288	0	
ycbJ	81	155	0.445128	0.936274402	0	7.54749E-05	0.024037	0	
yccT	188	50	4.7E-207	-1.910732662	0.00014238	0	0.015323	#DIV/0!	
ycdX	120	113	1.69E-12	-0.086711633	0.000160698	0	0.040276	#DIV/0!	
yceA	96	75	7.2E-20	-0.35614381	0	6.55784E-05	0.003307	0	
yceD	1573	1459	4.74E-08	-0.108538787	0.000705615	0.000300857	0.019147	2.345348564	
ycgB	414	359	9.64E-10	-0.205646924	0	4.19935E-05	0.005459	0	
yciE	99	44	1.09E-62	-1.169925001	0.000256991	4.05668E-05	0.044317	6.335020491	Y
yciG	566	202	1.7E-104	-1.48644676	0.000672501	0	0.028374	#DIV/0!	
yciH	47	41	2.09E-09	-0.197036847	0	0.000161046	0.032966	0	
ydcF	38	28	1.12E-18	-0.440572591	0.000178756	7.24421E-05	0.00062	2.467567147	
ydcI	120	94	1.59E-18	-0.352301744	0.000171436	6.56063E-05	0.046958	2.613099962	
ydcJ	282	135	2.08E-51	-1.062735755	0.000434863	0.000174466	0.079591	2.492531137	
yddE	43	38	9.58E-11	-0.178337241	0	0.000117018	0.002563	0	
ydfH	60	93	0.023708	0.632268215	0	0.000145993	0.016586	0	
ydfZ	37	96	0.001309	1.375509135	0.000368929	8.70637E-05	0.409746	4.237467331	Y
ydhF	199	148	3.45E-19	-0.427171255	0.000285339	0.000138692	0.014286	2.057350913	
ydjF	30	44	0.077116	0.552541023	0	0.00011261	0.003603	0	
yeaD	150	132	6.57E-13	-0.184424571	0.001216319	0.000418633	0.00296	2.905455216	
yebC	161	145	3.75E-13	-0.151007788	0.000154692	0.000341532	0.007178	0.452936909	
yecF	145	216	0.072005	0.574978412	0	0.001473493	0.010044	0	

yeeN	40	82	1	1.03562391	0	0.000257656	0.000429	0	
yegW	21	22	1	0.067114196	0	6.36417E-05	0.039616	0	
yehT	36	37	1.38E-06	0.039528364	0	0.000113146	0.030975	0	
yeiI	36	32	9.99E-11	-0.169925001	0	2.95744E-05	0.000249	0	
yeiQ	40	188	1.04E-12	2.232660757	0	7.61777E-05	0.067122	0	
yejG	244	832	0.001445	1.769702381	0.000381871	0.000227496	0.092459	1.678588137	
yfbT	164	139	2.72E-16	-0.238610932	0.000171327	0.000377376	0.030896	0.453995037	
yfcE	156	128	3.79E-17	-0.285402219	0	8.87233E-05	0.000249	0	
yfeC	183	395	1	1.110009005	0	0.000196242	0.019508	0	
yfeY	123	112	1.25E-12	-0.135159583	0	0.000112664	0.000249	0	
yffB	96	152	0.118254	0.662965013	0	0.000660941	0.002028	0	
yfgL	531	344	1.1E-16	-0.626303296	0.000126155	0.000390236	0.013651	0.323279424	
ygaD	81	56	4.34E-21	-0.532495081	0	0.000263136	0.016332	0	
ygaE	213	99	1.38E-64	-1.105353	0	3.78605E-05	0.195659	0	Y
ygaF	693	329	5.16E-35	-1.074767768	0.00024529	0.000136103	0.182692	1.802231078	
ygaM	1819	648	6.3E-107	-1.489079825	0.000630348	0.000311556	0.044331	2.023226556	
ygbI	35	29	1.59E-13	-0.271302022	0	0.00011527	0.01099	0	
ygeW	12	248	0	4.36923381	0	0.000232806	0.001965	0	
ygeX	6	124	0	4.36923381	0	0.000104971	0.031205	0	
ygeY	7	95	0	3.762500686	0	0.000499313	0.000144	0	
ygfB	116	161	0.00031	0.472935883	0	0.000140831	0.000249	0	
ygfK	9	78	1.27E-86	3.115477217	0	0.000130734	0.000359	0	
ygfM	11	60	3E-36	2.447458977	0	0.000122173	0.032966	0	
ygfZ	102	100	3.99E-11	-0.028569152	0.000120524	0.000383122	0.012488	0.314583268	
yggL	737	351	6.75E-59	-1.070193589	0.000506024	0.000421745	0.214091	1.199834931	
yggS	41	45	1.21E-05	0.134301092	0.00027941	0	0.041999	#DIV/0!	
yghA	81	35	2.89E-63	-1.210566986	0.000125688	6.23616E-05	0.101775	2.015464122	
ygiN	496	393	1.24E-16	-0.335810808	0.001419195	0.000708363	0.001146	2.003485064	
ygiX	13	10	1	-0.378511623	0	5.5445E-05	0.024525	0	
yhaR	15	243	0	4.017921908	0.000719748	0.003317112	0.067591	0.216980383	Y
yhcJ	40	30	2.63E-17	-0.415037499	0	0.000284215	0.00367	0	
yhhA	356	458	0.000468	0.363470357	0.00141851	0.000404783	0.012669	3.504376746	
yhiR	52	133	0.343182	1.354842717	0	0.000155955	0.012736	0	

yhjA	5	27	1	2.432959407	0	2.6512E-05	0.018841	0	
yhjM	154	115	5.38E-19	-0.42129649	0.000295243	0	0.002757	#DIV/0!	
yhjN	168	124	6.99E-14	-0.438121112	0.000471769	0.000216829	0.019369	2.175769871	
yhjW	14	27	1	0.94753258	0	3.92939E-05	0.036741	0	
yiaY	8	10	1	0.321928095	0	7.8867E-05	0.046605	0	
yibF	299	140	1.76E-66	-1.094718657	0.000684779	0.000401986	0.172493	1.703490892	
yibK	29	35	0.003334	0.271302022	0	0.000164555	0.039038	0	
yidB	221	107	3.52E-49	-1.046435573	0	0.00018276	0.004278	0	
yidC	188	225	0.000914	0.25919234	8.64947E-05	0.000241949	0.003005	0.357491809	
yieP	226	741	0.000251	1.71315077	0	6.10648E-05	0.204678	0	Y
yihI	189	181	3.8E-12	-0.062396537	0	0.000372316	0.012715	0	
yiiQ	21	20	1	-0.070389328	0	9.87846E-05	0.010188	0	
yjbJ	4273	1305	2.3E-119	-1.71119951	0.003567986	0.001490172	0.002759	2.394345143	
yjbK	75	139	0.39522	0.890122382	0	0.000113573	0.036361	0	
yjbN	35	34	8.91E-08	-0.041820176	7.24685E-05	0.000266717	0.011744	0.271705765	
yjcD	70	74	2.89E-09	0.080170349	0	4.30559E-05	0.040843	0	
yjdI	74	63	2.81E-10	-0.232173442	0	0.000154014	0.024525	0	
yjgB	86	39	3.24E-58	-1.140862536	0	1.01417E-05	0.42265	0	Y
yjgD	366	654	0.625004	0.837446987	0	0.000159447	0.019508	0	
yjgR	109	71	2.24E-28	-0.618437205	0.000352806	0.000116836	0.013806	3.019671323	
yjjI	13	38	0.0006	1.547487795	1.37359E-05	0.000156395	0.024093	0.087828125	Y
yjjV	42	27	1.35E-23	-0.637429921	9.24598E-05	0	0.003062	#DIV/0!	
ykfE	769	361	1.01E-54	-1.090984761	0.000795945	0.000904977	0.616152	0.879519536	
ykgE	22	31	1	0.494764692	0	7.57736E-05	0.009247	0	
ykgF	18	25	1	0.473931188	0	4.44991E-05	0.01794	0	
ymdB	308	147	2.39E-62	-1.067114196	8.38614E-05	0.00029111	0.139517	0.288074424	Y
ymjA	31	35	0.000564	0.175086707	0	0.000349182	0.012367	0	
ynfG	7	14	1	1	0	0.000111048	0.036741	0	
ynfK	90	163	0.230815	0.856875058	0	7.10969E-05	0.035658	0	
yoaH	91	83	1.38E-08	-0.132755209	0	0.000310044	0.009053	0	
yohN	99	58	7.92E-32	-0.771375625	0.000536773	0.000228214	0.035055	2.352060481	
ypeA	83	55	8.79E-23	-0.593679718	0	0.000197352	0.016332	0	
ypfH	134	67	1.08E-46	-1	0.000101328	0.00012857	0.620337	0.788111525	Y

yqcA	122	217	0.13383	0.830813895	0	0.000184371	0.011162	0
yqeA	15	50	1.31E-06	1.736965594	0	0.000125695	0.008907	0
yqeB	11	84	2.66E-74	2.932885804	0	3.747E-05	0.010188	0
yqgE	98	97	7.08E-10	-0.014797002	0.00025454	0.000121624	0.01229	2.09284254
yqhD	10	17	1	0.765534746	0	0.000201643	0.002984	0
yqjC	1841	1299	6.23E-15	-0.503088196	0.000669095	0.000225545	0.039457	2.966565624
yqjD	2400	1601	8.2E-17	-0.584061098	0.002276333	0.001075165	0.034761	2.117194051
yrbB	309	223	7.47E-24	-0.470563128	0	0.000183507	0.008563	0
yrbC	386	276	6.89E-20	-0.48393258	0.000954986	9.78332E-05	0.017637	9.761362664
yrbF	129	131	1.03E-09	0.022195746	0	0.000122118	0.007506	0
ytfE	12	13	1	0.115477217	0.000126447	0	0.033032	#DIV/0!
ytfG	12	12	1	0	0	0.000183468	0.021267	0

Note: Yellow denotes meeting the $p<0.05$ cut off. Green denotes meeting the 2-fold change (1 $\log_2$fc) cut off.

Table 3.2. Strains, plasmids, and primers used in this study.

Designator	Description	Source
Strains		
CL61	UTI89 *E. coli* Wild Type, bladder isolate	(62)
CL1175	UTI89 attB::*csgBAC*-eGFP electroporated with pCKR101- mCherry	(19)
	UTI89 *nrfA::kan*, Redswap mutant made with primers JP1 and JP2	This work
Plasmids		
pKD46	Arabinose-inducible red recombinase	(227)
pKD4	Contains kan cassette to use as template	(227)
pCKR101-mCherry	mCherry cloned into KpnI and XbaI sites of pCKR101	(19)
Primers		
JP1 RS Fwd.	5’ AAT AAA AAC CGC CAT TGC AAC AAT GGC GCA ATT CGG ATG AAG CCC TAT GGT GTA GGC TGG AGC TGC TTC 3’	
JP2 RS Rev.	5’ TTT TCC GCC CCT TGC GAG GCG GAA CGG GGT TAT TGG CTT AAC AGA CCG TTC ATA TGA ATA TCC TCC TTA G 3’	
JP3 Check Fwd.	5’ GAG CAA TGT CAT GAC AGT GTA GGT GC 3’	
JP4 Check Rev.	5’ TCC GTT CAG GCT CCA CAA CAG GC ‘3	

CHAPTER IV

Thiol Starvation Induces Redox-Mediated Dysregulation of *Escherichia coli* Biofilm Components

Abstract

A hallmark of bacterial biofilms is the production of an extracellular matrix (ECM) that encases and protects the community from environmental stressors. Biofilm formation is an integral portion of the uropathogenic *Escherichia coli* (UPEC) lifecycle. Approximately 2% of UPEC are cysteine auxotrophs. Here, we investigated how cysteine homeostasis impacted UPEC UTI89 strain biofilm formation and, specifically, the production of the ECM components curli and cellulose. Cysteine auxotrophs produced less cellulose and slightly more curli compared to wildtype (WT) strains, and cysteine auxotrophs formed smooth, non-rugose colonies. Cellulose production was restored in cysteine auxotrophs when YfiR was inactivated. YfiR is a redox-sensitive regulator of the diguanylate cyclase, YfiN. Curli production, a temperature-regulated appendage, was independent of temperature in UTI89 cysteine auxotrophs. In a screen of UPEC isolates, we found that ~60% of UPEC cysteine auxotrophs produced curli at 37°C, but only ~2% of cysteine prototrophic UPEC produced curli at 37˚C. Interestingly, sub-lethal concentrations of mecillinam and trimethoprim/sulfamethoxazole inhibited curli production, whereas strains auxotrophic for cysteine continued to produce curli even in the presence of mecillinam and trimethoprim/sulfamethoxazole. The dysregulation of ECM components and resistance to mecillinam in cysteine auxotrophs may be linked to hyper-oxidation, since the addition of

The contents of this chapter published by the *Journal of Bacteriology* by David A. Hufnagel, Janet E. Price, Rachel E. Stephenson, Jesse Kelley, Matthew F. Benoit, Matthew R. Chapman. D.A.H. and M.R.C. conceived and designed the experiments; D.A.H. and J.E.P. performed most of the experiments with help from J.K and M.F.B. The data was analyzed by D.A.H., J.E.P. and M.R.C. D.A.H. and J.E.P. co-wrote the manuscript with help from R.E.S. and M.R.C.

exogenous cysteine or glutathione restored WT biofilm phenotypes to strains unable to produce cysteine and glutathione.

Importance

Uropathogenic *Escherichia coli* (UPEC) are the predominant causative agent of urinary tract infections (UTIs). UTIs account for billions of dollars of financial burden to the healthcare industry in the United States annually. Biofilms are an important aspect of the UPEC pathogenesis cascade and for the establishment of chronic infections. Approximately ~2% of UPEC strains isolated from UTIs are cysteine auxotrophs, yet there is relatively little known on the biofilm formation of UPEC cysteine auxotrophs. Here we show that cysteine auxotrophs have dysregulated biofilm components due to a change in the redox state of the periplasm. Additionally, we show the relationship between cysteine auxotrophs, biofilms, and antibiotics frequently used to treat UTIs.

Introduction

Biofilms are communities of bacteria attached to a surface that produce an extracellular matrix (ECM) that is typically composed of polysaccharides, protein, and DNA (303). The ECM of *Escherichia coli* is predominately composed of the protein fiber curli and the polysaccharide cellulose (78). *E. coli* ECM production and biofilm formation generally occur in low salt, low nutrient, and low temperature conditions, although certain isolates of *E. coli* have been found to produce ECM components at higher temperatures (104, 117, 304-307). The redox state greatly influences biofilm formation by *E. coli* (87, 308), *Pseudomonas aeruginosa,* and *Bacillus subtilis* (295, 309, 310).

E. coli biofilm formation is typically dependent on the transcriptional regulator CsgD, which induces production of both curli and cellulose (77, 311). CsgD activates transcription of the *csgBAC* operon, which encodes the minor and major subunits of the curli fiber and the chaperone-like protein, CsgC (98, 311, 312). CsgD also transcriptionally up-regulates *adrA,* which encodes a diguanylate cyclase that produces the secondary messenger cyclic (c-) di-GMP (77). C-di-GMP is a secondary messenger involved in promoting biofilm formation and inhibiting sessile processes like motility (303). C-di-GMP binds to the cellulose synthase, BcsA, leading to its activation (77, 84). WT CsgD protein levels require c-di-GMP from both YfiN (DgcN) and YdaM (DgcM) (87, 248). YfiN is inhibited by the redox-sensitive periplasmic regulator YfiR and,

upon YfiR depletion, YfiN dimerizes leading to unregulated constitutive cellulose production (87).

Multiple cysteine biosynthesis and catabolic products have been implicated in biofilm formation and development (313-317). O-acetylserine (OAS) is a precursor to cysteine and has been found to inhibit biofilm formation in *E. coli* and *Providencia stuartii* (313) (Figure 4.1A). CysE is a serine acetyl transferase that converts serine and acetyl-CoA to OAS, whereas CysK and CysM are O-acetylserine sulfhydrylases, which convert OAS to cysteine (Figure 4.1A). Δ*cysE* strains that cannot produce OAS (Figure 4.1A) form hyper-biofilms, and addition of exogenous OAS inhibits biofilm formation in WT laboratory strains (313). Δ*cysB* strains produce hyper-biofilms, and CysB is regulated by N-acetylserine (NAS), a product of OAS (314). Phosphoadenosine 59-Phosphosulfate (PAPS), which is produced by CysC in the sulfur assimilation pathway, is a biofilm-activating compound that can increase production of curli (316, 317). Starvation of the cysteine precursor, serine, in *B. subtilis* leads to ribosome stalling on cysteine codons and biofilm upregulation (318). Additionally, work in *Vibrio fischeri* has found that cysteine auxotrophs are defective at forming wrinkled colonies (319). In summary, cysteine metabolism affects biofilm formation through multiple pathways in many microorganisms.

Cysteine auxotrophs of uropathogenic *E. coli* (UPEC) are commonly isolated from patients with an active urinary tract infection (UTI) (320). Approximately 1.5-2% of UPEC strains are cysteine auxotrophs (321, 322). Interestingly, cysteine auxotrophic UPEC strains can also be resistant to antibiotics such as mecillinam. Thulin *et al.* found that of 12 mecillinam resistant UPEC identified, each had mutations in the cysteine biosynthesis transcriptional regulator *cysB* (323).

We asked if UPEC cysteine auxotrophs produced curli and cellulose matrix components. We found that UPEC cysteine auxotrophs had increased curli and decreased cellulose levels. A lack of thiol reducing agents such as cysteine or glutathione altered cellular redox leading to aberrant ECM production. Oxidative stress has been implicated as a contributor to the efficacy of antibiotics (324, 325), although the specific mechanisms and contributions are still being considered (326, 327). We found that sub-inhibitory concentrations of mecillinam inhibited

biofilm formation. This may be a wide-spread mode of action, as the antibiotic trimethoprim/sulfamethoxazole also inhibited UPEC biofilm. Interestingly, cysteine auxotrophs were resistant to the curli-inhibition of both antibiotics. In summary, cysteine biosynthesis is necessary for the coupling of curli and cellulose production in UPEC biofilms.

Results

Colony wrinkling is inhibited in cysteine auxotrophs. Wild-type (WT) UTI89 colonies bind Congo red (CR), spread, and wrinkle when grown at 26° on YESCA media (Figure 4.1B) (87, 308). Colony spreading is dependent on both curli and cellulose, whereas cellulose alone can promote colony wrinkling (87). To investigate the roles of the biofilm modulatory compounds, cysteine and OAS, on UPEC biofilms and the production of curli and cellulose, we constructed Δ*cysE* and the *ΔcysKΔcysM* strains via lambda red mutagenesis. Both the Δ*cysE* and the *ΔcysKΔcysM* strains bound CR, but did not wrinkle or spread, indicating that there was likely a defect in cellulose production (Figure 4.1B). Addition of 20µL of 10% cysteine (w/v) to a sterile paper disk located 1cm away from the inoculation center restored colony wrinkling to cysteine auxotrophs (Figure 4.1B). To rule out colony morphology phenotypes observed in Figure 4.1B being caused by a lack of colony forming units (CFUs) in cysteine auxotrophs, the number of CFUs per colony was measured at 24 hours (Figure 4.1C). CFUs per colony of Δ*cysE* grown on YESCA or YESCA+cysteine plates were approximately equivalent, and so we concluded that a significant growth defect by the Δ*cysE* strain was not the reason for its smooth colony morphotype (Figure 4.1C). YESCA broth/plates have a calculated 99µM cysteine present according to BD bionutrients manual, enough for growth of cysteine auxotrophs (Figure 4.1C and Figure 4.9A), but not enough reducing capacity to support matrix production and rugose biofilm formation (Figure 4.1B). Since O-acetylserine (OAS) and cysteine have both been implicated in biofilm formation in laboratory strains, we probed our mutants with OAS. The addition of OAS restored wrinkling to *ΔcysE*, but not to *ΔcysKΔcysM* strains (Figure 4.1B), leading us to conclude that the smooth colony morphotype of UPEC cysteine auxotrophs was due to the lack of cysteine, not OAS. Wrinkling and spreading were restored in Δ*cysE* and *ΔcysKΔcysM* strains when these genes were complemented *in trans* (Figure 4.1D).

To determine if cysteine modulated UTI89 biofilm biomass similarly to laboratory strains, we performed pellicle biofilm assays with UTI89 WT and *ΔcysE.* WT UTI89 forms wrinkled pellicles, while the *ΔcysE* strain forms smooth pellicles, somewhat akin to the wrinkled (WT UTI89) and smooth (*ΔcysE*) colonies formed by these strains grown on YESCA plates (Figure 4.8A and Figure 4.1B). Interestingly, quantification of the pellicle biomass revealed that the *ΔcysE* pellicle had a greater amount of biomass, correlating with previously published research on *ΔcysE* strains as hyper-biofilm formers (Figure 4.8B) (323).

Cysteine auxotrophs have an altered ECM. Due to the altered colony biofilm in *ΔcysE* and *ΔcysKΔcysM*, we investigated the production of the extracellular matrix (ECM) components curli and cellulose in cysteine auxotrophs. UTI89 *ΔcsgBA* mutants do not make curli fibers, but bind CR and wrinkle due to cellulose production via the cellulose synthase, BcsA (77, 87, 308). The Δ*cysE*Δ*csgBA* strain had decreased CR binding compared to Δc*ysE*, and did not wrinkle under biofilm-inducing growth conditions unless exogenous cysteine was added in the medium (Figure 4.2A), suggesting that the Δc*ysE* strain is defective for cellulose production. To more carefully assess cellulose production, we used the cellulose-specific stain Pontamine Fast Scarlet 4B (S4B) (87). As predicted, Δ*cysE* colonies bound less S4B stain than WT colonies (Figure 4.2B). Additionally, the transcription of the cellulose activating diguanylate cyclase, *adrA,* was decreased in *ΔcysE* and *ΔcysKΔcysM* strains compared to WT (Figure 4.10). Staining with S4B was restored to WT levels when exogenous cysteine was added to the *cysE* mutant strain (Figure 4.2B). We measured curli production using antibodies against CsgA and CsgD. On YESCA plates at 26˚C, CsgD protein levels were comparable between WT and Δ*cysE* strains*,* while CsgA protein levels were increased in Δ*cysE* strains (Figure 4.2C and 2D). Increased curli production was also seen in the Δ*cysK*Δ*cysM* strain (Figure 4.11A). The addition of 250 µM cysteine to YESCA plates induced colony wrinkling in Δ*cysE* strains (Figure 4.2A), and restored CsgA protein to wild type levels (Figure 4.2D). Expression of CsgA was dependent on CsgD, as Δ*cysE*Δ*csgD* strains did not bind CR or produce CsgA (Figure 4.2C).

We next compared the CR phenotype of WT and *ΔcysE* with strains unable to produce curli, cellulose, or both. WT, a curli mutant (Δ*csgBA*), a cellulose mutant (Δ*bcsA*), a curli and

cellulose mutant (Δ*csgBAΔbcsA*), and a cysteine auxotroph (Δ*cysE*) were grown at 26°C on YESCA CR for 14 hours (Figure 4.3A). After 14 hours of growth at 26°C, WT colonies stained red, whereas the Δ*csgBA*Δ*bcsA* mutant (curli$^-$/cellulose$^-$) was white (Figure 4.3A). Both the Δ*csgBA* (curli$^-$/cellulose$^+$) and Δ*bcsA* (cellulose$^-$/curli$^+$) mutants simultaneously stained red at the 14 hour time point, indicating that curli and cellulose production are temporally synchronized. The Δ*cysE* mutant not only stained deep red at 14 hours, but was also the first strain to bind CR on the plate (Figure 4.3A). In contrast, Δ*cysEΔcsgBA* remained white until 18 hours of growth, suggesting that cysteine auxotrophy delayed cellulose synthesis (Figure 4.3A and data not shown). Addition of 250μM cysteine to the media resulted in Δ*cysEΔcsgBA* turning red at 14 hours (Figure 4.3A, right panel). Using time-lapse fluorescence microscopy, we assessed transcription from the *csgBAC* promoter using a chromosomal *csgBAC-mCherry* fusion in WT, Δ*cysE,* and Δ*csgBA* colonies on YESCA media without CR. Despite CR binding by Δ*cysE* at an earlier timepoint than WT, *csgBA* transcription was not appreciably increased in the Δ*cysE* colony compared to WT (Figure 4.3B). Additionally, we looked at expression of the *csgBAC* promoter via β-galactosidase transcriptional fusions (308, 328) and found similar transcription in WT, Δ*cysE,* and Δ*cysKM* mutant cells (Figure 4.10).

Cysteine auxotrophs have a defective ECM due to an altered redox state. Because there was no detectable growth defect of the cysteine auxotrophs when grown on YESCA plates (Fig. 1C), we speculated that the defect in cellulose production in cysteine auxotrophs might be due to an altered redox state of the colony. The amino acid cysteine reduces disulfide bonds (329). We hypothesized that cysteine auxotrophs might be hyper-oxidized since they would have fewer reduced thiols like cysteine and glutathione. Glutathione is a reducing agent of reactive oxygen species (ROS), participates in the glutaredoxin cytoplasmic disulfide reduction system (330) and is produced from cysteine (Figure 4.4A) (331, 332). We found that adding glutathione to a disk restored wrinkling and spreading to Δ*cysE* colonies (Figure 4.4B). Because glutathione can be converted back into cysteine by GshA and GshB (Figure 4.4A) (331), we constructed *ΔgshA, ΔgshB,* Δ*cysE gshA::kan* and *ΔcysE gshB::kan* strains. Δ*cysE gshA::kan* and Δ*cysE gshB::kan* phenocopied Δ*cysE* colonies on YESCA media (Figure 4.4B). The addition of either cysteine or

glutathione restored wrinkling to Δ*cysE gshA::kan* and Δ*cysE gshB::kan* (Figure 4.4C) and rescued shaking growth in a 96 well plate (Figure 4.9). It is possible that the slight difference in growth between cysteine and glutathione supplementation of cells comes from the action of γ-glutamyltranspeptidase (GTT), which breaks down glutathione to be used as a nitrate and cysteine source (333). This process is less efficient than cysteine addition and may account for the steady growth of glutathione supplemented cells to the level of cysteine supplemented cells (Figure 4.9B and C). Mutations *ΔgshA* or *ΔgshB* alone in the WT UTI89 background did not induce the cysteine auxotroph smooth colony morphotype (Figure 4.4B). These results suggest that hyper-oxidation of Δ*cysE* strains caused the non-spreading, smooth colony morphotype and that exogenous addition of glutathione or cysteine helped create reducing conditions that support cellulose production.

YfiR and c-di-GMP regulate the Δ*cysE* smooth colony morphotype. C-di-GMP is a critical signaling molecule for regulating matrix production, and at least part of c-di-GMP's action occurs through CsgD (87, 248). Decreased cellulose and *adrA* transcription in *ΔcysE* (Figure 4.2B and Figure 4.10) led us to hypothesize that c-di-GMP levels were globally misregulated in the *cysE* mutant strain. Motility can be used as a proxy for c-di-GMP levels as the flagellar brake YcgR is sensitive to c-di-GMP (334, 335). Δ*cysE* mutants displayed no statistical difference in motility from WT strains (Figure 4.12A). Mutation of flagella machinery, *fliC,* or the periplasmic inhibitor of an alternate c-di-GMP pathway, *yfiR,* in the *ΔcysE* background (87), show a significant decrease in swimming (Figure 4.11) indicating that any change in c-di-GMP levels of the Δ*cysE* strain were minimal or spatially unavailable to inhibit motility.

To better understand why Δ*cysE* strains produced smooth colonies at 26°C, transposon mutations were constructed in the Δ*cysE* background. Approximately 45,000 colonies from the Δ*cysE*+transposon library were screened on CR-indicator plates grown at 26°C for Δ*cysE*+transposon strains that gained the wrinkled colony phenotype (Table 4.1). We predicted that transposons that interrupted phosphodiesterase enzymes, which degrade c-di-GMP, would restore wrinkling to *cysE* strains. Indeed, we identified one strain with a transposon insertion in *yciR* (*pdeR*)*,* which encodes a phosphodiesterase (69). We identified a second strain with an

insertion found in *yfiR,* whose gene product inhibits activation of the diguanylate cyclase YfiN (87, 336).

Δ*cysE yfiR::kan* and Δ*cysE yciR::kan* strains were constructed by lambda red genome editing. Δ*cysE yciR::kan* did not restore wrinkling, while Δ*cysE yfiR::kan* had a robust wrinkled colony morphotype (Figure 4.5A). YfiR contains a disulfide bond that is sensitive to the oxidation state of the cell (87). Oxidized YfiR is more stable in the periplasm and can quench the diguanylate cyclase activity of YfiN (87, 336). Mutation of *yfiR* in Δ*cysE* limited motility, as c-di-GMP levels were increased (Figure 4.12).

These results, in combination with the ability of glutathione to restore wrinkling in cysteine auxotrophs, led us to hypothesize that *ΔcysE* strains have a more oxidized periplasm compared to WT, which increases YfiR stability and leads to decreased YfiN activation and decreased cellulose production. Consistent with this prediction, overexpression of *yfiR* conferred a smooth CR binding morphotype to WT colonies, similar to that of cysteine auxotrophs (Figure 4.5B). *ΔcysE* also displayed hyper susceptibility to H_2O_2 (Figure 4.13). The reducing agent, dithiothreitol (DTT), disrupts disulfide bonding in YfiR, causing it to misfold and leading to decreased YfiR levels in the periplasm (87). In agreement with cysteine auxotrophs having a smooth colony morphotype due to increased YfiR levels, DTT caused Δ*cysE* colonies to wrinkle at 26°C (Figure 4.5C) without rescuing cysteine auxotrophy (Figure 4.14). To further support, cysteine auxotrophs being affected by redox, mutations in both *hfq* and *oxyR* partially restored wrinkling in *cysE* biofilms (Figure 4.5A). Hfq stabilizes small RNAs like *oxyS* (337). OxyR is a cytoplasmic oxidation-sensitive transcription factor that regulates RpoS and the small RNA *oxyS* (338, 339).

Overexpression of curli in cysteine auxotrophs. Because cysteine auxotrophs had increased curli production at 26°C, we tested if cysteine auxotrophy also led to curli production under normally non-permissive temperatures. WT colonies are light red when grown on CR indicator plates at 37°C (Figure 4.6A). In contrast, Δ*cysE* and Δ*cysKΔcysM* colonies stained bright red on CR plates at 37°C (Figure 4.11B). Western blot analysis revealed increased levels of CsgD and a dramatic increase in CsgA in cysteine auxotrophs compared to WT (Figure 4.6B and Figure

4.11B). The red staining of *cysE* mutant colonies at 37°C was dependent on the curli genes *csgBA* and *csgD* as *ΔcysEΔcsgBA* and *ΔcysEΔcsgD* strains did not bind CR or produce CsgA protein (Figure 4.6A and B). Furthermore, when exogenous cysteine was provided to *ΔcysE* cells grown at 37°C curli production was undetectable (Figure 4.6A and B).

In order to determine if clinical UPEC strains can express curli at 37˚C, a collection of cysteine metabolizing and non-metabolizing isolates were tested for curli production at 37˚C. A recent study found that among 12 mecillinam (amdinocillin) resistant UPEC strains, all have mutations in *cysB* (323). Not surprisingly, these 12 mecillinam resistant strains and UTI89 Δ*cysE* were auxotrophic for cysteine biosynthesis (Figure 4.6C and Figure 4.15). More than half of the mecillinam resistant strains also bound to CR at 37°C (58.83%) (Figure 4.6C). Western blots confirmed that CsgA was produced by these 7 mecillinam-resistant strains at 37°C from Group2 (Figure 4.6D). We screened a collection of patient UPEC isolates from the University of Michigan hospital using CR-indicator plates to determine if they could express curli at 37°C. None of these strains were cysteine auxotrophs (Figure 4.6C) and only 1 bound CR at 37°C (1.89%) (Figure 4.6D).

Cysteine auxotroph resistance to antibiotic killing and biofilm inhibition. The tie between redox, antibiotics, and cysteine auxotrophy along with the resistance of UPEC *cysB* mutants to mecillinam led us to test whether the Δ*cysE* strain of UTI89 was mecillinam-resistant. When grown near mecillinam infused disks, there was no zone of clearing around the UTI89 Δ*cysE* strain, whereas WT UTI89 had a large zone of clearing (Figure 4.7A, top row). We hypothesized that hyper-oxidation was the cause of the antibiotic resistance phenotype. Cysteine and glutathione increased the susceptibility of Δ*cysE* UTI89 to mecillinam (Figure 4.7B), whereas addition of the reducing agent, DTT, caused an intermediate change in Δ*cysE* mecillinam susceptibility. Showing redox played a contributing role to Δ*cysE* mecillinam resistance.

Δ*cysE* and Δ*cysB* strains have previously been found to be resistant to mecillinam, so we sought to determine whether cysteine auxotrophy or other factors caused this resistance. We found that Δ*cysC* and Δ*cysKcysM* mutants were susceptible to killing by mecillinam with no statistical difference from WT (Figure 4.7A and C). Though a 96-well plate mecillinam challenge

assay Δ*cysE* cells were found to have 85µg/mL as minimum inhibitory concentration (MIC) of mecillinam, compared to 4µg/mL for WT cells (Figure 4.7D). The added sensitivity seen in plates supplemented with cysteine (Figure 4.7A and C) was supported in the MIC test, as Δ*cysE* cells grown with 250µM cysteine were found to have an MIC of 24.3µg/mL mecillinam (Figure 4.7D). Furthermore, the addition of other reductants, such as DTT and glutathione, were able to lower the MIC for Δ*cysE* cells supporting that any change to the global redox state of the cells can alter Δ*cysE* resistance. Susceptibility of other cysteine auxotrophs to mecillinam shows that the mecillinam resistance of Δ*cysE* and Δ*cysB* is not inherently due to their cysteine auxotrophy.

Various antibiotics have been implicated to cause oxidative stress in bacteria (324, 325), and redox plays a large role in UPEC biofilm formation (308). To test if sub-lethal doses of mecillinam could lead to perturbation of UPEC biofilm, we performed a disk diffusion assay, this time on YESCA CR plates at 26°C. Interestingly, WT CR binding was inhibited by sub-lethal concentrations of mecillinam, as a white line was clearly visible in the lawn of cells outside of the zone of clearing (Figure 4.7E). In contrast, Δ*cysE* bound CR in the sub-lethal zone of mecillinam (Figure 4.7E). Cells in the presence and absence of mecillinam were normalized by OD_{600}, serial diluted, and plated to confirm consistent viability (Figure 4.16). Cells were scraped from the lawn closest to the zone of clearing and further away from it and were subjected to western blot analysis. CsgA was decreased in WT in the presence of sub-inhibitory concentrations of mecillinam, while Δ*cysE* appears to be resistant to CsgA inhibition by mecillinam (Figure 4.7E).

Trimethoprim/sulfamethoxazole is the second most commonly prescribed antibiotic for UTIs in the US and kills bacteria by an alternative mechanism than mecillinam, through folate biosynthesis inhibition (340). Interestingly, sub-lethal levels of trimethoprim/sulfamethoxazole also inhibited CR binding and production of curli in WT strains. However, Δ*cysE* cells stained red and produced curli even in the presence of sub-lethal levels of trimethoprim/sulfamethoxazole and remained viable after dilution, similar to mecillinam (Figure 4.7F and Figure 4.16).

Discussion

The work here describes how the production of extracellular matrix components, curli and cellulose, becomes dysregulated due to redox perturbation in Δ*cysE* strains. In WT strains of *E. coli* the production of curli and cellulose appear to be expertly coordinated temporally (Figure 4.2), by the same regulator (77, 311), and are both influenced by the production of c-di-GMP (10). Cysteine auxotrophy greatly perturbs this process and leads to strong activation of curli, while inhibiting the production of cellulose, leading to an alternate smooth biofilm that accumulates biomass in static culture (Figure 4.1B and Figure 4.8B). The redox sensitive periplasmic protein YfiR is apparently responsible for repressing cellulose production in cysteine auxotrophs, as deletion of *yfiR* restores cellulose production to Δ*cysE* strains (Figure 4.5). Also, the addition of DTT, which is known to cause YfiR to misfold and become unstable (87), promotes a Δ*cysE* mutant strain to form wrinkled colonies (Figure 4.6C). We hypothesize that the lack of thiol reducing agents, such as cysteine and glutathione, in cysteine auxotrophs contributes to YfiR stability so that the YfiN diguanylate synthase is inactivated. In agreement, overexpression of *yfiR* in a WT strain abolishes colony wrinkling (Figure 4.6B). Interestingly, a screen for c-di-GMP inhibitors in *E. coli* uncovered another thiol compound, sulfathiazole (341). The thiol-responsive nature of YfiR makes it a potential target for this therapeutic compound's antibiofilm activity.

Many community and biofilm behaviors are influenced by various components of the cysteine biosynthesis pathway. OAS has been reported to be a biofilm inhibitory compound (313). Δ*cysK*Δ*cysM* mutants have a smooth colony morphotype and produce curli in the presence of OAS (Figure 4.1), as they cannot further anabolize OAS to cysteine. Therefore, the smooth colony morphotype of cysteine auxotrophs seen in UTI89 is due to the lack of cysteine not OAS. Glutathione functions as a reductant pool for glutaredoxins, which reduce disulfides of multiple proteins like ribonucleotide reductase and PAPs reductase (332). Without an active glutaredoxin system, PAPs reductase should be inactive and may accumulate PAPs, similar to the *cysH* mutants seen by Rossi *et al.* (316). Mutation of the PAPs biosynthesis enzyme, *cysC,* did not restore wrinkling to *ΔcysE* strains (Figure 4.17A). Additionally, mutation of the cysteine biosynthesis regulator, CysB, did not suppress the Δ*cysE* biofilm phenotype (Figure 4.16A). PAPs does not appear to affect the dysregulation of the curli overproduction phenotype in UTI89, as

neither a *cysC* mutation (Figure 4.17B) nor *cysH* overexpression (data not shown) in Δ*cysE* diminished 37ºC CR binding.

Previous work found that *cysE* and *cysB* mutant strains are resistant to mecillinam (342, 343). Thulin *et al.* 2015 screened a collection of UPEC for mecillinam resistance and found that all resistant strains isolated had mutations in *cysB* (323). UTI89 Δ*cysE* also showed increased resistance to mecillinam in comparison to WT (Figure 4.7A and C). UTI89 Δ*cysE* sensitivity could be partially restored with the addition of reducing compounds (Figure 4.7D), showing a distinct connection between cellular redox state and Δ*cysE* antibiotic resistance. We additionally made the novel discovery that this resistance is not mediated through cysteine auxotrophy, as the cysteine auxotrophs Δ*cysC* and Δ*cysK*Δ*cysM* are susceptible to mecillinam (Figure 4.7A and C). Tapsall and McIver found glutathione can rescue the small-colony phenotype of cysteine auxotrophs in *Klebsiella* and UPEC similar to our biofilm phenotype (344, 345).The Δ*cysE* biofilm suppressor transposon mutants are promising genetic targets for therapeutics to inhibit mecillinam resistance (Table 1).

Sub-inhibitory concentrations of mecillinam and trimethoprim/sulfamethoxazole inhibit production of curli in WT UPEC; however, cysteine auxotrophs are resistant to the curli-inhibitory effect (Figure 4.7E and F). Sub-inhibitory levels of antimicrobial compounds modulate biofilms of multiple species (346-348), but antibiotic-mediated inhibition of curli or resistance to these effects by cysteine auxotrophs have not been previously described. Perhaps the curli inhibitory effect of mecillinam and trimethoprim/sulfamethoxazole is part of the reason why these antibiotics are so effective against UPEC *in vivo.* The ECM can act as a barrier that inhibits antibiotics from reaching the cells in the biofilm (349, 350), and other antibiotics have been seen to disrupt the ECM (351). Δ*cysE* resistance to curli inhibition by sub-inhibitory concentrations of antibiotics may be a reason why cysteine auxotrophs are commonly selected for and isolated from chronic infections.

The ability of cysteine auxotrophs to produce curli at 37°C might impact how *E. coli* interacts with the host during an infection. Sepsis patients produce antibodies against curli (113), and UPEC strains that cause sepsis produce curli at 37°C at a higher rate than non-sepsis strains (352). Additionally, *Salmonella* that produce curli cause tightening of gut epithelial cell

junctions and, *in vivo,* have lower titers in the cecum and mesenteric tissue (353). Additionally, cysteine auxotrophs can be isolated from numerous types of *Enterobacteriaceae* infections (321, 322). Interestingly, the causative agents of 1.5-2% of UPEC infections and *Klebsiella spp.* UTIs are cysteine auxotrophs (322, 344, 345). Healthy patients have ~100uM cystine in their urine, similar to the levels present in YESCA media. Interestingly, cystinuria patients can have 3-4mM cystine in their urine (354) which might prevent curli production at 37˚C. The majority of cysteine auxotrophs isolated from the Gillespie, Borderon, and McIver studies are from chronic infections (320, 321, 344). Taken together, these results suggest that cysteine auxotrophs have an altered cellular redox state and that this environment lends itself to mecillinam resistance, increased curli production and decreased cellulose production compared with WT strains.

Material and Methods

Strains and growth conditions. All strains were grown in broth shaking overnight at 37°C. UTI89 strains (62) are all referred to by their genotypes and can be referenced in the supplemental material along with the primers used for strain construction. Cysteine auxotrophs were routinely grown in LB media supplemented with 250µM cysteine. Mutations were performed as previously described via lambda red recombination (87, 227). Genomic *csgBA-mCherry* transcriptional fusion was constructed previously (308).

Rugose biofilms are 4 µL dots of 1-OD_{600} cells washed twice in YESCA broth and then plated and incubated on YESCA (10g casamino acids and 1g yeast extract/L) CR (50µg/mL) media for 48 hours at 26°C as previously described (308). 37°C biofilms were incubated for 24 hours. For exogenous addition to biofilms, colonies were spotted 1 cm from sterile filter disks containing the compound of interest. For overexpression studies, 10 to 100µM of Isopropyl β-D-1-thiogalactopyranoside (IPTG) was added to the plates.

Pellicle biofilms assays were performed by inoculating 2mL culture in 24 well well plate with 2µL of overnight culture. Plates were then incubated at 26˚C for 48 hours prior to imaging and quantification. Pellicles were quantified by removal of broth culture without perturbation of the biofilm followed by a 5 minute staining with .1% (w/v) crystal violet for 5 minutes. Crystal

violet was then removed and the stained biofilm was washed 3x with sterile H_2O. After the wash steps, the pellicles were tissue homogenized and the OD_{600} was determined.

Spread plates for antibiotics assays were performed as follows: 0.1-OD_{600} cells were spread on plates with a sterile cotton swab, then the plate was rotated 60°, swabbed, rotated 60°, and swabbed again. Sterile filter disks contained 20µL of the compound of interest at the concentrations indicated in the text. ETEST strips (Biomerieux) contain increasing concentrations of compounds of interest.

Swim plates were made using YESCA (10g casamino acids and 1g yeast extract/L) with 0.25% agar added. Overnight cultures of tested cells were inoculated into plates by submerging pipette tips in the cultures and pricking the center of the plates. Plates were incubated at 37°C for 21 hours and the distance traveled was measured from the prick point to the swim front.

Growth Curves. Cells were harvested from overnight cultures, washed twice in fresh media (LB or M9 minimal media with nicotinamide and glucose) and brought to 0.1-OD_{600}. Cells were then diluted 1:10 to a volume of 200µL in supplemented media in a Corning Greneir flat, clear 96-well plate and sealed with Breathe-Easy. OD_{600} measurements were taken every 30 minutes using a Tecan Infinate 200 Pro plate reader with conditions of obital shaking at amplitude 4.5 and 37°C for 12 or 24 hours. All readings were performed in biological triplicate. Color coordinated error bars represent standard deviation.

MIC determination. Cells were harvested form overnight cultures, washed twice in fresh Mueller Hinton (MH) media (Fluka Analytical) and brought to an OD_{600} of 0.01. Cells were added 1:100 into a 96-well plate containing MH liquid media. Mecillinam concentration in MH was started at 256µg/mL and diluted 1:1 down the columns until the concentration was 1µg/mL. Cysteine, glutathione, and DTT were added to achieve concentrations of 250µM, 500µM, and 500µM respectively from stocks made in 200mM Tris, pH 8.6. Cells were allowed to shake at 37°C for 24 hours and OD_{600} readings were taken using a Tecan Infinite 200 plate reader at time of completion. All readings were performed in biological triplicate. Error bars represent the standard error of biological triplicate reactions.

S4B staining. Colonies were collected in 800 µL of 50 mM potassium phosphate buffer (pH7.2) (KPI) and homogenized on setting 3 of a Fisher Tissuemizer for 15 seconds. Cells were stained with 0.05mg/mL S4B (286), incubated for 10 min at room temperature in a shaker at 200 RPM. Cells were spun down and washed twice in KPI and resuspended in 100 µL of KPI. Stained cells were diluted 1:10 and imaged on a Tecan Infinite 200 plate reader at excitation 535 nm and emission 595 nm. Unstained cells treated similarly to stained cells were read and subtracted from the stained cell suspensions. Cell suspensions were normalized by OD_{600}. Error bars represent the standard deviation of biological triplicate reactions.

H_2O_2 Viability. assays were performed as previously described (308). Rugose colonies were grown at 26˚C for 48 hours prior to suspension in 50mM KPi (pH 7.2) and tissue homogenization with a Fisher Tissuemiser. 1-OD_{600} cells were suspended in 500µL 1% (v/v) H_2O_2 in KPi and incubated on the benchtop for 20 minutes. Reactions were stopped with 500µL of 1mg/mL catalase for 1 minutes. Cells were spun down and resuspended in KPi prior to serial dilution onto LB plates to determine CFU. % survival was the %CFUs after H_2O_2 treatment in comparison to a mock treatment without H_2O_2.

Statistics. Error bars represent standard deviation of a minimum of three biological replicates. Significance and *P* values were determined from a Student's two tailed T-Test (*P* values<.05).

Western Blot analysis. CsgA western blots were performed as previously described (87). Rugose biofilms were collected in 1 mL 50mM potassium phosphate buffer (KPI) (pH 7.2) and homogenized with a Fischer Tissuemizer for 10 seconds. 150µL of 1-OD_{600} cells were spun down and resuspended in hexafluoroisopropanol (HFIP) and then incubated in a Savant SPD SpeedVac at 45°C for 45 minutes before resuspension in 2x SDS-running buffer. Samples were heated at 95°C for 10 minutes then 8µL are loaded onto a 15% SDS-PAGE gel and run at 25mA for 45 min. The gel was transferred to PVDF at 25V for 10 minutes at room temperature using a semi-dry transfer apparatus. Non-CsgA blots were performed in the same manner with a few

modifications: HFIP was excluded and gels were wet transferred at 4°C at 12V for 12 hours. All blots were blocked in 5% skim milk Tris buffered saline-Tween 20 (TBST) overnight at 4°C. The membrane was incubated with primary antibody for 1 hour at room temperature (1:8000 CsgA, 1:5000 CsgD, 1:2000 His (ABGENT monoclonal San Diego, CA)) followed by 3x5 min washes in TBST. Secondary antibodies were applied for 1 hour at room temperature (1:15000 Licor IR dye anti-mouse and anti-rabbit) followed by 3x5min washes in TBST. Blots were visualized on Licor Odyssey CLX imager.

β-galactosidase assays. β-galactosidase assays were performed on rugose biofilms suspended in 1mL KPI and diluted 1:10 as previously described (87, 328). 90µL of reaction buffer, 7µL cells, were incubated for 20 min at 30°C before 4mg/mL ortho-nitrophenyl-β-galactoside (ONPG) was added. 50µL 1M NA_2CO_3 addition was added once a yellow color developed in the reaction. 420nm and 550nm absorbance on a Tecan Infinite 200 plate reader were measured in addition to the OD_{600} of 1:10 diluted cells. Results are the biological triplicate average for each strain minus the value of pRJ800 (promoterless *lacZ*) and normalized to the biological triplicate average of pRJ800-16s (16s promoter upstream of *lacZ*). All genes of interest were assayed in biological triplicate and significance was determined by a student's two-tailed T-test.

Transposon Screening. The screens were performed in UTI89 streptomycin resistant *ΔcysE* background and were plated on YESCA CR plates at 37°C or 26°C as previously described (87, 355). *ΔcysE* was conjugated with BW19851 pFD1 containing the IPTG inducible transposase (NDH587) via mixing, pelleting, and incubation on YESCA media plates at 37°C for 2.5 hours on a cellulose filter. Cells were collected in 1mM IPTG YESCA, incubated for 3 hours at 37°C, then pelleted and resuspended in 10 mL streptomycin and kanamycin YESCA to select for *ΔcysE* transposon mutants. Cells were diluted 1:10,000 prior to plating. Mutants were identified via random primer sequencing. Mariner 1 and mariner 2 primer colony PCR yielded DNA outside of the transposon and nested PCR with mariner 3 and 4 amplified this region. Sanger sequencing at University of Michigan Sequencing Core using mariner 4 revealed the location of transposon insertions.

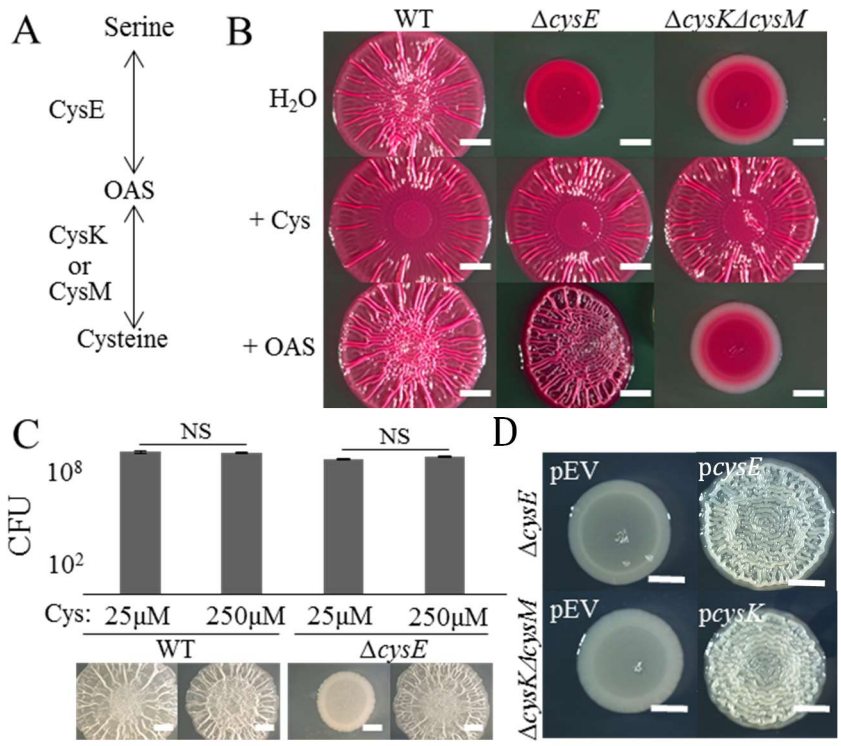

Figure 4.1. Cysteine is required for rugose biofilm formation. A) Cysteine biosynthesis. CysE converts Serine into OAS and OAS is converted into cysteine by either CysK or CysM. B) 4μL dots of 1-OD_{600} cells were spotted onto YESCA CR media and incubated at 26°C for 48 hours. 20μL of 10% (w/v) OAS or cysteine were added to sterile paper disks 1cm from the colonies. Cysteine auxotrophs formed smooth red colonies that wrinkled in the presence of cysteine. *ΔcysE* colonies wrinkled in the presence of OAS whereas Δ*cysK*Δ*cysM* mutants were still smooth. C) Colonies were resuspended in 1mL KPI and serial diluted and plated to determine CFUs. All measurements were done in biological triplicate. D) Δ*cysE* and Δ*cysK*Δ*cysM* were complemented with p*cysE* and p*cysK.* 4μL dots of 1-OD_{600} cells were spotted onto YESCA 100μM IPTG plates and incubated at 26˚C for 48 hours. Bars, 0.25cm.

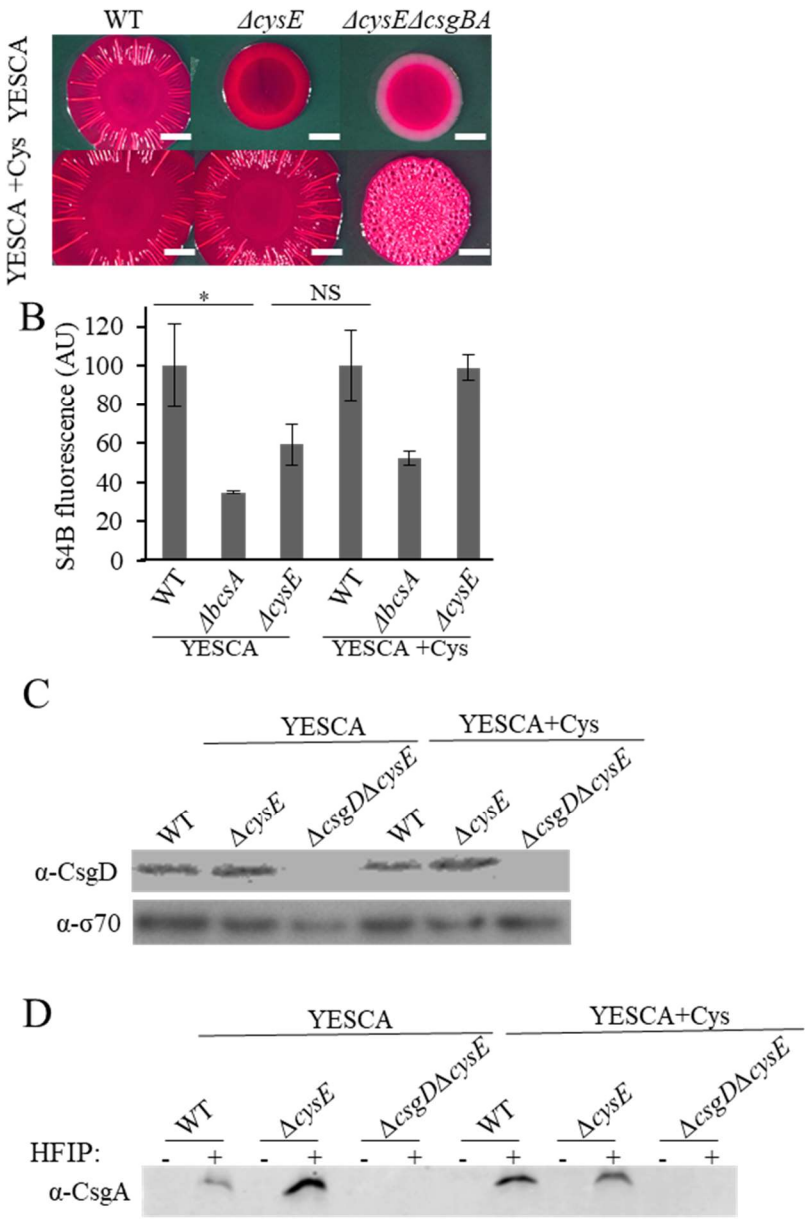

Figure 4.2. Cysteine auxotrophy uncouples curli and cellulose production. A) Rugose colonies were grown at 26°C for 48 hours on YESCA CR plates or YESCA CR plates with 250µM cysteine added to the plates. B) Pontamine Fast Scarlet 4B (S4B) was used to stain cells. Stained cells were washed prior to fluorescence readings. Higher fluorescence correlates with binding of more dye and cellulose production. C) Western blot analysis of rugose colonies grown at 26˚C for 24 hours revealed Δ*cysE* produces similar levels of CsgD to WT. D) CsgA western blot analysis revealed Δ*cysE* had increased CsgA production after 48 hour incubation at 26˚C. 250µM cysteine addition to the media decreased CsgA production in Δ*cysE.* Bars, 0.25cm. *-p value <0.05. NS-Not significant.

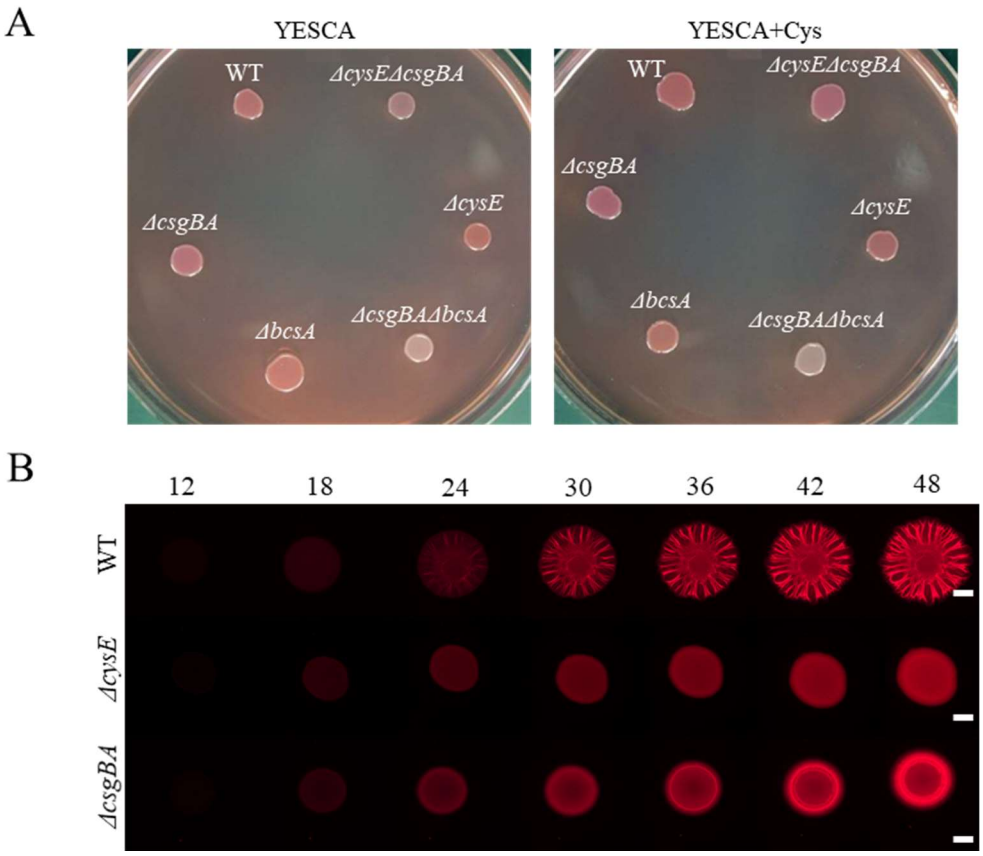

Figure 4.3. CR binding and curli transcription of rugose colonies. A) Rugose colonies were grown on YESCA CR plates or YESCA CR plates supplemented with 250µM cysteine and incubated at 26˚C for 14 hours. B) 2µL dots of WT, *ΔcysE*, and *ΔcsgBA* harboring *csgBA-mCherry* chromosomal insertions were grown in a stage incubator at 26°C and imaged at 12, 18, 24, 30, 36, 42, and 48 hours. Bars, 0.25cm.

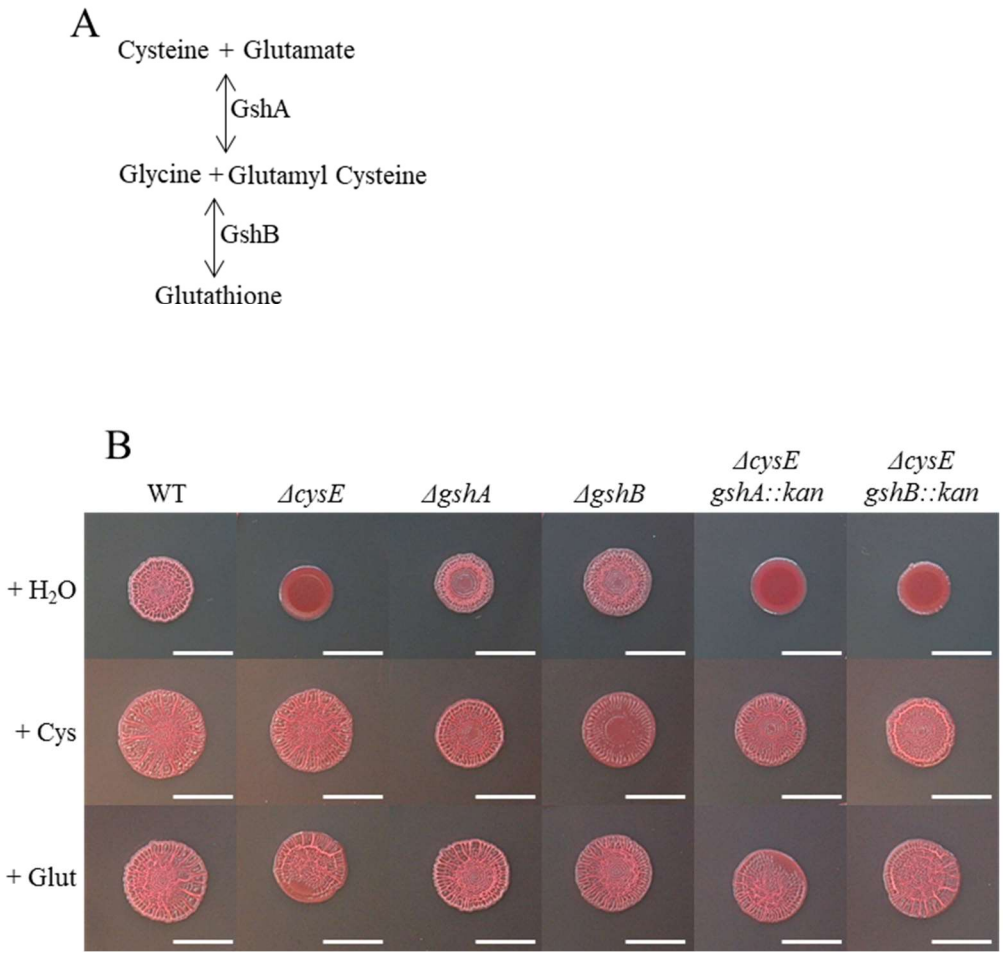

Figure 4.4. Glutathione and cysteine restore colony wrinkling to cysteine auxotrophs. A) Glutathione biosynthesis pathway. GshA converts cysteine and glutamate to glutamyl cysteine, and GshB converts glycine and glutamyl cysteine to glutathione. B) WT, *ΔcysE, ΔgshA, ΔgshB, ΔcysE gshA::kan,* and *ΔcysE gshB::kan* 26°C colonies after 48 hours of incubation in the presence of sterile disks containing cysteine or glutathione. Bars, .25cm.

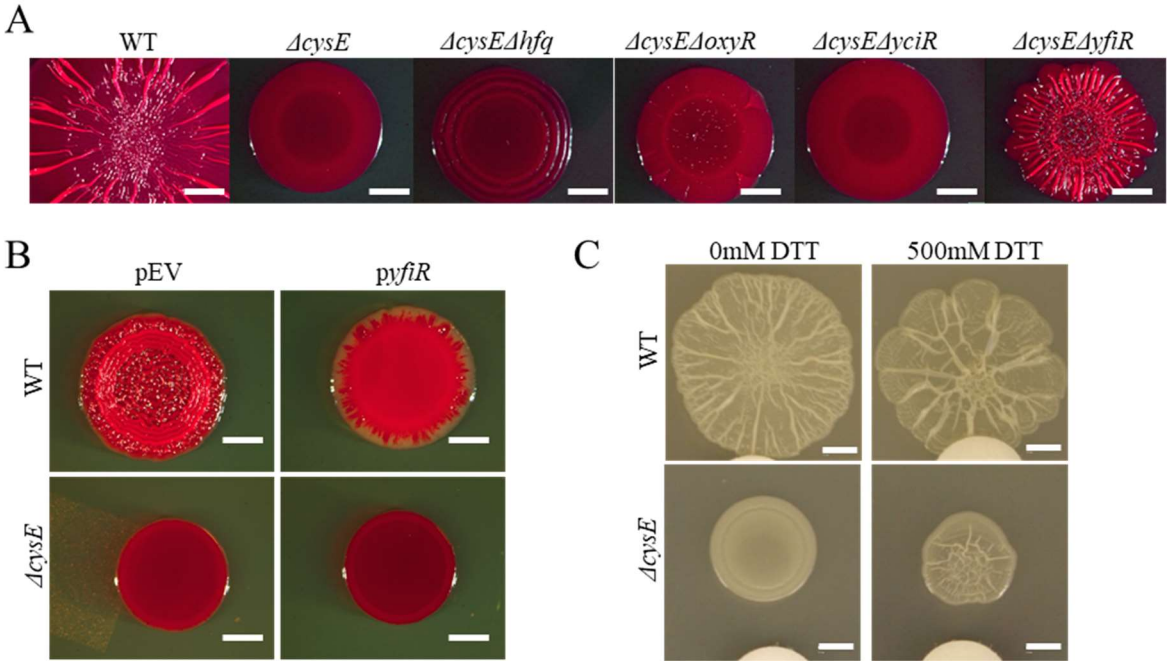

Figure 4.5. *yfiR* controls the smooth colony morphotype of *ΔcysE.* A) Secondary mutations found in 26°C transposon screen. 4µL dots of WT, *ΔcysE, ΔcysEΔhfq, ΔcysEΔoxyR, ΔcysEΔyciR,* and *ΔcysEΔyfiR* grown at 26°C for 48 hours. B) *yfiR* overexpression decreases WT colony wrinkling. WT and *ΔcysE* harboring p*yfiR-HIS* were grown at 26°C for 48 hours on YESCA CR 100µM IPTG plates. *yfiR* overexpression caused WT to phenocopy *ΔcysE*. C) 500mM DTT addition to a sterile paper disk (pictured as white circle at bottom of images) induced *ΔcysE* colony wrinkling and caused an increase in WT colony spreading.

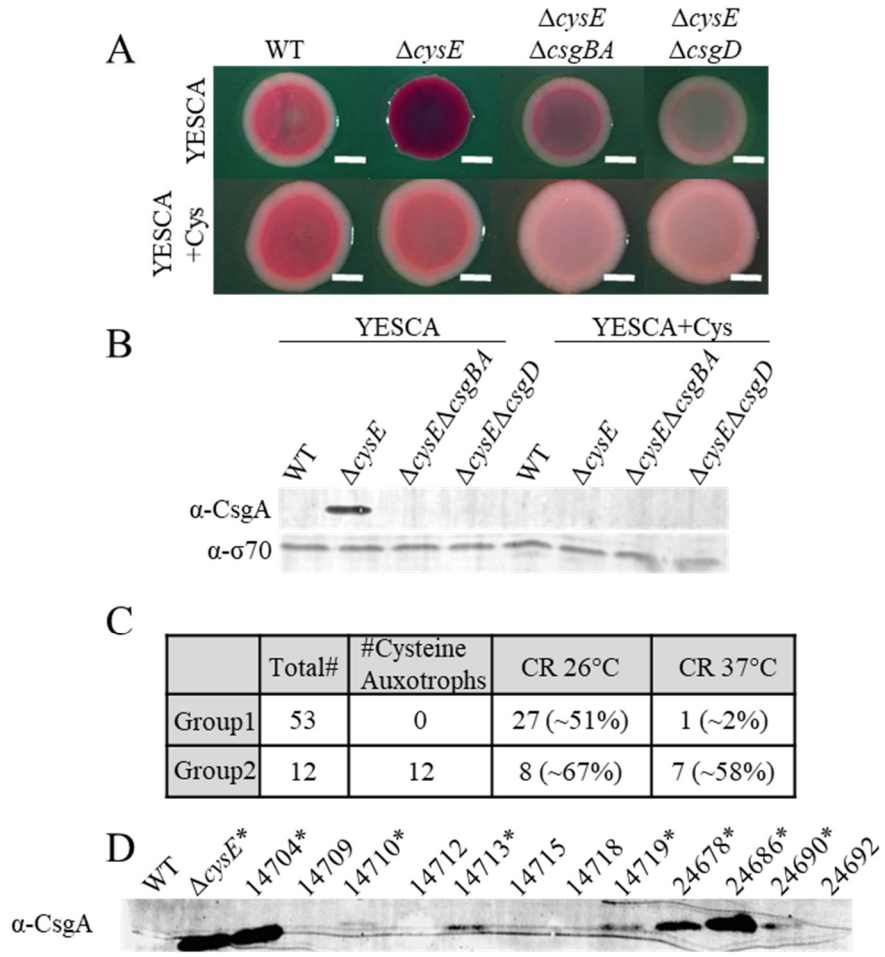

	Total#	#Cysteine Auxotrophs	CR 26°C	CR 37°C
Group1	53	0	27 (~51%)	1 (~2%)
Group2	12	12	8 (~67%)	7 (~58%)

Figure 4.6. Cysteine auxotrophs produce curli at 37°C. A) *ΔcysEΔcsgD* and *ΔcysEΔcsgBA* were unable to bind CR when grown 37°C for 24 hours on YESCA CR plates. B) α-CsgA western blot analysis of colonies grown at 37˚C for 24 hours. *csgBA* and *csgD* mutation in *ΔcysE* and 250μM cysteine addition abolished 37˚C curli production of *ΔcysE*. C) Table showing cysteine auxotrophs isolated from patients have an increased propensity to bind CR at 37°C. Two different sets of clinical isolates were grown as 4μL dots on YESCA CR plates at 26°C for 48 hours or 37°C for 24 hours. Auxotrophy was determined by growth on M9 minimal media with nicotinamide and glucose additions vs. growth on M9 minimal media with nicotinamide, glucose, and cysteine additions. Group 1 contained no cysteine auxotrophs and had 1 isolate that bound CR at 37°C. Group 2 contained all cysteine auxotrophs and 7/12 strains bound CR at 37°C. D) Isolates from Group 2 grown at 37°C for 24 hours on YESCA were subjected to western blot analysis against CsgA. CsgA was present in 14704, 14710, 14713, 14719, 24678, 24686, and 24690 (represented by *). Bars, 0.25cm.

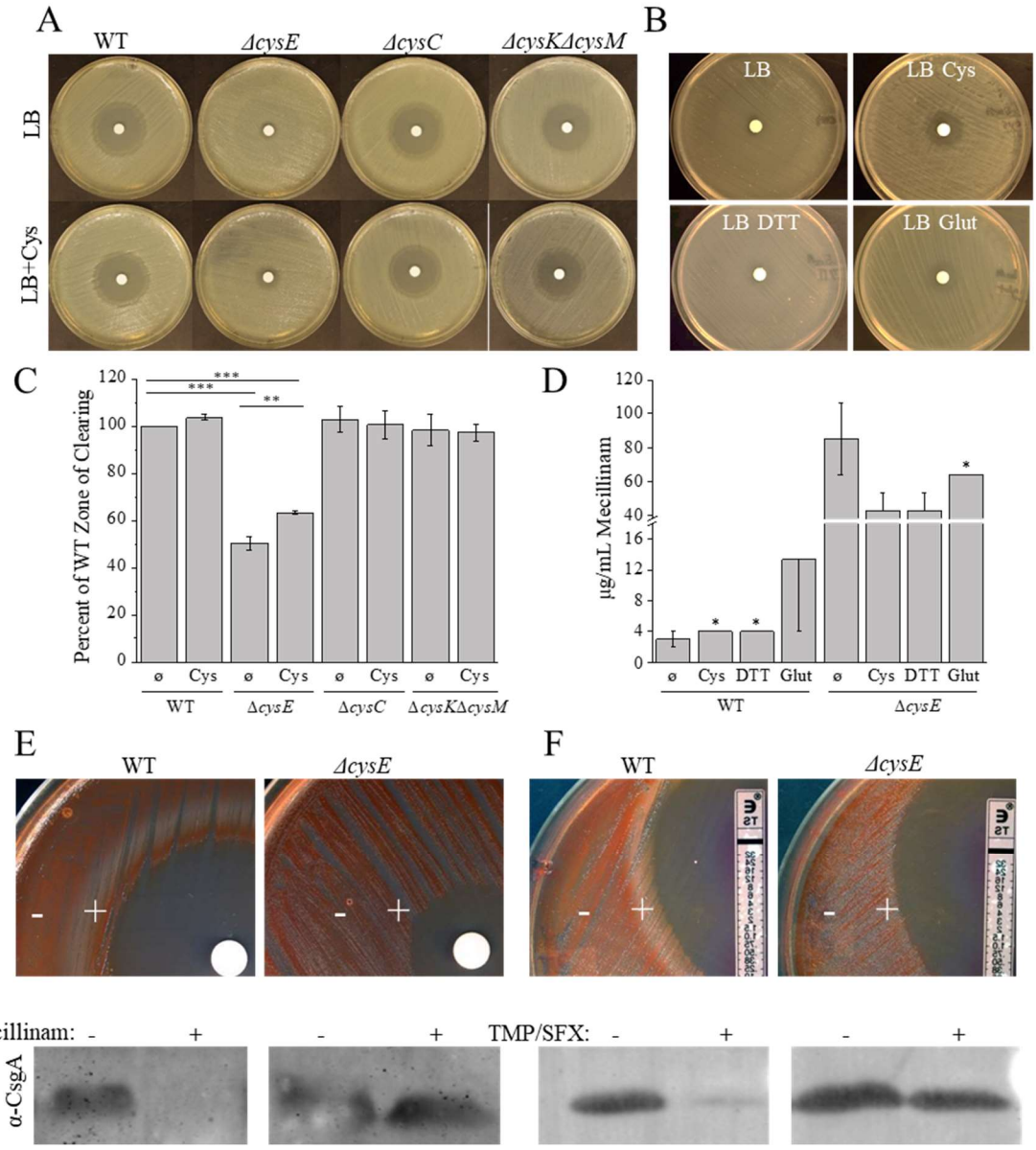

Figure 4.7. The effect of mecillinam on UTI89 biofilms. A) 0.1 OD_{600} bacteria were spread onto LB or LB supplemented with 250µM cysteine. Sterile disks containing 20µL 10mg/mL mecillinam were added prior to incubation at 37˚C for 24 hours. *ΔcysE* had a decreased zone of inhibition. B) *ΔcysE* colonies spread on YESCA plates supplemented with 250µM cysteine, 500µM DTT, or 500µM glutathione had a sterile filter disk containing 20µL of 10mg/ml mecillinam placed on top and were incubated at 37°C for 24 hours. The zone of inhibition of *ΔcysE* increased with the addition of cysteine, DTT, and glutathione.C) Quantification of zone of clearing from panel A. Bar graph represents three technical replicates. **- p>0.05, ***- p>0.01. D) Determination of MIC for WT and Δ*cysE* cells grown in MH media with or without supplementation of 250µM cysteine, 500µM DTT, or 500µM glutathione. Cells were challenged with decreasing concentrations of mecillinam and the concentration in which growth of cells was restored was recorded. Bar graph represents three technical replicates. * denotes replicates with identical

MIC. E) 0.1-OD_{600} WT and *ΔcysE* were spread onto YESCA CR plates with a sterile filter disk containing 20µL 10mg/mL of mecillinam and grown at 26°C for 48 hours. Pictures were taken prior to collecting cells at the edge of the plate (-mecillinam) and next to the zone of inhition (+mecillinam) that were then subjected to western blot analysis against CsgA. Mecillinam inhibited WT CR binding and curli production, but ΔcysE was resistant to the curli inhibition. F) Trimethoprim/sulfamethoxazole ETEST strips were laid onto WT and *ΔcysE* YESCA CR spread plates that were incubated at 26°C for 48 hours. Cells were collected at the edge of the plate (-mecillinam) and next to the zone of inhibition (+mecillinam) prior to testing for CsgA protein levels via western blot analysis.

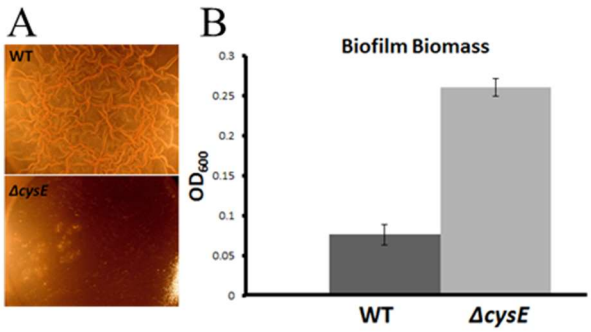

Figure 4.8. ΔcysE forms smooth and thick pellicles. A) 2µL of overnight culture were used to inoculate 2mL YESCA in 24 well dish. Biofilms were incubated statically at 26˚C for 48 hours prior to imaging. B) Pellicles were stained with crystal violet and washed to prior to tissue homogenization and quantification of biomass via OD_{600}.

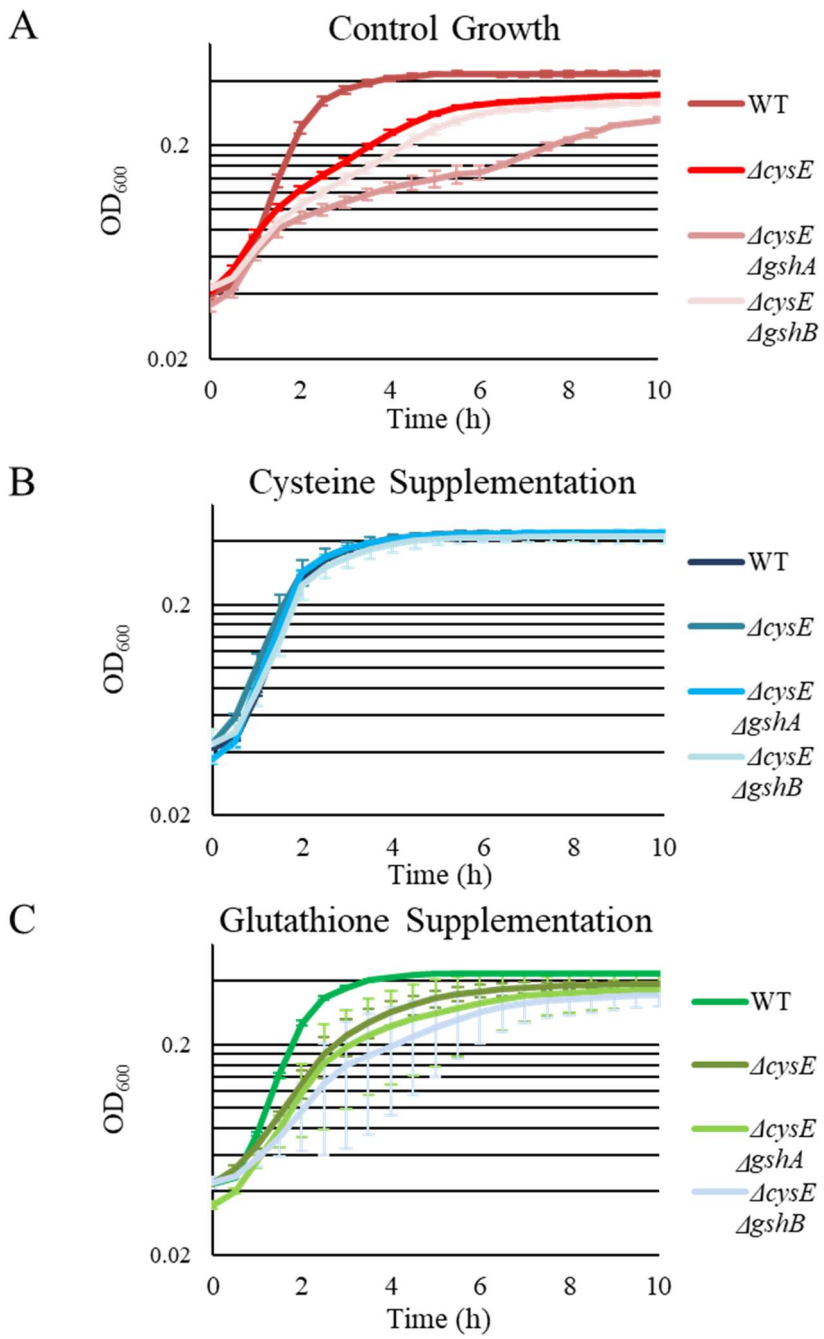

Figure 4.9. Growth defect of cysteine auxotrophs can be rescued by cysteine or glutathione supplementation. WT, *ΔcysE*, *ΔcysEgshA*, and *ΔcysEgshB* cells were grown in LB , LB + 250µM cysteine , or LB + 500µM glutathione for 12 hours. OD_{600} measurements were taken every 30 minutes. All readings were performed in biological triplicate. Color coordinated error bars represent standard deviation.

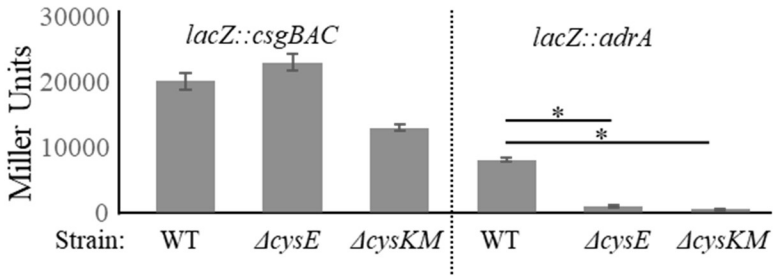

Figure 4.10. Transcription of ECM components in cysteine auxotrophs. Cysteine auxotrophs ECM transcription WT, *ΔcysE,* and *ΔcysKΔcysM* harboring prj800, prj800-*16s,* prj800-*csgBAC,* and prj800-*adrA* were grown as 4µL dots at 26°C for 48 hours on YESCA. β-galactosidase assays were done following previous studies (308). Base readings of prj800 were subtracted from each strain and Miller units were normalized by prj800-16s readings. All readings were performed in biological triplicate. Error bars represent standard deviation.

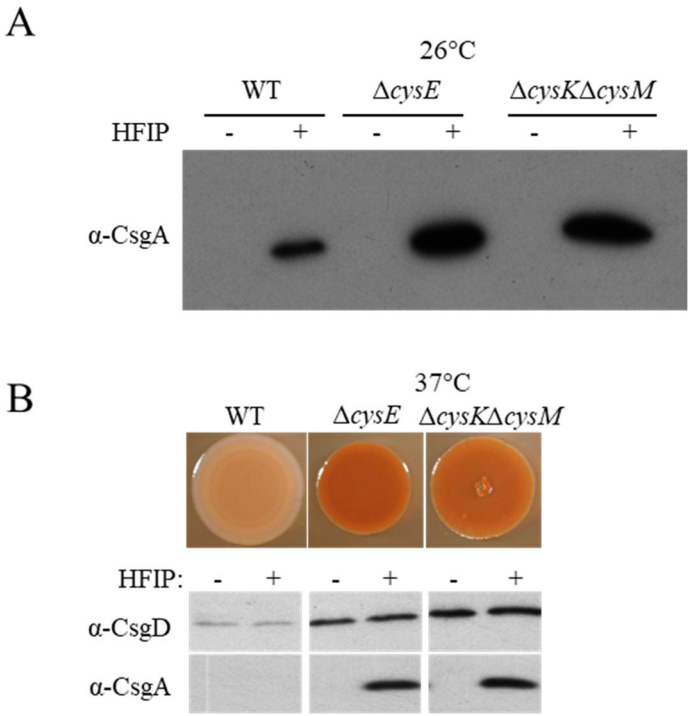

Figure 4.11. Cysteine auxotrophy leads to increased CsgA. A) Western blot analysis of CsgA on WT, *ΔcysE,* and *ΔcysKΔcysM* cells grown at 26°C for 48 hours on YESCA. B) Cysteine auxotrophs produce curli at 37˚C. WT, *ΔcysE* and *ΔcysKΔcysM* were grown on YESCA CR plates at 37°C for 24 hours. *ΔcysE* and *ΔcysKΔcysM* have increased CR binding. Western blot analysis of 37˚C rugose colonies revealed that *ΔcysE* and *ΔcysKΔcysM* have increased CsgD and CsgA in comparison to WT.

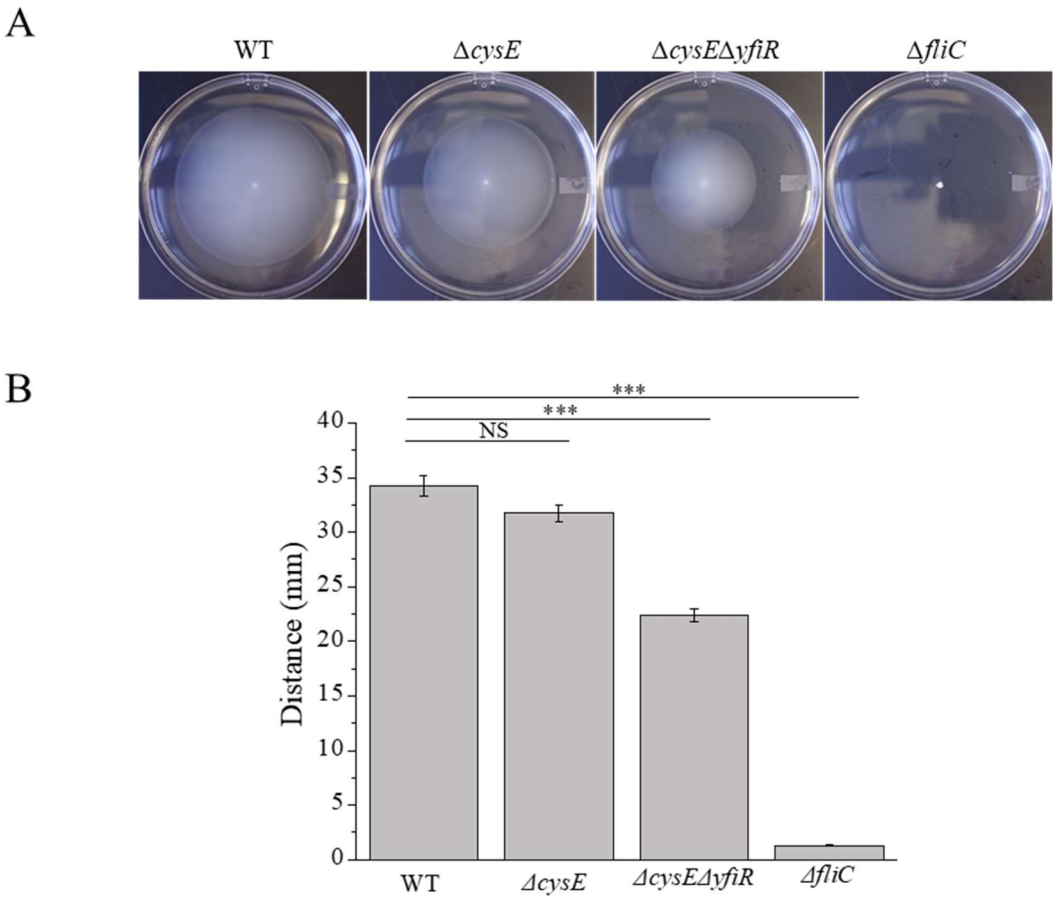

Figure 4.12. *ΔcysE* cells do not exhibit a swimming defect due to changes in c-di-GMP. A) Overnight cultures were stabbed into 0.25% agar plates and allowed to incubate at 26˚C for 21 hours. *ΔfliC* is a negative control. B) Quantification of swim distance. All readings were performed in biological triplicate. Error bars represent standard error. ***- p>0.01.

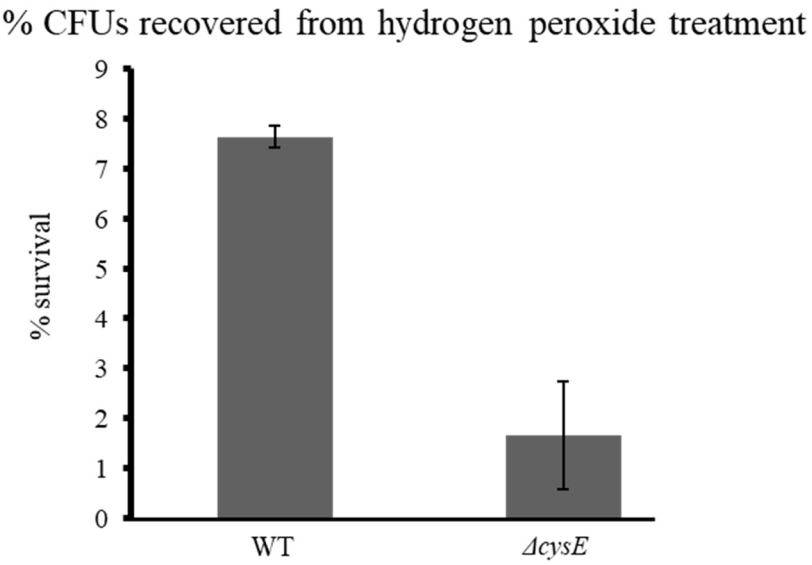

Figure 4.13. H_2O_2 viability assays. WT and ΔcysE rugose colonies were grown for 48 hours at 26˚C prior to harvesting, OD_{600} normalization, and 1% (v/v) H_2O_2 treatment. Reactions were stopped at 30 minutes prior to serial dilution and plating for CFU determination. % survival calculated from the percent CFU in H_2O_2 treatment compared to a mock treatment.

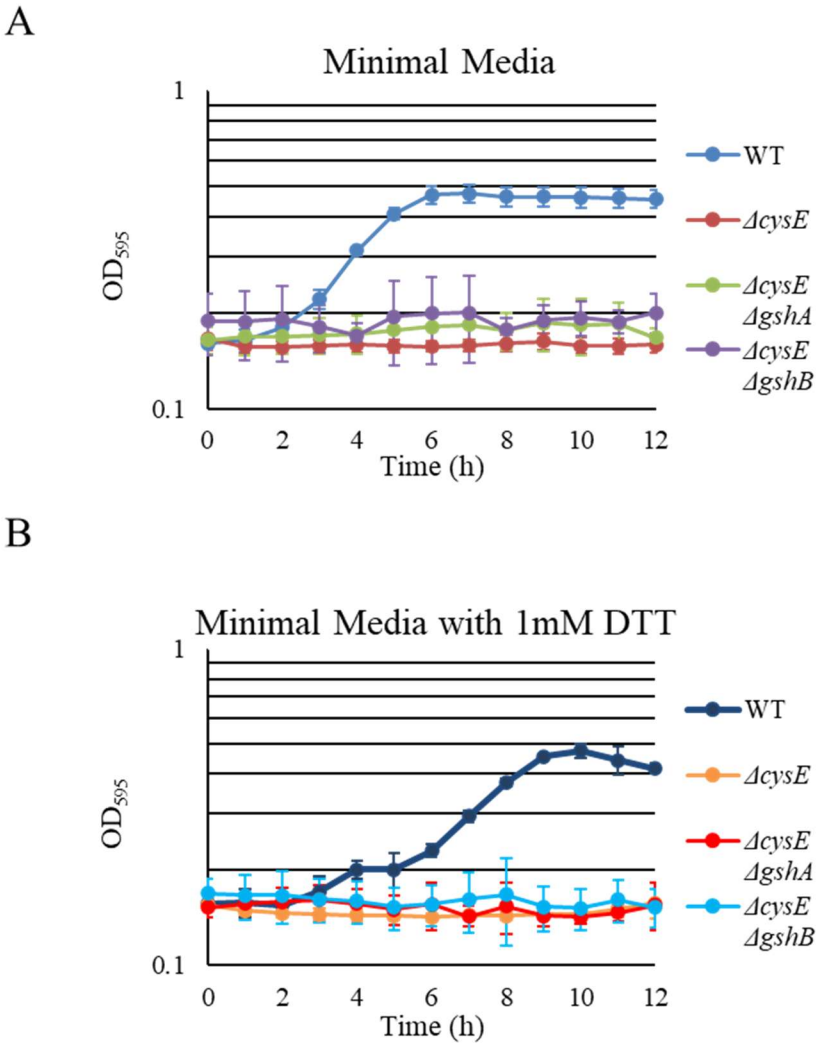

Figure 4.14. Exposing cysteine auxotrophs to the reductant DTT does not rescue growth in minimal media. WT, *ΔcysE*, *ΔcysEgshA*, and *ΔcysEgshB* cells were grown in A) M9 minimal media with nicotinamide and glucose or B) M9 minimal media with nicotinamide, glucose and 1mM DTT for 24 hours. OD_{600} measurements were taken every hour. All readings were performed in biological triplicate. Color coordinated error bars represent standard deviation.

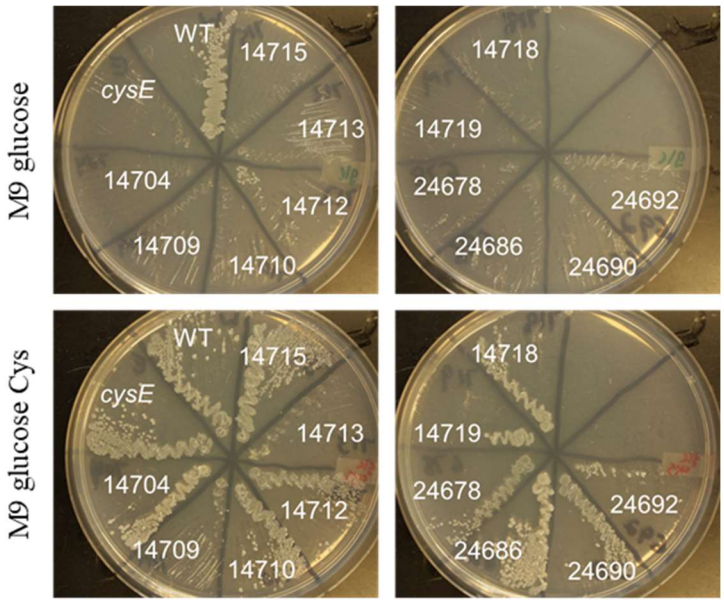

Figure 4.15. UTI89 *ΔcysE* and *cysB* hospital isolates are cysteine auxotrophs. WT UTI89, *ΔcysE,*and 12 *cysB* hospital isolates were grown on M9 minimal media with nicotinamide and glucose additions or M9 minimal media with nicotinamide, glucose, and cysteine additions. *ΔcysE* and *cysB* were unable to grow without the addition of cysteine to the media.

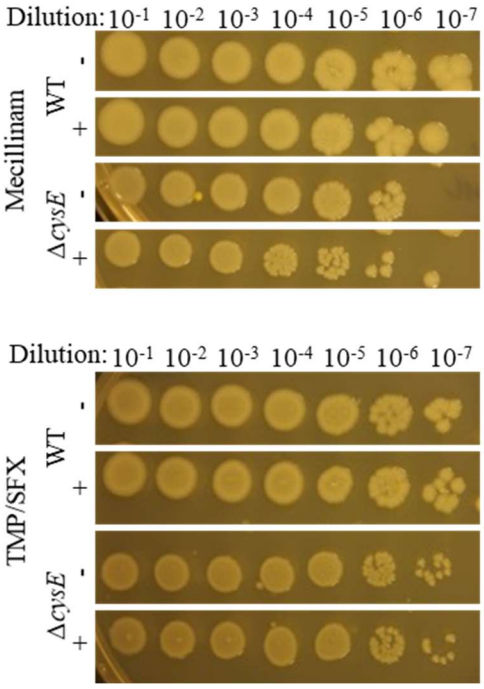

Figure 4.16. Cells harvested next to the zone of inhibition of mecillinam and trimethoprim/sulfamethoxazole are viable. Cells harvested in Figure 4.7C and Figure 4.7D for Western blot analysis were normalized by OD_{600} followed by serial dilution in KPI prior to plating 4µL dots onto LB plates for CFU determination. Plates were incubated at 37°C for 18 hours. Cells grown near and further from the zone of inhibition of both WT and *ΔcysE* had the same cell viability by CFU count.

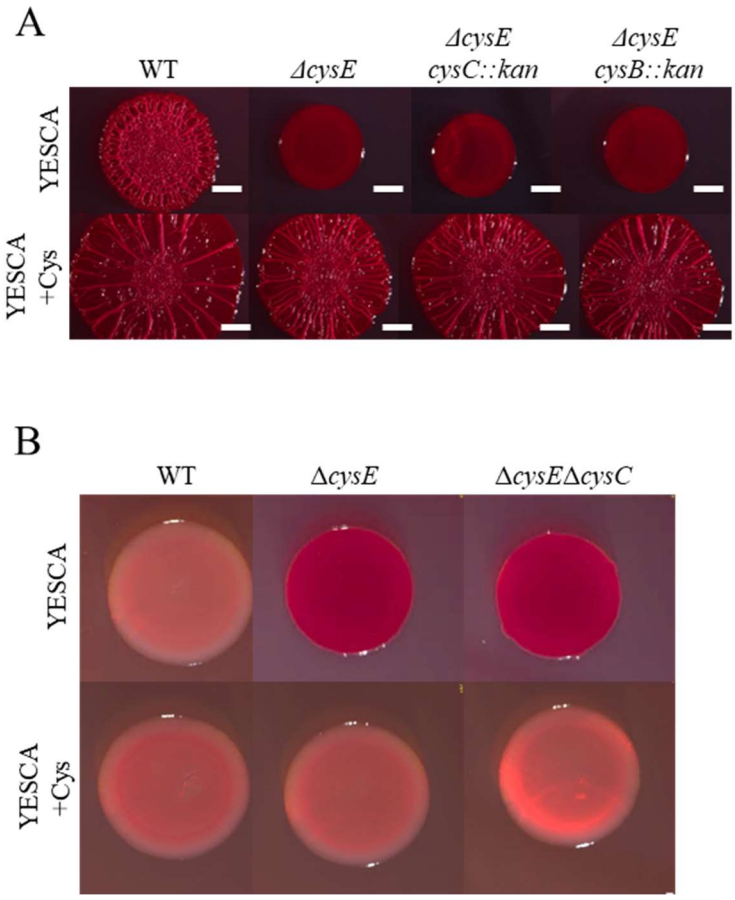

Figure 4.17. PAPs do not induce the *ΔcysE* smooth colony morphotype. A) 4µL dots of WT, *ΔcysE, ΔcysE cysC::kan,* and *ΔcysE cysB::kan* were plated on YESCA CR and YESCA 250µM cysteine CR plates and incubated at 26°C for 48 hours. *ΔcysE, ΔcysE cysC::kan,* and *ΔcysE cysB::kan* all displayed a smooth colony morphotype on YESCA, and a spreading and wrinkling colony on YESCA cysteine plates. B) 4µL dots of WT, *ΔcysE,* and *ΔcysEΔcysC* were plated on YESCA CR and YESCA 250µM cysteine CR plates and incubated at 37°C for 48 hours. Cysteine addition reverted *ΔcysE,* and *ΔcysEΔcysC* to no appreciable CR binding.

Table 4.1. Gene mutations that induce Δ*cysE* strains to wrinkle.

# isolated	Insertion gene	Function
1	*amyA*	cytoplasmic α-amylase
1	*degS*	cleaves misfolded outermembrane proteins and the anti sigma factor rseA
1	*dsbA*	periplasmic oxidoreductase
2	*dsbB*	periplasmic oxidoreductase
1	*hflX*	GTPase associated with ribosome located next to *hfq*
1	*hfq*	Protein that has been said to both increase and decrease stability of *csgD* transcript. Acts to stabilize other small RNAs
9	*mtlA*	mannitol permease
2	*opgG*	osmoregulated periplasmic glucan branching
5	*opgH*	osmoregulated periplasmic glucan glycosyl transferase
1	*serC*	in biosynthesis of serine and pyridoxine
1	*ssb*	Not found in lab strains additional SSB on UTI89 plasmid
1	*sufI*	stabilizes divisomal assembly during stress
1	*ugpC*	glycerol-3-phosphate import
1	*xylR*	Transcriptional regulator
1	*ychA*	Predicted transcriptional regulator
1	*yciR*	Phosphodiesterase paired with Ydam which increases *mlrA* and *csgD* transcription
1	*yfiR*	Periplasmic inhibitor of YfiN
1	*yhbE*	Unknown-has domain for cysteine/cystine export

Table 4.2. Plasmid list.

Plasmids	Reference
p*yfiR-his*	(68)
p*csgBAC*	(19)
p*adrA*	(19)
p*16s*	(68)
prj800	(127)
p*cysE*	(90)
p*cysK*	(90)

Table 4.3. Primer list.

Primers	Description	Sequence
DH1	*cysE* RS F	GCCCGCGCAGAACGGGCCGGTCATTATCTCATCGTGTGGAGTAAGCAATGGTGTAGGC TGGAGCTGCTTC
DH2	*cysE* RS *R*	TACATCGCATCCGGCACGATCACAGGACATTAGATCCCATCCCCATACTCCATATGAAT ATCCTCCTTAG
DH16	*cysK* RS F	GGT ATG CTA CCT GTT GTA TCC CAA TTT CAT ACA GTT AAG GAC AGG CCA TGG TGT AGG CTG GAG CTG CTT C
DH17	*cysK* RS R	CTT TTT TAC GCA TTT TTT ACA AGC TGG CAT TAC TGT TGC AGT TCT TTC TCC ATA TGA ATA TCC TCC TTA G
DH18	*cysM* RS F	AGA CGC GTA AGC GTC GCA TCA GGC AAC ACC ACG TAT GGA CAG AGA TCG TGG TGT AGG CTG GAG CTG CTT C
DH19	*cysM* RS R	ACG GAT AAA ACG GTG CCT GCG CAA TAA TCT TAA ATC CCC GCC CCC TGG CTC ATA TGA ATA TCC TCC TTA G
WD449	*hfq* RS F	GAA TCG AAA GGT TCA AAG TAC AAA TAA GCA TAT AAG GAA AAG AGA GAA TGG TGT AGG CTG GAG CTG CTT C
WD450	*hfq* RS R	CTC CCC GTG TAA AAA AAT AGC CCG AAA CCT TAT TCG GTT TCT TCG CTG TCC ATA TGA ATA TCC TCC TTA G
WD216	*oxyR* RS F	CTA TGC TAC CTA TCG CCG CGA ACT ATC GTG GCA ATG GAG GAT GGA TAA TGG TGT AGG CTG GAG CTG CTT C
WD217	*oxyR* RS R	AAG CCT ATC GGG TAG CTG CGC TAA ATG GCT TAA ACC GCC TGT TTT AAA ACC ATA TGA ATA TCC TCC TTA G
DH188	*cysC* RS F	CGC CAT TTC CCG CAT TGG GGT GCG CGC GAT TTA CTG GGA GAT AAA TAA TGG TGT AGG CTG GAG CTG CTT C
DH189	*cysC* RS R	CGA ACC GGG CAT GAA AAC CCG GTG GTG TCT CAG GAT CTG ATA ATA TCG TTC ATA TGA ATA TCC TCC TTA G
DH192	*cysB* RS F	GTG ACG AAA AAA CGA TGT TCT GAT GGC GTC TAA GTG GAT GGT TTA ACA TGG TGT AGG CTG GAG CTG CTT C
DH193	*cysB* RS R	ATA AAA GGT GCC GAA AAT AAC GCA AGA AAT TAT TTT TCC GGC AGT TTT ATC ATA TGA ATA TCC TCC TTA G
DH85	*Salmonella cysE* RS F	ACC CGC ACA GAA CGG GTT GGT CGT TTT CTG CCC GTC TGG AGT AAG CCA TGC ATA TGA ATA TCC TCC TTA G
DH86	*Salmonella cyseE* RS R	ACA GCG TTT TTT AGT TGT ACC GCG CAA TTC AGA TGC CGT CGC CAT ACT CAG TGT AGG CTG GAG CTG CTT C
WD439	*fliC* RS F	GTC AGT CTC AGT TAA TCA GGT TAC GGC GAT TAA CCC TGC AGC AGA GAC AGC ATA TGA ATA TCC TCC TTA G
WD440	*fliC* RS R	GGA AAC CCA AAA CGT AAT CAA CGA CTT GCA ATA TAG GAT AAC GAA TCA TGG TGT AGG CTG GAG CTG CTT C
DH232	*opgG* RS F	GCA CAC AAA GGG GGA AGT GCT TAC TAA TTA TGA AAC ATA AAC TAC AAA TGG TGT AGG CTG GAG CTG CTT C
DH233	*opgG* RS R	TGG GCA TTG CGT CAA TGT ACT CAG TTG TCT TAT TCA TTG GCA GGT AAC TGC ATA TGA ATA TCC TCC TTA G
DH236	*yciR* RS F	TAT AGC GCT AAG TAT ATA TAT TCA TCT ACT TAT GTG CGC TTC AGG TAG CGC ATA TGA ATA TCC TCC TTA G
DH237	*yciR* RS R	CCT TTT ATT TAA CTG CGG ACT CCG CTG TTA ACC GGA GGA TAT GCA TCA TGG TGT AGG CTG GAG CTG CTT C

Table 4.4. Strain list.

Strain name	Strain Genotype	Notes
	UTI89	**(62)**
	UTI89 *ΔcsgD*	(308)
	UTI89 *ΔcsgBA*	(308)
	UTI89 *ΔbcsA*	(308)
CL1166	UTI89 *ΔcysE*	kan cassette RS into *cysE* with DH1 and DH2 amplifying kan cassette. PCP20 used to remove kan cassette
CL1236	UTI89 *ΔcysKΔcysM*	kan cassette RS into *cysK* with DH16 and DH17 amplifying kan cassette, followed by kan cassette RS into *cysM* with DH18 and DH19 amplifying kan cassette. PCP20 used to remove kan cassettes
CL1483	UTI89 *ΔcysEΔcsgBA*	kan cassette RS into *cysE* in a *ΔcsgBA* strain with DH1 and DH2 amplifying kan cassette. PCP20 used to remove kan cassette
CL1564	UTI89 *ΔcsgD cysE::kan*	kan cassette RS into *cysE* with DH1 and DH2 in a *ΔcsgD* strain amplifying kan cassette. PCP20 used to remove kan cassette
CL1977	UTI89 *ΔgshA cysE::kan*	kan cassette RS into *cysE* with DH1 and DH2 in a *gshA::kan* strain amplifying kan cassette.
CL1980	UTI89 *ΔcysE ΔgshB*	kan cassette RS into *cysE* with DH1 and DH2 in *ΔgshB* strain. PCP20 used to remove kan cassette
CL2010	UTI89 *ΔcysE hfq::kan*	kan cassette RS into *hfq* with WD449 and WD450 in a *ΔcysE* strain amplifying kan cassette.
CL2036	UTI89 *ΔcysE oxyR::kan*	kan cassette RS into *oxyR* with WD 216 and WD217 in a *ΔcysE* strain amplifying kan cassette.
CL1979	UTI89 *ΔcysEΔyfiR*	kan cassette RS into *cysE* with DH1 and DH2 in a *ΔyfiR* strain amplifying kan cassette. PCP20 used to remove kan cassette
CL1502	UTI89 *ΔcysE* pckr101	*ΔcysE* strain transformed with pCKR101.
CL1962	UTI89 *ΔcysE* pckr101-*yfiR-his*	*ΔcysE* strain transformed with pCKR101-*yfiR-his*
CL1945	UTI89 *ΔcysE ΔcysC*	kan cassette RS into *cysE* with DH1 and DH2 in a *ΔcysC* strain amplifying kan cassette. PCP20 used to remove kan cassette
CL1948	UTI89 *ΔcysE cysB::kan*	kan cassette RS into *cysB* with DH192 and DH193 in a *ΔcysE* strain amplifying kan cassette.
CL1452	UTI89 *ΔcysE* prj800	*ΔcysE* strain transformed with pRJ800
CL1512	UTI89 *ΔcysE* prj800-csgBAC	*ΔcysE* strain transformed with pRJ800-*csgBAC*
CL1450	UTI89 *ΔcysE* prj800-*adrA*	*ΔcysE* strain transformed with pRJ800-*adrA*.
CL1545	UTI89 *ΔcysKΔcysM* prj800	*ΔcysKΔcysM* strain transformed with pRJ800
CL1547	UTI89 *ΔcysKΔcysM* prj800-*csgBAC*	*ΔcysKΔcysM* strain transformed with pRJ800-*csgBA*
CL1548	UTI89 *ΔcysKΔcysM* prj800-*adrA*	*ΔcysKΔcysM* strain transformed with pRJ800-*adrA*
CL1565	UTI89 *ΔfliC*	kan cassette RS into *fliC* with WD439 andWD440 amplifying kan cassette. PCP20 used to remove kan cassette
CL2015	UTI89 *ΔcysEΔugpQ*	kan cassette RS into *ΔcysE* with DH1 and DH2 in a *ugpQ* strain amplifying kan cassette. PCP20 used to remove kan cassette
CL2011	UTI89 *ΔcysEΔopgG*	kan cassette RS into *opgG* with DH233 and DH234 in a *ΔcysE* strain amplifying kan cassette. PCP20 used to remove kan cassette
CL2064	UTI89 *ΔcysE yciR::kan*	kan ca RS into *yciR* with DH236 and DH237 amplifying kan cassette in a *ΔcysE* strain.
CL2061	UTI89 *ΔcysE yfiN::kan*	kan cassette RS into *yfiN* in a *ΔcysE strain* amplifying kan cassette.

CHAPTER V

Future Directions and Concluding Remarks

Most of the bacteria we encounter are within biofilm, yet the full understanding of cellular processes involved in separating the matrix subpopulation from the underlying cells in a biofilm is unclear. Research has focused on the free-swimming and mature biofilm lifestyles while largely neglecting the crucial transition period. This work demonstrated the breadth of processes that alter and are required for biofilm formation. Our understanding of biofilm initiation has been limited to cells encountering a surface or experiencing starvation and stress conditions. Through this work biofilm formation is now known to require anaerobic respiration, multiple environment sensing transcription factors, a minimal cell wall, a functioning electron transport chain, and c-di-GMP from DgcN. Because there are so many effectors of biofilm formation, no one treatment will be the answer for biofilm inhibition. But this work also opens the possibilities of many new therapeutic targets that can be tested in combination to inhibit biofilm formation.

Future Directions

What role does purine synthesis play in biofilm formation?

Purine synthesis is involved in regulating matrix component production. De novo purine synthesis leads to adenine and guanine bases as well as the energetic triphosphate derivatives, ATP and GTP(356). Gene knockouts in the Keio collection that blocked purine synthesis (*purA*-*T*) reduced curli levels to those equal to *csgA* knockout mutants based on Congo red binding (Fig. 2.1C, Fig. 2.7, Table 2.5). This was originally argued to be a result of reduced growth or auxotrophy(357). The RNAseq and proteomic data further supported the idea that purine synthesis plays a more direct role in curli synthesis. While the *purA*-*T* transcripts and protein levels were not significantly changed between the Matrix subpopulation and Washout subpopulation within biofilms, the transcript/protein pairs involved in amino acid metabolism of histidine, thiamine, arginine, and asparagine were significantly increased in the Matrix producing cells (Fig 3.1 and Table 3.1). These amino acid metabolism pathways directly feed

into the purine synthesis pathway at multiple points(288). There are a couple possible reasons why purine synthesis is required for matrix component production. First, purine synthesis could be required for production of IMP to be used in c-di-GMP. High c-di-GMP levels are known to induce biofilm formation in *E. coli*(70, 83, 287). By increasing breakdown of amino acids into IMP, cells can produce more c-di-GMP and therefore increase matrix component production through activation of CsgD(47, 67, 68). Second, IMP is also a precursor of ADP and higher levels of ADP may be required to sustain high ATP levels in the cells. Matrix production is a energetically expensive undertaking for cells(272, 358). Matrix producing cells may require a higher pool of ADP to be rapidly phosphorylated and dephosporylated to allow for biofilm production in addition to normal cell functions. Third, purines may play a poorly understood role in stress mitigation. A study in *S. aureus* found that cells with mutations in purine synthesis genes were more susceptible to heat stress and the antibiotic *Rifampicin*(359). Future work should track usage of produced IMP within the cell. IMP is a branching point, and mutants could be made to restrict IMP to be metabolized only into GMP or AMP and the effect on matrix production measured.

How is subpopulation shape in *E. coli* biofilm determined?

Bacteria, and even some single-celled eukaryotes, form rugose biofilm colonies on agar plates that are similar in overall architecture(360). The colonies are rough in texture, usually with large wrinkles that radiate from the center of the biofilm towards the growing edge(360). The wrinkles have been shown to be important for nutrient and substrate movement within the biofilm(23, 277). But production of wrinkles is still poorly understood. *E. coli* biofilms that lack cellulose or curli do not wrinkle (Fig. 3.4A), indicating a cooperative interaction between cellulose and curli is required for wrinkling.

Causes of wrinkling are diverse and differ by bacterial species. Redox gradients are responsible for wrinkling in *P. aeruginosa*(361). In *V. cholerae* biofilm is wrinkled through cell-driven mechanical stress(362). And wrinkling is caused by localized cell death in *B. subtilis*(363, 364). I began work to test these different causes for wrinkling in UTI89 *E. coli.* I repeated the work of M. Asally *et al.* (363) using UTI89 *E. coli* at concentrations used in the paper and higher

concentrations to attempt to create wrinkles where the higher density cells were placed on the agar plate. After many attempts I was unable to create any shapes other than the WT structure, indicating *E. coli* utilize a different method to create wrinkles. In the case of redox gradients, we know that *E. coli* matrix component production is sensitive to the redox state of the cell, causing smooth biofilm colony morphology when hyper-oxidized (Fig. 4.1B)(19). This observed change in wrinkling was due to a decoupling of cellulose and curli production (Fig. 4.2 and 4.4). Cysteine auxotrophs were hyper-oxidized leading to increased curli production, decreased cellulose, and a biofilm without wrinkles (Fig. 4.2 and 4.4). When hyper-oxidized cells were supplemented with a reducing agent, curli and cellulose reverted to WT levels and biofilm morphology was wrinkled (Fig. 4.2 and 4.4). But cells being more oxidized alone does not drive wrinkling as the Washout biofilm subpopulation had an oxidized state higher than the Matrix subpopulation (Fig. 3.4D). Together, this indicates to me that the interaction between cellulose and curli is likely to drive wrinkling through cell contact stresses.

A high concentration of cellulose and curli on individual cells may be required for wrinkling. In *E. coli* biofilm, the matrix-associated cells form the Matrix subpopulation and the non-matrix cells form the Washout subpopulation. In UTI89 biofilm, approximately 40% of cells by OD_{600} are part of the Matrix subpopulation and putting curli and cellulose on their outer membrane. When we supplemented WT biofilm growth with nitrate (Fig 3.5) or blocked nitrite respiration with a *nrfA* knockout (Fig. 3.6), unwrinkled biofilm colonies formed. In these unwrinkled colonies the total amount of cellulose and curli were unchanged (Fig 3.5B and 3.6BC). This means that the local concentration of curli and cellulose per cell was higher in the WT Matrix cell subpopulation compared to the unwrinkled biofilms without subpopulations. In a colony biofilm, the aerobically respiring cells near the air-colony interface can use the available oxygen such that underlying cells are mostly anaerobic (Fig 3.3)(19). It is possible that energetically favorable oxygenic respiration is vital in early stages of biofilm formation due to the high energy cost of producing matrix components(272, 358). Having a mechanism to restrict matrix component production to cells that will be a part of the Matrix subpopulation may be a way to both ensure a high density of curli and cellulose per cell in only the Matrix cells as well as

ensuring that the available oxygen is disproportionately used by the Matrix subpopulation. Blocking matrix production in Washout cells also gives Washout cells the advantage of conserving energy. Anaerobic respiration is not as energetic as aerobic respiration, but we observed that the oxygen-limited Washout subpopulation had higher concentrations of ATP than the Matrix subpopulation (Fig. 3.4E). Having a biofilm 'off switch', potentially NarLP(Chapter 3), allows for judicious use of resources and potentially allows for Washout subpopulation cells to always primed for dispersal.

Remaining questions with the RNAseq data

One strength of the RNAseq analysis is the breadth of the returned information. Leads that I wanted to follow up include RstAB and YgeWXY. RstAB is a poorly characterized two-component system that had increased expression in the Matrix subpopulation as compared to the Washout subpopulation. *rstA*- had decreased curli in our screen for genes that altered curli production (Fig. 2.1) and has been shown to interact with the *csgD* promotor in response to acidic conditions(365). Given time I would have investigated RstAB role in host environment adaptation, as a change in pH is a strong signal for bacteria entering the host through both fecal-oral and rectal-ureter pathways(366). *ygeW* and the neighboring genes *ygeXY* were among those with the highest fold change difference between the Washout and Matrix subpopulation. While this is interesting enough alone to merit following up, *ygeW* is predicted to be a purine scavenger(356). Purine metabolism appears as important in the Matrix subpopulation (Fig 3.1), but the YgeW putative purine scavenger is upregulated in the Washout subpopulation. I am interested to see if this difference relates to how energy is conserved, potentially for nucleotide synthesis, or some other unknown mechanism. In addition to the WT Washout and WT Matrix subpopulations we sent for sequencing, I prepared and sent replicates for whole biofilms of WT, *csgD-, csgC-, yfiR-,* and *dgcN*-. These RNAseq samples had good variation between them and could be separated by principle component analysis (Fig. 5.1).

How is c-di-GMP produced by DgcN able to act selectively on *csgD* promotion?

There is an abundance of c-di-GMP during biofilm growth, but c-di-GMP produced by DgcN is required for basal CsgD levels(68). I began working on mutations in *dgcN* that would inhibit

GGDEF dimerization required for the production of c-di-GMP(83, 88). While the single mutant in the GGDEF domain was not sufficient to change the biofilm morphology, the GGAAAF mutant biofilm exhibited some loss of wrinkling. In parallel, mutations were being made in *mlrA* to inactivate 2 predicted PilZ domains that could potentially bind c-di-GMP. MlrA has been shown to bind the *csgD* promotor region in response to c-di-GMP(72, 73) and knockouts of *mlrA* exhibit no Congo Red binding (Fig 2.1)(54). Previously, the I-sites on MlrA were mutated, but did not block c-di-GMP binding (73). We were unable to complete this series of mutants but anticipate that DgcN acts as the beginning of a c-di-GMP signaling cascade that ends at MlrA to affect *csgD* expression specifically. This process has been characterized in K-12 *E.coli*(69) but DgcN has not been shown to be an active diguanylate cyclase in UTI89 *E. coli* and this signaling cascade effect on cellulose production remains unstudied. As DgcN senses redox through the periplasmic repressor YfiR and hyper-oxidized states lead to the uncoupling of curli and cellulose production (Chapter 4), it is possible that MlrA is responsible for cellulose and curli uncoupling. If MlrA increases recruitment of CsgD to the *csg* intragenic region, this may effectively sequester CsgD away from promoting *dgcC* and subsequently limit cellulose production.

Concluding Remarks

In my thesis I have investigated biofilm formation at the level of matrix component production, subpopulation structure, and regulation of initiation of *csgD* expression. Chapters 2 and 3 describe in detail the many cell processes that contribute to *E. coli* ability to form a biofilm. These chapters outlined the importance of environment sensing, directed amino acid breakdown leading to IMP production, and the critical role of anaerobic respiration. This work gives broader understanding to how pathogenic *E. coli* unable to respire anaerobically have reduced fitness in host environments(53, 54). Demonstrating *in vivo* that bacteria in the human GI tract live within biofilm is nearly impossible, as matrix components serve both general attachment and biofilm roles. The genes identified in this work can be used to better define what constitutes a biofilm, even in the complex host environment. Growth of subpopulations depends on a balance of the number matrix producing and non-producing cells (Chapter 3 and

4). Regulation of matrix production can be altered by the redox state of the cell, allowing for curli production at temperatures that normally inhibit curli production (Chapter 4). I predict that continued research will show even more clearly the complex of control over biofilm production, but also many new pathways to target with therapeutics and interventions to make biofilm cells susceptible to antibiotics.

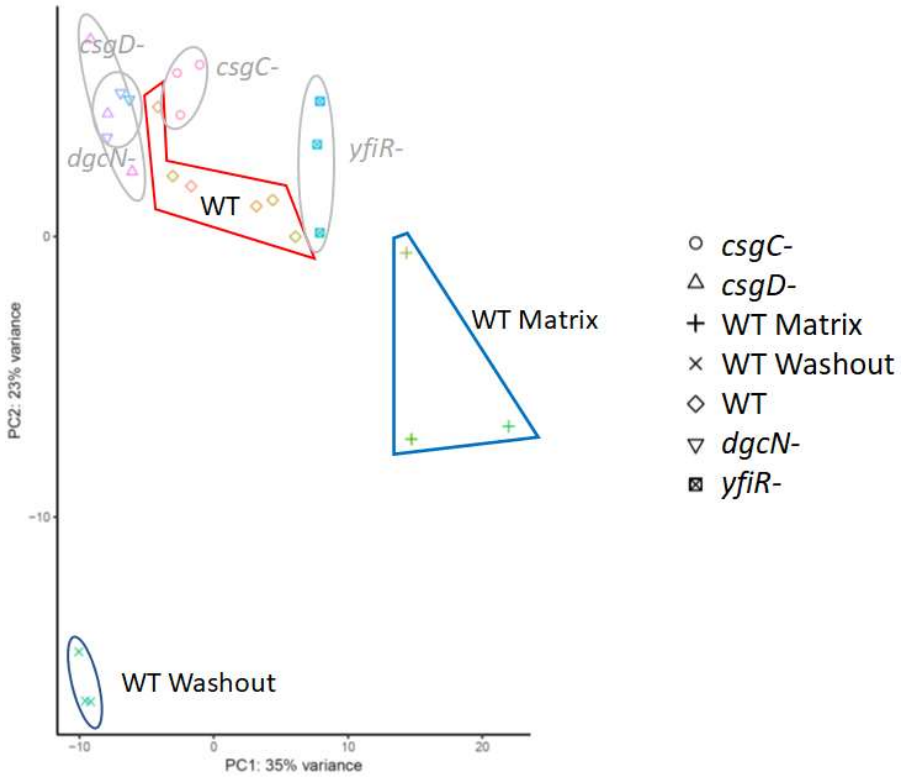

Figure 5.1. Principal component analysis of all UTI89 strains that underwent RNAseq analysis. RNA was harvested from UTI89 rugose biofilms in triplicate for use in RNA sequencing (6 replicates of WT). Comparing the variance of reads in the RNAseq data showed good grouping of replicates among the strains tested.

References

1. van Leewenhoeck A. 1677. Observations, Communicated to the Publisher by Mr. Antony van Leewenhoeck, in a Dutch Letter of the 9th of Octob. 1676. Here English'd: concerning Little Animals by Him Observed in Rain-Well-Sea. and Snow Water; as Also in Water Wherein Pepper Had Lain Infused. Philosophical Transactions (1665-1678) 12:821-831.

2. Gould SJ. 1976. This view of life - 5 Kingdoms. Natural History 85:30-&.

3. Hug LA, Baker BJ, Anantharaman K, Brown CT, Probst AJ, Castelle CJ, Butterfield CN, Hernsdorf AW, Amano Y, Ise K, Suzuki Y, Dudek N, Relman DA, Finstad KM, Amundson R, Thomas BC, Banfield JF. 2016. A new view of the tree of life. Nature Microbiology 1:16048.

4. Staley JT, Konopka A. 1985. Measurement of in situ activities of nonphotosynthetic microorganisms in aquatic and terrestrial habitats. Annu Rev Microbiol 39:321-46.

5. Costerton J, Lewandowski Z, Caldwell DE, Korber DR, Lappin-Scott HM. 1995. Microbial Biofilms. Annual Review of Microbiology 49:711-745.

6. Whitman WB, Coleman DC, Wiebe WJ. 1998. Prokaryotes: The unseen majority. Proceedings of the National Academy of Sciences 95:6578-6583.

7. Dodd MS, Papineau D, Grenne T, Slack JF, Rittner M, Pirajno F, O'Neil J, Little CT. 2017. Evidence for early life in Earth's oldest hydrothermal vent precipitates. Nature 543:60-64.

8. Glud RN, Wenzhöfer F, Middelboe M, Oguri K, Turnewitsch R, Canfield DE, Kitazato H. 2013. High rates of microbial carbon turnover in sediments in the deepest oceanic trench on Earth. Nature Geoscience 6:284-288.

9. Pol A, Barends TRM, Dietl A, Khadem AF, Eygensteyn J, Jetten MSM, Op den Camp HJM. 2014. Rare earth metals are essential for methanotrophic life in volcanic mudpots. Environmental Microbiology 16:255-264.

10. Amato P, Joly M, Besaury L, Oudart A, Taib N, Moné AI, Deguillaume L, Delort A-M, Debroas D. 2017. Active microorganisms thrive among extremely diverse communities in cloud water. PLOS ONE 12:e0182869.

11. Klintworth R, Reher HJ, Viktorov AN, Bohle D. 1999. Biological induced corrosion of materials II: New test methods and experiences from mir station. Acta Astronautica 44:569-578.

12. Zea L, McLean RJC, Rook TA, Angle G, Carter DL, Delegard A, Denvir A, Gerlach R, Gorti S, McIlwaine D, Nur M, Peyton BM, Stewart PS, Sturman P, Velez Justiniano YA. 2020. Potential biofilm control strategies for extended spaceflight missions. Biofilm 2:100026.

13. Kadner KRaRJ. June 20, 2019. Bacteria, p *In* (ed), Encyclopædia Britannica, ed vol Encyclopædia Britannica, inc, https://www.britannica.com/science/bacteria.

14. Stewart PS, Franklin MJ. 2008. Physiological heterogeneity in biofilms. Nature Reviews Microbiology 6:199-210.

15. Gannesen AV, Lesouhaitier O, Racine P-J, Barreau M, Netrusov AI, Plakunov VK, Feuilloley MGJ. 2018. Regulation of Monospecies and Mixed Biofilms Formation of Skin Staphylococcus aureus and Cutibacterium acnes by Human Natriuretic Peptides. Frontiers in Microbiology 9.

16. Lopes SP, Azevedo NF, Pereira MO. 2018. Quantitative assessment of individual populations within polymicrobial biofilms. Scientific Reports 8:9494.

17. Laskowska E, Kuczyńska-Wiśnik D. 2020. New insight into the mechanisms protecting bacteria during desiccation. Current Genetics 66:313-318.

18. Depas WH, Syed AK, Sifuentes M, Lee JS, Warshaw D, Saggar V, Csankovszki G, Boles BR, Chapman MR. 2014. Biofilm Formation Protects *Escherichia coli* against Killing by *Caenorhabditis elegans* and *Myxococcus xanthus*. Applied and Environmental Microbiology 80:7079-7087.

19. DePas WH, Hufnagel DA, Lee JS, Blanco LP, Bernstein HC, Fisher ST, James GA, Stewart PS, Chapman MR. 2013. Iron induces bimodal population development by *Escherichia coli*. Proceedings of the National Academy of Sciences of the United States of America 110:2629-2634.

20. Borriello G, Werner E, Roe F, Kim AM, Ehrlich GD, Stewart PS. 2004. Oxygen limitation contributes to antibiotic tolerance of *Pseudomonas aeruginosa* in biofilms. Antimicrobial Agents and Chemotherapy 48:2659-2664.

21. Hufnagel DA, Price JE, Stephenson RE, Kelley J, Benoit MF, Chapman MR. 2017. Thiol Starvation induces redox-mediated dysregulation of *Escherichia coli* biofilm components. J Bacteriol doi:10.1128/jb.00389-17.

22. Hall-Stoodley L, Costerton JW, Stoodley P. 2004. Bacterial biofilms: from the Natural environment to infectious diseases. Nature Reviews Microbiology 2:95-108.

23. Rasmussen K, Lewandowski Z. 1998. Microelectrode measurements of local mass transport rates in heterogeneous biofilms. Biotechnology and Bioengineering 59:302-309.

24. Serra DO, Hengge R. 2014. Stress responses go three dimensional - the spatial order of physiological differentiation in bacterial macrocolony biofilms. Environmental Microbiology 16:1455-1471.

25. Prax M, Bertram R. 2014. Metabolic aspects of bacterial persisters. Front Cell Infect Microbiol 4:148.

26. Lacqua A, Wanner O, Colangelo T, Martinotti MG, Landini P. 2006. Emergence of Biofilm-Forming Subpopulations upon Exposure of *Escherichia coli* to Environmental Bacteriophages. Applied and Environmental Microbiology 72:956-959.

27. Kaur GDC, Sanjivani SM. 2015. Biofilm Formation and Antimicrobial Resistance Pattern Among Uropathogens. International Journal of Medical Research & Health Sciences 4:339-344.

28. Khatoon Z, McTiernan CD, Suuronen EJ, Mah TF, Alarcon EI. 2018. Bacterial biofilm formation on implantable devices and approaches to its treatment and prevention. Heliyon 4:e01067.

29. Starner TD, Zhang N, Kim GH, Apicella MA, McCray PB. 2006. *Haemophilus influenzae* forms biofilms on airway epithelia - Implications in cystic fibrosis. American Journal of Respiratory and Critical Care Medicine 174:213-220.

30. Kirketerp-Moller K, Jensen PO, Fazli M, Madsen KG, Pedersen J, Moser C, Tolker-Nielsen T, Hoiby N, Givskov M, Bjarnsholt T. 2008. Distribution, organization, and ecology of bacteria in chronic wounds. Journal of Clinical Microbiology 46:2717-2722.

31. Graziottin A, Zanello PP. 2015. Pathogenic Biofilms as Triggers of Recurrent Vaginitis and Cystitis, p 3-11. *In* BenRafael Z (ed), 20th World Congress on

Controversies in Obstetrics, Gynecology & Infertility. Monduzzi Editore S P A, Bologna.

32. Conover MS, Ruer S, Taganna J, Kalas V, De Greve H, Pinkner JS, Dodson KW, Remaut H, Hultgren SJ. 2016. Inflammation-Induced Adhesin-Receptor Interaction Provides a Fitness Advantage to Uropathogenic *E. coli* during Chronic Infection. Cell Host Microbe 20:482-492.

33. Potera C. 1999. Forging a Link Between Biofilms and Disease. Science 283:1837-1839.

34. Wolcott RD, Rhoads DD, Bennett ME, Wolcott BM, Gogokhia L, Costerton JW, Dowd SE. 2010. Chronic wounds and the medical biofilm paradigm. Journal of Wound Care 19:45-53.

35. Romling U, Kjelleberg S, Normark S, Nyman L, Uhlin BE, Akerlund B. 2014. Microbial biofilm formation: a need to act. Journal of Internal Medicine 276:98-110.

36. Chmielewski RAN, Frank JF. 2003. Biofilm Formation and Control in Food Processing Facilities. Comprehensive Reviews in Food Science and Food Safety 2:22-32.

37. Fitridge I, Dempster T, Guenther J, de Nys R. 2012. The impact and control of biofouling in marine aquaculture: a review. Biofouling 28:649-669.

38. Teng F, Guan YT, Zhu WP. 2008. Effect of biofilm on cast iron pipe corrosion in drinking water distribution system: Corrosion scales characterization and microbial community structure investigation. Corrosion Science 50:2816-2823.

39. Sun H, Shi B, Lytle DA, Bai Y, Wang D. 2014. Formation and release behavior of iron corrosion products under the influence of bacterial communities in a simulated water distribution system. Environmental Science: Processes & Impacts 16:576-585.

40. Geesey GG, Richardson WT, Yeomans HG, Irvin RT, Costerton JW. 1977. Microscopic examination of natural sessile bacterial populations from an alpine stream. Canadian Journal of Microbiology 23:1733-1736.

41. J W Costerton, K J Cheng, G G Geesey, T I Ladd, J C Nickel, M Dasgupta a, Marrie TJ. 1987. Bacterial Biofilms in Nature and Disease. Annual Review of Microbiology 41:435-464.

42. Beloin C, Roux A, Ghigo JM. 2008. *Escherichia coli* biofilms. Curr Top Microbiol Immunol 322:249-89.

43. Kostakioti M, Hadjifrangiskou M, Hultgren SJ. 2013. Bacterial biofilms: development, dispersal, and therapeutic strategies in the dawn of the postantibiotic era. Cold Spring Harb Perspect Med 3:a010306.

44. Goodwine J, Gil J, Doiron A, Valdes J, Solis M, Higa A, Davis S, Sauer K. 2019. Pyruvate-depleting conditions induce biofilm dispersion and enhance the efficacy of antibiotics in killing biofilms in vitro and in vivo. Scientific Reports 9:16.

45. Petrova OE, Sauer K. 2016. Escaping the biofilm in more than one way: desorption, detachment or dispersion. Current Opinion in Microbiology 30:67-78.

46. Ho CL, Chong KSJ, Oppong JA, Chuah MLC, Tan SM, Liang ZX. 2013. Visualizing the Perturbation of Cellular Cyclic di-GMP Levels in Bacterial Cells. Journal of the American Chemical Society 135:566-569.

47. Lee VT, Matewish JM, Kessler JL, Hyodo M, Hayakawa Y, Lory S. 2007. A cyclic-di-GMP receptor required for bacterial exopolysaccharide production. Molecular Microbiology 65:1474-1484.

48. Srivastava D, Hsieh ML, Khataokar A, Neiditch MB, Waters CM. 2013. Cyclic di-GMP inhibits Vibrio cholerae motility by repressing induction of transcription and inducing extracellular polysaccharide production. Molecular Microbiology 90:1262-1276.

49. Shulman ST, Friedmann HC, Sims RH. 2007. Theodor Escherich: the first pediatric infectious diseases physician? Clin Infect Dis 45:1025-9.

50. Tenaillon O, Skurnik D, Picard B, Denamur E. 2010. The population genetics of commensal *Escherichia coli*. Nat Rev Microbiol 8:207-17.

51. Smith HW. 1965. Observations on the Flora of the Alimentary Tract of Animals and Factors Affecting its Composition. J Pathol Bacteriol 89:95-122.

52. Jones SA, Chowdhury FZ, Fabich AJ, Anderson A, Schreiner DM, House AL, Autieri SM, Leatham MP, Lins JJ, Jorgensen M, Cohen PS, Conway T. 2007. Respiration of *Escherichia coli* in the Mouse Intestine. Infection and Immunity 75:4891-4899.

53. Jones SA, Gibson T, Maltby RC, Chowdhury FZ, Stewart V, Cohen PS, Conway T. 2011. Anaerobic Respiration of *Escherichia coli* in the Mouse Intestine. Infection and Immunity 79:4218-4226.

54. Martín-Rodríguez AJ, Rhen M, Melican K, Richter-Dahlfors A. 2020. Nitrate Metabolism Modulates Biosynthesis of Biofilm Components in Uropathogenic *Escherichia coli* and Acts as a Fitness Factor During Experimental Urinary Tract Infection. Front Microbiol 11:26.

55. Kaas RS, Friis C, Ussery DW, Aarestrup FM. 2012. Estimating variation within the genes and inferring the phylogeny of 186 sequenced diverse *Escherichia coli* genomes. BMC Genomics 13:577.

56. Bachmann BJ. 1972. Pedigrees of some mutant strains of *Escherichia coli* K-12. Bacteriol Rev 36:525-57.

57. Vidal O, Longin R, Prigent-Combaret C, Dorel C, Hooreman M, Lejeune P. 1998. Isolation of an *Escherichia coli* K-12 mutant strain able to form biofilms on inert surfaces: involvement of a new ompR allele that increases curli expression. J Bacteriol 180:2442-9.

58. Hooton TM, Scholes D, Hughes JP, Winter C, Roberts PL, Stapleton AE, Stergachis A, Stamm WE. 1996. A prospective study of risk factors for symptomatic urinary tract infection in young women. N Engl J Med 335:468-74.

59. Schappert SM. 1999. Ambulatory care visits to physician offices, hospital outpatient departments, and emergency departments: United States, 1997. Vital Health Stat 13:i-iv, 1-39.

60. Yamamoto S, Tsukamoto T, Terai A, Kurazono H, Takeda Y, Yoshida O. 1997. Genetic Evidence Supporting the Fecal-Perineal-Urethral Hypothesis in Cystitis Caused by *Escherichia coli*. The Journal of Urology 157:1127-1129.

61. Hufnagel DA, Depas WH, Chapman MR. 2015. The Biology of the *Escherichia coli* Extracellular Matrix. Microbiology Spectrum 3.

62. Mulvey MA, Schilling JD, Hultgren SJ. 2001. Establishment of a persistent *Escherichia coli* reservoir during the acute phase of a bladder infection. Infect Immun 69:4572-4579.

63. Vogeleer P, Tremblay YDN, Mafu AA, Jacques M, Harel J. 2014. Life on the outside: role of biofilms in environmental persistence of Shiga-toxin producing *Escherichia coli*. Frontiers in Microbiology 5.

64. Volz K. 1993. Structural conservation in the CheY superfamily. Biochemistry 32:11741-53.

65. Olsén A, Arnqvist A, Hammar M, Sukupolvi S, Normark S. 1993. The RpoS sigma factor relieves H-NS-mediated transcriptional repression of *csgA*, the subunit gene of fibronectin-binding curli in *Escherichia coli*. Mol Microbiol 7:523-36.

66. Evans ML, Chapman MR. 2013. Curli biogenesis: Order out of disorder. Biochim Biophys Acta doi:10.1016/j.bbamcr.2013.09.010.

67. Ahmad I, Cimdins A, Beske T, Römling U. 2017. Detailed analysis of c-di-GMP mediated regulation of *csgD* expression in *Salmonella typhimurium*. BMC Microbiology 17:27.

68. Hufnagel DA, DePas WH, Chapman MR. 2014. The Disulfide Bonding System Suppresses CsgD-Independent Cellulose Production in *Escherichia coli*. Journal of Bacteriology 196:3690-3699.

69. Lindenberg S, Klauck G, Pesavento C, Klauck E, Hengge R. 2013. The EAL domain protein YciR acts as a trigger enzyme in a c-di-GMP signalling cascade in *E. coli* biofilm control. Embo Journal 32:2001-2014.

70. Römling U, Gomelsky M, Galperin MY. 2005. C-di-GMP: the dawning of a novel bacterial signalling system. Molecular Microbiology 57:629-639.

71. Sommerfeldt N, Possling A, Becker G, Pesavento C, Tschowri N, Hengge R. 2009. Gene expression patterns and differential input into curli fimbriae regulation of all GGDEF/EAL domain proteins in *Escherichia coli*. Microbiology 155:1318-1331.

72. Brown PK, Dozois CM, Nickerson CA, Zuppardo A, Terlonge J, Curtiss R, 3rd. 2001. MlrA, a novel regulator of curli (AgF) and extracellular matrix synthesis by *Escherichia coli* and *Salmonella enterica* serovar Typhimurium. Mol Microbiol 41:349-63.

73. Ogasawara H, Yamamoto K, Ishihama A. 2010. Regulatory role of MlrA in transcription activation of *csgD*, the master regulator of biofilm formation in *Escherichia coli.* FEMS Microbiol Lett 312:160-8.

74. Guttenplan SB, Kearns DB. 2013. Regulation of flagellar motility during biofilm formation. FEMS Microbiol Rev 37:849-71.

75. Ogasawara H, Yamamoto K, Ishihama A. 2011. Role of the Biofilm Master Regulator CsgD in Cross-Regulation between Biofilm Formation and Flagellar Synthesis. J Bacteriol 193:2587-97.

76. Chapman MR, Robinson LS, Pinkner JS, Roth R, Heuser J, Hammar M, Normark S, Hultgren SJ. 2002. Role of *Escherichia coli* Curli Operons in Directing Amyloid Fiber Formation. Science 295:851-855.

77. Zogaj X, Nimtz M, Rohde M, Bokranz W, Romling U. 2001. The multicellular morphotypes of *Salmonella typhimurium* and *Escherichia coli* produce cellulose as the second component of the extracellular matrix. Mol Microbiol 39:1452-63.

78. McCrate OA, Zhou X, Reichhardt C, Cegelski L. 2013. Sum of the parts: composition and architecture of the bacterial extracellular matrix. Journal of molecular biology 425:4286-94.

79. Gorgieva S, Trček J. 2019. Bacterial Cellulose: Production, Modification and Perspectives in Biomedical Applications. Nanomaterials (Basel) 9.

80. Gualdi L, Tagliabue L, Bertagnoli S, Ierano T, De Castro C, Landini P. 2008. Cellulose modulates biofilm formation by counteracting curil-mediated colonization of solid surfaces in *Escherichia coli*. Microbiology-Sgm 154:2017-2024.

81. Serra DO, Richter AM, Hengge R. 2013. Cellulose as an architectural element in spatially structured *Escherichia coli* biofilms. J Bacteriol 195:5540-54.

82. Hung C, Zhou Y, Pinkner JS, Dodson KW, Crowley JR, Heuser J, Chapman MR, Hadjifrangiskou M, Henderson JP, Hultgren SJ. 2013. *Escherichia coli* Biofilms Have an Organized and Complex Extracellular Matrix Structure. mBio 4:e00645-13.

83. Ryjenkov DA, Tarutina M, Moskvin OV, Gomelsky M. 2005. Cyclic diguanylate is a ubiquitous signaling molecule in bacteria: insights into biochemistry of the GGDEF protein domain. J Bacteriol 187:1792-8.

84. Omadjela O, Narahari A, Strumillo J, Melida H, Mazur O, Bulone V, Zimmer J. 2013. BcsA and BcsB form the catalytically active core of bacterial cellulose synthase sufficient for in vitro cellulose synthesis. Proc Natl Acad Sci U S A 110:17856-61.

85. Morgan JL, McNamara JT, Zimmer J. 2014. Mechanism of activation of bacterial cellulose synthase by cyclic di-GMP. Nat Struct Mol Biol 21:489-96.

86. Da Re S, Ghigo JM. 2006. A CsgD-independent pathway for cellulose production and biofilm formation in *Escherichia coli*. J Bacteriol 188:3073-87.

87. Hufnagel DA, DePas WH, Chapman MR. 2014. The disulfide bonding system suppresses CsgD-independent cellulose production in *Escherichia coli*. J Bacteriol 196:3690-9.

88. Hengge R, Galperin MY, Ghigo JM, Gomelsky M, Green J, Hughes KT, Jenal U, Landini P. 2016. Systematic Nomenclature for GGDEF and EAL Domain-Containing Cyclic Di-GMP Turnover Proteins of *Escherichia coli*. J Bacteriol 198:7-11.

89. Barnhart MM, Chapman MR. 2006. Curli biogenesis and function. Annu Rev Microbiol 60:131-47.

90. Zhou Y, Smith DR, Hufnagel DA, Chapman MR. 2013. Experimental manipulation of the microbial functional amyloid called curli. Methods Mol Biol 966:53-75.

91. Goyal P, Krasteva PV, Van Gerven N, Gubellini F, Van den Broeck I, Troupiotis-Tsailaki A, Jonckheere W, Pehau-Arnaudet G, Pinkner JS, Chapman MR, Hultgren SJ, Howorka S, Fronzes R, Remaut H. 2014. Structural and mechanistic insights into the bacterial amyloid secretion channel CsgG. Nature 516:250-253.

92. Robinson LS, Ashman EM, Hultgren SJ, Chapman MR. 2006. Secretion of curli fibre subunits is mediated by the outer membrane-localized CsgG protein. Mol Microbiol 59:870-81.

93. Shu Q, Krezel AM, Cusumano ZT, Pinkner JS, Klein R, Hultgren SJ, Frieden C. 2016. Solution NMR structure of CsgE: Structural insights into a chaperone and regulator protein important for functional amyloid formation. Proceedings of the National Academy of Sciences doi:10.1073/pnas.1607222113.

94. Nenninger AA, Robinson LS, Hultgren SJ. 2009. Localized and efficient curli nucleation requires the chaperone-like amyloid assembly protein CsgF. Proc Natl Acad Sci U S A 106:900-5.

95. Yan Z, Yin M, Chen J, Li X. 2020. Assembly and substrate recognition of curli biogenesis system. Nature Communications 11:241.

96. Zhang M, Shi H, Zhang X, Zhang X, Huang Y. 2020. Cryo-EM structure of the nonameric CsgG-CsgF complex and its implications for controlling curli biogenesis in Enterobacteriaceae. PLOS Biology 18:e3000748.

97. Evans ML, Chorell E, Taylor JD, Aden J, Gotheson A, Li F, Koch M, Sefer L, Matthews SJ, Wittung-Stafshede P, Almqvist F, Chapman MR. 2015. The Bacterial Curli System Possesses a Potent and Selective Inhibitor of Amyloid Formation. Molecular Cell 57:445-455.

98. Hammer ND, Schmidt JC, Chapman MR. 2007. The curli nucleator protein, CsgB, contains an amyloidogenic domain that directs CsgA polymerization. Proc Natl Acad Sci U S A 104:12494-9.

99. Zhou Y, Smith D, Leong BJ, Brännström K, Almqvist F, Chapman MR. 2012. Promiscuous cross-seeding between bacterial amyloids promotes interspecies biofilms. J Biol Chem 287:35092-103.

100. Dressaire C, Moreira RN, Barahona S, Alves de Matos AP, Arraiano CM. 2015. BolA Is a Transcriptional Switch That Turns Off Motility and Turns On Biofilm Development. mBio 6:e02352-14.

101. Flemming H-C, Wingender J. 2010. The biofilm matrix. Nature Reviews Microbiology 8:623-633.

102. Baba T, Ara T, Hasegawa M, Takai Y, Okumura Y, Baba M, Datsenko KA, Tomita M, Wanner BL, Mori H. 2006. Construction of *Escherichia coli* K-12 in-frame, single-gene knockout mutants: the Keio collection. Mol Syst Biol 2:2006 0008.

103. Chapman MR, Robinson LS, Pinkner JS, Roth R, Heuser J, Hammar M, Normark S, Hultgren SJ. 2002. Role of *Escherichia coli* curli operons in directing amyloid fiber formation. Science 295:851-5.

104. Collinson SK, Emody L, Muller KH, Trust TJ, Kay WW. 1991. Purification and characterization of thin, aggregative fimbriae from *Salmonella enteritidis.* J Bacteriol 173:4773-81.

105. Kikuchi T, Mizunoe Y, Takade A, Naito S, Yoshida S. 2005. Curli fibers are required for development of biofilm architecture in *Escherichia coli* K-12 and enhance bacterial adherence to human uroepithelial cells. Microbiol Immunol 49:875-84.

106. Uhlich GA, Cooke PH, Solomon EB. 2006. Analyses of the red-dry-rough phenotype of an *Escherichia coli* O157:H7 strain and its role in biofilm formation and resistance to antibacterial agents. Appl Environ Microbiol 72:2564-72.

107. Ryu JH, Beuchat LR. 2005. Biofilm formation by *Escherichia coli* O157:H7 on stainless steel: effect of exopolysaccharide and Curli production on its resistance to chlorine. Appl Environ Microbiol 71:247-54.

108. Jeter C, Matthysse AG. 2005. Characterization of the binding of diarrheagenic strains of *E. coli* to plant surfaces and the role of curli in the interaction of the bacteria with alfalfa sprouts. Mol Plant Microbe Interact 18:1235-42.

109. Barak JD, Gorski L, Naraghi-Arani P, Charkowski AO. 2005. *Salmonella enterica* virulence genes are required for bacterial attachment to plant tissue. Appl Environ Microbiol 71:5685-91.

110. White AP, Gibson DL, Kim W, Kay WW, Surette MG. 2006. Thin aggregative fimbriae and cellulose enhance long-term survival and persistence of *Salmonella*. J Bacteriol 188:3219-27.

111. Wang X, Rochon M, Lamprokostopoulou A, Lunsdorf H, Nimtz M, Romling U. 2006. Impact of biofilm matrix components on interaction of commensal *Escherichia coli* with the gastrointestinal cell line HT-29. Cell Mol Life Sci 63:2352-63.

112. Gophna U, Barlev M, Seijffers R, Oelschlager TA, Hacker J, Ron EZ. 2001. Curli fibers mediate internalization of *Escherichia coli* by eukaryotic cells. Infect Immun 69:2659-65.

113. Bian Z, Brauner A, Li Y, Normark S. 2000. Expression of and cytokine activation by *Escherichia coli* curli fibers in human sepsis. J Infect Dis 181:602-12.

114. Hammar M, Arnqvist A, Bian Z, Olsen A, Normark S. 1995. Expression of two *csg* operons is required for production of fibronectin- and congo red-binding curli polymers in *Escherichia coli* K-12. Mol Microbiol 18:661-70.

115. Romling U, Bian Z, Hammar M, Sierralta WD, Normark S. 1998. Curli fibers are highly conserved between *Salmonella typhimurium* and *Escherichia coli* with respect to operon structure and regulation. J Bacteriol 180:722-31.

116. Jensen LJ, Kuhn M, Stark M, Chaffron S, Creevey C, Muller J, Doerks T, Julien P, Roth A, Simonovic M, Bork P, von Mering C. 2009. STRING 8--a global view on proteins and their functional interactions in 630 organisms. Nucleic Acids Res 37:D412-6.

117. Romling U, Sierralta WD, Eriksson K, Normark S. 1998. Multicellular and aggregative behaviour of *Salmonella typhimurium* strains is controlled by mutations in the *agfD* promoter. Mol Microbiol 28:249-64.

118. Bian Z, Normark S. 1997. Nucleator function of CsgB for the assembly of adhesive surface organelles in *Escherichia coli*. Embo J 16:5827-36.

119. Hammar M, Bian Z, Normark S. 1996. Nucleator-dependent intercellular assembly of adhesive curli organelles in *Escherichia coli.* Proc Natl Acad Sci U S A 93:6562-6.

120. Loferer H, Hammar M, Normark S. 1997. Availability of the fibre subunit CsgA and the nucleator protein CsgB during assembly of fibronectin-binding curli is limited by the intracellular concentration of the novel lipoprotein CsgG. Mol Microbiol 26:11-23.

121. Epstein EA, Reizian MA, Chapman MR. 2009. Spatial clustering of the curlin secretion lipoprotein requires curli fiber assembly. J Bacteriol 191:608-15.

122. Nenninger AA, Robinson LS, Hammer ND, Epstein EA, Badtke MP, Hultgren SJ, Chapman MR. 2011. CsgE is a curli secretion specificity factor that prevents amyloid fibre aggregation. Mol Microbiol 81:486-99.

123. Gibson DL, White AP, Rajotte CM, Kay WW. 2007. AgfC and AgfE facilitate extracellular thin aggregative fimbriae synthesis in *Salmonella enteritidis*. Microbiology 153:1131-40.

124. Taylor JD, Zhou Y, Salgado PS, Patwardhan A, McGuffie M, Pape T, Grabe G, Ashman E, Constable SC, Simpson PJ, Lee W-c, Cota E, Chapman MR, Matthews SJ. 2011. Atomic Resolution Insights into Curli Fibre Biogenesis Structure in press.

125. Pham CLL, Kwan AH, Sunde M. 2014. Functional amyloid: widespread in Nature, diverse in purpose, p 207-219. *In* Perrett S (ed), Amyloids in Health and Disease, vol 56. Portland Press Ltd, London.

126. Ogasawara H, Yamada K, Kori A, Yamamoto K, Ishihama A. 2010. Regulation of the *E. coli csgD* Promoter: Interplay between Five Transcription Factors. Microbiology.

127. Barnhart MM, Lynem J, Chapman MR. 2006. GlcNAc-6P levels modulate the expression of Curli fibers by *Escherichia coli.* J Bacteriol 188:5212-9.

128. Hammar M. 1997 Assembly and adhesive properties of curli. . PhD thesis at Karolinska Institute, Stockholm, Sweden.

129. Ishii S, Ksoll WB, Hicks RE, Sadowsky MJ. 2006. Presence and Growth of Naturalized *Escherichia coli* in Temperate Soils from Lake Superior Watersheds. Applied and Environmental Microbiology 72:612-621.

130. Hassett DJ, Sutton MD, Schurr MJ, Herr AB, Caldwell CC, Matu JO. 2009. *Pseudomonas aeruginosa* hypoxic or anaerobic biofilm infections within cystic fibrosis airways. Trends in Microbiology 17:130-138.

131. Collinson SK, Doig PC, Doran JL, Clouthier S, Trust TJ, Kay WW. 1993. Thin, aggregative fimbriae mediate binding of *Salmonella enteritidis* to fibronectin. J Bacteriol 175:12-8.

132. Powell S, Szklarczyk D, Trachana K, Roth A, Kuhn M, Muller J, Arnold R, Rattei T, Letunic I, Doerks T, Jensen LJ, von Mering C, Bork P. 2012. eggNOG v3.0: orthologous groups covering 1133 organisms at 41 different taxonomic ranges. Nucleic Acids Res 40:D284-9.

133. Keseler IM, Mackie A, Peralta-Gil M, Santos-Zavaleta A, Gama-Castro S, Bonavides-Martinez C, Fulcher C, Huerta AM, Kothari A, Krummenacker M, Latendresse M, Muniz-Rascado L, Ong Q, Paley S, Schroder I, Shearer AG, Subhraveti P, Travers M, Weerasinghe D, Weiss V, Collado-Vides J, Gunsalus RP, Paulsen I, Karp PD. 2013. EcoCyc: fusing model organism databases with systems biology. Nucleic Acids Res 41:D605-12.

134. Galperin MY, Makarova KS, Wolf YI, Koonin EV. 2015. Expanded microbial genome coverage and improved protein family annotation in the COG database. Nucleic Acids Res 43:D261-9.

135. Lipman DJ, Souvorov A, Koonin EV, Panchenko AR, Tatusova TA. 2002. The relationship of protein conservation and sequence length. BMC Evol Biol 2:20.

136. Misra RV, Horler RS, Reindl W, Goryanin, II, Thomas GH. 2005. EchoBASE: an integrated post-genomic database for *Escherichia coli*. Nucleic Acids Res 33:D329-33.

137. Shimada T, Fujita N, Yamamoto K, Ishihama A. 2011. Novel Roles of cAMP Receptor Protein (CRP) in Regulation of Transport and Metabolism of Carbon Sources. PLOS ONE 6:e20081.

138. Tatusov RL, Koonin EV, Lipman DJ. 1997. A genomic perspective on protein families. Science 278:631-7.

139. Weiner JH, Li L. 2008. Proteome of the *Escherichia coli* envelope and technological challenges in membrane proteome analysis. Biochim Biophys Acta 1778:1698-713.

140. Pradel E, Schnaitman CA. 1991. Effect of *rfaH* (*sfrB*) and temperature on expression of *rfa* genes of *Escherichia coli* K-12. J Bacteriol 173:6428-31.

141. Raetz CR, Whitfield C. 2002. Lipopolysaccharide endotoxins. Annu Rev Biochem 71:635-700.

142. Schnaitman CA, Klena JD. 1993. Genetics of lipopolysaccharide biosynthesis in enteric bacteria. Microbiol Rev 57:655-82.

143. Klein G, Müller-Loennies S, Lindner B, Kobylak N, Brade H, Raina S. 2013. Molecular and structural basis of inner core lipopolysaccharide alterations in *Escherichia coli*: incorporation of glucuronic acid and phosphoethanolamine in the heptose region. J Biol Chem 288:8111-27.

144. Anriany Y, Sahu SN, Wessels KR, McCann LM, Joseph SW. 2006. Alteration of the rugose phenotype in *waaG* and *ddhC* mutants of *Salmonella enterica* serovar Typhimurium DT104 is associated with inverse production of curli and cellulose. Appl Environ Microbiol 72:5002-12.

145. Kim SH, Kim YH. 2004. *Escherichia coli* O157:H7 adherence to HEp-2 cells is implicated with curli expression and outer membrane integrity. J Vet Sci 5:119-24.

146. Ma Q, Wood TK. 2009. OmpA influences *Escherichia coli* biofilm formation by repressing cellulose production through the CpxRA two-component system. Environ Microbiol 11:2735-46.

147. Coleman WG, Jr. 1983. The *rfaD* gene codes for ADP-L-glycero-D-mannoheptose-6-epimerase. An enzyme required for lipopolysaccharide core biosynthesis. J Biol Chem 258:1985-90.

148. Kneidinger B, Marolda C, Graninger M, Zamyatina A, McArthur F, Kosma P, Valvano MA, Messner P. 2002. Biosynthesis pathway of ADP-L-glycero-beta-D-manno-heptose in *Escherichia coli*. J Bacteriol 184:363-9.

149. Kuznetsova E, Proudfoot M, Gonzalez CF, Brown G, Omelchenko MV, Borozan I, Carmel L, Wolf YI, Mori H, Savchenko AV, Arrowsmith CH, Koonin EV, Edwards AM, Yakunin AF. 2006. Genome-wide analysis of substrate specificities of the *Escherichia coli* haloacid dehalogenase-like phosphatase family. J Biol Chem 281:36149-61.

150. Parker CT, Kloser AW, Schnaitman CA, Stein MA, Gottesman S, Gibson BW. 1992. Role of the *rfaG* and *rfaP* genes in determining the lipopolysaccharide core structure and cell surface properties of *Escherichia coli* K-12. J Bacteriol 174:2525-38.

151. Weissborn AC, Liu Q, Rumley MK, Kennedy EP. 1994. UTP: alpha-D-glucose-1-phosphate uridylyltransferase of *Escherichia coli*: isolation and DNA sequence of the *galU* gene and purification of the enzyme. J Bacteriol 176:2611-8.

152. Karp PD, Keseler IM, Shearer A, Latendresse M, Krummenacker M, Paley SM, Paulsen I, Collado-Vides J, Gama-Castro S, Peralta-Gil M, Santos-Zavaleta A, Penaloza-Spinola MI, Bonavides-Martinez C, Ingraham J. 2007. Multidimensional annotation of the *Escherichia coli* K-12 genome. Nucleic Acids Res 35:7577-90.

153. Boos W, Ehmann U, Forkl H, Klein W, Rimmele M, Postma P. 1990. Trehalose transport and metabolism in *Escherichia coli*. J Bacteriol 172:3450-61.

154. Genevaux P, Bauda P, DuBow MS, Oudega B. 1999. Identification of Tn10 insertions in the *rfaG*, *rfaP*, and *galU* genes involved in lipopolysaccharide core biosynthesis that affect *Escherichia coli* adhesion. Arch Microbiol 172:1-8.

155. Rosenberg M, D. Gutnick, and E. Rosenberg. 1980. Adherence of bacteria to hydrocarbons: a simple method for measuring cell surface hydrophobicity. FEMS Microbiol Lett 9:29-33.

156. Nikaido H, Vaara M. 1985. Molecular basis of bacterial outer membrane permeability. Microbiol Rev 49:1-32.

157. de Cock H, Tommassen J. 1996. Lipopolysaccharides and divalent cations are involved in the formation of an assembly-competent intermediate of outer-membrane protein PhoE of *E.coli*. Embo J 15:5567-73.

158. de Maagd RA, Wientjes FB, Lugtenberg BJ. 1989. Evidence for divalent cation (Ca2+)-stabilized oligomeric proteins and covalently bound protein-peptidoglycan complexes in the outer membrane of *Rhizobium leguminosarum*. J Bacteriol 171:3989-95.

159. Rahman A, Barr K, Rick PD. 2001. Identification of the structural gene for the TDP-Fuc4NAc:lipid II Fuc4NAc transferase involved in synthesis of enterobacterial common antigen in *Escherichia coli* K-12. J Bacteriol 183:6509-16.

160. Danese PN, Oliver GR, Barr K, Bowman GD, Rick PD, Silhavy TJ. 1998. Accumulation of the enterobacterial common antigen lipid II biosynthetic intermediate stimulates *degP* transcription in *Escherichia coli.* J Bacteriol 180:5875-84.

161. Serra DO, Mika F, Richter AM, Hengge R. 2016. The green tea polyphenol EGCG inhibits *E. coli* biofilm formation by impairing amyloid curli fibre assembly and downregulating the biofilm regulator CsgD via the σE-dependent sRNA RybB. Molecular Microbiology 101:136-151.

162. Vines ED, Marolda CL, Balachandran A, Valvano MA. 2005. Defective O-antigen polymerization in *tolA* and pal mutants of *Escherichia coli* in response to extracytoplasmic stress. J Bacteriol 187:3359-68.

163. Chaba R, Alba BM, Guo MS, Sohn J, Ahuja N, Sauer RT, Gross CA. 2011. Signal integration by DegS and RseB governs the σE-mediated envelope stress response in *Escherichia coli*. Proceedings of the National Academy of Sciences 108:2106-2111.

164. Ahuja N, Korkin D, Chaba R, Cezairliyan BO, Sauer RT, Kim KK, Gross CA. 2009. Analyzing the interaction of RseA and RseB, the two negative regulators of the sigmaE envelope stress response, using a combined bioinformatic and experimental strategy. J Biol Chem 284:5403-13.

165. Missiakas D, Mayer MP, Lemaire M, Georgopoulos C, Raina S. 1997. Modulation of the *Escherichia coli* sigmaE (RpoE) heat-shock transcription-factor activity by the RseA, RseB and RseC proteins. Mol Microbiol 24:355-71.

166. Rhodius VA, Suh WC, Nonaka G, West J, Gross CA. 2006. Conserved and variable functions of the sigmaE stress response in related genomes. PLoS Biol 4:e2.

167. Bury-Mone S, Nomane Y, Reymond N, Barbet R, Jacquet E, Imbeaud S, Jacq A, Bouloc P. 2009. Global analysis of extracytoplasmic stress signaling in *Escherichia coli.* PLoS Genet 5:e1000651.

168. Tam C, Missiakas D. 2005. Changes in lipopolysaccharide structure induce the sigma(E)-dependent response of *Escherichia coli*. Mol Microbiol 55:1403-12.

169. Klein G, Stupak A, Biernacka D, Wojtkiewicz P, Lindner B, Raina S. 2016. Multiple Transcriptional Factors Regulate Transcription of the *rpoE* Gene in *Escherichia coli* under Different Growth Conditions and When the Lipopolysaccharide Biosynthesis Is Defective. J Biol Chem 291:22999-23019.

170. Missiakas D, Betton JM, Raina S. 1996. New components of protein folding in extracytoplasmic compartments of *Escherichia coli* SurA, FkpA and Skp/OmpH. Mol Microbiol 21:871-84.

171. Jiang SS, Lin TY, Wang WB, Liu MC, Hsueh PR, Liaw SJ. 2010. Characterization of UDP-glucose dehydrogenase and UDP-glucose pyrophosphorylase mutants of *Proteus mirabilis*: defectiveness in polymyxin B resistance, swarming, and virulence. Antimicrob Agents Chemother 54:2000-9.

172. Klein G, Lindner B, Brabetz W, Brade H, Raina S. 2009. *Escherichia coli* K-12 Suppressor-free Mutants Lacking Early Glycosyltransferases and Late Acyltransferases: minimal lipopolysaccharide structure and induction of envelope stress response. J Biol Chem 284:15369-89.

173. Dorel C, Vidal O, Prigent-Combaret C, Vallet I, Lejeune P. 1999. Involvement of the Cpx signal transduction pathway of *E. coli* in biofilm formation. FEMS Microbiol Lett 178:169-75.

174. Jubelin G, Vianney A, Beloin C, Ghigo JM, Lazzaroni JC, Lejeune P, Dorel C. 2005. CpxR/OmpR interplay regulates curli gene expression in response to osmolarity in *Escherichia coli*. J Bacteriol 187:2038-49.

175. Yamamoto K, Ishihama A. 2005. Transcriptional response of *Escherichia coli* to external zinc. J Bacteriol 187:6333-40.

176. Egler M, Grosse C, Grass G, Nies DH. 2005. Role of the extracytoplasmic function protein family sigma factor RpoE in metal resistance of *Escherichia coli*. J Bacteriol 187:2297-307.

177. De Las Penas A, Connolly L, Gross CA. 1997. The sigmaE-mediated response to extracytoplasmic stress in *Escherichia coli* is transduced by RseA and RseB, two negative regulators of sigmaE. Mol Microbiol 24:373-85.

178. Perrenoud A, Sauer U. 2005. Impact of global transcriptional regulation by ArcA, ArcB, Cra, Crp, Cya, Fnr, and Mlc on glucose catabolism in *Escherichia coli*. J Bacteriol 187:3171-9.

179. Nanchen A, Schicker A, Revelles O, Sauer U. 2008. Cyclic AMP-dependent catabolite repression is the dominant control mechanism of metabolic fluxes under glucose limitation in *Escherichia coli*. J Bacteriol 190:2323-30.

180. Saier MH, Jr., Ramseier TM. 1996. The catabolite repressor/activator (Cra) protein of enteric bacteria. J Bacteriol 178:3411-7.

181. Zheng D, Constantinidou C, Hobman JL, Minchin SD. 2004. Identification of the CRP regulon using in vitro and in vivo transcriptional profiling. Nucleic Acids Res 32:5874-93.

182. Neidhardt FC, Curtiss III R, Ingraham JL, Lin ECC, Low Jr. KB, Magasanik B, Reznikoff WS, Riley M, Schaechter M, Umbarger HE. 1996. *Escherichia coli* and *Salmonella*: Cellular and Molecular Biology, 2nd ed. ASM Press, Washington, D.C.

183. Hufnagel DA, Evans ML, Greene SE, Pinkner JS, Hultgren SJ, Chapman MR. 2016. CRP-cAMP regulates *csgD* and biofilm formation by uropathogenic *Escherichia coli*. Journal of Bacteriology doi:10.1128/jb.00652-16.

184. Ramseier TM, Bledig S, Michotey V, Feghali R, Saier MH, Jr. 1995. The global regulatory protein FruR modulates the direction of carbon flow in *Escherichia coli*. Mol Microbiol 16:1157-69.

185. White AP, Weljie AM, Apel D, Zhang P, Shaykhutdinov R, Vogel HJ, Surette MG. 2010. A global metabolic shift is linked to *Salmonella* multicellular development. PLoS One 5:e11814.

186. Alteri CJ, Smith SN, Mobley HL. 2009. Fitness of *Escherichia coli* during urinary tract infection requires gluconeogenesis and the TCA cycle. PLoS Pathog 5:e1000448.

187. Yoon SS, Hennigan RF, Hilliard GM, Ochsner UA, Parvatiyar K, Kamani MC, Allen HL, DeKievit TR, Gardner PR, Schwab U, Rowe JJ, Iglewski BH, McDermott TR, Mason RP, Wozniak DJ, Hancock REW, Parsek MR, Noah TL, Boucher RC, Hassett DJ. 2002. *Pseudomonas aeruginosa* Anaerobic Respiration in Biofilms. Developmental Cell 3:593-603.

188. Mangalea MR, Plumley BA, Borlee BR. 2017. Nitrate Sensing and Metabolism Inhibit Biofilm Formation in the Opportunistic Pathogen *Burkholderia pseudomallei* by Reducing the Intracellular Concentration of c-di-GMP. Frontiers in Microbiology 8:1353.

189. Van Alst NE, Picardo KF, Iglewski BH, Haidaris CG. 2007. Nitrate Sensing and Metabolism Modulate Motility, Biofilm Formation, and Virulence in *Pseudomonas aeruginosa*. Infection and Immunity 75:3780-3790.

190. Kalamorz F, Reichenbach B, Marz W, Rak B, Gorke B. 2007. Feedback control of glucosamine-6-phosphate synthase GlmS expression depends on the small RNA GlmZ and involves the novel protein YhbJ in *Escherichia coli*. Mol Microbiol 65:1518-33.

191. Reichenbach B, Maes A, Kalamorz F, Hajnsdorf E, Gorke B. 2008. The small RNA GlmY acts upstream of the sRNA GlmZ in the activation of *glmS* expression and is subject to regulation by polyadenylation in *Escherichia coli*. Nucleic Acids Res 36:2570-80.

192. Gruber CC, Sperandio V. 2015. Global Analysis of Posttranscriptional Regulation by GlmY and GlmZ in Enterohemorrhagic *Escherichia coli* O157:H7. Infection and Immunity 83:1286-1295.

193. Urban JH, Vogel J. 2008. Two seemingly homologous noncoding RNAs act hierarchically to activate *glmS* mRNA translation. PLoS Biol 6:e64.

194. Mengin-Lecreulx D, van Heijenoort J. 1996. Characterization of the essential gene *glmM* encoding phosphoglucosamine mutase in *Escherichia coli*. J Biol Chem 271:32-9.

195. Pedersen AG, Jensen LJ, Brunak S, Staerfeldt HH, Ussery DW. 2000. A DNA structural atlas for *Escherichia coli*. J Mol Biol 299:907-30.

196. Teramoto J, Yoshimura SH, Takeyasu K, Ishihama A. 2010. A novel nucleoid protein of *Escherichia coli* induced under anaerobiotic growth conditions. Nucleic Acids Res 38:3605-18.

197. Tamayo R, Pratt JT, Camilli A. 2007. Roles of cyclic diguanylate in the regulation of bacterial pathogenesis. Annu Rev Microbiol 61:131-48.

198. Hengge-Aronis R. 2002. Signal transduction and regulatory mechanisms involved in control of the sigma(S) (RpoS) subunit of RNA polymerase. Microbiol Mol Biol Rev 66:373-95, table of contents.

199. Bohringer J, Fischer D, Mosler G, Hengge-Aronis R. 1995. UDP-glucose is a potential intracellular signal molecule in the control of expression of sigma S and sigma S-dependent genes in *Escherichia coli*. J Bacteriol 177:413-22.

200. Loewen PC, Hu B, Strutinsky J, Sparling R. 1998. Regulation in the rpoS regulon of *Escherichia coli*. Can J Microbiol 44:707-17.

201. Sevcik M, Sebkova A, Volf J, Rychlik I. 2001. Transcription of *arcA* and *rpoS* during growth of *Salmonella typhimurium* under aerobic and microaerobic conditions. Microbiology 147:701-8.

202. Lange R, Fischer D, Hengge-Aronis R. 1995. Identification of transcriptional start sites and the role of ppGpp in the expression of *rpoS*, the structural gene for the sigma S subunit of RNA polymerase in *Escherichia coli*. J Bacteriol 177:4676-80.

203. Brown L, Gentry D, Elliott T, Cashel M. 2002. DksA affects ppGpp induction of RpoS at a translational level. J Bacteriol 184:4455-65.

204. Jiang M, Sullivan SM, Wout PK, Maddock JR. 2007. G-protein control of the ribosome-associated stress response protein SpoT. J Bacteriol 189:6140-7.

205. Kostakioti M, Hadjifrangiskou M, Pinkner JS, Hultgren SJ. 2009. QseC-mediated dephosphorylation of QseB is required for expression of genes associated with virulence in uropathogenic *Escherichia coli*. Mol Microbiol 73:1020-31.

206. Pesavento C, Becker G, Sommerfeldt N, Possling A, Tschowri N, Mehlis A, Hengge R. 2008. Inverse regulatory coordination of motility and curli-mediated adhesion in *Escherichia coli*. Genes Dev 22:2434-46.

207. Dyszel JL, Soares JA, Swearingen MC, Lindsay A, Smith JN, Ahmer BM. 2010. *E. coli* K-12 and EHEC genes regulated by SdiA. PLoS One 5:e8946.

208. Leaphart AB, Thompson DK, Huang K, Alm E, Wan X-F, Arkin A, Brown SD, Wu L, Yan T, Liu X, Wickham GS, Zhou J. 2006. Transcriptome Profiling of *Shewanella oneidensis* Gene Expression following Exposure to Acidic and Alkaline pH. Journal of Bacteriology 188:1633-1642.

209. Popp D, Iwasa M, Narita A, Erickson HP, Maéda Y. 2009. FtsZ Condensates: An In Vitro Electron Microscopy Study. Biopolymers 91:340-350.

210. Pogliano J, Dong JM, De Wulf P, Furlong D, Boyd D, Losick R, Pogliano K, Lin EC. 1998. Aberrant cell division and random FtsZ ring positioning in *Escherichia coli cpxA** mutants. J Bacteriol 180:3486-90.

211. Inoue T, Shingaki R, Hirose S, Waki K, Mori H, Fukui K. 2007. Genome-wide screening of genes required for swarming motility in *Escherichia coli* K-12. J Bacteriol 189:950-7.

212. Harshey RM. 2003. Bacterial motility on a surface: many ways to a common goal. Annu Rev Microbiol 57:249-73.

213. Pirooznia M, Nagarajan V, Deng Y. 2007. GeneVenn - A web application for comparing gene lists using Venn diagrams. Bioinformation 1:420-2.

214. Hadjifrangiskou M, Gu AP, Pinkner JS, Kostakioti M, Zhang EW, Greene SE, Hultgren SJ. 2012. Transposon Mutagenesis Identifies Uropathogenic *Escherichia coli* Biofilm Factors. Journal of Bacteriology 194:6195-6205.

215. Niba ET, Naka Y, Nagase M, Mori H, Kitakawa M. 2007. A genome-wide approach to identify the genes involved in biofilm formation in *E. coli*. DNA Res 14:237-46.

216. Römling U, Rohde M, Olsén A, Normark S, Reinköster J. 2000. AgfD, the checkpoint of multicellular and aggregative behaviour in *Salmonella typhimurium* regulates at least two independent pathways. Molecular Microbiology 36:10-23.

217. Garavaglia M, Rossi E, Landini P. 2012. The pyrimidine nucleotide biosynthetic pathway modulates production of biofilm determinants in *Escherichia coli*. PLoS One 7:e31252.

218. Monteiro C, Papenfort K, Hentrich K, Ahmad I, Le Guyon S, Reimann R, Grantcharova N, Romling U. 2012. Hfq and Hfq-dependent small RNAs are major contributors to multicellular development in *Salmonella enterica* serovar Typhimurium. RNA Biol 9:489-502.

219. Andresen L, Sala E, Koiv V, Mae A. 2010. A role for the Rcs phosphorelay in regulating expression of plant cell wall degrading enzymes in *Pectobacterium carotovorum* subsp. carotovorum. Microbiology 156:1323-34.

220. Mika F, Busse S, Possling A, Berkholz J, Tschowri N, Sommerfeldt N, Pruteanu M, Hengge R. 2012. Targeting of *csgD* by the small regulatory RNA RprA links stationary phase, biofilm formation and cell envelope stress in *Escherichia coli*. Mol Microbiol 84:51-65.

221. Jorgensen MG, Nielsen JS, Boysen A, Franch T, Moller-Jensen J, Valentin-Hansen P. 2012. Small regulatory RNAs control the multi-cellular adhesive lifestyle of *Escherichia coli*. Mol Microbiol 84:36-50.

222. Zhang A, Schu DJ, Tjaden BC, Storz G, Gottesman S. 2013. Mutations in interaction surfaces differentially impact *E. coli* Hfq association with small RNAs and their mRNA targets. J Mol Biol 425:3678-97.

223. Mika F, Hengge R. 2014. Small RNAs in the control of RpoS, CsgD, and biofilm architecture of *Escherichia coli*. RNA Biology 11:494-507.

224. Tsay JT, Oh W, Larson TJ, Jackowski S, Rock CO. 1992. Isolation and characterization of the beta-ketoacyl-acyl carrier protein synthase III gene (*fabH*) from *Escherichia coli* K-12. J Biol Chem 267:6807-14.

225. Dehesh K, Tai H, Edwards P, Byrne J, Jaworski JG. 2001. Overexpression of 3-Ketoacyl-Acyl-Carrier Protein Synthase IIIs in Plants Reduces the Rate of Lipid Synthesis. Plant Physiology 125:1103-1114.

226. Lai C-Y, Cronan JE. 2003. β-Ketoacyl-Acyl Carrier Protein Synthase III (FabH) Is Essential for Bacterial Fatty Acid Synthesis. Journal of Biological Chemistry 278:51494-51503.

227. Datsenko KA, Wanner BL. 2000. One-step inactivation of chromosomal genes in *Escherichia coli* K-12 using PCR products. Proc Natl Acad Sci U S A 97:6640-5.

228. Wang X, Smith DR, Jones JW, Chapman MR. 2007. In Vitro Polymerization of a Functional *Escherichia coli* Amyloid Protein. Journal of Biological Chemistry 282:3713-3719.

229. Marolda CL, Lahiry P, Vines E, Saldias S, Valvano MA. 2006. Micromethods for the characterization of lipid A-core and O-antigen lipopolysaccharide. Methods Mol Biol 347:237-52.

230. Stead MB, Agrawal A, Bowden KE, Nasir R, Mohanty BK, Meagher RB, Kushner SR. 2012. RNAsnap: a rapid, quantitative and inexpensive, method for isolating total RNA from bacteria. Nucleic Acids Res 40:e156.

231. Pfaffl MW. 2001. A new mathematical model for relative quantification in real-time RT-PCR. Nucleic Acids Res 29:e45.

232. Zhang XS, García-Contreras R, Wood TK. 2007. YcfR (BhsA) influences *Escherichia coli* biofilm formation through stress response and surface hydrophobicity. J Bacteriol 189:3051-62.

233. Rosenberg M. 1984. Ammonium sulphate enhances adherence of *Escherichia coli* J-5 to hydrocarbon and polystyrene. FEMS Microbiology Letters 25:41-45.

234. Arnqvist A, Olsén A, Pfeifer J, Russell DG, Normark S. 1992. The Crl protein activates cryptic genes for curli formation and fibronectin binding in *Escherichia coli* HB101. Mol Microbiol 6:2443-52.

235. Bougdour A, Lelong C, Geiselmann J. 2004. Crl, a low temperature-induced protein in *Escherichia coli* that binds directly to the stationary phase sigma subunit of RNA polymerase. J Biol Chem 279:19540-50.

236. Pratt LA, Silhavy TJ. 1998. Crl stimulates RpoS activity during stationary phase. Mol Microbiol 29:1225-36.

237. Gerstel U, Park C, Römling U. 2003. Complex regulation of *csgD* promoter activity by global regulatory proteins. Mol Microbiol 49:639-54.

238. Arnqvist A, Olsén A, Normark S. 1994. Sigma S-dependent growth-phase induction of the *csgBA* promoter in *Escherichia coli* can be achieved in vivo by sigma 70 in the absence of the nucleoid-associated protein H-NS. Mol Microbiol 13:1021-32.

239. Saldaña Z, Xicohtencatl-Cortes J, Avelino F, Phillips AD, Kaper JB, Puente JL, Girón JA. 2009. Synergistic role of curli and cellulose in cell adherence and biofilm formation of attaching and effacing *Escherichia coli* and identification of Fis as a negative regulator of curli. Environ Microbiol 11:992-1006.

240. Vianney A, Jubelin G, Renault S, Dorel C, Lejeune P, Lazzaroni JC. 2005. *Escherichia coli* tol and rcs genes participate in the complex network affecting curli synthesis. Microbiology 151:2487-2497.

241. Uhlich GA, Gunther NWt, Bayles DO, Mosier DA. 2009. The CsgA and Lpp proteins of an *Escherichia coli* O157:H7 strain affect HEp-2 cell invasion, motility, and biofilm formation. Infect Immun 77:1543-52.

242. Ferrières L, Clarke DJ. 2003. The RcsC sensor kinase is required for normal biofilm formation in *Escherichia coli* K-12 and controls the expression of a regulon in response to growth on a solid surface. Mol Microbiol 50:1665-82.

243. Ogasawara H, Hasegawa A, Kanda E, Miki T, Yamamoto K, Ishihama A. 2007. Genomic SELEX search for target promoters under the control of the PhoQP-RstBA signal relay cascade. J Bacteriol 189:4791-9.

244. Lee J, Maeda T, Hong SH, Wood TK. 2009. Reconfiguring the quorum-sensing regulator SdiA of *Escherichia coli* to control biofilm formation via indole and N-acylhomoserine lactones. Appl Environ Microbiol 75:1703-16.

245. Tschowri N, Busse S, Hengge R. 2009. The BLUF-EAL protein YcgF acts as a direct anti-repressor in a blue-light response of *Escherichia coli*. Genes Dev 23:522-34.

246. Kader A, Simm R, Gerstel U, Morr M, Römling U. 2006. Hierarchical involvement of various GGDEF domain proteins in rdar morphotype development of *Salmonella enterica* serovar Typhimurium. Mol Microbiol 60:602-16.

247. Simm R, Lusch A, Kader A, Andersson M, Römling U. 2007. Role of EAL-containing proteins in multicellular behavior of *Salmonella enterica* serovar Typhimurium. J Bacteriol 189:3613-23.

248. Weber H, Pesavento C, Possling A, Tischendorf G, Hengge R. 2006. Cyclic-di-GMP-mediated signalling within the sigma network of *Escherichia coli*. Molecular microbiology 62:1014-34.

249. Solano C, García B, Latasa C, Toledo-Arana A, Zorraquino V, Valle J, Casals J, Pedroso E, Lasa I. 2009. Genetic reductionist approach for dissecting individual roles of GGDEF proteins within the c-di-GMP signaling network in *Salmonella*. Proc Natl Acad Sci U S A 106:7997-8002.

250. Ishihama A. 2010. Prokaryotic genome regulation: multifactor promoters, multitarget regulators and hierarchic networks. FEMS Microbiol Rev 34:628-45.

251. Stenutz R, Weintraub A, Widmalm G. 2006. The structures of *Escherichia coli* O-polysaccharide antigens. FEMS Microbiol Rev 30:382-403.

252. Jensen KF. 1993. The *Escherichia coli* K-12 "wild types" W3110 and MG1655 have an *rph* frameshift mutation that leads to pyrimidine starvation due to low *pyrE* expression levels. J Bacteriol 175:3401-7.

253. Holmqvist E, Reimegård J, Sterk M, Grantcharova N, Römling U, Wagner EG. 2010. Two antisense RNAs target the transcriptional regulator CsgD to inhibit curli synthesis. Embo j 29:1840-50.

254. Brombacher E, Dorel C, Zehnder AJB, Landini P. 2003. The curli biosynthesis regulator CsgD co-ordinates the expression of both positive and negative determinants for biofilm formation in *Escherichia coli*. Microbiology 149:2847-2857.

255. Brombacher E, Baratto A, Dorel C, Landini P. 2006. Gene Expression Regulation by the Curli Activator CsgD Protein: Modulation of Cellulose Biosynthesis and Control of Negative Determinants for Microbial Adhesion. Journal of Bacteriology 188:2027-2037.

256. Chirwa NT, Herrington MB. 2003. CsgD, a regulator of curli and cellulose synthesis, also regulates serine hydroxymethyltransferase synthesis in *Escherichia coli* K-12. Microbiology 149:525-535.

257. Chirwa NT, Herrington MB. 2004. Role of MetR and PurR in the activation of *glyA* by CsgD in *Escherichia coli* K-12. Can J Microbiol 50:683-90.

258. Gibson DL, White AP, Snyder SD, Martin S, Heiss C, Azadi P, Surette M, Kay WW. 2006. *Salmonella* produces an O-antigen capsule regulated by AgfD and important for environmental persistence. J Bacteriol 188:7722-30.

259. Gualdi L, Tagliabue L, Landini P. 2007. Biofilm Formation-Gene Expression Relay System in *Escherichia coli*: Modulation of σ^S-Dependent Gene Expression by the CsgD Regulatory Protein via σ^S Protein Stabilization. Journal of Bacteriology 189:8034-8043.

260. Latasa C, Roux A, Toledo-Arana A, Ghigo J-M, Gamazo C, Penadés JR, Lasa I. 2005. BapA, a large secreted protein required for biofilm formation and host colonization of *Salmonella enterica* serovar Enteritidis. Molecular Microbiology 58:1322-1339.

261. Zakikhany K, Harrington CR, Nimtz M, Hinton JCD, Römling U. 2010. Unphosphorylated CsgD controls biofilm formation in *Salmonella enterica* serovar Typhimurium. Molecular Microbiology 77:771-786.

262. Prigent-Combaret C, Brombacher E, Vidal O, Ambert A, Lejeune P, Landini P, Dorel C. 2001. Complex regulatory network controls initial adhesion and biofilm formation in *Escherichia coli* via regulation of the *csgD* gene. J Bacteriol 183:7213-23.

263. Blattner FR, Plunkett G, Bloch CA, Perna NT, Burland V, Riley M, Collado-Vides J, Glasner JD, Rode CK, Mayhew GF, Gregor J, Davis NW, Kirkpatrick HA, Goeden MA, Rose DJ, Mau B, Shao Y. 1997. The Complete Genome Sequence of *Escherichia coli* K-12. Science 277:1453-1462.

264. Chen SL, Hung C-S, Xu J, Reigstad CS, Magrini V, Sabo A, Blasiar D, Bieri T, Meyer RR, Ozersky P, Armstrong JR, Fulton RS, Latreille JP, Spieth J, Hooton TM, Mardis ER, Hultgren SJ, Gordon JI. 2006. Identification of genes subject to positive selection in uropathogenic strains of *Escherichia coli*: A comparative genomics approach. Proceedings of the National Academy of Sciences 103:5977-5982.

265. Mulvey MA, Lopez-Boado YS, Wilson CL, Roth R, Parks WC, Heuser J, Hultgren SJ. 1998. Induction and evasion of host defenses by type 1-piliated uropathogenic *Escherichia coli*. Science 282:1494-7.

266. Campbell A. 1961. Conditions for the Existence of Bacteriophage. Evolution 15:153-165.

267. Casadaban MJ. 1976. Transposition and fusion of the *lac* genes to selected promoters in *Escherichia coli* using bacteriophage lambda and Mu. J Mol Biol 104:541-55.

268. Peters JE, Thate TE, Craig NL. 2003. Definition of the *Escherichia coli* MC4100 genome by use of a DNA array. J Bacteriol 185:2017-21.

269. Xiao H, Kalman M, Ikehara K, Zemel S, Glaser G, Cashel M. 1991. Residual guanosine 3',5'-bispyrophosphate synthetic activity of *relA* null mutants can be eliminated by *spoT* null mutations. J Biol Chem 266:5980-90.

270. Amann E, Ochs B, Abel KJ. 1988. Tightly regulated *tac* promoter vectors useful for the expression of unfused and fused proteins in *Escherichia coli*. Gene 69:301-15.

271. Costanzo A, Ades SE. 2006. Growth phase-dependent regulation of the extracytoplasmic stress factor, sigmaE, by guanosine 3',5'-bispyrophosphate (ppGpp). J Bacteriol 188:4627-34.

272. Saville RM, Rakshe S, Haagensen JAJ, Shukla S, Spormann AM. 2011. Energy-Dependent Stability of *Shewanella oneidensis* MR-1 Biofilms. Journal of Bacteriology 193:3257-3264.

273. McCrate OA, Zhou XX, Reichhardt C, Cegelski L. 2013. Sum of the Parts: Composition and Architecture of the Bacterial Extracellular Matrix. Journal of Molecular Biology 425:4286-4294.

274. Hufnagel DA, Price JE, Stephenson RE, Kelley J, Benoit MF, Chapman MR. 2018. Thiol Starvation Induces Redox-Mediated Dysregulation of *Escherichia coli* Biofilm Components. Journal of Bacteriology 200:e00389-17.

275. Garnett JA, Martínez-Santos VI, Saldaña Z, Pape T, Hawthorne W, Chan J, Simpson PJ, Cota E, Puente JL, Girón JA, Matthews S. 2012. Structural insights into the biogenesis and biofilm formation by the *Escherichia coli* common pilus. Proceedings of the National Academy of Sciences 109:3950-3955.

276. Wood TK. 2009. Insights on *Escherichia coli* biofilm formation and inhibition from whole-transcriptome profiling. Environ Microbiol 11:1-15.

277. Seminara A, Angelini TE, Wilking JN, Vlamakis H, Ebrahim S, Kolter R, Weitz DA, Brenner MP. 2012. Osmotic spreading of *Bacillus subtilis* biofilms driven by an extracellular matrix. Proceedings of the National Academy of Sciences of the United States of America 109:1116-1121.

278. Tseng BS, Zhang W, Harrison JJ, Quach TP, Song JL, Penterman J, Singh PK, Chopp DL, Packman AI, Parsek MR. 2013. The extracellular matrix protects *Pseudomonas aeruginosa* biofilms by limiting the penetration of tobramycin. Environ Microbiol 15:2865-78.

279. Lee SW, Gu H, Kilberg JB, Ren D. 2018. Sensitizing bacterial cells to antibiotics by shape recovery triggered biofilm dispersion. Acta Biomater 81:93-102.

280. Vidakovic L, Singh PK, Hartmann R, Nadell CD, Drescher K. 2018. Dynamic biofilm architecture confers individual and collective mechanisms of viral protection. Nature Microbiology 3:26-31.

281. Fox EP, Cowley ES, Nobile CJ, Hartooni N, Newman DK, Johnson AD. 2014. Anaerobic bacteria grow within *Candida albicans* biofilms and induce biofilm formation in suspension cultures. Curr Biol 24:2411-6.

282. McClure R, Balasubramanian D, Sun Y, Bobrovskyy M, Sumby P, Genco CA, Vanderpool CK, Tjaden B. 2013. Computational analysis of bacterial RNA-Seq data. Nucleic Acids Res 41:e140.

283. Tjaden B. 2015. *De novo* assembly of bacterial transcriptomes from RNA-seq data. Genome Biology 16:1.

284. Goodarzi H, Elemento O, Tavazoie S. 2009. Revealing Global Regulatory Perturbations across Human Cancers. Molecular Cell 36:900-911.

285. Consortium TU. 2018. UniProt: a worldwide hub of protein knowledge. Nucleic Acids Research 47:D506-D515.

286. Hoch HC, Galvani CD, Szarowski DH, Turner JN. 2005. Two new fluorescent dyes applicable for visualization of fungal cell walls. Mycologia 97:580-8.

287. Simm R, Morr M, Kader A, Nimtz M, Romling U. 2004. GGDEF and EAL domains inversely regulate cyclic di-GMP levels and transition from sessility to motility. Molecular Microbiology 53:1123-1134.

288. Kanehisa M, Goto S. 2000. KEGG: kyoto encyclopedia of genes and genomes. Nucleic Acids Res 28:27-30.

289. Kanehisa M, Sato Y, Furumichi M, Morishima K, Tanabe M. 2019. New approach for understanding genome variations in KEGG. Nucleic Acids Res 47:D590-d595.

290. Kang Y, Weber KD, Qiu Y, Kiley PJ, Blattner FR. 2005. Genome-Wide Expression Analysis Indicates that FNR of *Escherichia coli* K-12 Regulates a Large Number of Genes of Unknown Function. Journal of Bacteriology 187:1135-1160.

291. Beebout CJ, Eberly AR, Werby SH, Reasoner SA, Brannon JR, De S, Fitzgerald MJ, Huggins MM, Clayton DB, Cegelski L, Hadjifrangiskou M. 2019. Respiratory Heterogeneity Shapes Biofilm Formation and Host Colonization in Uropathogenic *Escherichia coli*. mBio 10:e02400-18.

292. Moreira RN, Dressaire C, Barahona S, Galego L, Kaever V, Jenal U, Arraiano CM. 2017. BolA Is Required for the Accurate Regulation of c-di-GMP, a Central Player in Biofilm Formation. mBio 8.

293. Ogasawara H, Ishizuka T, Hotta S, Aoki M, Shimada T, Ishihama A. 2020. Novel regulators of the *csgD* gene encoding the master regulator of biofilm formation in *Escherichia coli* K-12. Microbiology doi:https://doi.org/10.1099/mic.0.000947.

294. Smith DR, Price JE, Burby PE, Blanco LP, Chamberlain J, Chapman MR. 2017. The Production of Curli Amyloid Fibers Is Deeply Integrated into the Biology of *Escherichia coli*. Biomolecules 7.

295. Kolodkin-Gal I, Elsholz AK, Muth C, Girguis PR, Kolter R, Losick R. 2013. Respiration control of multicellularity in *Bacillus subtilis* by a complex of the cytochrome chain with a membrane-embedded histidine kinase. Genes Dev 27:887-99.

296. Rabin RS, Stewart V. 1993. Dual response regulators (NarL and NarP) interact with dual sensors (NarX and NarQ) to control nitrate- and nitrite-regulated gene expression in *Escherichia coli* K-12. Journal of Bacteriology 175:3259-3268.

297. Smith JD. 2003. Signals, switches, regulons and cascades: Control of bacterial gene expression: Hodgson, D. A., and Thomas, C. M. (eds). Biochemistry and Molecular Biology Education 31:274-274.

298. Darwin AJ, Tyson KL, Busby SJ, Stewart V. 1997. Differential regulation by the homologous response regulators NarL and NarP of *Escherichia coli* K-12 depends on DNA binding site arrangement. Mol Microbiol 25:583-95.

299. Van Alst NE, Picardo KF, Iglewski BH, Haidaris CG. 2007. Nitrate Sensing and Metabolism Modulate Motility, Biofilm Formation, and Virulence in *Pseudomonas aeruginosa*. Infection and Immunity 75:3780-3790.

300. Browning DF, Lee DJ, Wolfe AJ, Cole JA, Busby SJ. 2006. The *Escherichia coli* K-12 NarL and NarP proteins insulate the *nrf* promoter from the effects of integration host factor. J Bacteriol 188:7449-56.

301. Browning DF, Cole JA, Busby SJ. 2004. Transcription activation by remodelling of a nucleoprotein assembly: the role of NarL at the FNR-dependent *Escherichia coli nir* promoter. Mol Microbiol 53:203-15.

302. Stewart V. 1993. Nitrate regulation of anaerobic respiratory gene expression in *Escherichia coli*. Mol Microbiol 9:425-34.

303. Stewart PS, Franklin MJ. 2008. Physiological heterogeneity in biofilms. Nat Rev Microbiol 6:199-210.

304. Olsen A, Arnqvist A, Hammar M, Normark S. 1993. Environmental regulation of curli production in *Escherichia coli*. Infect Agents Dis 2:272-4.

305. Gerstel U, Romling U. 2001. Oxygen tension and nutrient starvation are major signals that regulate *agfD* promoter activity and expression of the multicellular morphotype in *Salmonella* typhimurium. Environ Microbiol 3:638-48.

306. Bokranz W, Wang X, Tschape H, Romling U. 2005. Expression of cellulose and curli fimbriae by *Escherichia coli* isolated from the gastrointestinal tract. Journal of Medical Microbiology 54:1171-82.

307. Jubelin G, Vianney A, Beloin C, Ghigo JM, Lazzaroni JC, Lejeune P, Dorel C. 2005. CpxR/OmpR interplay regulates curli gene expression in response to osmolarity in *Escherichia coli*. J Bacteriol 187:2038-2049.

308. Depas WH, Hufnagel DA, Lee JS, Blanco LP, Bernstein HC, Fisher ST, James GA, Stewart PS, Chapman MR. 2013. Iron induces bimodal population development by *Escherichia coli*. Proc Natl Acad Sci U S A 110:2629-34.

309. Dietrich LE, Okegbe C, Price-Whelan A, Sakhtah H, Hunter RC, Newman DK. 2013. Bacterial community morphogenesis is intimately linked to the intracellular redox state. J Bacteriol 195:1371-80.

310. Dietrich LE, Teal TK, Price-Whelan A, Newman DK. 2008. Redox-active antibiotics control gene expression and community behavior in divergent bacteria. Science 321:1203-6.

311. Hammar M, Arnqvist A, Bian Z, Olsen A, Normark S. 1995. Expression of two *csg* operons is required for production of fibronectin- and Congo red-binding curli polymers in *Escherichia coli* K-12. Mol Microbiol 18:661-670.

312. Evans ML, Chorell E, Taylor JD, Aden J, Gotheson A, Li F, Koch M, Sefer L, Matthews SJ, Wittung-Stafshede P, Almqvist F, Chapman MR. 2015. The bacterial curli system possesses a potent and selective inhibitor of amyloid formation. Mol Cell 57:445-55.

313. Sturgill G, Toutain CM, Komperda J, O'Toole GA, Rather PN. 2004. Role of CysE in production of an extracellular signaling molecule in Providencia stuartii and *Escherichia coli*: Loss of *cysE* enhances biofilm formation in *Escherichia coli*. Journal of Bacteriology 186:7610-7617.

314. Ren DC, Zuo RJ, Barrios AFG, Bedzyk LA, Eldridge GR, Pasmore ME, Wood TK. 2005. Differential gene expression for investigation of *Escherichia coli* biofilm inhibition by plant extract ursolic acid. Applied and Environmental Microbiology 71:4022-4034.

315. Lee J, Bansal T, Jayaraman A, Bentley WE, Wood TK. 2007. Enterohemorrhagic *Escherichia coli* biofilms are inhibited by 7-hydroxyindole and stimulated by isatin. Applied and Environmental Microbiology 73:4100-4109.

316. Rossi E, Motta S, Mauri P, Landini P. 2014. Sulfate assimilation pathway intermediate phosphoadenosine 5 '-phosphosulfate acts as a signal molecule affecting production of curli fibres in *Escherichia coli*. Microbiology-Sgm 160:1832-1844.

317. Longo F, Motta S, Mauri P, Landini P, Rossi E. 2016. Interplay of the modified nucleotide phosphoadenosine 5'-phosphosulfate (PAPS) with global regulatory proteins in *Escherichia coli*: modulation of cyclic AMP (cAMP)-dependent gene expression and interaction with the HupA regulatory protein. Chem Biol Interact doi:10.1016/j.cbi.2016.04.016.

318. Subramaniam AR, Deloughery A, Bradshaw N, Chen Y, O'Shea E, Losick R, Chai Y. 2013. A serine sensor for multicellularity in a bacterium. Elife 2:e01501.

319. Singh P, Brooks JF, 2nd, Ray VA, Mandel MJ, Visick KL. 2015. CysK Plays a Role in Biofilm Formation and Colonization by *Vibrio fischeri*. Appl Environ Microbiol 81:5223-34.

320. Gillespie WA. 1952. Biochemical mutants of coliform *bacilli* in infections of the urinary tract. J Pathol Bacteriol 64:551-7.

321. Borderon E, Horodniceanu T. 1978. Metabolically deficient dwarf-colony mutants of *Escherichia coli*: deficiency and resistance to antibiotics of strains isolated from urine culture. J Clin Microbiol 8:629-34.

322. KS. GTaG. 2002. Cysteine-Dependent Uropathogens:Isolation, Identification and Susceptibility to Antimicrobial Agents. JamahiriyaMed J 2:52-54.

323. Thulin E, Sundqvist M, Andersson DI. 2015. Amdinocillin (Mecillinam) resistance mutations in clinical isolates and laboratory-selected mutants of *Escherichia coli*. Antimicrob Agents Chemother 59:1718-27.

324. Dwyer DJ, Belenky PA, Yang JH, MacDonald IC, Martell JD, Takahashi N, Chan CTY, Lobritz MA, Braff D, Schwarz EG, Ye JD, Pati M, Vercruysse M, Ralifo PS, Allison KR, Khalil AS, Ting AY, Walker GC, Collins JJ. 2014. Antibiotics induce redox-related physiological alterations as part of their lethality. Proceedings of the National Academy of Sciences of the United States of America 111:E2100-E2109.

325. Belenky P, Ye JD, Porter CBM, Cohen NR, Lobritz MA, Ferrante T, Jain S, Korry BJ, Schwarz EG, Walker GC, Collins JJ. 2015. Bactericidal Antibiotics Induce Toxic Metabolic Perturbations that Lead to Cellular Damage. Cell Reports 13:968-980.

326. Keren I, Wu Y, Inocencio J, Mulcahy LR, Lewis K. 2013. Killing by bactericidal antibiotics does not depend on reactive oxygen species. Science 339:1213-6.

327. Liu YY, Imlay JA. 2013. Cell Death from Antibiotics Without the Involvement of Reactive Oxygen Species. Science 339:1210-1213.

328. Miller J. 1972. Experiments in Molecular Genetics. Cold Spring Harbor Lab Press, Cold Spring Harbor, NY.

329. Finley JW. SJ, Johnston PH., and Friedman M. 1978. Inhibition of lysinoalanine formation in food protein. Journal of Food Science 43:619-621.

330. Meyer Y, Buchanan BB, Vignols F, Reichheld JP. 2009. Thioredoxins and glutaredoxins: unifying elements in redox biology. Annu Rev Genet 43:335-67.

331. Apontoweil P, Berends W. 1975. Glutathione biosynthesis in *Escherichia coli* K 12. Properties of the enzymes and regulation. Biochim Biophys Acta 399:1-9.

332. Toledano MB, Kumar C, Le Moan N, Spector D, Tacnet F. 2007. The system biology of thiol redox system in *Escherichia coli* and yeast: differential functions in oxidative stress, iron metabolism and DNA synthesis. FEBS Lett 581:3598-607.

333. Okada T, Suzuki H, Wada K, Kumagai H, Fukuyama K. 2006. Crystal structures of γ-glutamyltranspeptidase from *Escherichia coli*, a key enzyme in glutathione metabolism, and its reaction intermediate. Proceedings of the National Academy of Sciences 103:6471-6476.

334. Ryjenkov DA, Simm R, Romling U, Gomelsky M. 2006. The PilZ domain is a receptor for the second messenger c-di-GMP: the PilZ domain protein YcgR controls motility in enterobacteria. Journal of Biological Chemistry 281:30310-4.

335. Fang X, Gomelsky M. 2010. A post-translational, c-di-GMP-dependent mechanism regulating flagellar motility. Molecular Microbiology 76:1295-1305.

336. Malone JG, Jaeger T, Manfredi P, Dotsch A, Blanka A, Bos R, Cornelis GR, Haussler S, Jenal U. 2012. The YfiBNR Signal Transduction Mechanism Reveals Novel Targets for the Evolution of Persistent *Pseudomonas aeruginosa* in Cystic Fibrosis Airways. PLoS Pathog 8.

337. Wassarman KM, Repoila F, Rosenow C, Storz G, Gottesman S. 2001. Identification of novel small RNAs using comparative genomics and microarrays. Genes & Development 15:1637-1651.

338. Storz G, Tartaglia LA, Ames BN. 1990. The Oxyr Regulon. Antonie Van Leeuwenhoek International Journal of General and Molecular Microbiology 58:157-161.

339. Altuvia S, WeinsteinFischer D, Zhang AX, Postow L, Storz G. 1997. A small, stable RNA induced by oxidative stress: Role as a pleiotropic regulator and antimutator. Cell 90:43-53.

340. Kallen AJ, Welch HG, Sirovich BE. 2006. Current antibiotic therapy for isolated urinary tract infections in women. Arch Intern Med 166:635-9.

341. Antoniani D, Bocci P, Maciag A, Raffaelli N, Landini P. 2010. Monitoring of diguanylate cyclase activity and of cyclic-di-GMP biosynthesis by whole-cell assays suitable for high-throughput screening of biofilm inhibitors. Appl Microbiol Biotechnol 85:1095-104.

342. Oppezzo OJ, Anton DN. 1995. Involvement of *cysB* and *cysE* genes in the sensitivity of *Salmonella* typhimurium to mecillinam. J Bacteriol 177:4524-7.

343. Lilic M, Jovanovic M, Jovanovic G, Savic DJ. 2003. Identification of the CysB-regulated gene, *hslJ*, related to the *Escherichia coli* novobiocin resistance phenotype. FEMS Microbiol Lett 224:239-46.

344. Mciver CJ, Tapsall JW. 1993. Study of Growth Requirements Other Than Cysteine of Naturally-Occurring *Escherichia coli* and *Klebsiella* Spp Auxotrophic for Cysteine. Journal of Clinical Microbiology 31:2790-2793.

345. Mciver CJ, Tapsall JW. 1987. Cysteine Requirements of Naturally-Occurring Cysteine Auxotrophs of *Escherichia coli*. Pathology 19:361-363.

346. Rachid S, Ohlsen K, Witte W, Hacker J, Ziebuhr W. 2000. Effect of subinhibitory antibiotic concentrations on polysaccharide intercellular adhesin expression in biofilm-forming *Staphylococcus epidermidis*. Antimicrob Agents Chemother 44:3357-63.

347. Hoffman LR, D'Argenio DA, MacCoss MJ, Zhang Z, Jones RA, Miller SI. 2005. Aminoglycoside antibiotics induce bacterial biofilm formation. Nature 436:1171-5.

348. Limoli DH, Rockel AB, Host KM, Jha A, Kopp BT, Hollis T, Wozniak DJ. 2014. Cationic antimicrobial peptides promote microbial mutagenesis and pathoadaptation in chronic infections. PLoS Pathog 10:e1004083.

349. Ganeshnarayan K, Shah SM, Libera MR, Santostefano A, Kaplan JB. 2009. Poly-N-Acetylglucosamine Matrix Polysaccharide Impedes Fluid Convection and Transport of the Cationic Surfactant Cetylpyridinium Chloride through Bacterial Biofilms. Applied and Environmental Microbiology 75:1308-1314.

350. Doroshenko N, Tseng BS, Howlin RP, Deacon J, Wharton JA, Thurner PJ, Gilmore BF, Parsek MR, Stoodley P. 2014. Extracellular DNA Impedes the Transport of Vancomycin in *Staphylococcus epidermidis* Biofilms Preexposed to Subinhibitory Concentrations of Vancomycin. Antimicrobial Agents and Chemotherapy 58:7273-7282.

351. Klinger-Strobel M, Stein C, Forstner C, Makarewicz O, Pletz MW. 2017. Effects of colistin on biofilm matrices of *Escherichia coli* and *Staphylococcus aureus*. Int J Antimicrob Agents 49:472-479.

352. Hung C, Marschall J, Burnham CAD, Byun AS, Henderson JP. 2014. The Bacterial Amyloid Curli Is Associated with Urinary Source Bloodstream Infection. PLoS One 9.

353. Oppong GO, Rapsinski GJ, Newman TN, Nishimori JH, Biesecker SG, Tukel C. 2013. Epithelial cells augment barrier function via activation of the Toll-like receptor 2/phosphatidylinositol 3-kinase pathway upon recognition of *Salmonella enterica* serovar Typhimurium curli fibrils in the gut. Infect Immun 81:478-86.

354. Claes DJ, Jackson E. 2012. Cystinuria: mechanisms and management. Pediatric Nephrology 27:2031-2038.

355. Rubin EJ, Akerley BJ, Novik VN, Lampe DJ, Husson RN, Mekalanos JJ. 1999. *In vivo* transposition of mariner-based elements in enteric bacteria and mycobacteria. Proc Natl Acad Sci U S A 96:1645-50.

356. Xi H, Schneider BL, Reitzer L. 2000. Purine catabolism in *Escherichia coli* and function of xanthine dehydrogenase in purine salvage. J Bacteriol 182:5332-41.

357. Shaffer CL, Zhang EW, Dudley AG, Dixon B, Guckes KR, Breland EJ, Floyd KA, Casella DP, Algood HMS, Clayton DB, Hadjifrangiskou M. 2017. Purine Biosynthesis Metabolically Constrains Intracellular Survival of Uropathogenic *Escherichia coli*. Infect Immun 85.

358. Smith DR, Chapman MR. 2010. Economical Evolution: Microbes Reduce the Synthetic Cost of Extracellular Proteins. mBio 1:e00131-10.

359. Yee R, Cui P, Shi W, Feng J, Zhang Y. 2015. Genetic Screen Reveals the Role of Purine Metabolism in *Staphylococcus aureus* Persistence to Rifampicin. Antibiotics (Basel) 4:627-42.

360. Haussler S, Fuqua C. 2013. Biofilms 2012: new discoveries and significant wrinkles in a dynamic field. J Bacteriol 195:2947-58.

361. Kåhrström CT. 2013. Survival of the wrinkliest. Nature Reviews Microbiology 11:149-149.

362. Yan J, Fei C, Mao S, Moreau A, Wingreen NS, Košmrlj A, Stone HA, Bassler BL. 2019. Mechanical instability and interfacial energy drive biofilm morphogenesis. eLife 8:e43920.

363. Asally M, Kittisopikul M, Rué P, Du Y, Hu Z, Çağatay T, Robinson AB, Lu H, Garcia-Ojalvo J, Süel GM. 2012. Localized cell death focuses mechanical forces during 3D patterning in a biofilm. Proceedings of the National Academy of Sciences 109:18891-18896.

364. Aguilar B, Ghaffarizadeh A, Johnson CD, Podgorski GJ, Shmulevich I, Flann NS. 2018. Cell death as a trigger for morphogenesis. PLOS ONE 13:e0191089.

365. Ogasawara H, Yamada K, Kori A, Yamamoto K, Ishihama A. 2010. Regulation of the *Escherichia coli csgD* promoter: interplay between five transcription factors. Microbiology 156:2470-2483.

366. Ramos-Morales F. 2012. Acidic pH. Virulence 3:103-106.